NMR Spectroscopic Investigations on Photocatalytic Reactions and Photochromic Materials

Dissertation

zur Erlangung des Doktorgrades der Naturwissenschaften

(Dr. rer. nat.)

an der Fakultät für Chemie und Pharmazie

der Universität Regensburg

vorgelegt von

Hanna Bartling

aus Rosenheim

August 2016

Die vorliegende Dissertation beruht auf Arbeiten, die zwischen August 2012 und August 2016 am Arbeitskreis von Frau Professor Dr. Ruth M. Gschwind am Institut für Organische Chemie der Universität Regensburg durchgeführt wurden.

Promotionsgesuch eingereicht am 19.08.2016

Die Arbeit wurde angeleitet von:	Prof. Dr. Ruth M. Gschwind
Promotionsausschuss:	
Vorsitzender:	PD Dr. Rainer Müller
1. Gutachter:	Prof. Dr. Ruth M. Gschwind
2. Gutachter:	Prof. Dr. Burkhard König
3. Prüfer:	Prof. Dr. Werner Kremer

An dieser Stelle möchte ich mich bei allen bedanken, ohne deren Hilfe und Unterstützung diese Arbeit nicht möglich gewesen wäre.

Zuallererst gilt mein Dank meiner Doktormutter Frau Prof. Dr. Ruth M. Gschwind für die interessante Themenstellung und die intensiven und fruchtbaren Diskussionen, die ganz entscheidend zum Gelingen dieser Arbeit beigetragen haben. Darüber hinaus möchte ich mich für die Möglichkeit bedanken, ein Teil des Graduiertenkollegs 1626 „chemical photocatalysis" zu sein, durch das ich meine Kompetenzen über das Fachliche hinaus erweitern konnte.

Herrn Prof. Dr. Burkhard König danke ich für die Übernahme des Zweitgutachtens, für die erfolgreiche Kooperation bei dem THIQ Projekt und die Betreuung im Rahmen des GRK 1626.

Bei Herrn Prof. Dr. Werner Kremer und Herrn PD Dr. Rainer Müller möchte ich mich für die Ausübung des Amtes als Prüfer bzw. als Vorsitzende recht herzlich bedanken.

Der Deutschen Forschungsgemeinschaft (DFG) danke ich für die finanzielle Unterstützung im Rahmen des Graduiertenkollegs 1626 „Chemische Photokatalyse".

Meiner Kooperationspartnerin des THIQ Projekts Anna Eisenhofer gilt mein besonderer Dank für ihr großes Engagement und ihr Fachwissen, das sie in dieses Projekt eingebracht und ihre Geduld mit der sie die vielen gemeinsamen Stunden intensiver Arbeit bereichert hat. Ohne sie wäre dieses Projekt so nicht möglich gewesen. Den Forschungspraktikanten Nane Eiber und Daniel Schneider danke ich für ihre Mitarbeit und ihr Engagement.

Meinen Kooperationspartnern des Spiropyran/Merocyanine Projekts, Frau Prof. Dr. Christina Thiele, Dr. Christiane Wolff und Jonas Kind möchte ich herzlich für die Möglichkeit danken, unseren LED Aufbau auf ein neues Feld der Chemie auszuweiten und gemeinsam an diesem Projekt zu arbeiten.

Herr Dr. Christian Feldmeier danke ich für die intensive Zusammenarbeit, die vielen Anregungen und Gespräche, die mir den Einstieg in die Photokatalyse sehr erleichtert haben. Zudem möchte ich mich für die Möglichkeit, an den gemeinsamen Projekten des LED-Aufbaus und der Flavin-Katalyse mitzuwirken, bedanken.

Einen besonderen Dank möchte ich all meinen aktuellen und ehemaligen Kollegen aussprechen, die mir stets mit Rat und Tat zur Seite standen und mit so manchen Uni- und Freizeitaktivitäten für ein angenehmes Arbeitsklima sorgten. Dr. Diana Drettwan, Dr. Evelyn Hartmann, Dr. Maria Neumeier, Dr. Christian Feldmeier, Dr. Felicitas von Rekowski, Dr. Carina Koch, Dr. Michael Haindl, Michael Hammer, Nils Sorgenfrei, Florian Hastreiter, Julian Greindl, Andreas Seegerer, Kerstin Rothermel, Philipp Nitschke, unseren PostDocs Dr. Johnny Hioe, Dr. Fabio Morana, Dr. Maxime Melikian, Dr. Polyssena Renzi, Dr. Lokesh Nanjundappa, dem Nachwuchs Nele Berg, Verena Streitferdt und Daniel Schneider. Euch allen vielen vielen Dank! Ein riesiges Dankeschön geht an meine Unimädels Franziska Fendt, Veronika Kropf, Carina Koch und Kathrin Magerl für die unzähligen Kaffepausen, Feierabendbiere, o.ä. welche für den nötigen Ausgleich sorgten und nicht zuletzt für eure Unterstützung in allen Lebenslagen. Ihr seid die Besten!

Den Mitarbeitern der NMR-Abteilung, Dr. Ilya Shenderovich, Fritz Kastner, Annette Schramm, Georgine Stühler, sowie unserer TA Nikola Kastner-Pustet und unserer Sekretärin Ulrike Weck gilt mein Dank für ihre Hilfe und Unterstützung in allen technischen und bürokratischen Fragen.

Ein großes Dankeschön geht auch an meine Freunde innerhalb und außerhalb der Uni, da sie stets Verständnis aufbrachten, ein offenes Ohr für mich hatten oder einen wichtigen Ausgleich zum Arbeitsalltag schufen.

Vor allem aber gilt mein Dank meiner Familie und meinem Freund Stephan, ohne deren Rückhalt, Zuspruch, Verständnis und Glaube an mich diese Arbeit nicht zustande gekommen wäre. Danke für euer Vertrauen, eure Geduld und eure Unterstützung.

Vielen Dank!

NMR Spectroscopic Investigations on Photocatalytic Reactions and Photochromic Materials

Table of Content

1 Introduction and Outline 1

2 LED based NMR Illumination Device for Mechanistic Studies on Photochemical Reactions – Versatile and Simple, yet Surprisingly Powerful ... 5

2.1 Abstract 7

2.2 Introduction 9

2.3 Materials and Methods 10

2.4 Results and Discussion 13

2.5 Conclusions 16

2.6 Additional Findings 17

2.7 References 18

3 The Photocatalyzed Aza-Henry Reaction of *N*-Aryltetrahydro-isoquinolines — Comprehensive Mechanism, $H^{\bullet}$- versus H^{+}-Abstraction and Background Reactions 21

3.1 Abstract 23

3.2 Introduction 25

3.3 Results and Discussion 28

3.4 Summary of the Mechanistic Proposal and Conclusion 40

3.5 Supporting Information 43

3.6 Additional Findings 71

3.7 NMR spectra 90

3.8 References 96

4 LED-illuminated NMR Studies of Flavin-Catalyzed Photo-oxidations Reveal Solvent Control of the Electron-Transfer Mechanism 103

4.2 Introduction 107

4.3 Materials and Methods 107

4.4 Results and Discussion 109

4.5 Conclusions 112

4.6 Supporting Information[1] 113

4.7 References 132

5 Spiropyran/Merocyanine — Studies of a Photochromic Model System Using NMR with *Ex-Situ* and *In-Situ* Irradiation Devices 137

5.1 Abstract 139

5.2 Introduction 141

5.3 Materials and Methods 142

5.4 Results and Discussion 143

5.5 Conclusions 150

5.6 Supporting Information 152

5.7 Additional Information 159

5.8 References 161

6 Summary 165

7 Zusammenfassung 169

1 Introduction and Outline

The idea of using sunlight to promote chemical processes has been growing, since Giacomo Ciamician proclaimed the impending energy problematic in 1912. Very early he realized that the sun is the most efficient sustainable energy source mankind can harness. However, only in the last decades the urgency to replace fossil materials by sustainable sources and therewith the use of sunlight for a multitude of applications has increased tremendously. Nowadays, the adoption of visible light became a major topic in organic synthesis, which is reflected in the fast increasing number of publications. In contrast to the multitude of synthetic applications, only an evanescent number of mechanistic studies investigating photochemical and photocatalytic reactions have been published. However, an in-depth knowledge of the reaction mechanisms and the ongoing processes is of utmost importance for an efficient reaction design. The method of choice for the investigation of light absorbing processes constitutes UV/Vis spectroscopy, due to its ultrashort time resolution, even enabling the detection and characterization of excited states and electron transfer processes. Until now, NMR spectroscopy played only a minor role for the investigation of photochemical and photocatalytic reactions, due to its comparatively low sensitivity and time resolution. Nevertheless, it is a powerful spectroscopic method, providing structural information not only of light absorbing molecules but all kinds of diamagnetic species, as well as insights into aggregation and solvent effects or chemical exchange processes. Taking into account the laser based compositions, commonly used for Photo-CIDNP studies, we developed an LED based NMR illumination device. Due to their high energy lasers are not prone to follow chemical reactions, as they often lead to fast degradation processes. In contrast, LEDs exhibit many advantages for the monitoring of photocatalytic reactions and offer comparability with the synthetically used light sources. By applying a new strategy for the sample illumination inside the magnet the full capacity of this powerful method NMR spectroscopy can be exploited for the investigation of light induced processes. After implementation of the illumination setup prominent model reactions were chosen to examine the potential as well as the limitations of the setup. Demonstrating the diversity, central photocatalytic reactions as well as photochromic materials were investigated, using excitation wavelengths ranging from ultraviolet to visible light.

In chapter 2 the LED based illumination device is presented. This setup allows for the *in situ* illumination of NMR samples thus, providing a new approach for the detection and characterization of photochemical processes by NMR spectroscopy. The setup consists of an optical fiber, guiding the light of the LEDs into the sample placed inside the magnet. The operation of the LEDs by the spectrometer hardware enables both continuous illumination as well as pulsed mode. The application of short duty cycles in combination with reasonable high light intensities made the setup suitable even for time resolved Photo-CIDNP spectroscopy.

In chapter 3 the cross-dehydrogenative coupling reactions of *N*-aryl-tetrahydroisoquinolines and in particular the aza-Henry reaction were investigated. An in depth mechanistic study including *in situ* and *ex situ* NMR techniques, ESR measurements and synthetic strategies revealed, that the aza-Henry reaction can be divided into three main reaction types: the back-

ground reaction independent of light, the light-induced background reaction and the photocatalyzed process. The latter can be further separated into a hydrogen atom abstraction and a deprotonation pathway, depending on the terminal oxidant. The study combined NMR and ESR spectroscopy as well as synthetic strategies, to provide an exceptional comprehensive picture of the overall mechanism.

In chapter 4 the flavin-catalyzed photooxidation of benzyl alcohol was studied by using the *in situ* illumination setup. The reaction was performed in acetonitrile and acetonitrile/D_2O mixtures, since from synthesis strongly deviating reaction rates were known, however their origin remained so far unclear. The NMR spectra and reaction profiles, supported by Photo-CIDNP and UV/Vis measurements revealed the solvent dependent stabilization of a flavin semiquinone radical. The solvent properties turned out to be responsible for the stabilization of the zwiterionic ion pair and thus for the subsequent reaction mechanism. Depending on the experimental conditions flavin was found to be capable of acting as a one- or two-electron acceptor in solution, which has so far only been observed for proteins.

In chapter 5 the *in situ* illumination setup is applied for the investigation of photochromic materials. A spiropyran/merocyanine structure was selected to examine the switching behavior of this model system before embedding the photo switch into polymers. The photochromic properties of the compounds were studied in dependency on solvent, sample concentration, temperature, light intensity and irradiation wavelength. Regarding additional information e.g. about the excitation process of the metastable compound, the *in situ* setup revealed to be superior to the *ex situ* illumination. Furthermore, insights into the stationary states could be gained and the setup provided access to two dimensional NMR spectroscopy and carbon chemical shifts, unknown before.

2 LED based NMR Illumination Device for Mechanistic Studies on Photochemical Reactions – Versatile and Simple, yet Surprisingly Powerful

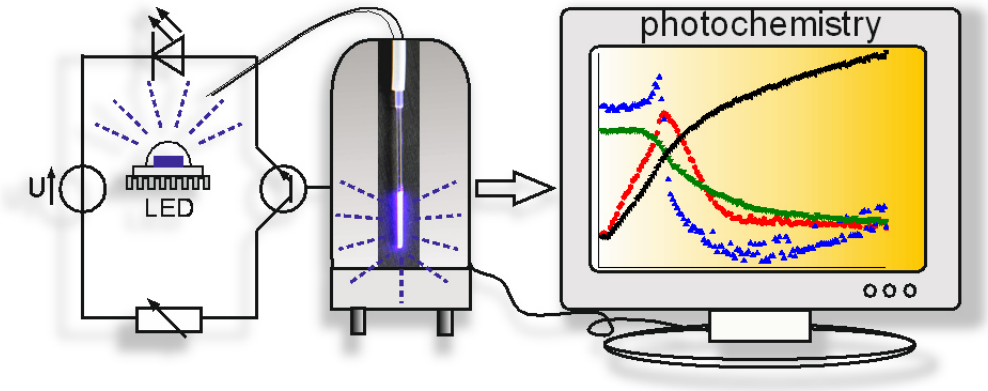

The setup was developed and tested in close collaboration with Dr. C. Feldmeier. The preparation of the fiber tip and the corresponding measurements were conducted by H. Bartling.

Christian Feldmeier, Hanna Bartling, Eberhard Riedle, Ruth M. Gschwind
J. Magn. Reson. **2013**, *232*, 39–44.
DOI: 10.1016/j.jmr.2013.04.011

2.1 Abstract

An LED based illumination device for mechanistic studies on photochemical reactions by means of NMR spectroscopy is presented. The LEDs are directly switched by the NMR spectrometer with the help of a one-stage electronic circuit. This allows for continuous or alternatively pulsed operation of the LEDs. Continuous operation provides direct comparability with conditions in synthetic chemistry, in pulsed operation the short time light power can be enhanced ninefold. The LEDs are efficiently coupled to a 1000 µm core optical fiber guiding the light into the spectrometer by simply bringing it in close contact to the fiber. The tip of the fiber is roughened by sandblasting and thus emits light in a uniform and efficient way over the full length of the receiver coil. The combination of these techniques tremendously increases the amount of light brought into the NMR sample and makes LEDs an easy, versatile and handy light source for the *in situ* illumination of NMR samples allowing even for single millisecond time resolved Photo-CIDNP spectroscopy.

2.2 Introduction

A detailed understanding of the mechanisms of chemical reactions is essential for their application and further development. In classical catalytic reactions such as applied in organocatalysis and transition metal catalysis, NMR has proven to be a very powerful tool for revealing diamagnetic intermediate species and for mechanistic investigations. For example, recently the elusive enamine intermediates,[1] the Breslow intermediate,[2] the key intermediate in enantioselective palladium catalyzed allylic substitution,[3] or Brønsted acid catalysis intermediates[4] were detected and characterized by means of NMR. However, to apply the whole variety of NMR methods to photochemical reactions it is essential to be able to run the reaction inside the spectrometer, which implies that the NMR sample has to be illuminated inside the spectrometer. This not only allows the *in situ* detection of diamagnetic intermediates in photoreactions but also the analysis of the kinetics and reaction mechanisms. *In situ* illumination of NMR samples is applied in various different fields such as organometallic photochemistry[5] or monitoring the kinetics of protein folding.[6,7]

In addition to the standard NMR spectroscopic approaches feasible for reactions in the dark, there is a special hyperpolarization technique applicable exclusively to photoreactions, the Photo-CIDNP spectroscopy.[8-10] Caused by the influence of the nuclear spin state on the intersystem crossing in radical pairs the Photo-CIDNP effect results in anomalous NMR signal intensities. The power of the CIDNP effect is that even extremely short-lived precursor radicals, not detectable in ESR, leave traces in the signal intensity pattern of their diamagnetic products detectable by NMR.[11,12] In this way not only standard NMR techniques can be used for mechanistic studies on photocatalytic systems but even paramagnetic radical intermediates can be detected and characterized by means of NMR. However, both the application of well-established NMR techniques to photochemical reactions and the Photo-CIDNP spectroscopy require the illumination of the samples inside the spectrometer.

Various approaches have been reported to illuminate the sample inside the spectrometer and to guide the light into the sample using lasers or various lamps as light sources.[5,13] The illumination of the sample from the side or from below by selected types of light guides is an approach compatible with both continuous wave light sources and intense pulsed lasers, but requires modifications of the NMR probe and hampers uniform illumination of the NMR sample. By using an optical fiber to guide the light into the spectrometer the sample can be illuminated from the inside by placing the tip of the optical fiber into a coaxial insert.[14] Illumination uniformity is improved by replacing the coaxial insert by a cone shaped insert[6,7] or by tapering the optical fiber stepwise[13] making the tip of the fiber emit light over the whole range of the receiver coil, instead of just from above. A shutter placed in the optical path and synchronized with the NMR spectrometer controls the illumination of the sample and allows the implementation of well-defined light pulses in NMR pulse sequences.[14,15]

LEDs provide an extraordinarily inexpensive, energy saving and easy to handle light source available in a huge diversity of wavelengths in the infrared, visible and ultraviolet range. Among other reasons LEDs have therefore become the light source of choice in the recently rapidly expanding area of photocatalysis.[16-20] Despite these indisputable advantages LEDs have so far not been used as light sources for systematic illumination of NMR samples to the best of our knowledge.

Here we present a notably versatile, easy and inexpensive setup for the illumination of NMR samples using LEDs as light source. To achieve maximal and uniform illumination of the sample (i) the LEDs are switched directly by the spectrometer, (ii) they are brought in direct contact with the optical fiber and (iii) the tip of the optical fiber inserted in the sample is roughened by sandblasting. This setup allows both, the investigation of photo catalytic reactions under synthetic conditions and by pulsed operation of the LEDs even millisecond time resolved Photo-CIDNP spectroscopy.

2.3 Materials and Methods

2.3.1 Circuit – light source

As light source different LEDs are used for the described setup. The high power LEDs are controlled by an electronic circuit, shown schematically in Figure 2.1 a. It consists of a power supply, the LED, a potentiometer to regulate the current through the LEDs and a transistor switched by a TTL signal from the time control unit of the spectrometer. With this circuit the LED can be switched on and off directly by the spectrometer. The potentiometer controls the current through the LEDs and so they can be operated as (i) continuous wave (cw) devices (at specified maximum cw operation currents or below) or (ii) in a pulsed manner at much higher currents. By pulsing the LEDs significantly higher short time powers for the duration of a short pulse in a low duty cycle can be achieved. The currents applied to the LEDs are usually limited by the heat the LEDs produce. However, if heating is minimized by a combination of short light pulses, proper heat dissipation methods realized by an aluminum heat sink, and low duty cycles currents higher by as much as a factor of 9 than those recommended for continuous operation can be used and significantly higher peak output light powers can be achieved. This technique is used in various different fields such as imaging flow velocimetry,[21] high speed photography[22] or laser-flash-photolysis.[23]

Additionally, an opto-isolator is placed between the time control unit of the spectrometer and the LED circuit in order to isolate the two units galvanically and thus to protect the spectrometer time control unit from high and rapidly changing currents from the LED circuit.

In the described way the LED light can be controlled by a spare spectrometer time control unit output. However, to implement defined light pulses into pulse sequences for time resolved CIDNP-spectroscopy[12] it is important to know how fast the LEDs respond with respect to the TTL signal from the spectrometer. Additionally to the intrinsic response time of the LEDs the circuit with the opto-isolator causes an delay between the TTL output signal of the spectrometer and the LED light. To determine the total delay between the TTL pulse and the response of the LED light a photo resistor was used. The total delay was determined by simultaneously measuring the voltage at the TTL signal input and the voltage across a photo resistor illuminated by the LED at the time when the LED was switched on and off, Figure 2.1 b. The upper graph shows the LED response (LED output) for a 10 ms pulse of the spectrometer output on the millisecond time scale. The lower graph reveals on the microsecond time scale that the response time of the LED in this setup is about 3-8 µs. For millisecond time resolved experiments this delay is insignificant. However, for time resolved experiments on smaller time scales it has to be considered when the pulse sequences are implemented. The exponentially

increasing light output in the first few µs is most likely due to heating of the LED that increases the efficiency. If this variation in illumination power is of concern, it can readily be compensated with an improved current control circuit that applies a slightly higher voltage and current initially and then decreases it over the next few µs.

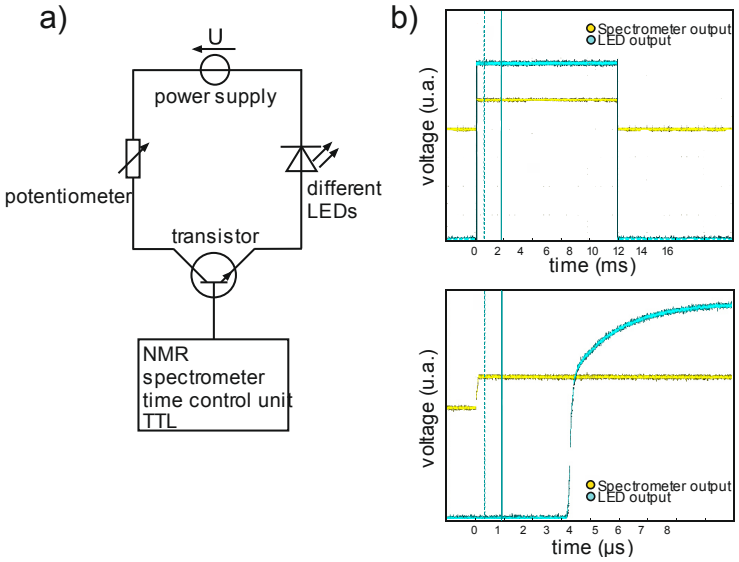

Figure 2.1 (a) Scheme of the circuit used to control and to pulse the LEDs, consisting of a power supply, a potentiometer to adjust the current through the LED and a transistor controlled by the spectrometer. (b) The upper graph shows the response of the LED to a 10 ms pulse from the spectrometer output on a milliseconds time scale and the lower graph reveals at microsecond time resolution that the response time of the LED in this setup is about 3-8 µs.

2.3.2 Light source – optical fiber

The light from the high power LEDs is guided into the sample by 14 m of a BFH optical fiber with 1000 µm diameter purchased from Thorlabs. Due to the direct switching of the LED by the spectrometer, a shutter in the light path as it is often described in the literature[11,12,14] can be omitted. As a result it is possible to bring the LED in direct contact with the end of the optical fiber, enabling much higher light intensities by avoiding loss due to the strongly diverging LED output or due to additional optics. The light emitting area of the LED is about the same size as the cross section of the optical fiber core. The silicone lens of the LED is cut off and so the optical active part of the LED is brought in even closer contact with the end of the fiber guaranteeing optimal coupling of the LED to the fiber. As LEDs we found the following models well suited for our application, but other are likely equally suitable: Cree XP-E, Nichia SMD, LUXEON Rebel LXML, LUXEON K2 LXK2.

2.3.3 Optical fiber - sample

The light guided by the optical fiber from the LEDs into the spectrometer has to illuminate the NMR sample in a way that the whole sample inside the measurement coils is illuminated efficiently and uniformly.

For this the claddings of the optical fiber tip were stripped off, the main part of the fiber was masked and the 21 mm at the tip of the fiber were sandblasted to roughen its surface and thus make it emit light over this whole range instead of just from its tip. Siliciumcarbid 180

was used as the abrasive mineral. Figure 2.2 a and b show the light emission of the untreated fiber compared to the light emission of the roughened fiber. Whereas the untreated fiber emits light in a cone-shaped manner just from its tip, the roughened fiber emits light over the whole roughened area. Roughening the optical fiber is a remarkable easy, fast and hazard-free method to treat the tip of the optical fiber compared to other reported techniques as the etching with hydrofluoric acid.[13]

Optimal and uniform illumination of the NMR sample in the measuring coils of the spectrometer is ensured by aligning the light emitting area of the fiber to the coils, schematically shown in Figure 2.2 c. For this the optical fiber is inserted in a standard Rototec-Spintec stem coaxial insert which is retained in a Rototec-Spintec 5 mm NMR-Tube 7 inch 535-PP-7 similar as in the setup presented by Scheffler *et al.*.[14] The coaxial insert centers the optical fiber in the NMR tube and the shim coils. Moreover the insert prevents direct contact of the fiber with the sample and thus makes it very easy to handle.

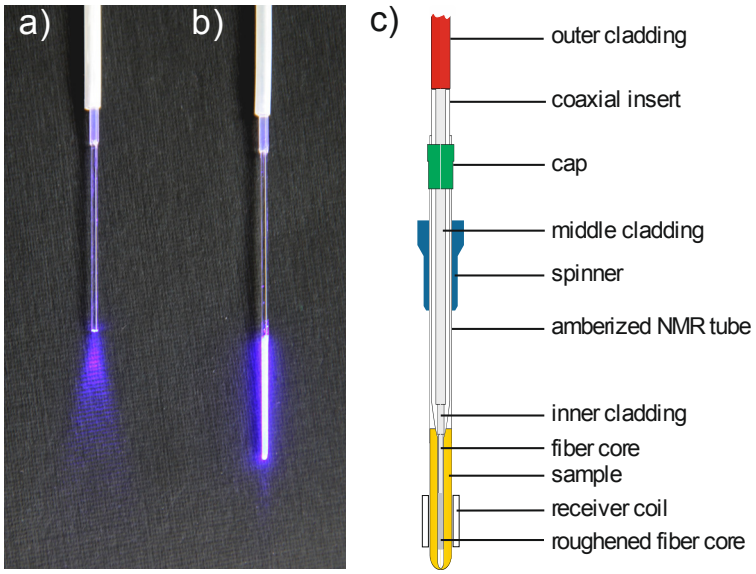

Figure 2.2 (a) Picture of an untreated fiber tip emitting light from just its tip in a cone- shaped manner. (b) Picture of the roughened fiber tip emitting light uniformly over the whole roughened range. (c) Scheme of the optical fiber inserted in a coaxial inlet inside the NMR tube. To guarantee uniform illumination along the z-axis the tip of the fiber is roughened over the whole range of the receiver coil.

Optimal and uniform illumination of the NMR sample in the measuring coils of the spectrometer is ensured by aligning the light emitting area of the fiber to the coils, schematically shown in Figure 2.2 c. For this the optical fiber is inserted in a standard Rototec-Spintec stem coaxial insert which is retained in a Rototec-Spintec 5 mm NMR-Tube 7 inch 535-PP-7 similar as in the setup presented by Scheffler *et al.*.[14] The coaxial insert centers the optical fiber in the NMR tube and the shim coils. Moreover the insert prevents direct contact of the fiber with the sample and thus makes it very easy to handle.

2.3.4 Sample preparation - measurement

With the described setup all photochemical reactions tested so far can be followed by NMR spectroscopy. In addition, with this setup the identical light sources can be used for synthetic applications and NMR investigations allowing for direct comparisons. No deviations in the

products, reactivities, yields or trends found by the synthetically working chemists were found in the reactions tested so far, like in the flavin catalyzed photo oxidations,[24-26] the arylation of heteroarenes with diazonium salts,[27] the photocatalytic coupling of N-arylamines with nucleophiles[28,29] or in spiropyran photochromism.[30]

The most demanding test for the scope and limitations of LEDs used for the illumination of NMR samples and connected mechanistic studies are Photo-CIDNP and especially time resolved Photo-CIDNP experiments, because there, short light pulses of high intensities are required.[12] The intensity of the CIDNP signals is directly proportional to the photochemical turnover.[12] Therefore the intensity of a Photo-CIDNP signal is used as a direct measure for the amount of light brought into the NMR sample and to test the effect of the three innovations.

As a test reaction the flavin catalyzed photo oxidation of benzyl alcohols to the corresponding aldehydes was used.[24-26,31] The reduced flavin is reoxidized by oxygen. Flavins in general are a common model system for CIDNP studies, because falvin radicals have suitable magnetic properties and are prone to show CIDNP-signals. For this reason flavins are often employed as photosensitizers for CIDNP-studies on proteins.[11,32]

For the measurements 2 mM riboflavin tetra acetate (RFT) and 20 mM methoxybenzyl alcohol (MBA) were dissolved in CD_3CN and the sample was purged with argon for 1 h. NMR spectra were recorded on a Bruker Avance 600 spectrometer with a 5 mm broadband triple resonance z-gradient probe. The temperature of 300 K was controlled by a Bruker BVTE 3000 unit. As a light source a Cree XP-E high power LED with a center wavelength of 455 nm and 500 mW optical output power was used, according to the absorption maximum of RFT.[26] To determine the current through the LED the voltage on a resistance in series with the LED was measured. As a measure for the light intensity in the sample the Photo-CIDNP signal intensity of the aromatic proton of RFT at 7.89 ppm was chosen (Figure 2.3 a) because this proton shows a well baseline separated and emissive Photo-CIDNP signal. The CIDNP-spectra were taken as the difference spectra between the ^1H spectra of the illuminated sample and the dark sample.

2.4 Results and Discussion

In the following the three innovations for the *in situ* illumination of NMR samples are tested. This was done by measuring the Photo-CIDNP polarization of the flavin aromatic proton with altered setups. First, the new easy and efficient way to roughen the fiber tip and thus to improve illumination uniformity over the whole sample is tested. Second, the effective coupling of the LED with the optical fiber possible through the direct switching of the LED by the spectrometer was investigated. Third, the pulsed operation of the LEDs to achieve higher short time powers was tested.

The effect of the roughened fiber tip was tested by measuring the Photo-CIDNP polarization of the flavin aromatic proton. For that the light ^1H spectra were measured with a 30° rf pulse and 16 scans, while illuminating the sample with a constant LED current of 1 A and with the LED directly coupled to the optical fiber. Alternating dark ^1H spectra with a 30° rf pulse and 16 scans were measured and subtracted from the illuminated spectra to yield the Photo-CIDNP spectra.

The ^{1}H spectra with maximum CIDNP-intensity are shown in Figure 2.3 b. With the setup the difference in the CIDNP intensities between the two tips of the optical fiber is pleasantly large. Using the roughened fiber instead of the untreated one the maximal CIDNP polarization was increased by a factor of about 3. These results are due to the improved uniform illumination by the roughened tip. The untreated fiber emits light in a cone-shaped manner just from its tip, whereas the roughened fiber emits light over the whole roughened range (see Figure 2.3 a and b).

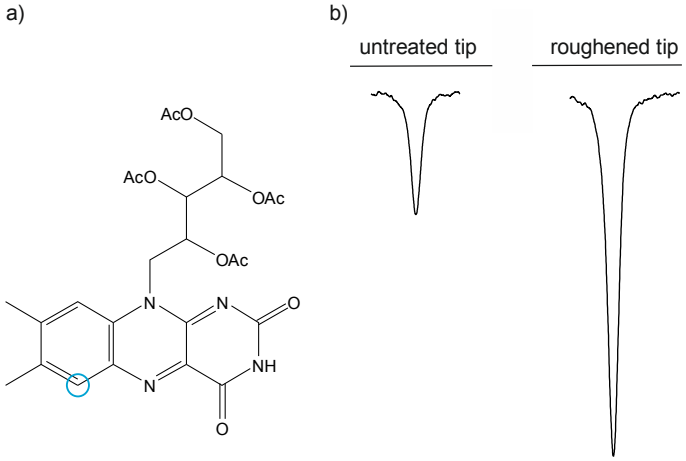

Figure 2.3 (a) Structure of riboflavin tetraacetate. The emissive Photo-CIDNP signal of the encircled aromatic proton appearing at a chemical shift of 7.89 ppm was observed for the Photo-CIDNP experiments. (b) ^{1}H Photo-CIDNP intensities of the aromatic RFT proton for the concentration of 2 mM RFT and 20 mM MBA in acetonitrile, measured with the untreated tip (left) and the roughened tip of the optical fiber (right).

So as a first achievement, roughening the optical fiber by sand blasting is a remarkable easy, fast and hazard-free method to treat the tip and make it emit light over the whole area of the receiver coil in a very efficient and uniform manner.

Next the effect of an optimized coupling of the glass fiber with the LEDs was tested. For that purpose (a) a setup leaving 0.5 cm space for a shutter, (b) a setup with direct attachment of the glass fiber to the LED and (c) a setup with direct attachment of the LED with a cut off silicone lens to the optical fiber were compared, see Figure 2.4. For that the Photo-CIDNP polarization of the aromatic proton of RFT are used as the difference spectra of illuminated and dark ^{1}H spectra with a 30° rf pulse and 16 scans each and illumination during the whole measurement. The reduction of the distance between diode and the end of the fiber core leads to a huge increase in light power and thus CIDNP polarization. The setup without the need of a shutter in the light path increases the signal intensity by a factor of about 20 (Figure 2.4 B). Further reduction of the distance between diode and fiber core by cutting off the LED silicone lens leads to a further increase in light intensity and CIDNP polarization (Figure 2.4 C). In total the signal intensity is increased by a factor of about 30 compared to the setup with space for a shutter. The output power of the optical fiber coupled in the described way was measured to be about 50 mW.

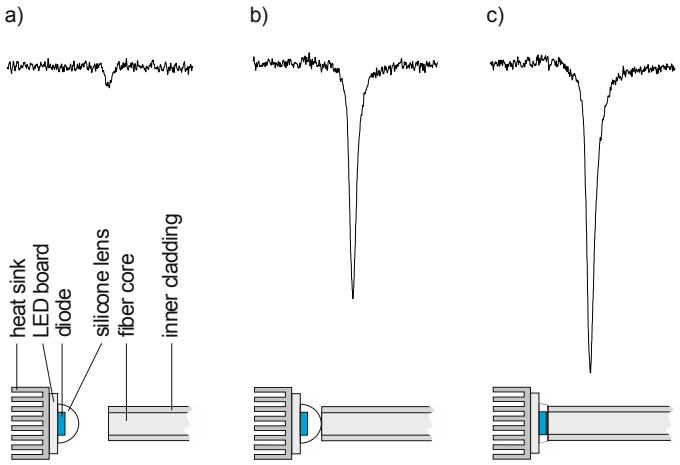

Figure 2.4 (a) Setup with 0.5 cm space for a shutter between the optical fiber and the LED and the corresponding Photo-CIDNP signal of the aromatic proton of RFT. (b) Setup with the LED in direct contact with the optical fiber and the effect on the Photo-CIDNP signal. (c) Setup with the silicone lens of the LED cut off and direct contact to the optical fiber and the effect on the Photo-CIDNP signal.

The described setup provides an extraordinary easy and efficient way to couple the LEDs to the optical fiber without the need of specially designed and cumbersome optics.

Finally the gain in CIDNP-intensity and thus in light intensity by the pulsed operation of the LEDs was investigated. For this purpose the sample was illuminated by a short light pulse of only 1 ms length after a relaxation delay D1 of 120 s. The relaxation delay ensures the complete relaxation of all polarization and a sufficiently low duty cycle of the LED. The light pulse was directly followed by a 30° rf pulse on the proton channel and acquisition. Then the same pulse sequence was applied without the light pulse to record the dark spectrum which was then subtracted from the light spectrum to yield the Photo-CIDNP spectrum. Both the light and the dark spectrum were recorded with one single scan only. In this way five different Photo-CIDNP spectra were acquired with rising currents through the LED. Starting with the manufacturer recommended maximum current of 1 A the current was raised in steps of 2 A up to 9 A. Figure 2.5 shows the Photo-CIDNP intensity in dependence on the current through the LED. At a current of 1 A no Photo-CIDNP signal is detectable for the aromatic proton of RFT. A detectable signal with low signal to noise ratio appears at 3 A. Further increase of the current strongly enhances the Photo-CIDNP signal. Figure 2.5 b reveals that the increase of the Photo-CIDNP signal is proportional to the LED current which results in an increase of the signal by a factor of about 9 for the presented measurements. The LED used for the tests broke down at currents higher than 9 A. With shorter light pulses, with other LEDs or with additional cooling of the LEDs a further increase of the light intensities and thus the Photo-CIDNP signals can be expected. This shows that the pulsed operation of the LEDs enables light intensities much higher than at standard operation. Through these high light intensities Photo-CIDNP signals can be enhanced tremendously and otherwise not detectable signals become detectable even at the millisecond time scale. This paves the way to millisecond time resolved Photo-CIDNP spectroscopy even with this comparativly simple setup.

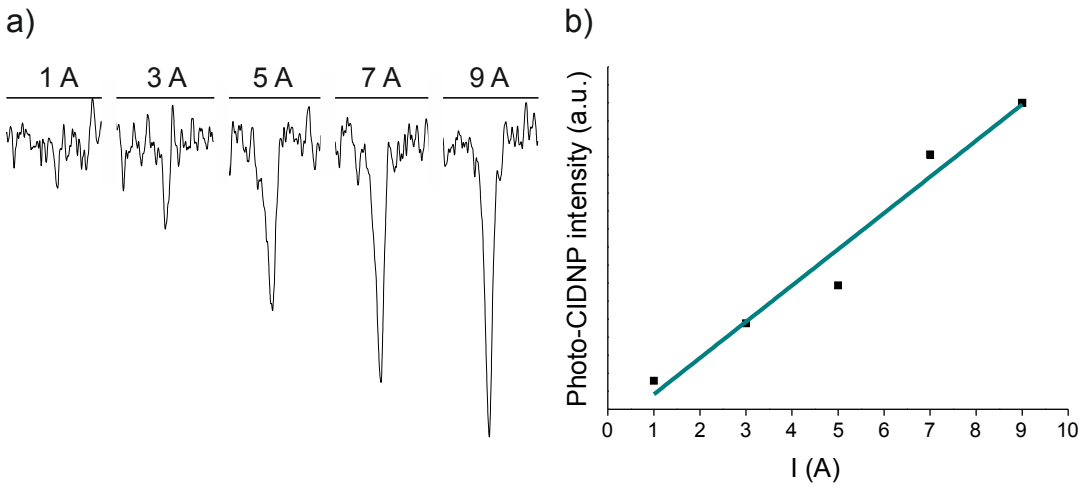

Figure 2.5: (a) The Photo-CIDNP signal of the RFT aromatic proton for light pulses of 1 ms length and for LED currents of 1 A (maximum current for continuous operation) up to 9 A. (b) The Photo-CIDNP intensity shows a linear dependency on the current through the LED.

2.5 Conclusions

Despite the clear benefits of LEDs compared to other light sources, such as easy handling, low cost, availability in a huge variety of wavelengths and direct comparability with conditions in synthetic chemistry LEDs have not been used as light sources for the systematic illumination of a NMR sample yet. Here an innovative LED based device for the *in situ* illumination of NMR samples is presented. The combination of an efficient coupling of the LEDs to the optical fiber, a specially prepared fiber tip and the high power pulsed operation of the LEDs allows for tremendous increases in the amount of light brought into the NMR sample. The LEDs are directly switched by the NMR spectrometer. This allows for continuous LED operation at standard currents and for pulsed LED operation at much higher currents. By using the LEDs in continuous operation the whole variety of NMR methods can be applied directly to photochemical reactions and the use of LEDs provides direct comparability with conditions in synthetic chemistry. Pulsed operation of the LEDs allows for currents and light intensities well above the maximal currents of continuous operation. This makes time resolved Photo-CIDNP spectroscopy on a millisecond time scale possible even with this simple setup.

Switching the LED directly by the spectrometer makes a shutter that is commonly used to control the illumination redundant. Therefore the light emitting area of the LED can be brought in direct contact with the end of the optical fiber guiding the light from the LED into the NMR sample. This provides a remarkably easy, versatile and efficient coupling without the need of any further optical components.

To provide uniform and efficient illumination of the whole NMR sample along the measuring coils the tip of the optical fiber inserted in the sample was roughened by sand blasting which is an extraordinarily fast, simple and hazard-free preparation method.

2.6 Additional Findings

2.6.1 Specification of the LEDs

For the illumination setup described above a variety of different LEDs was tested, see Figure 2.6. The application of LEDs offered many advantages, as they are inexpensive, easy to handle in comparison to laser systems and commercially available in a broad spectrum of emission wavelength, ranging from ultraviolet to infrared. However, the application of UV LEDs is limited, as the transmission of the optical fiber (Thorlabs BFH48-1000), between 99.9% and 99% in the visible range, drastically decreases for wavelength below 400 nm. Thus, the shortest wavelength applied to this setup was 367 nm.

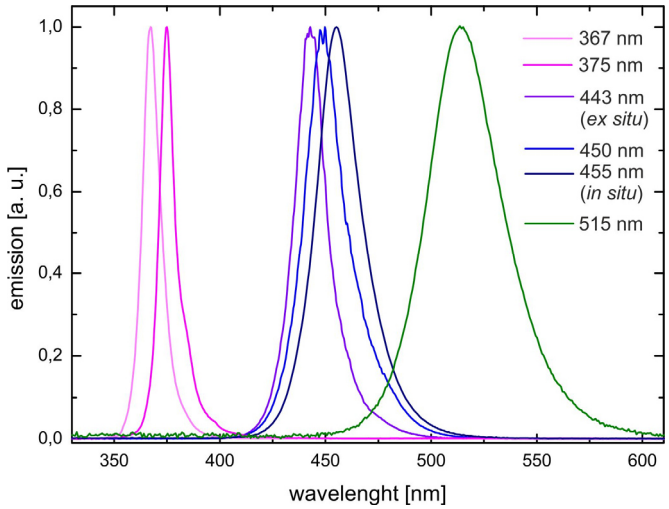

Figure 2.6 Emission spectra of the LEDs applied to the optical fiber. The intensities are normed.

The LEDs shown in Figure 2.6 are: 367 nm (Nichia SMD LED UV NCSU033B, 325 mW); 375 (Conrad P8D237, 230 mW) 443 nm (Osram Oson SSL 80, royal blue, 700 mA), 450 and 455 nm (Cree XP-E, royal blue, 700 mA); 515 nm (Luxeon K2 LXK2-PM14-U00, 130 lm, 100 mA). Additionally a white LED has been applied (Seoul Z-LED P4, 240 lm, spectrum not shown).

2.7 References

[1] M. B. Schmid, K. Zeitler, R. M. Gschwind, *Angew. Chemie - Int. Ed*. **2010**, *49*, 4997–5003.

[2] A. Berkessel, S. Elfert, V.R. Yatham, J. M. Neudörfl, N. E. Schlörer, J. H. Teles, *Angew. Chemie - Int. Ed*. **2012**, *51*, 12370–12374.

[3] B. Böttcher, V. Schmidts, J. A. Raskatov, C. M. Thiele, *Angew. Chemie - Int. Ed*. **2010**, *49*, 205–209.

[4] M. Fleischmann, D. Drettwan, E. Sugiono, M. Rueping, R. M. Gschwind, *Angew. Chemie - Int. Ed*. **2011**, *50*, 6364–6369.

[5] G. E. Ball, *in Spectrosc. Prop.* Inorg. Organomet. Compd. Tech. Mater. Appl., The Royal Society of Chemistry, London, **2010**, pp. 262–287.

[6] T. Kühn, H. Schwalbe, *J. Am. Chem. Soc.* **2000**, *122*, 6169–6174.

[7] J. Wirmer, T. Kühn, H. Schwalbe, *Angew. Chemie - Int. Ed*. **2001**, *40*, 4248–4251.

[8] H. R. Ward, R. G. Lawler, *J. Am. Chem. Soc*. **1967**, *89*, 5518–5519.

[9] J. Bargon, H. Fischer*, Zeitschrift für Naturforsch*. **1967**, *A22*, 1556–1562.

[10] J. Bargon, H. Fischer, *Zeitschrift für Naturforsch*. **1967**, *A22*, 1551–1555.

[11] P. J. Hore, *Prog. NMR Spectrosc*. **1993**, *25*, 345–402.

[12] M. Goez, *in Annu. Reports NMR Spectrosc*. Vol 66 (Ed.: G.A. Webb), Academic Press, **2009**, pp. 77–147.

[13] I. Kuprov, P.J. Hore, *J. Magn. Reson*. **2004**, *171*, 171–175.

[14] J. E. Scheffler, C. E. Cottrell, L. J. Berliner, *J. Magn. Reson*. **1985**, *63*, 199–201.

[15] I. Kuprov, M. Goez, P. A. Abbott, P. J. Hore, *Rev. Sci. Instrum*. **2005**, *76*, 84103.

[16] J. W. Tucker, Y. Zhang, T. F. Jamison, C. R. J. Stephenson, *Angew. Chemie - Int. Ed*. **2012**, *51*, 4144–4147.

[17] M. Cherevatskaya, M. Neumann, S. Füldner, C. Harlander, S. Kümmel, S. Dankesreiter, A. Pfitzner, K. Zeitler, B. König, *Angew. Chemie - Int. Ed*. **2012**, *51*, 4062–4066.

[18] R. Lechner, S. Kümmel, B. König*, Photochem. Photobiol. Sci*. **2010**, *9*, 1367–1377.

[19] M. Neumann, S. Füldner, B. König, K. Zeitler, *Angew. Chemie - Int. Ed*. **2011**, *50*, 951–954.

[20] U. Megerle, R. Lechner, B. König, E. Riedle, *Photochem. Photobiol. Sci*. **2010**, *9*, 1400–1406.

[21] C. Willert, B. Stasicki, J. Klinner, S. Moessner, *Meas. Sci. Technol*. **2010**, *21*, 075402 (11pp).

[22] W. Hiller, H. M. Lent, G. E. A. Meier, B. Stasicki, *Exp. Fluids* **1987**, *5*, 141–144.

[23] U. Schmidhammer, S. Roth, E. Riedle, A. A. Tishkov, H. Mayr, *Rev. Sci. Instrum*. **2005**, *76*, 093111.

[24] H. Schmaderer, P. Hilgers, R. Lechner, B. König, *Adv. Synth. Catal*. **2009**, *351*, 163–174.

[25] J. Svoboda, H. Schmaderer, B. König, *Chem. - A Eur. J*. **2008**, *14*, 1854–1865.

[26] U. Megerle, M. Wenninger, R.-J. Kutta, R. Lechner, B. König, B. Dick, E. Riedle, *Phys. Chem. Chem. Phys*. **2011**, *13*, 8869–8880.

[27] D. P. Hari, P. Schroll, B. König, *J. Am. Chem. Soc*. **2012**, *134*, 2958–2961.

[28] D. P. Hari, B. Kӧnig, *Org. Lett.* **2011**, *13*, 3852–3855.

[29] A. G. Condie, J. C. González-Gómez, C. R. J. Stephenson, *J. Am. Chem. Soc*. **2010**, *132*, 1464–1465.

[30] B. S. Lukyanov, M. B. Lukyanova, *Chem. Heterocycl. Compd*. **2005**, *41*, 281–311.

[31] J. Daďová, S. Kümmel, C. Feldmeier, J. Cibulková, R. Pažout, J. Maixner, R. M. Gschwind, B. König, R. Cibulka, *Chem. – A Eur. J*. **2013**, *19*, 1066–1075.

[32] G. Richter, S. Weber, W. Römisch, A. Bacher, M. Fischer, W. Eisenreich, *J. Am. Chem. Soc*. **2005**, *127*, 17245–17252.

3 The Photocatalyzed Aza-Henry Reaction of *N*-Aryltetrahydroisoquinolines — Comprehensive Mechanism, $H^{\bullet}$- versus H^{+}-Abstraction and Background Reactions

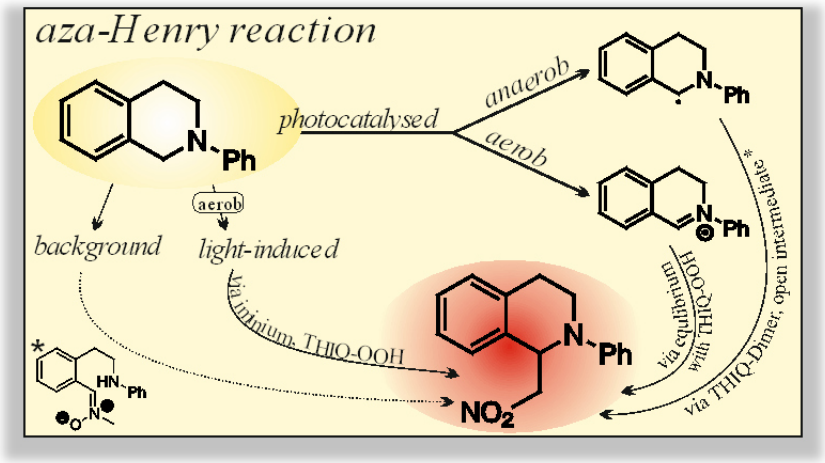

The study of the light-induced background reaction was in main parts performed by A. Eisenhofer. The study of the photocatalyzed reaction was in main parts performed by H. Bartling. Investigations on the dimer kinetic, the background reaction in the dark, the ESR and radical trapping experiments were planned and conducted with equal contributions.

A. Eisenhofer and H. Bartling contributed equally to this paper.

Hanna Bartling, Anna Eisenhofer, Burkhard König, Ruth M. Gschwind

submitted

3.1 Abstract

The cross-dehydrogenative coupling (CDC) reaction of *N*-aryltetrahydroisoquinolines (THIQ) is one of the most exploited photocatalytic transformation and a test reaction for an exceptional variety of catalysts. However, its mechanism remained unclear concerning involved intermediates, reactive pathways of the amine radical cation and the influence of oxygen and the light source. Therefore, NMR-, ESR- and synthetic methods were combined to provide a comprehensive picture of the reaction mechanism using $Ru(bpy)_3Cl_2$ as a photocatalyst under aerobic and anaerobic conditions. The reaction profiles and involved intermediates were monitored and analyzed by NMR spectroscopy. Several intermediates contributing to product formation were identified, the iminium ion, the hydroperoxide and dimer of THIQ, and a new ring opened intermediate, cleaved at the benzylic C-N bond. Mechanistic evidence is given that under anaerobic conditions preferentially the α-amino radical is formed by deprotonation, in contrast to the formation of iminium ions via H˙-abstraction in the presence of oxygen. Further, the light-induced background reaction in the absence of the catalyst was studied in detail, revealing that the product formation rate is correlated to the intensity and wavelength of the light source and that oxygen is essential for an efficient conversion. The reaction rate and efficiency is comparable to previously reported photocatalytic systems, performed under aerobic conditions in combination with intense blue light sources. Thus, the multitude of reaction parameters investigated reveals the preference for hydrogen atom or proton abstraction in photoreactions and allows to assess the influence of experimental conditions on the mechanistic pathways.

3.2 Introduction

The direct and efficient transformation of C-H groups into C-C bonds under mild reaction conditions is of high interest in organic synthesis.[1–3] In the last decade, visible-light photoredox catalysis developed into a powerful method for the activation of C-H bonds under mild conditions.[4–16] In this context, the visible light photocatalytic C-H functionalization of tertiary amines adjacent to nitrogen atoms became a valuable extension of transition-metal-catalyzed,[17] electrochemical[18–20] and DDQ-mediated reactions,[21–24] and for UV-light-induced photochemical approaches.[25–27] Since in 2010 Stephenson *et al.*[28] published an efficient concept for the visible-light mediated photocatalytic aza-Henry reaction of nitromethane with *N*-aryl-tetrahydroisoquinolines (THIQ) using air as terminal oxidant several synthetic applications emerged. [7,11,15,16] The aza-Henry reaction of THIQ represents one of the most exploited photocatalytic transformations and an exceptional variety of visible-light absorbing photocatalysts has been applied for the CDC of the THIQ substrate with nitromethane: metal complexes containing ruthenium,[29,30] iridium,[28,31] palladium,[32] platinum,[33] cobalt[34] or copper,[35] organic dyes,[36–43] and heterogeneous photocatalysts like TiO_2,[44] Cu_2O,[45] CdS,[46] or mpg-C_3N_4,[47] metal-organic frameworks,[48,49] or cross-linked polymers.[50–54]

Despite the plethora of different catalytic systems, a mechanistic overlap exists in the initial electron transfer step from the lone pair of the amine substrate to the photoexcited catalyst generating an amine radical cation.[55] Mechanistic evidence was given by early studies of Whitten *et al.* by luminescence quenching of the frequently used photocatalyst $Ru(bpy)_3Cl_2$ (tris(bipyridine) ruthenium(II)chloride hexahydrate) with triethylamine.[56,57] Recent spectroscopic investigations confirmed a reductive quenching of the photoexcited state of the respective catalyst by THIQ substrates for a series of catalytic systems described above.[28,37,38,58,59] In addition, Wu *et al.* could prove the existence of the THIQ $\mathbf{1}^{+\bullet}$ by transient absorption spectroscopy in combination with the spectroelectrochemical absorption spectrum of THIQ $\mathbf{1}^{+\bullet}$.[58,60]

The amine radical cation provides unique properties for the α-C-H functionalization. Compared with the neutral amine the bond dissociation energy and the pKa value[61] are reduced significantly, which opens different mechanistic pathways dependent on the reaction conditions (Scheme 3.1).[11,15]

Oxidative coupling reactions of tertiary amines are generally supposed to proceed via the electrophilic iminium ion, which is formed from the amino radical cation and can be intercepted by nucleophiles. The intermediacy of iminium ions was confirmed for transition-metal[62] and DDQ-catalyzed reactions,[22] as well as for photocatalyzed systems using $BrCCl_3$ as terminal oxidant.[29,63]

However, for the photocatalytic aza-Henry reaction mechanistic evidence is missing, if the iminium ion is directly formed via hydrogen atom abstraction from the amine radical cation or by deprotonation generating the α-amino radical followed by a subsequent electron transfer. Investigations of the influence of the terminal oxidant on those reaction pathways are lacking. Furthermore, the question remains, whether the iminium species **2** is the only intermediate, which contributes to the product formation or if other mechanistic pathways are operating. In some cases intermediates have been observed, but their role within the catalytic cycle remained unclear.[37,41] The existence of the α-amino radical of THIQ **7** was proven by Xiao and

Lu for the α-allylation of amines in a dual catalytic approach, by ESR spectroscopy.[64] Whitten *et al.* detected the respective α-amino radical of triethylamine with a spin trap by ESR spectroscopy.[57]

Scheme 3.1 Activation of tertiary amines by photoredox catalysis and amine radical cation modes of reactivity. Values for the bond dissociation energy (BDE) and oxidation potentials (vs. SCE) are given for triethylamine (R^1=-CH_3, R^2=R^3= -CH_2-CH_3). (SET = single electron transfer, BET = back electron transfer)[11,15,56,57,65–69]

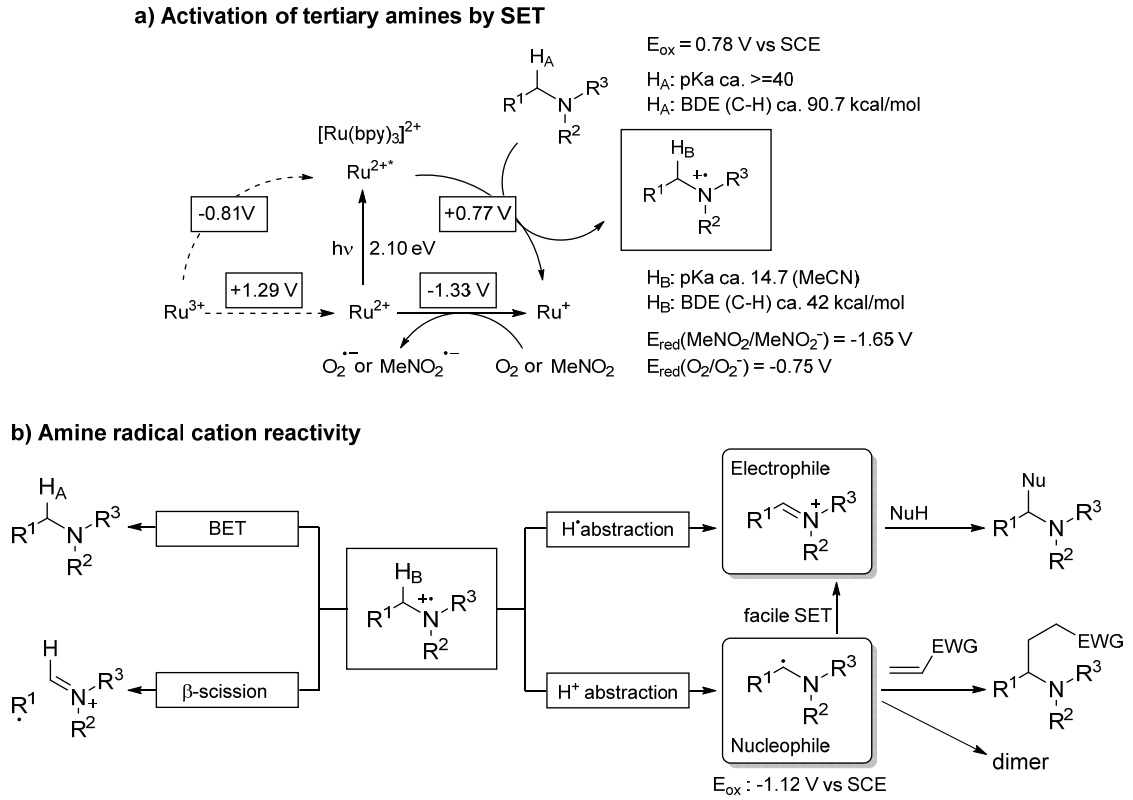

The question of reactive key intermediates and the active pathways remains also a topic of debate for the related transition-metal catalyzed reaction. Previous studies of Murahashi, Li, Che, Klussmann and Doyle led to divergent mechanistic models.[70] Mechanistic studies of Klussmann *et al.* demonstrated that varying the oxidant/catalyst pair from $CuCl_2 \cdot 2H_2O/O_2$ to CuBr/*tert*-butyl hydroperoxide (TBHP) in the oxidative coupling of THIQ **1** lead to major changes in the catalytic cycle (Scheme 3.2).[71–73] For $CuCl_2 \cdot 2H_2O/O_2$ the iminium ion **2a** was found as the key intermediate, which originate from a direct oxidation of THIQ **1** by the Cu-catalyst. The role of oxygen was limited to the reoxidation of the catalyst. The solvent methanol stabilized the iminium ion **2a** by formation of stable reservoirs in an off-cycle equilibrium,[74] which provides the active iminium species **2a** in a controlled fashion. The roles of the oxidant and the catalyst change for the CuBr/TBHP system. CuBr converts TBHP in a Kharasch type reaction to the *tert*-butyl peroxy radical and the respective *tert*-butyloxy radical, which activates THIQ **1** by a hydrogen atom transfer (HAT). Radical recombination formed the THIQ peroxy species **8** as a true intermediate, which is converted to the iminium ion **2b** assisted by CuBr acting as a Lewis acid.

In light of transition metal-catalyzed studies the question arises, if in the photocatalyzed system similar off-cycle equilibria are operative and to what extent the terminal oxidant influ-

ences the mechanism. Notwithstanding the variety of elaborated spectroscopic and mechanistic studies, that have been performed under different conditions – all dealing with photocatalyzed CDC reactions of *N*-arylamines and with the aza-Henry reaction in particular – to the best of our knowledge no comprehensive study regarding the pathways of the amine radical cation and involved intermediate species with respect to the terminal oxidant of the photocatalyzed reaction of THIQ **1** with nitromethane **5a** has been reported so far.

Scheme 3.2 Mechanistic proposals of Klussmann *et al.* for the Cu-catalyzed oxidative coupling of THIQ **1** using oxygen or *tert*-butyl hydroperoxide (TBHP) as oxidant.[71–73]

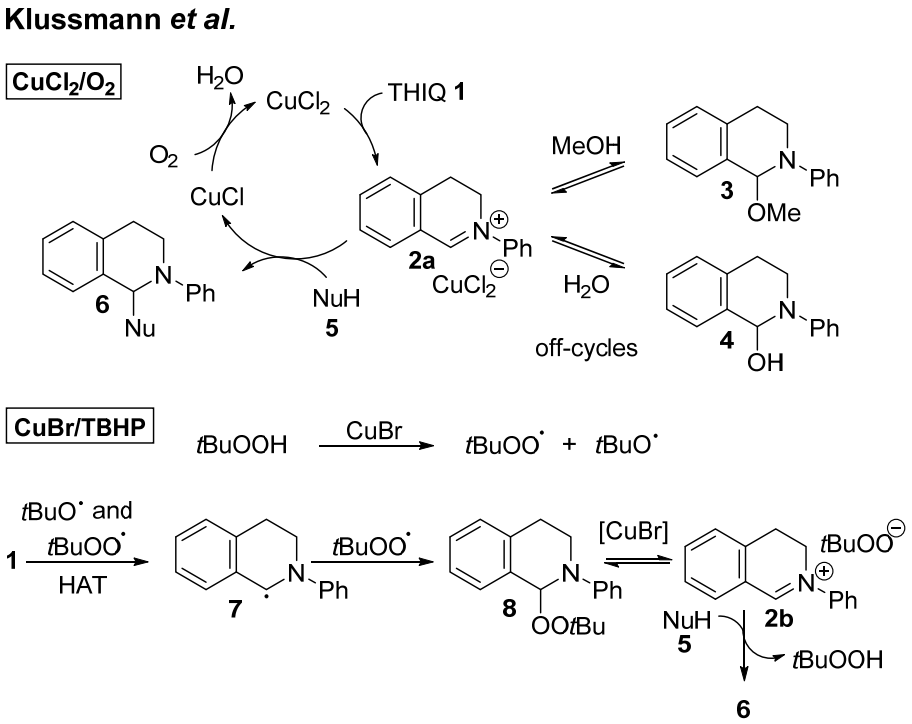

In light of transition metal-catalyzed studies the question arises, if in the photocatalyzed system similar off-cycle equilibria are operative and to what extent the terminal oxidant influences the mechanism. Notwithstanding the variety of elaborated spectroscopic and mechanistic studies, that have been performed under different conditions – all dealing with photocatalyzed CDC reactions of *N*-arylamines and with the aza-Henry reaction in particular – to the best of our knowledge no comprehensive study regarding the pathways of the amine radical cation and involved intermediate species with respect to the terminal oxidant of the photocatalyzed reaction of THIQ **1** with nitromethane **5a** has been reported so far.

Herein, we present our mechanistic study of the CDC reaction of THIQ with nitromethane investigating the reaction profiles, (elusive) intermediates and the necessity of the photocatalyst, together with the role of oxygen and light in different reaction setups by NMR and ESR spectroscopy. Furthermore, the role of the reaction intermediates within the catalytic cycle is discussed and background reactions are investigated. Based on our results we divided the reaction into different pathways, which are presented in detail.

3.3 Results and Discussion

In order to elucidate the reactive pathway ($H^{\bullet}$- vs. H^{+}-abstraction) of the photocatalytically generated amine radical cation and the involved intermediates dependent on the reaction conditions, we systematically studied different reaction parameters. The aza-Henry reaction stands out from the photocatalyzed CDC reactions as the nucleophile nitromethane itself is feasible of regenerating the catalyst and can act as a terminal oxidant albeit with a reduced reaction rate compared to oxygen. Thus, no external terminal oxidant is required (Scheme 3.1).[28,37,41] This enabled us to investigate the role of oxygen separately with respect to $H^{\bullet}$- vs. H^{+}- abstraction pathways. First, the influence of the terminal oxidant – in particular the presence or absence of oxygen – on the catalytic cycle and the correlation to involved intermediate species and the reaction profiles were investigated by NMR spectroscopy.

3.3.1 Setup

The control of the oxygen concentration was accomplished by a variation of the reaction setups, which are depicted schematically in Figure 3.1 and are referred to as *in situ* and *ex situ*. Almost anaerobic conditions were achieved with the *in situ* technique developed by Feldmeier *et al*.,[75] which allows the illumination of the sample with an LED inside the spectrometer. This setup provides a unique possibility monitoring reaction profiles as well as the detection and characterization of elusive intermediates and products of photochemical reactions. However, due to the conditions of the setup (closed system, no boundary layer to air, only diffusion) the corresponding aerobic sample cannot be monitored with this technique. Therefore, the aerobic sample was irradiated open to air outside of the spectrometer (*ex situ* strategy). While the reaction proceeded, aliquot samples were taken and the reaction profile was monitored by NMR spectroscopy.

3.3.2 Aerobic and Anaerobic Reaction Profiles

For both kinetics, THIQ **1** (200 mM) and 1 mol% of $Ru(bpy)_3Cl_2$ in deuterated nitromethane-d3 **5a** were irradiated with blue LEDs (for specification see section 3.5.3) at room temperature (Figure 3.1 a,b). The nucleophile nitromethane was used as solvent. The *in situ* experiment was repeated with 50 mM THIQ **1** and an increased catalyst loading of 10 mol% of $Ru(bpy)_3Cl_2$ (Figure 3.1 c). The intermediates THIQ dimer **9** and THIQ nitrone **10** showed the same profiles and relative intermediate ratios, but with 10 mol% of $Ru(bpy)_3Cl_2$ a reduced reaction time and an increased absolute amount of intermediates was observed (Figure 3.1 b,c). To facilitate the assignment and to reduce measurement time the following *in situ* experiments were conducted at these conditions.

Under anaerobic conditions (*in situ*), two main intermediates were observed, the dimerization product **9** of the THIQ substrate and a ring opened THIQ-nitrone **10** cleaved at the benzylic C-N bond (for NMR data and assignment see 3.5.6.6). The dimer **9** and the ring opened intermediate **10** could also be observed as intermediates for the aerobic sample, but the main intermediate constitutes the THIQ hydroperoxide **11**, reaching a maximum of 20%. All detected THIQ species showed maxima in their reaction profile under photocatalytic conditions, indicating their role as intermediate or as off-cycle resting state in the reaction mechanism.

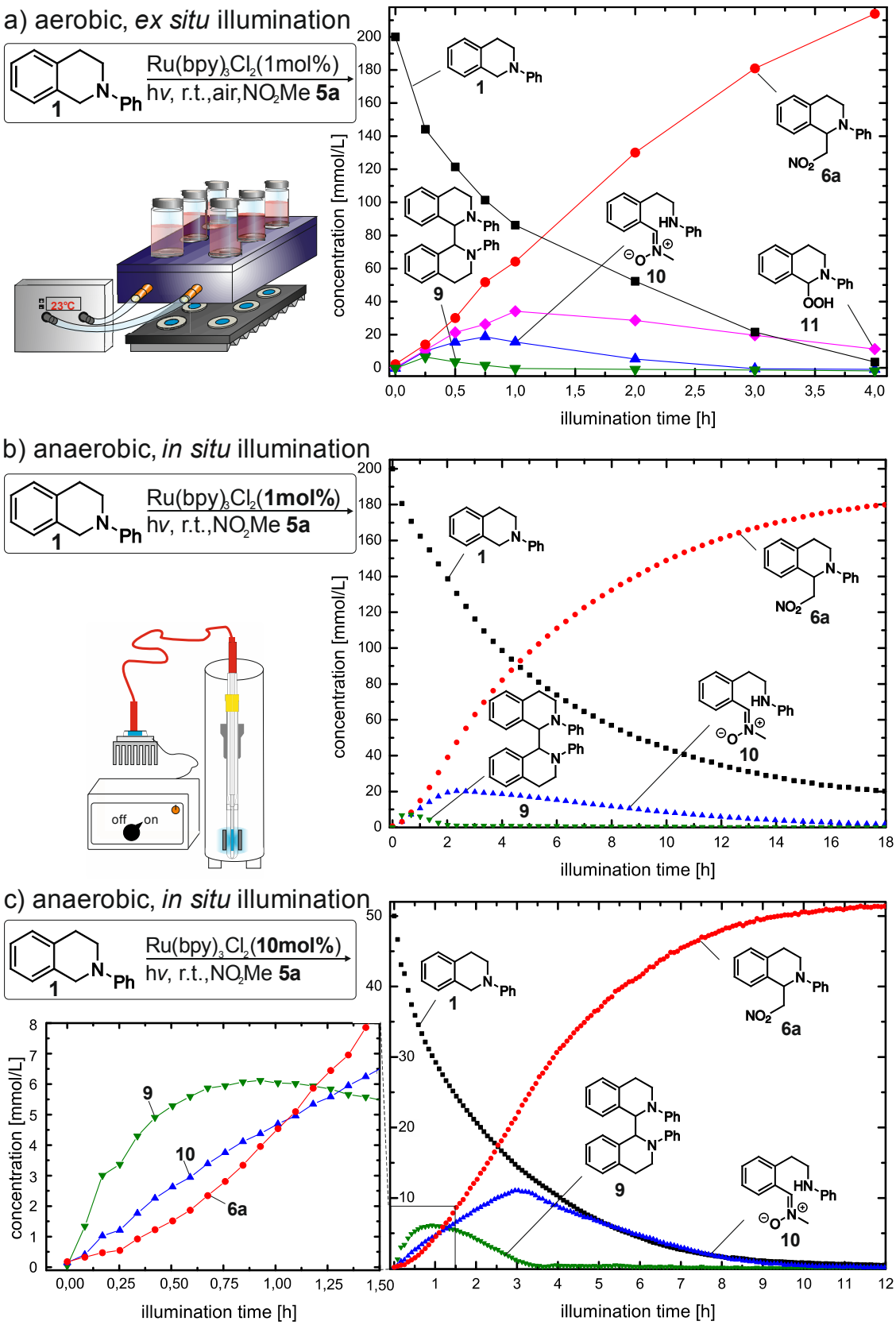

Figure 3.1 Reaction conditions, setups and ^{1}H NMR kinetics of the photocatalytic coupling reaction of THIQ **1** and nitromethane-d_3 **5a** shown for aerobic *ex situ* (a) and anaerobic *in situ* illumination with 1 mol% (b) and 10 mol% (c) catalyst loading.

The ^{1}H reaction profiles of the dimer **9** and ring opened intermediate **10** of the *ex situ* illuminated reaction basically follow the same pattern as the reaction under *in situ* conditions.

In the initial minutes of the *ex situ* and *in situ* reaction THIQ iminium ion **2**[76] was detected. In addition, traces of THIQ-OOH **11** were observed in the *in situ* ^{1}H NMR reaction profile due to residual oxygen. However, these species are not depicted in Figure 3.1 a-3.1 c because of concentrations below 2% and fast decrease within 30 minutes. For NMR spectra under *in situ* conditions showing all detected THIQ species, please refer to Figure 3.3 and Figure 3.13.

The aerobic reaction proceeds significantly faster, which is in agreement with literature reports.[28,37,41] After 3 h, 90% of product **6a** were obtained compared to 18 h of reaction time in the *in situ* system. This indicates that oxygen plays an important role in the reaction process, either by accelerating the efficiency of the catalyst turnover or by involvement in follow up reactions of the amine radical cation or by a combination of both.

THIQ starting material **1** decreased exponentially under aerobic and anaerobic conditions. While the product curve showed a linear increase for the aerobic (*ex situ*) experiment (for additional proof refer to Figure 3.16), a sigmoidal shape was obtained for the *in situ* measurement. The latter indicates the product formation from (transient) species, which are accumulated during the reaction. A possible explanation for this sigmoidal reaction progression would be the nitromethane nucleophile requiring activation to a tautomeric, but thermodynamically unfavorable aci-form for the nucleophilic attack.[77–81] Klussmann *et al*. reported increasing pH values with reaction progress.[72] Higher pH values result in an increased formation of the reactive deprotonated aci-form of nitromethane and finally lead to an increased product formation rate. This would be in good accordance with the observed sigmoidal curve of product formation. However, if the delayed product formation can exclusively be ascribed to the activation of nitromethane the aerobic and the dimer **9** kinetic (see Figure 3.2 c and text below) should also exhibit a sigmoidal shape. As for both of them a linear product formation rate was observed, we explain the disparity of the curves by different underlying reaction mechanisms.

3.3.3 Intermediate Formation Mechanisms

3.3.3.1 THIQ Dimer 9

The intermediate providing the first maximum during the course of the reaction is the dimerization product **9** of THIQ, which is commonly accepted to occur via a radical pathway by homocoupling of two amine radicals **7**.[82,83] König *et al.* developed a method for the radical homocoupling of THIQ on polycrystalline CdS.[46] The formation of the THIQ dimer **9** gives evidence, that the deprotonation pathway proceeds under aerobic and anaerobic conditions (see Scheme 3.1). This is remarkable as amino radicals are very strong reducing agent and are thus prone to oxidation. Even molecular oxygen ($E_{red}(O_2/O_2^{\cdot-})$ = -0.75 V vs. SCE)[68] is able to oxidize α-amino radicals ($E_{ox}(Et_2N^{-\cdot}CHCH_3/\ Et_2N^{+}{=}CHCH_3)$ = -1.12 V vs. SCE) thermodynamically.[66] Therefore, synthetic applications of the α-amino radical are conducted under inert atmosphere conditions e.g. the addition to electron-deficient alkenes.[82–84] However, Jiang and coworkers recently published a radical cascade reaction between the α-

amino radical of THIQ **7** and *N*-itaconimides under aerobic conditions, which is in line with our observations.[85–88]

3.3.3.2 THIQ-OOH 11

The elucidation of the mechanistic pathway for the formation of THIQ-OOH **11** is more challenging. The intermediate species THIQ-OOH **11** was anticipated by Wu *et al*., but no full characterization was provided.[37] The formation of the THIQ hydroperoxide species **11** requires an incorporation of oxygen. Based on the amine radical cation of THIQ $\mathbf{1}^{+\bullet}$ different mechanistic pathways are possible (see Scheme 3.3). As discussed above, the amine radical cation can undergo hydrogen atom abstraction or deprotonation. Superoxide radical anion $O_2^{\bullet-}$, which is formed after regeneration of the photocatalyst, can initiate both pathways as $O_2^{\bullet-}$ is reported in literature as H•- and H^+-acceptor.[68,89–98] The intermediate superoxide radical anion was confirmed by ESR spectroscopy after trapping with the radical probe DMPO (see section 3.5.11). The attributed role of the superoxide radical anion varies also within the suggested mechanism reported for the aza-Henry reaction.[28,37,99,100] The product of the H•-abstraction pathway is the iminium ion **2**, which can be intercepted by the generated OOH^- to form THIQ-OOH **11**. The hydroperoxide is in a pH-dependent equilibrium with the iminium species **2**, which was shown by Klussmann *et al.* for the THIQ-iminium **2b**/THIQ-*tert*-butyl hydroperoxide **8** couple (Scheme 3.2).[72] Nevertheless, also the amino radical **7**, formed via the deprotonation pathway, could deliver the respective amino peroxide **11** by a radical coupling with •OOH.[101] Furthermore, it is known that α-amino radicals **7** can react very fast with atmospheric molecular oxygen in an autoxidation type mechanism (see Scheme 3.3 and Scheme 3.9).[73,102–105] The formed oxygen centered peroxyl radical adduct **12** can provide the THIQ-OOH **11** in a chain propagation step together with another amino radical **7**.

Scheme 3.3 Possible pathways for the formation of THIQ hydroperoxide **11**.

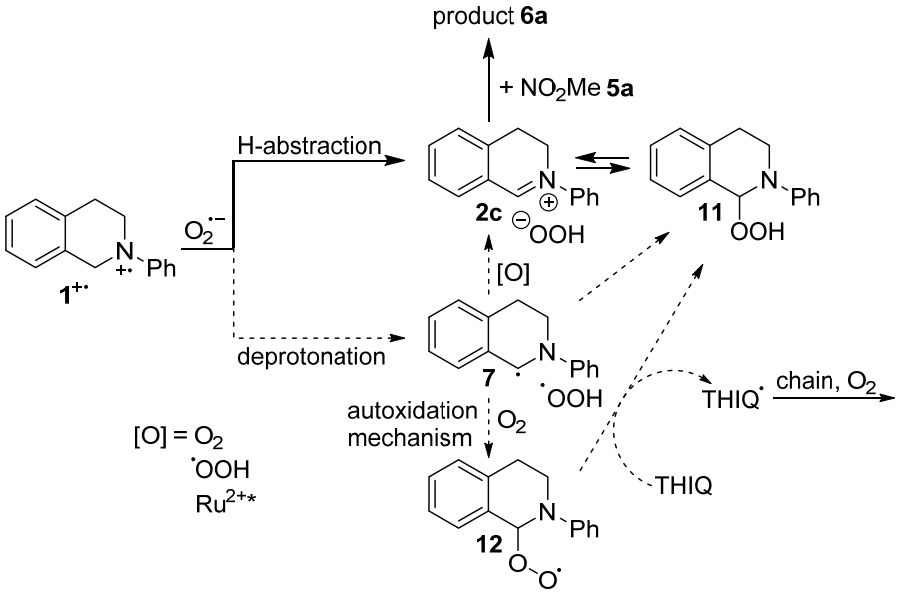

To probe if THIQ-OOH **11** is formed via the iminium **2** (H•-abstraction pathway) or the amino radical **7** (deprotonation pathway) the reaction profiles were investigated in the presence of the radical inhibitor TEMPO.

The addition of TEMPO slowed down the aerobic reaction (for details see 3.5.12). However, due to extensive line broadening – indicating the presence of radical species – no reliable reaction yields could be achieved. The reaction profiles elucidate that the formation of the dimer **9** and the nitrone **10** are completely suppressed, whereas the THIQ-OOH **11** could be observed throughout the kinetic, increasing within the first hour of the reaction (for details see Figure 3.27). This specific suppression of two intermediates strongly indicates that both the dimer **9** and the open intermediate **10** are formed via a radical pathway. The formation of THIQ-OOH intermediate **11** in the presence of TEMPO also corroborates the existence of an additional productive reaction pathway, not occurring via the amino radical **7**. Based on these results we propose that the superoxide radical anion acts preferentially as a hydrogen atom acceptor leading to iminium ion **2c**. This hydrogen abstraction pathway was later supported by the detection of both iminium ion **2** and THIQ-OOH **11** in the photocatalyst free studies (see Effective Background Reaction with Light and Figure 3.5). We further suggest that THIQ hydroperoxide **11** is formed in an off-cycle equilibrium from the iminium ion **2c** (Scheme 3.3, bold line).

3.3.3.3 Ring opened Intermediate 10

The intermediate **10** is detected for the first time and only one previous publication anticipated a C-N cleavage within the route to product formation.[69] The mechanistic evidence for radical species involved in the formation of the ring opened intermediate **10** under aerobic conditions (see above) was corroborated by the addition of TEMPO under anaerobic conditions. Again, the reaction was slowed down and the formation of the dimer **9** and the open intermediate **10** were completely suppressed. Based on this observation in conjunction with the product structure determined by NMR (see 3.5.6.6) we propose a radical coupling between the α-amino radical **7** and a hydroxylamine radical **13** (Scheme 3.4). The formation of the hydroxylamine radical **13** is reported for a stepwise reduction of nitromethane by metal catalysts[106], electrochemically[107] or via dissociation or disproportionation of nitromethane.[108] Here, the electrons come from the reoxidation of the photocatalyst (see Scheme 3.1 a). The initial strong formation of dimer **9** (see Figure 3.1 c) supports this mechanistic proposal, since three electrons are required for the formation of one hydroxylamine radical **13.** Furthermore, we assume that the ring opened intermediate **10** is in a pH-dependent equilibrium with the reactive iminium species **2** and thus constitutes a true, productive intermediate (Scheme 3.5). This assumption is supported by a formation of *N*-methylhydroxylamine **14**, which was detected in the NMR spectra with progressing reaction (Scheme 3.5 and section 3.5.6.7).[109]

Scheme 3.4 Proposed radical mechanism for the formation of the ring opened intermediate **10**.

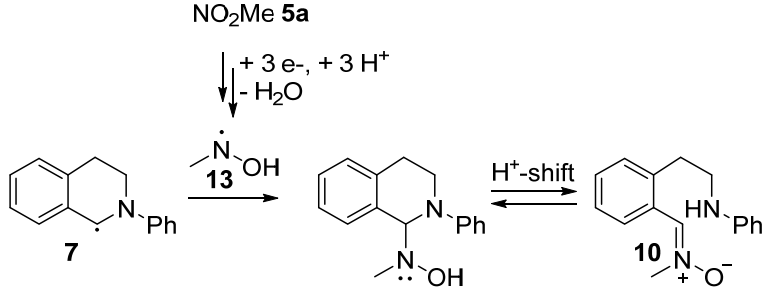

Scheme 3.5 Proposed reaction mechanism for the formation of the coupling product **6a** and *N*-methylhydroxylamine **14** from the ring opened intermediate **10**.

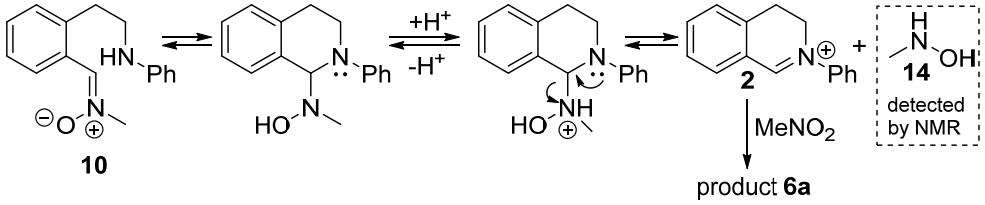

3.3.4 Light On-Off Studies and Identification of Productive Intermediates

The role of the intermediates was further investigated by light on-off studies to address the question which intermediates are directly involved in the product formation and the influence of light for the transformation. Therefore, the intermediates were accumulated during an irradiation period (*in situ* and *ex situ*) followed by the measurement of the NMR reaction profiles in the dark (see Figure 3.2 a,b). The reaction kinetic of the dark period for the *in situ* (anaerobe) light on-off study showed that the ring opened intermediate **10** is a direct precursor of the aza-Henry product **6a**. Even in the dark, the gradient of the product **6a** formation remains unchanged, as long as the intermediate **10** is present. After the intermediate **10** is fully consumed the rate of the product formation drops to zero. In contrast, the concentration of the dimer **9** is constant in the dark (Figure 3.2 a).

The light on-off studies of the externally irradiated aerobic system (see Figure 3.2 b) are in accordance with the *in situ* observation considering the behavior of the ring opened intermediate **10** and the dimer **9** in the dark. In addition, the hydroperoxide species **11** also contributes to the product formation in the absence of light. This is in agreement with Klussmann *et al.*; they observed a similar trend for the conversion of THIQ-OO^{t}Bu **8** to the product in the absence of the respective metal catalyst albeit with a reduced rate. This was explained by a Lewis acid activation by the CuBr catalyst (Scheme 3.2).[72] The accumulation of intermediates, which can be converted to the product in the dark is in line with the report of Wu *et al.* for the TBA-eosin Y catalyzed reaction of THIQ and nitromethane. They observed an increase in yield of the aza-Henry product from 75% to 92% when they continued stirring for 12 h in the dark after irradiation for 4 h. They assumed the intermediacy of THIQ-OOH **11**, but no structural proof was given.[37]

In both systems, the concentration of dimer **9** remains unchanged in the dark (see Figure 3.2 a and 3.2 b). However, the kinetic profile showed a reversible behavior under photocatalytic conditions without decomposition as the mass balance is almost 100% (see Figure 3.1 c).

This observation incited us to investigate the influence of light on the reversibility of the dimer **9** formation. For that reason, the dimer **9** was prepared according to a literature-known procedure[46] and subjected to *in situ* NMR measurements. The illumination of dimer **9** in nitromethane-d_3 **5a** only led to a slow product formation in the absence of the catalyst (see Figure 3.2 c). The addition of $Ru(bpy)_3Cl_2$ (10 mol%) to the reaction mixture drastically increased the reaction rate and gave 80% of product **6a** after 2 h. The ring opened intermediate **10** was detected, but its formation was considerably delayed with respect to the product **6a** formation and only a maximum amount of 10% was reached (see Figure 3.2 c). Based on the results we assume that the amino radical cation of the dimer $\mathbf{9}^{+\bullet}$ is generated by an electron

transfer to the catalyst, which can undergo homolytic C-C bond cleavage resulting in a α-amino radical **7** and the iminium ion **2** (Scheme 3.6).[110–112]

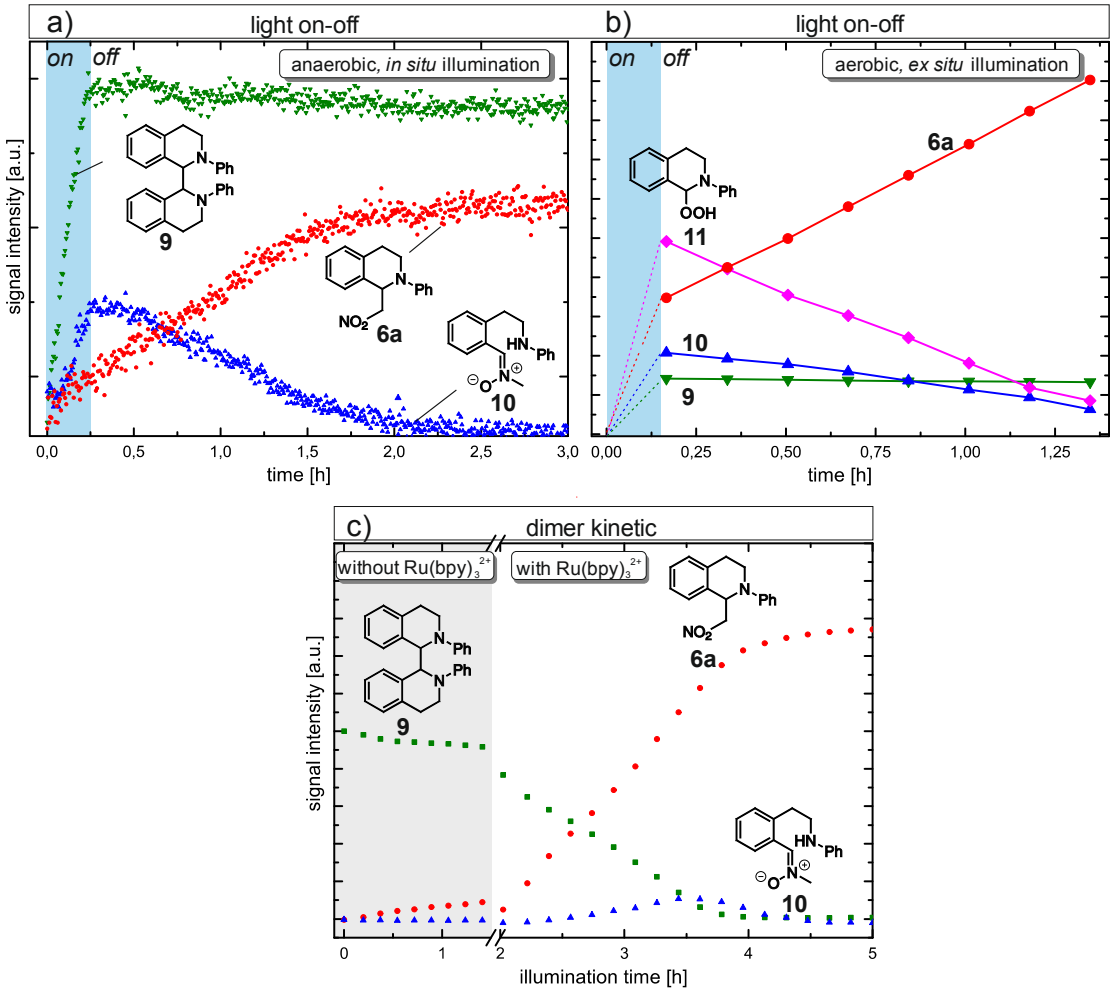

Figure 3.2 Product **6a** formation from intermediates **10** and **11** in the dark (a,b) and light and photocatalyst dependent product **6a** formation from THIQ dimer **9** (c). The ^{1}H NMR reaction profiles of the photocatalyzed CDC reaction of THIQ **1** and nitromethane **5a**, irradiated for 15 minutes (a) anaerob or (b) aerob were monitored regarding their contribution to the product formation **6a** in the dark. (c) ^{1}H NMR kinetic of THIQ dimer **9** and nitromethane **5a** under continuous illumination with blue LEDs at 300 K in the absence and presence of $Ru(bpy)_3Cl_2$ as photocatalyst.

Scheme 3.6 Proposed mechanism for the photocatalytic C-C cleavage of dimer **9**.

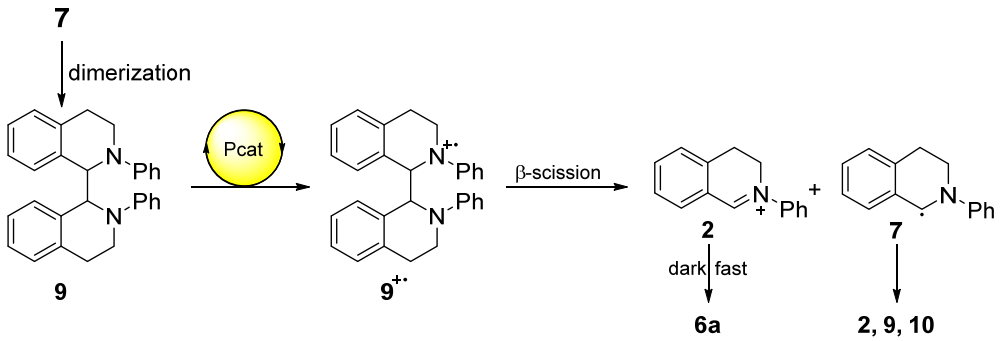

Remarkably, in contrast to the *in situ* kinetic no sigmoidal product formation curve was observed. Instead, a linear curve with a high product formation rate was detected (compare Figure 3.1 c and Figure 3.2 c). We ascribe the linear product formation rate to the iminium species **2**, irreversibly formed by β-scission of the dimer radical cation $\mathbf{9}^{+\bullet}$. This observation gives further evidence that the sigmoidal shape and thus the delayed product formation under anaerobic conditions is not caused by the accumulation of the reactive aci-nitromethane species (see above). Furthermore, the differences in the initial product formation curves (sigmoidal vs. linear) of the *in situ* ^{1}H kinetic of the photocatalytic aza-Henry reaction (Figure 3.1 c) with the photocatalytic dimer **9** cleavage (Figure 3.2 c) rule out the direct formation of THIQ iminium **2** from THIQ **1** under anaerobic conditions. Based on these results the participation of the H$^\bullet$-abstraction pathway under anaerobic conditions is unlikely. Further support comes from the change of the sigmoidal shape of the curve to a linear slope at the maximum dimer **9** concentration of the *in situ* kinetic (Figure 3.1 c). The offset between the maximum of the dimer **9** and the maximal slope of the product formation (Figure 3.1 b,c) is due to the additional contribution of the ring opened intermediate **10**. The absence of the iminium ion **2** during the initial hour also excludes a fast oxidation of the α-amino radical **7** under *in situ* conditions. The α-amino radical is sufficiently stable to react under the applied conditions by radical recombination.

On the basis of the experimental results we propose that the dimer **9** is a productive intermediate and not an undesired byproduct for the iminium ion **2** generation, as described in literature[82]. In addition, these data indicate that the reduced nitromethane species $MeNO2^{\bullet-}$ solely functions as base and not as hydrogen atom acceptor.

In summary, the two terminal oxidants lead to different intermediate distributions and pathways. A radical pathway, opened by $MeNO_2^{\bullet-}$, generates the amino radical **7**, a precursor of the intermediates **9** and **10**. After formation of a certain concentration of **9** and **10**, these intermediates were converted to product **6a** via the iminium ion **2**, leading to an increase in the reaction rate over time and thus to a sigmoidal product curve. Under anaerobic conditions this pathway is exclusively operating. In addition to the radical pathway an iminium pathway is opened by $O_2^{\bullet-}$ under aerobic conditions. Besides the formation of **9** and **10**, the main intermediate now constitutes the THIQ-OOH **11** in equilibrium with iminium ion **2**, latter directly resulting from the radical cation $\mathbf{1}^{+\bullet}$ not taking the detour via **9** and **10**. The dominance of the iminium pathway is reflected in the linear product formation and the accelerated reaction rate.

3.3.5 Slow Background Reaction in the Dark

After mixing THIQ **1,** $Ru(bpy)_3Cl_2$ (10 mol%) and nitromethane **5a** under *in situ* conditions we observed the THIQ iminium ion **2** accompanied by a delayed formation of the THIQ hydroperoxide species **11**.[113] The first ten minutes of the photocatalyzed reaction are depicted by a row of stacked proton spectra in Figure 3.3. After initiation of the reaction by visible light, dimer **9** arises followed by product **6a** and the ring opened THIQ species **10**. The reaction profiles of the iminium THIQ **2** and THIQ hydroperoxide **11** are correlated, which indicates that the iminium ion **2** is converted into the amino hydroperoxide species **11** directly.

Surprisingly, the maximum amount of THIQ iminium ion **2** is already generated in the dark (indicated with 0 s of irradiation in Figure 3.3) and rapidly decreases below the detection limit after irradiation.

Control measurements showed that the initial formation of the iminium ion **2** upon mixing THIQ **1** with nitromethane **5a** in the dark is independent of the presence or absence of photocatalyst or air. Up to 2% of THIQ iminium ion **2** were already detected in the dark, even if the sample is prepared directly at the spectrometer (elapsed time before measurement 60-90 s). However, the efficiency of the background reaction in the dark is low, as only negligible yields were obtained under anaerobic conditions in the presence of 10 mol% $Ru(bpy)_3^{2+}$ (6% after 18 h) and without catalyst in air (2% after 20 h). Therefore, we investigated the origin of the background reaction in the dark. Upon mixing the pure white THIQ **1** and colorless nitromethane **5a** a color change to fade pale yellow was observed. The THIQ iminium **2** as well as the color change could not be detected when nitromethane was substituted by $CDCl_3$, DMF-d_7 or MeCN-d_3. The formation does not require light, air or a photocatalyst, but nitromethane **5a**. Therefore, we assume a direct interaction of nitromethane **5a** and THIQ **1** in form of redox or acid-base equilibria. However, a comparison of the pKa values [114] and measured redox potentials by cyclic voltammetry[115] (for detailed considerations see section 3.5.9) show that the equilibria reside strongly on the side of the neutral species explaining the ineffectiveness of the background reaction.

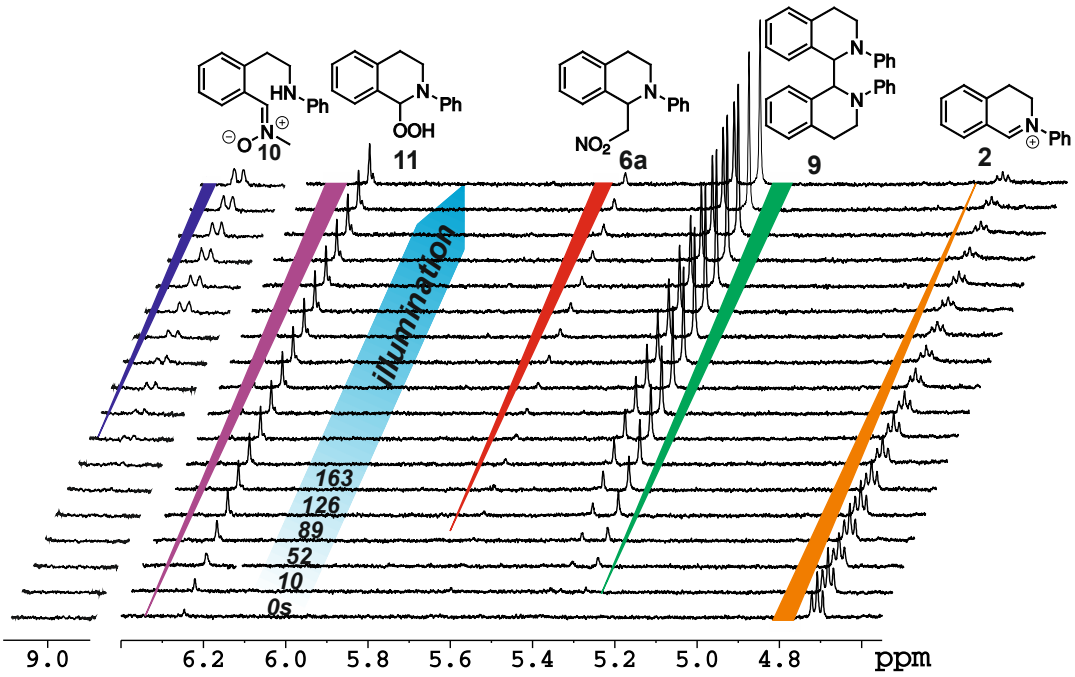

Figure 3.3 The formation of iminium ion **2** in the dark and subsequent formation of THIQ-OOH **11** is shown by a row of stacked ^{1}H-NMR spectra (initial 10 min, 50 mM THIQ **1** and nitromethane **5a** with $Ru(bpy)_3Cl_2$ (10 mol%) in nitromethane-d_3 under continuous irradiation with blue LEDs at 300 K).

3.3.6 Effective Background Reaction with Light

More control experiments addressing the light-induced background reaction were performed. Surprisingly, reactions without photocatalyst but under air in combination with an intense visible light source (blue LEDs) gave 80% of the coupling product after 24 h.

Stephenson *et al.* already reported a slow background reaction in the absence of the catalyst by irradiation with a fluorescent bulb, but prolonged reaction times were required. The product of the aza-Henry reaction was obtained with 83% conversion after 180 h in contrast to 92% yield after 10 h when $Ir(ppy)_2(dtbbpy)PF_6$ was applied as photocatalyst.[28] However, we observed a remarkable increase of the reaction rate for the light-induced "background" reaction, by changing the irradiation setup to use high power LEDs with defined emission spectra, see Table 3.1. Upon mixing of the pure white crystalline THIQ **1** with nitromethane, a solution possessing a stable fade pale yellow color was obtained. We assume the formation of an electron donor acceptor (EDA) complex between THIQ **1** and nitromethane **5a**. Literature evidence is given by spectroscopic studies for similar systems. Andrabi *et al.*[116] proposed CT complexes of aromatic amines with nitromethane. They described the formation of weak 1:1 molecular CT complexes of nitromethane with different *N,N*-dialkylanilines (N,N-diethylaniline: λ_{CT} = 377 nm, K(25°C) = 0.31 l mol^{-1}), a structural motif, which is present in THIQs. The color change upon addition of tertiary amines to nitromethane was also reported by Constantinou *et al.*; they assigned it to the formation of charge transfer complexes.[117] For THIQ systems significant light-induced background reactions were detected in some cases.[63,85,118] Rovis and coworkers observed a high background reaction in the absence of catalyst for the α-acylation of THIQ with aldehydes using *m*-DNB (*m*-dinitrobenzene) as terminal oxidant. They propose the formation of an EDA complex between *m*-DNB and THIQ.[118] Zeitler *et al.* recently published a photocatalyst-free method for the α-C-H functionalization of THIQ; mechanistically they assume the involvement of EDA complexes between THIQ and $BrCCl_3$, which was added as terminal oxidant.[63]

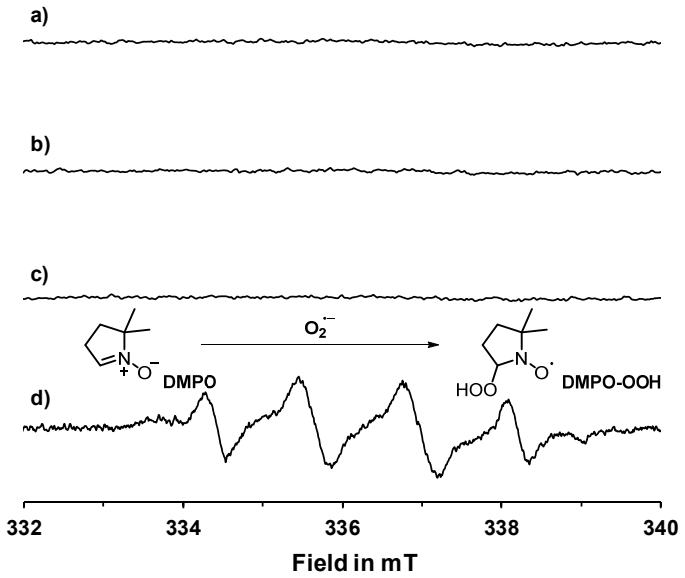

Figure 3.4 Detection of $O_2^{\bullet-}$ using DMPO as radical trap by ESR. (a) and (b): ESR spectra of DMPO (2.0×10^{-2} $molL^{-1}$) in air-saturated nitromethane in the dark (a) and under the irradiation of blue LEDs

(b); c) and d): ESR spectra of a solution of THIQ **1** (1.5 x 10^{-3} molL^{-1}) and DMPO (2.0 x 10^{-2} molL^{-1}) in air-saturated nitromethane in the dark (c) and under the irradiation of blue LEDs (d).

When the reaction was carried out under an argon atmosphere only a low yield of the desired cross-coupling product **6a** was obtained (7% after 20 h). This shows, that oxygen is essential for the visible light induced aza-Henry reaction, in contrast to the photocatalyzed reaction. In order to elucidate the role of oxygen and the involved reactive oxygen species ESR spectroscopic measurements were performed.[119] DMPO (5,5-dimethyl-1-pyrroline-N-oxide) was employed as a probe for superoxide radical anion confirming the formation of $O_2^{\bullet-}$ by the characteristic signal of the superoxide-DMPO adduct (Figure 3.4). Superoxide radical anion was exclusively formed upon irradiation with blue LEDs and the presence of both reaction partners (THIQ **1** and nitromethane **5a**). By exclusion of light or THIQ **1** no $O_2^{\bullet-}$ was detected.

The influence of intensity and wavelength of the light source on the reaction rate was further investigated. For that reason, we examined high power LEDs with different wavelengths. In order to have a comparable value to the literature reported photo-background reaction of Stephenson *et al.*[28] we also applied a household energy-saving bulb as irradiation source (Table 3.1).

The reactions were performed under aerobic conditions and the conversions were compared after 24 h. The expected β-nitroamine coupling product **6a** was obtained for all investigated light sources (Table 3.1, entries 1-4). In agreement with the literature reported values, we observed low conversion of THIQ **1** when an energy-saving bulb was used as irradiation source (Table 3.1, entry 4). By changing the light source to high power LEDs a significant acceleration of the reaction rate was observed. Almost full conversion of the THIQ **1** was achieved after 24 h using LEDs with a peak wavelength λ_{max} of 400 nm or 440 nm providing the desired cross coupling product **6a** with good yields in reasonable reaction times. Applying LEDs with longer wavelength the product formation decreases (Table 3.1, entry 3). Further experiments were conducted with blue LEDs (440 nm) as they are most suitable for an efficient product formation.

Table 3.1 Wavelength dependence of the light-induced aza-Henry reaction without photocatalyst.

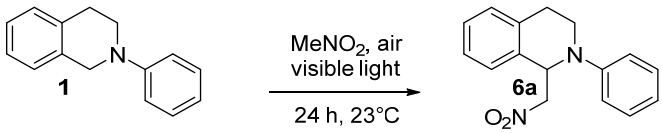

Entry	Light source[a]	Recovered THIQ **1**[b]	Yield **6a** [%][b]
1	400 nm LED	3	74
2	440 nm LED	8	80
3	520 nm LED	62	38
4	Energy saving bulb	85	15

[a]For a detailed specification see section 3.5.3.
[b]Based on NMR analysis using 2,5-dimethylfuran as an internal standard.

Using filters with different transmission values (25-75%) we further examined the impact of the light intensity on the reaction rate (Figure 3.22). As expected a decrease in product formation was observed by reduced transmission. The influence of wavelength and intensity on the product formation clearly proofs the importance of the reaction parameter light.

In analogy to the photocatalyzed *ex situ* studies ^{1}H-NMR kinetics were recorded to gain mechanistic insights and to elucidate the involved intermediates. The conditions are identical to the *ex situ* study described above, apart from the exclusion of the photocatalyst. In contrast to the aerobic photocatalyzed reaction (see Figure 3.1 a) no dimer **9** and intermediate **10** were detected during the kinetic measurement (see Figure 3.5). THIQ hydroperoxide **11** constitutes the main intermediate, with constant amount of 10-15% over the reaction time. A moderate amount of iminium ion **2** is detected. The differences in the reaction profile - the absence of dimer **9** and open intermediate **10**, which we assume is derived from the α-amino radical **7** - indicate that the iminium pathway is operative and gave evidence that $O_2^{\bullet-}$ exclusively act as an hydrogen atom acceptor.

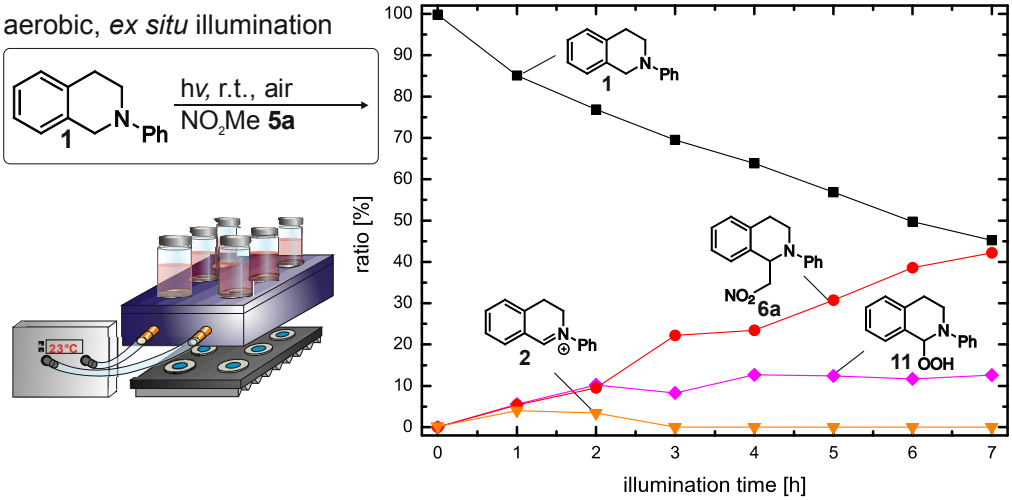

Figure 3.5 The photocatalyst free ^{1}H NMR kinetic shows the intermediates iminium ion **2** and THIQ hydroperoxide **11,** indicating an iminium pathway.

In analogy to the results of the photocatalyzed studies, light on-off studies revealed that THIQ hydroperoxide **11** is build up photo-induced. The reaction from THIQ-OOH **11** to the product **6a** and hydrogen peroxide also proceeds independent from light and catalyst in the dark (see Figure 3.21).

However, the involvement of the amino radical **7** or other radical species cannot be completely excluded as BHT[120] (2,6-di-tert-butyl-4-methylphenol), a radical inhibitor, decreased the rate of product formation from 62-65% (without BHT) to 31-33% (with 1.3 equiv. BHT) after 15 h of irradiation.[121] Due to this effect an autoxidation mechanism[105,122,123] for the formation of THIQ-OOH **11** as reported for the acetic acid promoted[104] and sulfuryl chloride initiated[103] CDC of THIQ **1** with nucleophiles cannot be excluded (for detailed mechanism of the autoxidation see Scheme 3.9).

Despite the suppressing effect of the radical inhibitor, the reaction profile and the absence of intermediates formed on the radical pathway (e.g. dimer **9**) suggest that THIQ hydroperoxide **11** is predominantly generated via the iminium ion **2** and not via the amino radical **7**. This

topic is also discussed for the metal-catalyzed CDC reaction of THIQ **1** with different nucleophiles using *tert*-butyl hydroperoxide as terminal oxidant. Doyle *et al.*[70] suggested the formation of the respective *tert*-butyl peroxide species in analogy to our proposal via iminium ions, whereas Klussmann *et al.*[72] proposed a radical pathway for the formation of amino *tert*-butyl hydroperoxide (see Figure 3.2) for a similar reaction system.

On the basis of these results we propose the following mechanism for the light induced background reaction presented in Scheme 3.7. THIQ **1** and nitromethane **5a** form an EDA complex. Upon irradiation with visible light the electron transfer from the lone pair of THIQ to nitromethane is promoted, which provides a pair of radical ions. Oxygen is anticipated to prevent back electron transfer to the neutral components by accepting the electron from the radical anion of nitromethane ($E_{red}(MeNO_2/MeNO_2^-)$ = -1.65 V vs. SCE, $E_{red}(O_2/O_2^{\bullet-})$ = -0.75 V vs. SCE)[68] making the process efficient. The resulting superoxide radical anion abstracts a hydrogen atom to produce the iminium ion **2,** which can be intercepted by nucleophiles including the formed peroxide anion.

Scheme 3.7 Proposed mechanism of the light induced reaction of THIQ **1** and nitromethane **5a** in the presence of oxygen.

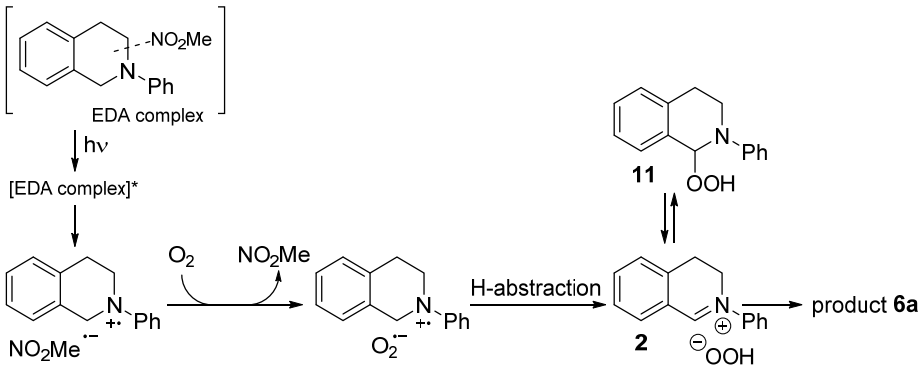

3.4 Summary of the Mechanistic Proposal and Conclusion

The results are summarized in a mechanistic proposal depicted in Scheme 3.8. The photocatalyzed aza-Henry reaction is initiated by a reductive quenching of the photoexcited state of $Ru(bpy)_3Cl_2$ upon irradiation with visible light generating the THIQ amine radical cation $\mathbf{1}^{+\bullet}$(Scheme 3.8 c). The subsequent reactive mode of $\mathbf{1}^{+\bullet}$ depends on the nature of the terminal oxidant regenerating the photocatalyst. Under anaerobic conditions, nitromethane acts as terminal oxidant exclusively. The resulting $MeNO_2^{\bullet-}$ is assumed to deprotonate THIQ $\mathbf{1}^{+\bullet}$ initiating the radical pathway via the α-amino radical **7**, characterized by a sigmoidal product formation. On this pathway, dimer **9** and a new ring opened species **10** are detected as intermediates, which are found to be productive towards **6a** in the dark (**10**) or light dependent (**9**). In the presence of radical inhibitors the intermediates **9** and **10** cannot be observed and the reaction is slowed down. Further experiments starting from dimer **9** show a very effective linear product formation via an iminium ion intermediate **2** under anaerobic conditions. All of these data indicate that $MeNO_2^{\bullet-}$ acts as a base and opens an effective radical pathway, while $H^{\bullet}$- abstraction followed by the iminium ion pathway is negligible.

Under aerobic conditions O_2 as well as nitromethane operate as terminal oxidants in the photocatalyzed reaction. Now, the $MeNO_2^{\bullet-}$ based radical pathway is active (see above). In addition, THIQ hydroperoxide **11** is detected as intermediate and a fast and linear product formation is observed. THIQ hydroperoxide **11** is an off cycle resting state of the iminium ion pathway. In studies without photocatalyst ($O_2^{\bullet-}$/**1**$^{+\bullet}$ interaction) the intermediates **9** and **10** of the radical pathway are not detected. With the radical inhibitor TEMPO only the iminium ion pathway is observed. All of these data indicate that $O_2^{\bullet-}$ functions mainly as radical species and initiates via H•- abstraction the highly effective iminium ion pathway.

Even without photocatalyst a productive light dependent reaction is observed with rates comparable to previously reported photocatalyzed systems (Scheme 3.8 b). A correlation between the rate of product formation, the light intensity and the wavelengths was found. With strong light sources (blue LEDs) and O_2 after 24 h full conversion is reached (compared to 4 h with $Ru(bpy)_3Cl_2$ and O_2 as well as 12 h with $Ru(bpy)_3Cl_2$ and without O_2). Oxygen proved to be mandatory and exclusively $O_2^{\bullet-}$ as well as THIQ hydroperoxide **11** and the iminium ion **2** intermediates were found. This is in accordance with the photocatalytic iminium pathway and corroborates that $O_2^{\bullet-}$ acts mainly via H•- abstraction. We assume that three features promote this light dependent background reaction to become effective. Firstly, light excitation facilitates the charge transfer in an electron-donor-acceptor (EDA)-complex between nitromethane and THIQ **1** to generate the respective radical ion pair. Secondly**,** back electron transfer (BET) is prevented by electron transfer from $MeNO_2^{\bullet-}$ to dissolved oxygen providing $O_2^{\bullet-}$. Thirdly, $O_2^{\bullet-}$ initiates an effective product formation via H•-abstraction and iminium pathway. In the absence of light the charge transfer is inefficient (2% yield after 20 h). With light but without oxygen, the combination of BET and less reactive radical pathway leads to only 7% after 20 h (Scheme 3.8 a).

The comprehensive picture of the aza-Henry reaction presented herein reveals the influence of reaction conditions on the mechanistic pathways in photocatalytic reactions in detail. The possibility to switch between the operative reaction pathways (H^+-or H•-abstraction) provides a more accurate prediction and planning of the experimental setup in photoreactions.

Scheme 3.8 Overview of the proposed mechanism of the aza-Henry reaction, divided into three parts: the photocatalyzed aza-Henry reaction (c), the light induced reaction in the absence of a photocatalyst (b) and the background reaction of THIQ and nitromethane in the dark (a). The respective reactions were investigated in the presence (aerobic, red) and absence (anaerobic, blue) of oxygen. The pathways active under both conditions are dashed in red and blue. (c) The under photocatalytic conditions stated iminium and radical pathways are highlighted in grey.

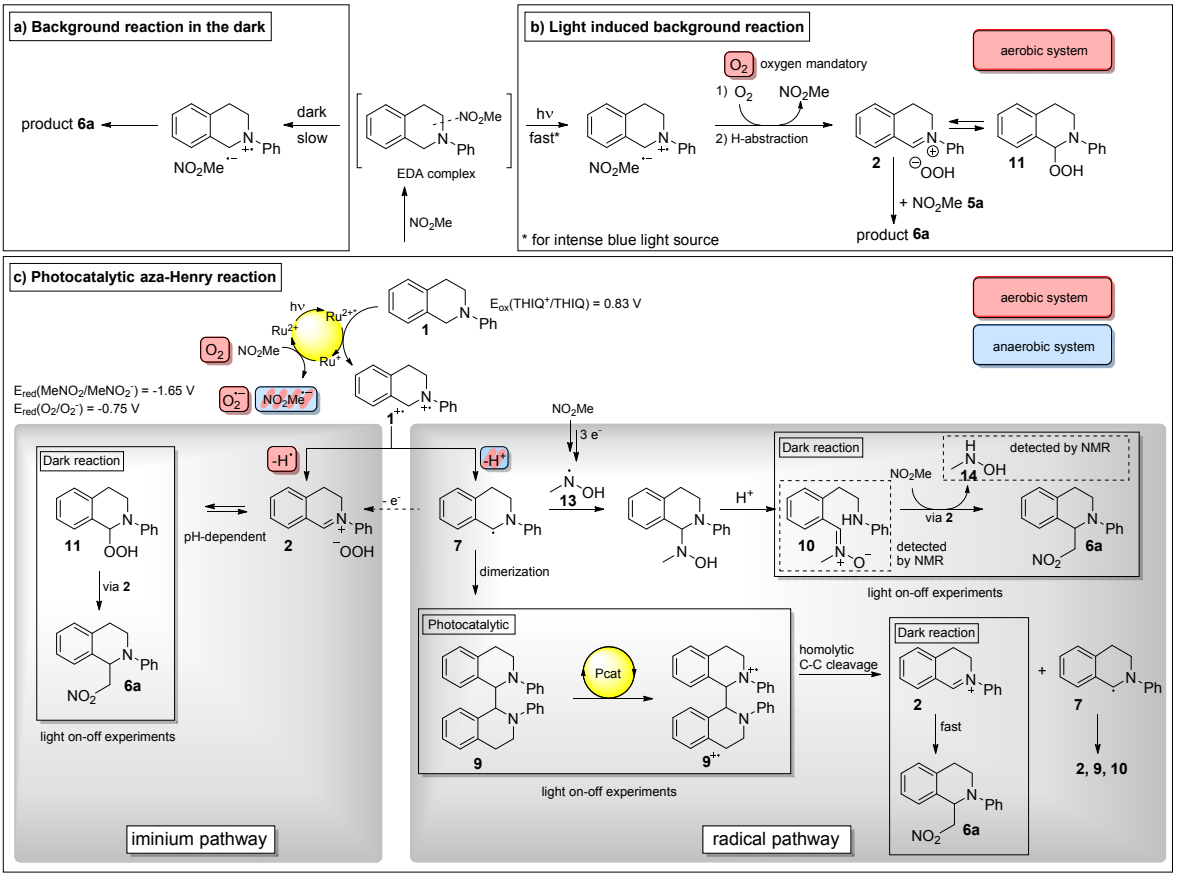

3.5 Supporting Information

3.5.1 General Methods

Commercial reagents and starting materials were purchased and used without further purification.

The NMR-measurements were recorded on a Bruker Avance III 600 MHz spectrometer with a 5 mm TBI-C, TBI-P or TBI-F probe or Prodigy BBO-probe or on a Bruker Avance III 600 MHz spectrometer with Cryo probe. For temperature control a BCU II unit was used. For analysis Bruker Avance 400 (^{1}H: 400 MHz, ^{13}C: 101 MHz, T = 300 K) or Bruker Avance 300 (^{1}H: 300 MHz, ^{13}C: 75 MHz, T = 295 K) spectrometer were used. Tetramethylsilane (δ = 0 ppm) or the solvent residual peak (NO_2Me-d_3: ^{1}H δ= 4.33 ppm; ^{13}C δ= 63.0 ppm; ^{15}N δ= 380.9 ppm (280 K); $CDCl_3$: ^{1}H δ= 7.26 ppm; ^{13}C δ= 77.0 ppm) was used as reference. The data were processed with Brukers Topspin 3.2. Multiplicities are indicated, s (singlet), d (doublet), t (triplet), q (quartet), quint (quintet), sept (septet), m (multiplet); coupling constants (*J*) are in Hertz (Hz).

Reactions were monitored by thin-layer chromatography using silica gel plates ALUGRAM Xtra SIL G/UV254 from Macherey-Nagel; visualization was accomplished with UV light (254 nm or 366 nm). Flash column chromatography was performed on a Biotage Isolera Spektra One automated flash purification system with UV-Vis detector using Merck silica gel 60 M (0.040-0.063 mm, 230-440 mesh) for normal phase or pre-packed Biotage SNAP cartridges (KP-C18-HS) for reversed phase chromatography.

UV-Vis measurements were performed on an Agilent 8453 spectrophotometer. Hellma quartz cuvettes were used (2 mm and 10 mm).

Cyclic voltammetry (CV) measurements were performed with the three-electrode potentiostat galvanostat PGSTAT302N from Metrohm Autolab.

Electron-spin resonance (ESR) measurements were performed on a Magnettech MiniScope MS400 ESR spectrometer at 9.2-9.6 GHz. The measurements were recorded at room temperature. For the *in situ* irradiation of the samples a blue LED (OSRAM Oslon SSL 80, royal blue) was used.

Mass spectra were recorded on Finnigan MAT95 (EI-MS), Agilent Q-TOF 6540 UHD (ESI-MS, APCI-MS), Finnigan MAT SSQ 710 A (EI-MS, CI-MS) or ThermoQuest Finnigan TSQ 7000 (ES-MS, APCI-MS) spectrometer.

3.5.2 General procedures

3.5.2.1 General procedure for the preparation of 2-phenyl-1,2,3,4-tetrahydro-isoquinoline 1[124,125]

A Schlenk tube containing copper(I) iodide (200 mg, 1.0 mmol) and potassium phosphate (4.25 g, 20.0 mmol) was evacuated and back filled with nitrogen. 2-Propanol (10.0 mL), ethylene glycol (1.11 mL, 20.0 mmol), 1,2,3,4-tetrahydroisoquinoline (2.0 mL, 15.0 mmol) and iodobenzene (1.12 mL, 10.0 mmol) were added successively at room temperature. The reaction mixture was heated at 85-90 °C and kept for 24 h and then allowed to cool to room

temperature. Diethyl ether (20 mL) and water (20 mL) were then added to the reaction mixture. The aqueous layer was extracted with diethyl ether (2 × 20 mL). The combined organic phases were washed with brine and dried over sodium sulfate. The solvent was removed by rotary evaporation and purified by repeated automated flash column chromatography on silica gel using hexane/ethyl acetate as eluent and was further purified by recrystallization in ethanol. A white solid was obtained.

3.5.2.2 General procedure for the preparation of 2-phenyl-3,4-dihydroisoquinolinium bromide 2d[63]

An oven-dried Schlenk tube with a magnetic stir bar was evacuated and backfilled with argon. 2-phenyl-1,2,3,4-tetrahydroisoquinoline (0.25 mmol, 1.0 equiv) was dissolved in dry acetonitrile. Bromotrichloromethane (0.375 mmol, 1.5 equiv) was added under nitrogen and the tube was then irradiated with blue LEDs for 1 h at room temperature. A color change from transparent to deep blue to brown was visible. The THIQ iminium bromide **2d** was precipitated by addition of dry diethyl ether to the sluggish solution. A light brown solid was obtained.

3.5.2.3 General procedure for the preparation of 2,2′-diphenyl-1,1′,2,2′,3,3′,4,4′-octahydro-1,1′-biisoquinoline 9[46]

The dimer **9** was prepared according to previously reported procedure.[46] Purification was achieved by filtration over a short plug of silica gel to remove CdS and subsequent reversed phase automated flash column chromatography (MeCN/water, 50-100% MeCN).

3.5.3 NMR Studies: General procedures for the aza-Henry reaction

3.5.3.1 In situ illumination (A)

The LED based device for *in situ* illumination described in Feldmeier *et al*.[75] was used. For standard reactions THIQ (1 equiv.) and $Ru(bpy)_3Cl_2$ (0.1 equiv.) were dissolved in deuterated nitromethane-d_3 (0.05 mmol/mL). The samples were directly prepared in 5 mm amberized NMR tubes of spintec which were used together with an insert for the optical fibre. As light source Cree XP-E LEDs (**royal blue** 500 mW) with a peak wavelength (λ_{Peak}) of 449 nm were used. The LEDs were operated at 500 mA. The temperature as indicated was kept constant by the BCU II unit of the spectrometer.

For the dimer kinetic, dimer **9** (1 equiv., 0.01 mmol/mL) in deuterated nitromethane was irradiated for 1.5 h, then $Ru(bpy)_3Cl_2$ (0.1 equiv.) was added and the irradiation was continued for 3 h.

3.5.3.2 Ex situ illumination

For the external illumination a setup consisting of a LED array and a temperature control unit was used (see Figure 3.6). The samples were irradiated through the vial's plane bottom side and cooled from the side using custom made aluminum cooling blocks connected to a thermostat. High Power LEDs of different wavelengths and an energy-saving bulb were used for irradiation of the reaction mixtures (for emission spectra of the light sources see 3.5.10.5):[1]

[1] We want to thank OSRAM Opto Semiconductors GmbH (Regensburg) for spectral characterization of the used light sources.

- OSRAM Oslon SSL 80 (λ_{Peak} = 440 nm, **royal blue**, operated at 700 mA, LT-1960)
- Edison Edixeon 3W Emitter (λ_{Peak} = 400 nm, **purple**, operated at 700 mA, EDEV-SLC1-03)
- CREE XP-E Q4 (λ_{Peak} = 520 nm, **green**, operated at 700 mA, LT-2048)
- Megaman (SP0405)

3.5.3.3 Ex situ method (B)

In a 5 mL snap vial equipped with a magnetic stirring bar THIQ (1 equiv.) and if mentioned $Ru(bpy)_3Cl_2$ (0.01 equiv.) were dissolved in nitromethane-d_3 (0.20 mmol/mL) and the resulting mixture was irradiated with 440 nm LEDs (OSRAM Oslon SSL 80, royal blue) for the indicated time. In some cases, decane or octamethylcyclotetrasiloxane were used as internal standards and were added at the beginning of the reaction. If not otherwise mentioned the reaction was performed under air. For samples under inert atmosphere the solvent was degassed by freeze, pump and thaw method and backfilled with argon. The temperature was kept constant at 23 °C. For the measurements a stock solution in deuterated nitromethane-d_3 was prepared and either the whole reaction mixture or aliquot samples were taken and directly measured by NMR spectroscopy. The concentrations were calculated using Brukers *Eretic 2* or by the signal ratios relative to the internal standard.

3.5.3.4 Ex situ method (C) – (Table 3.1)

In a 5 mL snap vial equipped with a magnetic stirring bar THIQ (1 equiv.) was dissolved in nitromethane (0.20 mmol/mL) and the resulting mixture was irradiated by LEDs with the indicated wavelength or a fluorescent bulb for 24 h. The reaction was performed under air and the temperature was kept constant at 23 °C. After 24 h of irradiation the solvent was evaporated under reduced pressure and the internal standard 2,5-dimethylfuran[126] was added. The mixture was redissolved in $CDCl_3$. The yield was calculated by integrating the ^1H NMR spectrum.

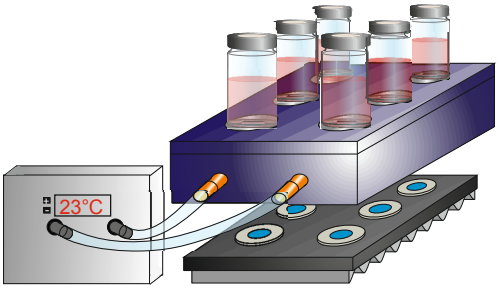

Figure 3.6 External illumination setup.

3.5.4 Autoxidation mechanism

The radical initiated autoxidation mechanism is described in literature for the acetic acid[104] promoted and sulfuryl chloride[103] initiated cross-dehydrogenative coupling reaction of THIQ **1** with different nucleophiles. In both publications the origin of the radical initiator is not completely elucidated. It is assumed, that in the initiation step the radical initiator is abstracting a hydrogen atom from the benzylic position of THIQ **1**. The generated amine radical **7** can undergo an addition reaction with molecular oxygen providing the oxygen-centered peroxyl radical **12**. The propagation step involves another hydrogen atom

abstraction step from THIQ starting material **1** to the peroxyl radical **12**, resulting in THIQ peroxide **11**. The THIQ peroxide **11** is in an equilibrium with the THIQ iminium ion **2c**, which can be intercepted by nucleophiles, leading to the coupling product **6** and hydrogen peroxide.

Scheme 3.9 Proposed reaction mechanism for the autoxidative CDC reaction of THIQ **1**.

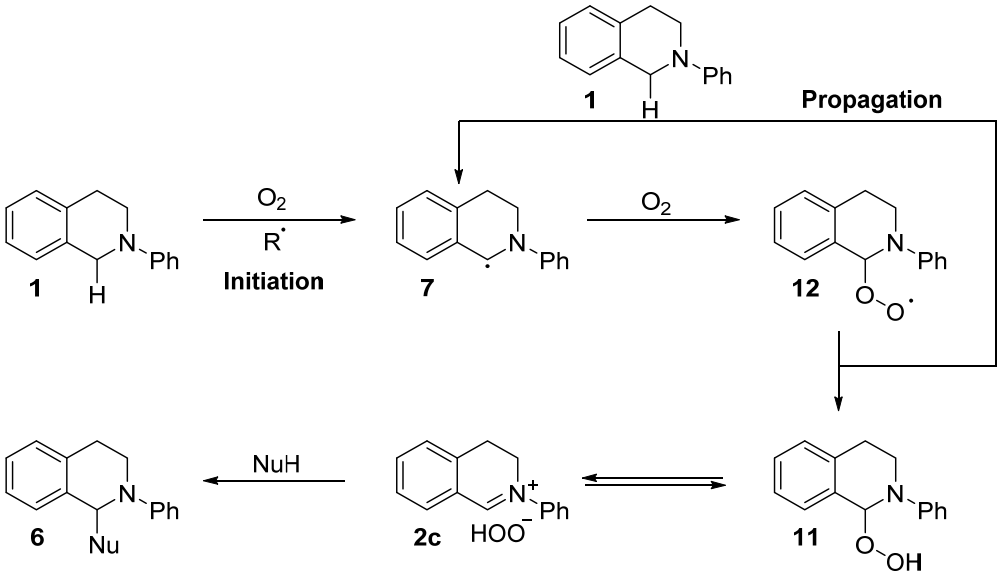

3.5.5 Ring opened intermediate 10

We propose the formation of the ring opened intermediate **10** to occur via the α-amino radical **7**, as discussed in detail in the main text. A more detailed proposal of the mechanism is given in Scheme 3.9. After multistep reduction of nitromethane by the catalyst a hydroxylamine radical **13** can be formed[106], which can undergo radical recombination with the α-amino radical **7**. A H^+-shift and subsequent rearrangement lead to a C-N bond cleavage and a secondary aniline is formed. A similar ring opening by retro-aza-Michael reaction has been anticipated before, though no experimental proof for the structure was given.[69]

Scheme 3.10 Proposed reaction mechanism for the formation of the ring opened intermediate **10** via a radical pathway.

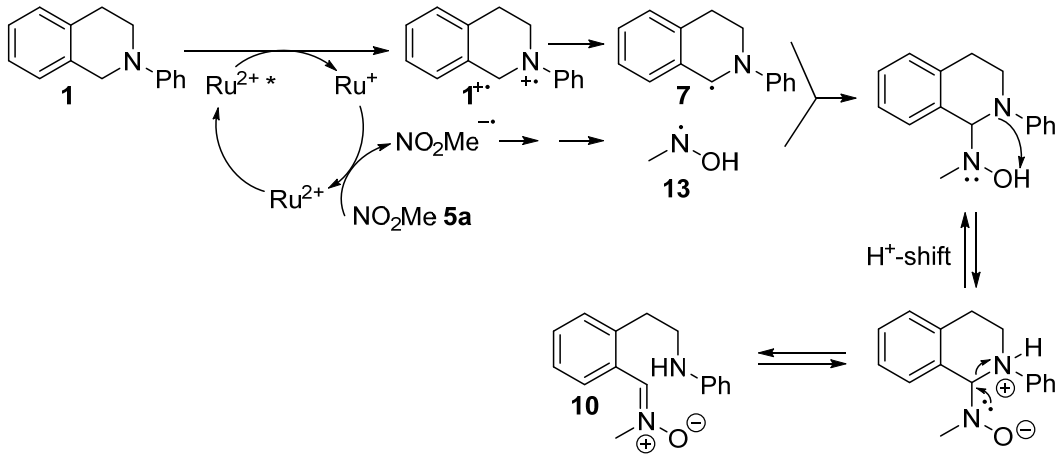

3.5.6 NMR Assignment of the THIQ species

3.5.6.1 2-Phenyl-1,2,3,4-tetrahydroisoquinoline (1)

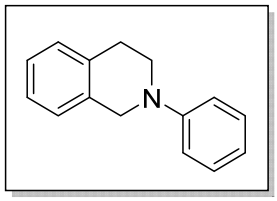

Synthesized according to the general procedure. NMR data are in accordance with literature reported values.[63,124,125]

^{1}H NMR (600 MHz, NO_2Me-d_3, 300 K): δ [ppm] = 7.29 – 7.25 (m, 2H), 7.23-7.17 (m, 4H), 7.04 (d, *J* = 7.7 Hz, 2H), 6.79 (t, *J* = 6.9 Hz, 1H), 4.41 (s, 2H), 3.59 (t, *J* = 5.8 Hz, 2H), 2.99 (t, *J* = 5.6 Hz, 2H).

^{13}C NMR (150 MHz, NO_2Me-d_3, 300 K): δ [ppm] = 152.4, 136.8, 136.4, 130.7, 130.1, 128.2, 127.9, 127.5, 119.9, 116.6, 51.8, 47.9, 29.9.

3.5.6.2 2-Phenyl-3,4-dihydroisoquinolinium bromide (2d)

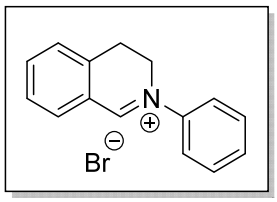

Synthesized according to the general procedure. NMR data are in accordance with literature reported values.[63,71]

^{1}H NMR (600 MHz, NO_2Me-d_3, 300 K): δ [ppm] = 9.42 (s, 1H), 8.10 (d, *J* = 7.7 Hz, 1H), 7.93 (t, *J* = 7.4 Hz, 1H), 7.84-7.82 (m, 2H), 7.72-7.70 (m, 3H), 7.66-7.62 (m, 2H), 4.72 (t, *J* = 7.9 Hz, 2H), 3.59 (t, *J* = 7.9 Hz, 2H).

^{13}C NMR (150 MHz, NO_2Me-d_3, 300 K): δ [ppm] = 167.9, 140.7, 138.6, 136.5, 131.8, 131.8, 129.9, 129.7, 123.5, 52.8, 26.4.

3.5.6.3 2,2′-Diphenyl-1,1′,2,2′,3,3′,4,4′-octahydro-1,1′-biisoquinoline (9)

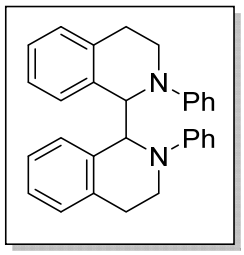

Synthesized according to the general procedure. NMR data are in accordance with literature reported values. [82] Two diastereomers (ratio 42:58) are observed in nitromethane-d_3 at 298 K.

^{1}H NMR (600 MHz, NO_2Me-d_3, 298 K): δ [ppm] = 7.21-7.14, 7.13-7.08, 7.08-7.02, 6.99-6.93, 6.82-6.78, 6.67-6.60, 5.36 (s, 2H), 3.83-3.77 (m, 2H), 3.47-3.40 (m, 2H), 2.99-2.93 (m,

2H), 2.83-2.76 (m, 2H); 5.30 (s, 2H), 3.69-3.63 (m, 2H), 3.58-3.53 (m, 2H), 3.06-2.99 (m, 2H), 2.92-2.85 (m, 2H).

^{13}C NMR (150 MHz, NO_2Me-d_3, 298 K): δ [ppm] = 150.8, 137.3, 130.7, 130.3, 130-127, 64.9, 44.3, 28.4

3.5.6.4 1-(Nitromethyl)-2-phenyl-1,2,3,4-tetrahydroisoquinoline (6a)

Synthesized according to the general procedure B. NMR data are in accordance with literature reported values.[28]

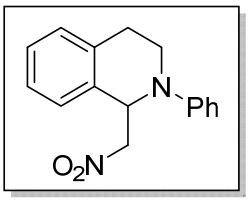

^{1}H NMR (600 MHz, NO_2Me-d_3, 300 K): δ [ppm] = 7.29-7.22 (m, 4H), 7.25 (m, 2H), 7.05 (d, *J* = 8.7 Hz, 2H), 6.81 (td, *J* = 7.3 Hz, *J* = 0.8 Hz, 1H), 5.64 (dd, *J* = 9.1 Hz, *J* = 6.2 Hz, 1H), 5.0 (dd, *J* = 12.3 Hz, *J* = 8.9 Hz, 1H), 4.80 (dd, *J* = 12.3 Hz, *J* = 6.1 Hz, 1H), 3.81-3.67 (m, 2H), 3.11-3.05 (m, 1H), 2.82 (dt, *J* = 16.7 Hz, *J* = 4.2 Hz, 1H).

^{13}C NMR (150 MHz, NO_2Me-d_3, 300 K): δ [ppm] = 150.5, 137.5, 134.5, 130.9, 130.8, 129.5, 128.8, 127.9, 120.7, 116.9, 79.9, 59.2, 42.9, 27.0.

New THIQ species

The intermediates were characterized and assigned by NMR in the reaction mixture.

3.5.6.5 1-Hydroperoxy-2-phenyl-1,2,3,4-tetrahydroisoquinoline (11)

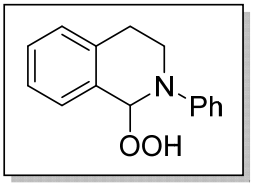

^{1}H NMR (600 MHz, NO_2Me-d_3, 270 K): δ [ppm] = 9.15 (br s, 1H), 7.43 (m, 1H), 7.36 (m, 2H), 7.32 (m, 2H), 7.27 (m, 1H), 7.15 (m, 2H), 6.87 (t, *J* = 7.5 Hz, 1H), 6.24 (s, 1H), 3.72-3.52 (m, 2H), 3.05-2.89 (m, 2H).

^{13}C NMR (150 MHz, NO_2Me-d_3, 270 K): δ [ppm] = 150.5, 138.9, 130.8, 130.8, 130.5, 130.0, 120.8, 116.4, 93.6, 43.6, 29.1.

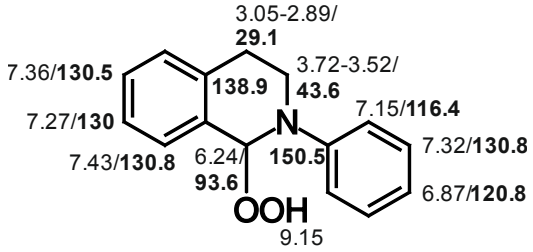

Figure 3.7 Chemical shift assignment of THIQ peroxide **11** in nitromethane-d_3 at 270 K.

The assignment of THIQ-OOH **11** is verified by the addition of hydrogen peroxide (30 w% in water) to an irradiated reaction mixture of THIQ **1**, $Ru(bpy)_3Cl_2$ and nitromethane-d_3, see Figure 3.8. After addition of H_2O_2 to the sample the THIQ peroxide **11** signals at 6.24 ppm and 9.15 ppm (br) drastically increase. The new signal at 8.8 ppm (br) is assigned to H_2O_2.

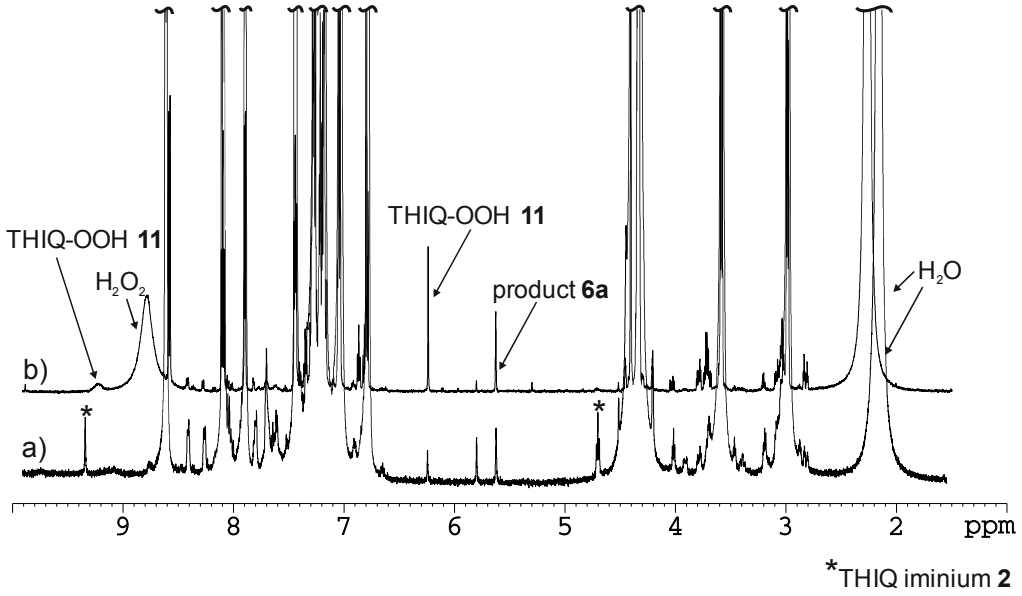

Figure 3.8 ^{1}H NMR spectra of THIQ **1** and $Ru(bpy)_3Cl_2$ photocatalyst in nitromethane-d_3 during illumination at 300 K (a) before and (b) after addition of hydrogen peroxide to the solution.

3.5.6.6 *N*-Methyl-1-(2-(2-(phenylamino)ethyl)phenyl)methanimine oxide (10)

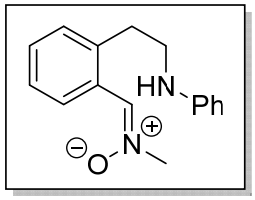

^{1}H NMR (600 MHz, NO_2Me-d_3, 280 K): δ [ppm] = 9.03 (d, *J* = 7.9 Hz, 1H), 7.73 (s, 1H), 7.38 (m, 1H), 7.37 (m, 1H), 7.32 (m, 1H), 7.17 (m, 2H), 6.67 (m, 3H), 3.39 (t, *J* = 7.2 Hz, 2H), 3.03 (t, *J* = 7.2 Hz, 2H).

^{13}C NMR (150 MHz, NO_2Me-d_3, 280 K): δ [ppm] = 150.1, 140.5, 133.3, 131.6, 131.4, 131.0, 130.8, 129.0, 127.8, 118.4, 114.1, 55.4, 46.1, 33.8.

^{15}N NMR (60 MHz, NO_2Me-d_3, 280 K): δ [ppm] =277.9.

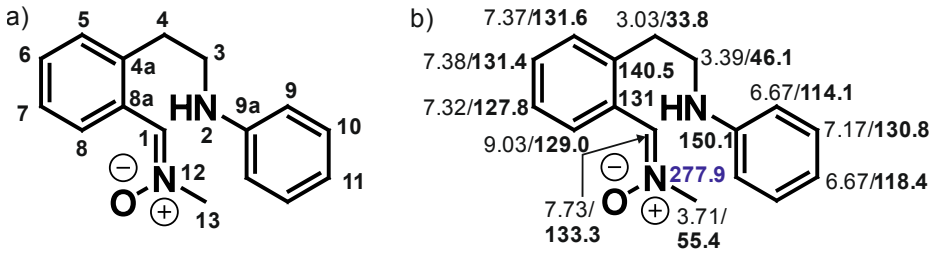

Figure 3.9 (a) Structure and numbering of the ring opened intermediate **10** and (b) chemical shift assignment in nitromethane-d_3 at 280 K.

The intermediate species **10** was assigned by 1D (^{1}H, ^{13}C) and 2D (^{1}H,^{1}H-noesy, ^{1}H,^{1}H-cosy, ^{1}H,^{1}H-tocsy ^{1}H,^{13}C-hmbc, ^{1}H,^{13}C-hsqc, ^{1}H,^{15}N-hmbc) NMR experiments. The species depicted in Figure 3.9 a is determined to be the most reliable one among the possible structures shown in Figure 3.10. The intermediate holds the motif of the THIQs, see Figure 3.10 a, however the missing ^{1}H,^{13}C-hmbc cross peak (refer to Figure 3.11 b) between C1 and C3 - detectable for all other THIQ species – hints towards a spin barrier between C1 and C3, which can occur because of a ring opening or insertion of a nitrogen or oxygen atom between position C1 and N2, as the C3-C9a coupling is not affected (Figure 3.10). The carbon atom at position C3 is shifted upfield from 48.0 ppm @280 K (THIQ **1**) to 46.1 ppm @280 K (intermediate **10**). Compared to literature values[127–130] the C3 carbon is expected to be shifted downfield for oxygen addition to N2 (refer to Figure 3.10 b, R_2=O and Figure 3.10 c) and upfield for protonation of N2 (refer to Figure 3.10 b, R_2=H). Based on this we assume a NH group, rather than N-O or N-N. The spectra of the *N*-oxide THIQ (see Figure 3.10 e) published by Prabhu *et al*.[131] corroborate our assignment.[2] Further, a ring closure between ^{15}N12 and N2 would result in a $^{3}J_{NH}$ coupling of N12 and H3 which in analogy to the product should be detectable in the ^{1}H,^{15}N-hmbc and a $^{2}J_{CN}$ coupling of N12 and C3, which should be detectable in the proton decoupled ^{13}C spectra. None of them was observed in the spectra. Based on the coupling patterns and the chemical shift changes we conclude a ring opening and a protonation of the N2 atom. The amine proton H2 was not detectable, but this can be due to fast exchange in the presence of H_2O. Further support is given by ^{1}H-dosy measurements, showing that the size of the intermediate species is in the range of the product and selective 1D tocsys, revealing four separate spin systems: C1; C3-C4; C5-C8 and C9-C11. The integral (1H) and carbon chemical shift at C1 hint towards a double bond at this position. The coupling between the nitrogen atom N12 and C1 was proven by ^{15}N labeled nitromethane, showing ^{1}H,^{15}N-hmbc cross peaks between N12-H1 and N12-H13 (see Figure 3.11). The cross peak detected in the ^{1}H,^{13}C-hmbc between C1 and C13 is due to a $^{3}J_{CH}$ coupling, because a $^{2}J_{CH}$ coupling would imply a $^{3}J_{HH}$ coupling between H1 and H13, what is not the case. Furthermore, both C1-N12 and C13-N12 can be assigned to $^{1}J_{CN}$ couplings, because of coupling constants of $^{1}J_{CN}$ = 10.3 Hz ($^{1}J_{CN}$ = 8.6 Hz for nitromethane) for C13-N12 and $^{1}J_{CN}$ = 21.0 Hz for C1-N12, refer to[132] for C-N coupling constants.

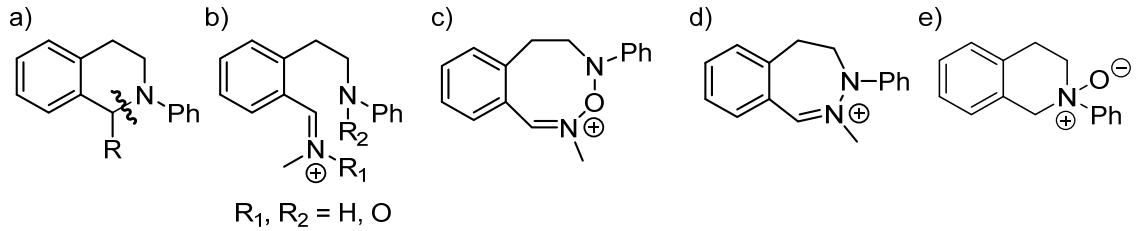

Figure 3.10 Possible intermediate structures showing the C-N bond cleavage (a) the ring opened intermediate (b) closed intermediates incorporating an additional O- (c) or N-atom (d) and the *N*-oxide THIQ (e).

[2] The assignment is taken from the Supporting Information, pp. 22-23.

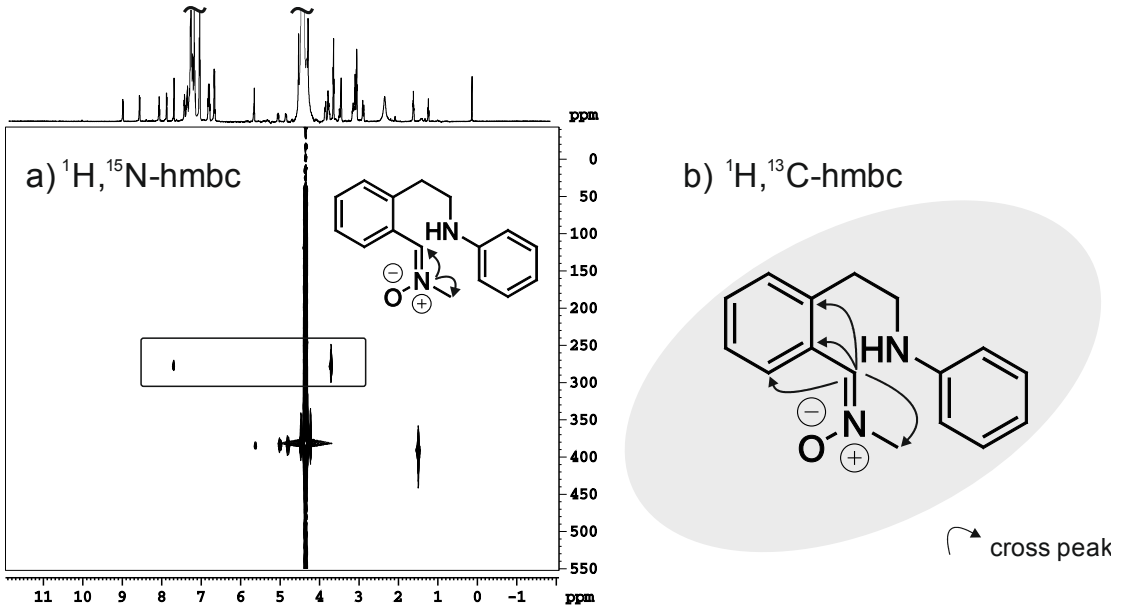

Figure 3.11 ^{1}H,^{15}N-hmbc of the ring opened intermediate **10** using ^{15}N-labeled nitromethane in nitromethane-d_3 at 280 K (a) and ^{1}H,^{13}C-hmbc cross peak pattern of C1 depicted by arrows (b).

3.5.6.7 *N*-Methylhydroxylamine (14)

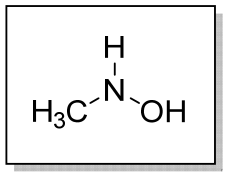

^{1}H NMR (600 MHz, NO_2Me-d_3, 280 K): δ [ppm] = 2.61 (s, br).

^{13}C NMR (150 MHz, NO_2Me-d_3, 280 K): δ [ppm] = 41.5.

^{15}N NMR (60 MHz, NO_2Me-d_3, 280 K): δ [ppm] = 118.3.

By phase sensitive ^{1}H,^{13}C-hsqc spectra a cross peak between 2.61 and 41.5 ppm (CH or CH_3 group) was detected. Additionally, this CH/CH_3-groupe is bound to a nitrogen atom, as ^{1}H,^{15}N-hmbc spectra revealed a cross peak between 2.61 and 118.3 ppm. The amine and hydroxyl proton could not be observed due to fast exchange in water. The ^{15}N chemical shifts reported for hydroxylamine[132] and the downfield shift from primary to tertiary amines (see Figure 3.12) are in good agreement with the observed chemical shift and corroborate the assignment of the structure to *N*-methylhydroxylamine **14**.

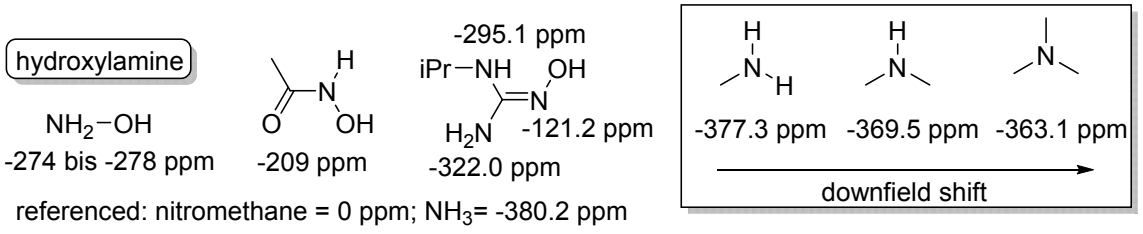

Figure 3.12 Literature reported ^{15}N chemical shifts and trends of hydroxylamines and amines.[132]

3.5.7 *In situ* illumination of the photocatalytic system

3.5.7.1 Reaction kinetic

The photocatalytic CDC reaction of THIQ **1** (50 mM) and nitromethane-d_3 **5a** was monitored *in situ* by NMR spectroscopy according to general procedure A. A ^{1}H NMR reaction profile of the initial 40 minutes of the reaction is depicted in Figure 3.13, additionally showing the curves of THIQ iminium ion **2** and THIQ peroxide **11**. The concentrations of THIQ iminium ion **2** and THIQ-OOH **11** are below 1 mM and rapidly decrease during irradiation. THIQ dimer **9** and a ring opened THIQ intermediate **10** were formed as intermediates which are converted to the product **6a** during the reaction time course.

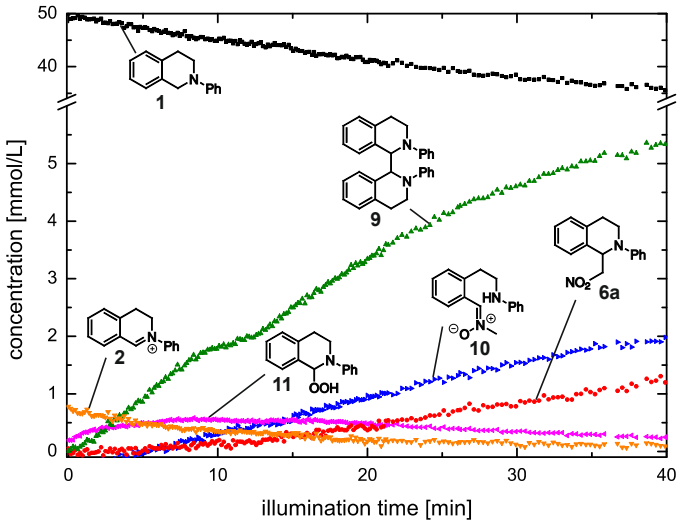

Figure 3.13 ^{1}H NMR reaction profile of the initial 40 minutes of the CDC reaction of THIQ **1** (50 mM) and $Ru(bpy)_3Cl_2$ (10 mol%) in nitromethane-d_3 under continuous irradiation with blue LEDs at 300 K.

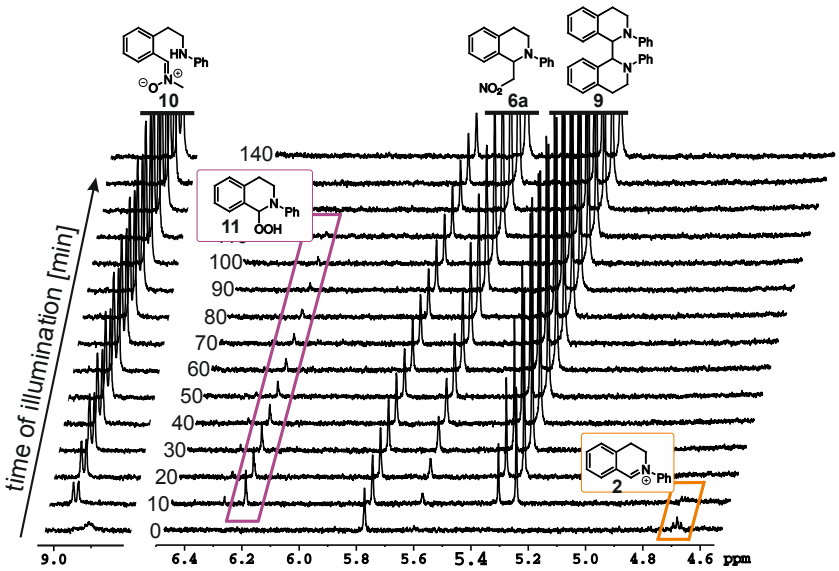

Figure 3.14 A row of stacked ^{1}H NMR spectra showing the first 2.5 h of the aza-Henry reaction of 50 mM THIQ **1** and nitromethane **5a** via $Ru(bpy)_3Cl_2$ (10 mol%) catalyst in nitromethane-d_3 under continuous irradiation with blue LEDs at 300 K.

Figure 3.13 and Figure 3.14 show the fast decrease of THIQ iminium ion **2** accompanied by the formation of THIQ peroxide **11** followed by its decrease as well.

3.5.7.2 Light on-off study (*in situ*)

Light on-off studies were performed inside the spectrometer (see Figure 3.15) according to general procedure A.

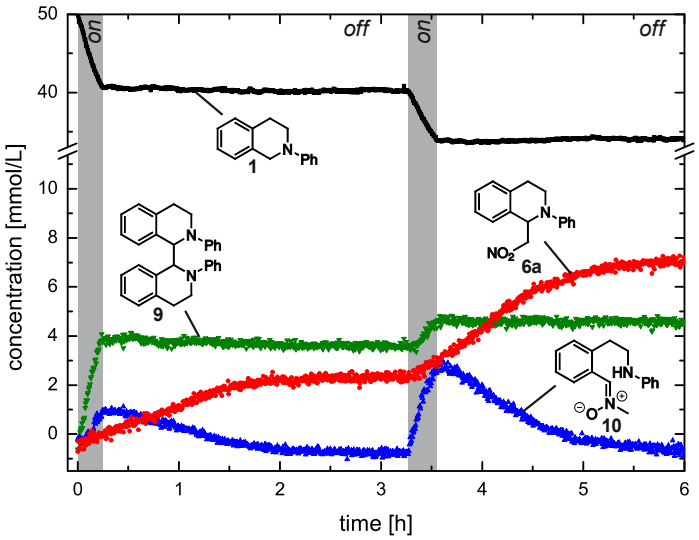

Figure 3.15 ^{1}H NMR reaction profile of a light on-off study of the CDC reaction of THIQ **1** and nitromethane-d_3 **5a**. The sample was *in situ* alternatingly irradiated for 15 minutes and kept in the dark inside the spectrometer for 3 h.

The sample was alternatingly illuminated for 15 minutes and then kept in the dark. While the sample was irradiated with blue LEDs the concentration of THIQ **1** decreased and the concentrations of THIQ dimer **9**, ring opened intermediate **10** and coupling product **6a** increased. In the absence of light the concentration of THIQ **1** and THIQ dimer **9** remained constant. In contrast, the ring opened intermediate **10** is fully converted to the product **6a** in the dark. The rate of the product formation stays constant as long as the ring opened intermediate **10** is present in the reaction mixture. After full consumption of the intermediate **10** the formation of the product **6a** drops close to zero. By this experiment we could show, that the ring opened intermediate **10** is a direct precursor for the product formation, without the need of further activation by light.

3.5.8 *Ex situ* illumination of the photocatalytic system

3.5.8.1 Reaction kinetic

When the *ex situ* illuminated kinetic is repeated using octamethylcyclotetrasiloxane (OMS) as internal standard the linear product formation became even more obvious. In the first hour of the reaction the product **6a** formation gradient is linear, resulting in an exponential curve and complete conversion to product **6a** after 4 h. However, the application of OMS lead to reduced concentrations of THIQ-OOH **11** and open intermediate **10** in contrast to the reaction kinetic under standard conditions, see Figure 3.16.

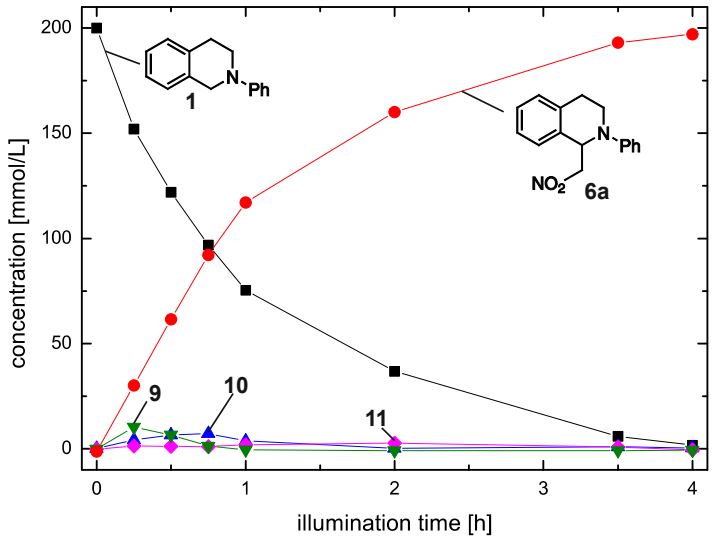

Figure 3.16 ^{1}H NMR reaction kinetic of THIQ **1** (200 mM) and $Ru(bpy)_3Cl_2$ (1 mol%) in nitromethane-d_3 under irradiated with blue LEDs at 23°C using octamethylcyclotetrasiloxane as internal standard.

3.5.8.2 Light on-off study (*ex situ*) and temperature dependence of the dark reaction

A sample containing THIQ **1** and $Ru(bpy)_3Cl_2$ 1mol% in nitromethane-d_3 was illuminated external according to general procedure B under air for 15 min and then the reaction profile was monitored in the dark by ^{1}H NMR. Furthermore the influence of the temperature was investigated by comparing the kinetics in the dark at 291 K and 300 K (Figure 3.17). The THIQ peroxide **11** and the ring opened intermediate **10** are converted into the stable product **6a** in the dark. The slope of THIQ-OOH **11** is steeper decreasing, suggesting a faster product forming reaction. The reaction rate is accelerated by increasing temperatures. The concentration of the dimer **9** remained constant without illumination at both temperatures as observed before.

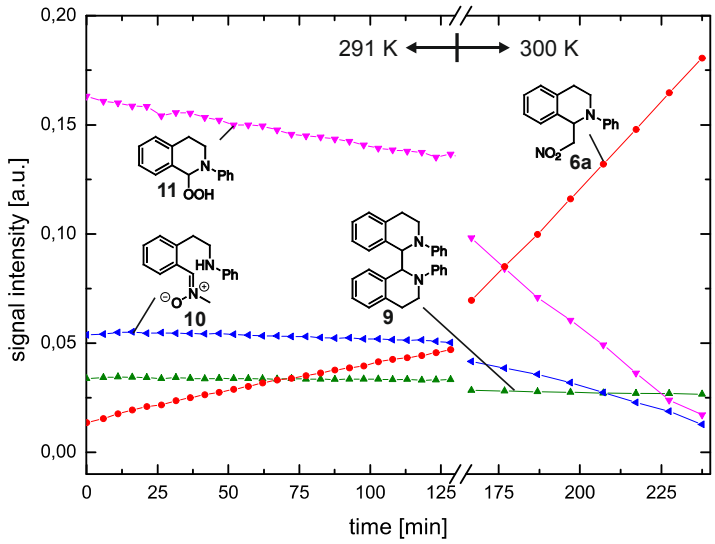

Figure 3.17 ^{1}H NMR kinetic of the light independent conversion to product **6a** at 291 K and 300 K. A sample of THIQ **1** and $Ru(bpy)_3Cl_2$ (1 mol%) in nitromethane-d_3, external irradiated with blue LEDs for 15 minutes at 23°C, is transferred into the NMR and a ^{1}H NMR reaction profile is measured in the dark.

3.5.9 Background reaction in the dark

At the initial minutes after mixing THIQ **1** and nitromethane **5a**, we could observe the THIQ iminium ion **2** independent of the presence or absence of photocatalyst, air or light. The THIQ iminium ion **2** was already detectable when the sample was prepared directly at the spectrometer in the dark (elapsed time before measurement 60-90 s). However the background reaction in the dark is slow and results in negligible yields after 20 h. Due to the formation independent from light, air and photocatalyst we assume a direct interaction of nitromethane and THIQ **1** in form of redox (EDA complex) or acid-base equilibria.

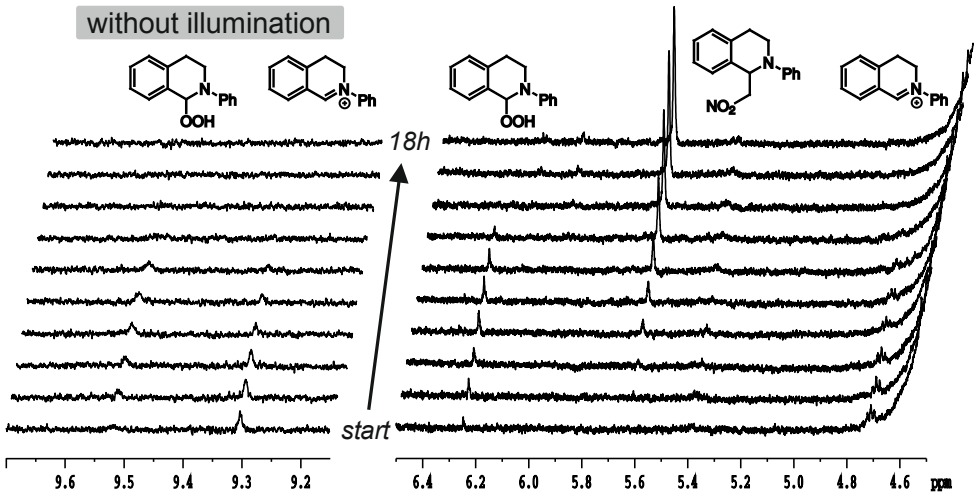

Figure 3.18 A row of stacked ^{1}H-NMR spectra (1 number of scans) of the aza-Henry reaction of 50 mM THIQ **1** and nitromethane-d_3 **5a** using 10 mol% $Ru(bpy)_3Cl_2$ in the dark at 300 K, monitored over a time of 18 h. Setup according to general procedure A.

The intermediate distribution in the dark in the presence of 10 mol% $Ru(bpy)_3Cl_2$ differs from the respective irradiated sample. In the absence of light no dimerization product **9** and ring opened intermediate **10** were formed. At the beginning of the dark reaction THIQ iminium ion **2** is detected. THIQ-OOH **11** (due to residual oxygen) arises with a short delay, followed by the coupling product **6a**, see Figure 3.18.

3.5.9.1 Solvent screening

Different solvents ($CDCl_3$, DMF-d_7, MeCN-d_3) were tested to gain more information about the solvent influence on the THIQ iminium ion **2** formation. THIQ **1** (50 mM) and the respective solvent were mixed in the dark and immediately measured (elapsed time before measurement 60-90 s). Then the photocatalyst $Ru(bpy)_3Cl_2$ was added to the solution and the samples were measured again in the dark at 298 K.

The THIQ iminium ion **2** could not be detected when nitromethane-d_3 was substituted by $CDCl_3$, DMF-d_7 or MeCN-d_3 in the absence of catalyst, indicating that nitromethane **5a** is directly involved in the THIQ iminium ion **2** formation. In the presence of $Ru(bpy)_3Cl_2$ the iminium ion **2** was observed in DMF-d_7, however in concentration of < 0.5%.

Table 3.2 Influence of solvents on the initial THIQ iminium ion **2** formation.

Entry	Substrate	Catalyst	Solvent	Iminium ion 2 (%)	Product 6a (%)
1	THIQ **1**	No	$CDCl_3$	n.d.	n.d.
2	THIQ **1**	No	DMF-d_7	n.d.	n.d.
3	THIQ **1**	No	MeCN-d_3	n.d.	n.d.
4	THIQ **1**	$Ru(bpy)_3Cl_2$	$CDCl_3$	n.d.	n.d.
5	THIQ **1**	$Ru(bpy)_3Cl_2$	DMF-d_7	<0.5	n.d.
6	THIQ **1**	$Ru(bpy)_3Cl_2$	MeCN-d_3	n.d.	n.d.

n.d. = not detected

3.5.9.2 Redox reaction

In order to determine the feasibility of an electron transfer from THIQ **1** to nitromethane **5a** the oxidation and reduction potential were measured by cyclic voltammetry.

CV measurements

Cyclic voltammetry measurements were performed with the three-electrode potentiostat galvanostat PGSTAT302N from Metrohm Autolab. A glassy carbon working electrode and a platinum counter electrode were used. As reference electrode a silver wire was used. The potentials were given relative to the Fc/Fc^+ redox couple with ferrocene as internal standard. The control of the measurement instrument, the acquisition and processing of the cyclic voltammetric data were performed with the software Metrohm Autolab NOVA 1.10.4.

The measurements were carried out as follows: 6 mL of a 0.1 M solution of the supporting electrolyte in the respective solvent was placed in the measuring cell and the solution was degassed by a stream of argon for 5 min. After measuring of the baseline the electroactive species was added (1 mL of 0.01 M for THIQ **1** and 1 µL (neat) for nitromethane) and the solution was degassed by argon purge for 5 min. The cyclic voltammogram was recorded with one to three scans at a scan rate of 50 mV/s. Finally ferrocene (2.2 mg, 12 µmol) was added to the solution. The solution was degassed by argon purge for another 5 min and the measurement was performed again with one to three scans. The potentials were converted to SCE according to V. V. Pavlishchuk and A. W. Addison.[133]

Table 3.3 Redox potentials of nitromethane **5a** and THIQ **1**.

Analyte	Supporting Electrolyte	Solvent	E vs. SCE [V][a]
Nitromethane **5a**	Tetrabutylammonium hexafluorophosphate	MeCN	-1.65
THIQ **1**	Tetrabutylammonium hexafluorophosphate	$MeNO_2$	+0.83

[a] Irreversible peak potentials.

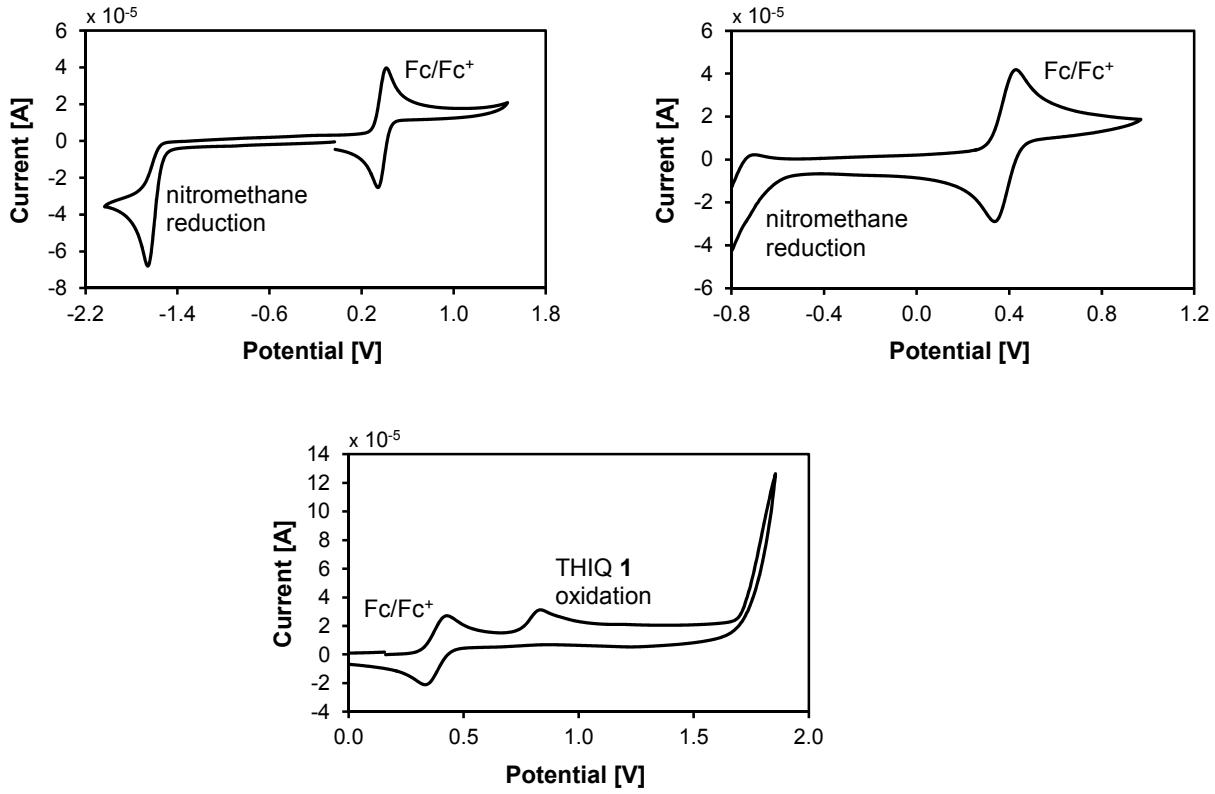

Figure 3.19 Cyclic voltammograms of (a) nitromethane **5a** (solvent, electrochemical window), (b) nitromethane **5a** (1 µL) in MeCN, (c) THIQ **1** in nitromethane **5a**. Tetrabutylammonium hexafluorophosphate was used as supporting electrolyte. The potentials are given in Volt vs. SCE. Ferrocene was used as internal standard.[133]

The electron transfer from THIQ **1** to nitromethane **5a** is an endothermic redox reaction. Nevertheless it is reported that follow-up reactions or transformations can kinetically drive a thermodynamically unfavorable process against a potential gradient toward product. This concept is exploited in the application of mediators in electroorganic synthesis.[134] As a rule of thumb, for outer-sphere electron transfer processes potential differences of up to 0.5 V and for inner-sphere electron transfer processes even up to 2.0 V can be overcome. Higher potential differences results in inefficient reactions with slow reaction rates. The formation of charge transfer complexes (EDA complexes) prior to the electron transfer step are typical examples for inner-sphere electron transfer processes. Typical fast and thermodynamically favorable follow-up reactions are for example the deprotonation of radical cations.[134] As we anticipate the formation of a EDA complex between nitromethane **5a** and THIQ **1** as well as a subsequent deprotonation/hydrogen atom abstraction step of the THIQ radical cation $\mathbf{1}^{+\bullet}$, we rationalize the background reaction due to a redox initiated process with a fast follow-up reaction under the limitations described above. However, the potential difference of the substrates is still high, which is reflected in the low yield of the background reaction in the dark. We assume that for the light induced aza-Henry coupling the initial electron transfer within the EDA complex is promoted by visible light irradiation resulting in an increased rate (see 3.3 and 3.5.10). The observation that oxygen is mandatory for fast conversion of the light induced aza-Henry reaction can be rationalized by a subsequent electron transfer from reduced

nitromethane to molecular oxygen producing superoxide radical anion, which can undergo follow up-reactions by H•-abstraction.

3.5.9.3 Acid-base equilibrium

Nitromethane **5a** and THIQ **1** are in an acid-base equilibrium, producing the aci-anion of nitromethane and protonated THIQ. Comparing the pKa values for nitromethane and protonated THIQ, the equilibrium resides strongly on the side of the neutral species. Gupta and coworker[135] described possible follow-up reactions of the nitromethane aci-anion with nitromethane itself to produce radical species (depicted in Scheme 3.11), which can serve as possible radical starter in chain processes. The formation of radical starter can be an explanation for the observed background reaction in the dark.

Scheme 3.11 Generation of radical starter by acid-base equilibrium.[135,136]

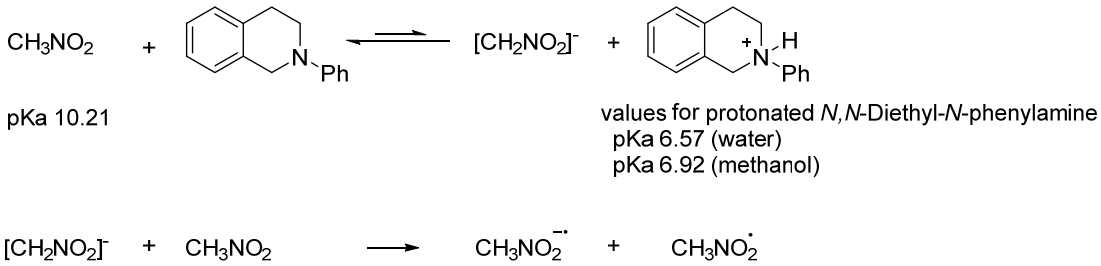

The aci-anion form of nitromethane has a characteristic ^{13}C signal at 102.8-104.9 ppm.[80] We performed NMR investigations in order to visualize the proton transfer reaction. Despite the use of ^{13}C labeled nitromethane and prolonged measuring time, the peak of the aci-anion could not be detected, indicating that the proton transfer either didn`t proceed or that the concentration of the aci-anion is below the detection limit of the NMR. A downfield shift from THIQ to the protonated form[83] could not be monitored either. We assume this is due to concentration below the detection limit.

3.5.10 Light induced CDC reaction

3.5.10.1 Reaction kinetic

The application of octamethylcyclotetrasiloxane as internal standard leads to a reduced THIQ peroxide **11** formation (compare Figure 3.16). However, the shapes of the curves are not affected, showing a reproducible reaction profile.

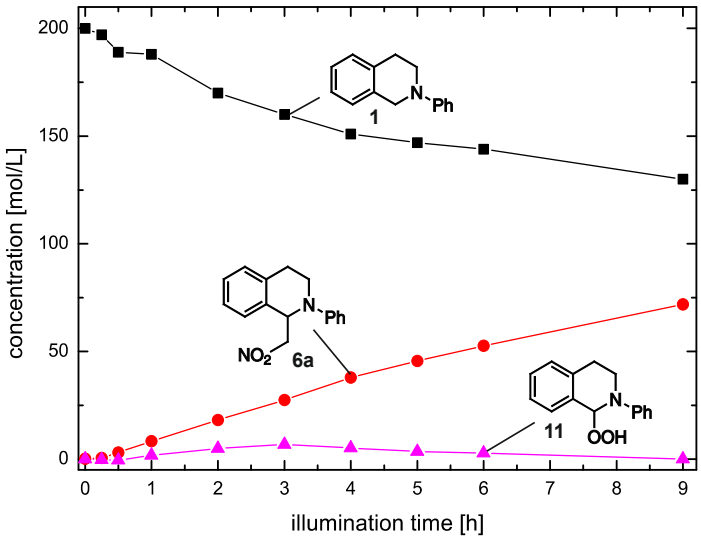

Figure 3.20 ^{1}H NMR reaction kinetic of THIQ **1** (200 mM) in nitromethane-d_3 under irradiated with blue LEDs at 23°C using octamethylcyclotetrasiloxane as internal standard. Conditions and setup according to general procedure B.

3.5.10.2 Reaction conditions

Performing the aza-Henry reaction without catalyst shows that the reaction conditions are decisive for an effective product formation. The exclusion of light or air results in reduced reaction rates and negligible product formation (Table 3.4).

Table 3.4 Summary of different reactions and reaction conditions.

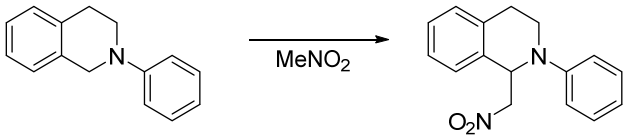

Entry	t [h]	Yield [%]	Light Source	Catalyst	Conditions
1	18	6	-	10 mol% $Ru(bpy)_3Cl_2$	0.05 M, 300 K, *in situ* (anaerobic)
2	20	6	LEDs (blue)	-	0.05 M, 300 K, *in situ* (anaerobic)
3	20	7	LEDs (blue)	-	0.4 M, r.t., *ex situ*, argon atmosphere (glovebox)
4	15	7	LEDs (blue)	-	0.05 M, 300 K, *in situ* (anaerobic), 7equiv. H_2O_2
5	24	80	LEDs (blue)	-	0.2 M, 291 K, *ex situ*, air
6	20	2	-	-	0.2 M, 291 K, *ex situ*, air

3.5.10.3 Light on-off studies (*ex situ*)

A sample of THIQ **1** in nitromethane-d_3 was irradiated for 20 minutes with blue LEDs according to the general procedure B. Within the irradiation period THIQ peroxide **11** and product

6a were formed. Then ^{1}H spectra of the sample were measured in the dark in variable time intervals and the correlation between THIQ **1**, product **6a** and the intermediate THIQ-OOH **11** was investigated. Figure 3.21 shows the proton kinetic depicting the decrease of THIQ **1** and THIQ-OOH **11**and the increase of H_2O_2 and the coupling product **6a** in the dark.

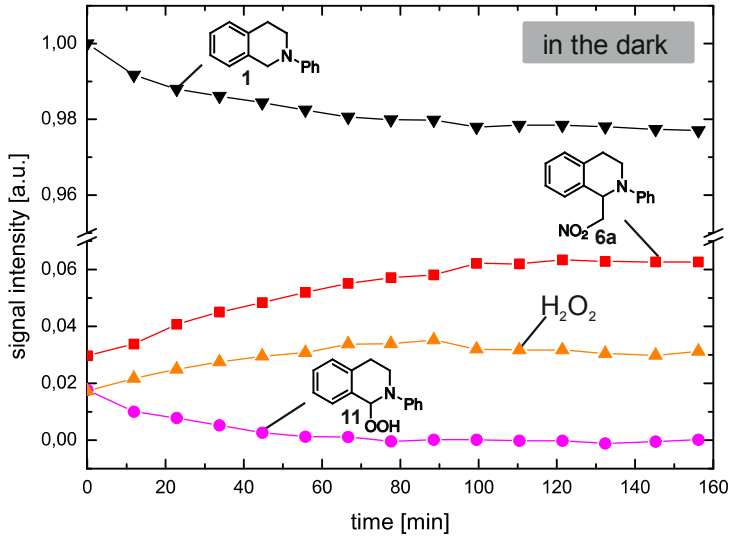

Figure 3.21 A mixture of THIQ **1** (200 mM) and nitromethane-d_3 was external illuminated for 20 minutes, then a row of ^{1}H spectra was measured *in situ* at 300 K in the dark.

A sample of THIQ **1** in nitromethane-d_3 was irradiated for 20 minutes with blue LEDs according to the general procedure B. Within the irradiation period THIQ peroxide **11** and product **6a** were formed. Then ^{1}H spectra of the sample were measured in the dark in variable time intervals and the correlation between THIQ **1**, product **6a** and the intermediate THIQ-OOH **11** was investigated. Figure 3.21 shows the proton kinetic depicting the decrease of THIQ **1** and THIQ-OOH **11** and the increase of H_2O_2 and the coupling product **6a** in the dark.

3.5.10.4 Light intensity

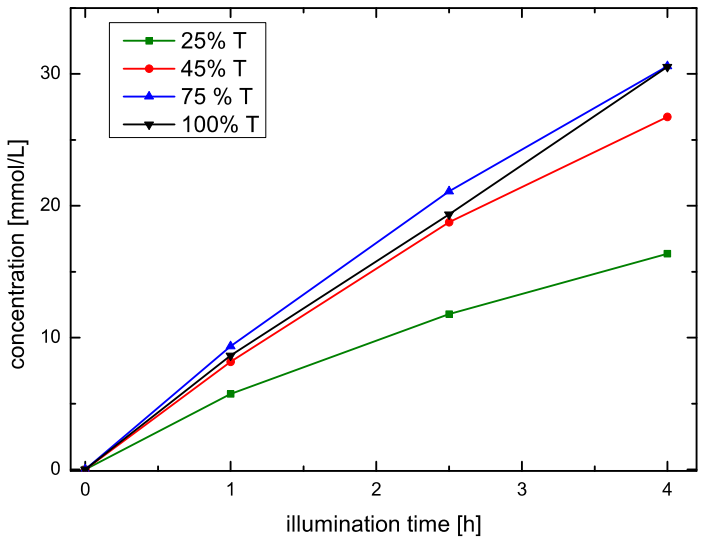

Figure 3.22 Dependence of the formation rate of product **6a** from the light intensity by application of filters with defined transmission.

In order to display the effect of the light intensity on the reaction rate different filters with defined transmission were placed between the reaction vessel and the blue LED. The reactions were prepared according to general procedure B. A correlation between the intensity of the LED and rate could be observed (see Figure 3.22). A comparison of the curves indicates that the system reached saturation between 45 and 75% transmission.

3.5.10.5 UV/Vis-Measurements

In order to rationalize the high visible light induced background reaction we investigated the spectroscopic characteristics of the single components and the reaction mixture. Figure 3.23 depicts the absorption spectra of THIQ **1** (0.4 mM in MeCN, pathlength d = 2 mm) and nitromethane (200 mM in MeCN, pathlength d = 2 mm) at UV-Vis concentrations and the emission spectra of the applied light sources (see 3.5.3 for specification of the light sources). The absorption spectra of the single components and the emission of the light source showed no overlap. Upon mixing the pure white crystalline THIQ **1** with nitromethane **5a**, a solution with a stable fade pale yellow color was obtained. The absorption spectrum of THIQ **1** in nitromethane **5a** at the reaction concentration (200 mM and 50 mM, pathlength d = 2 mm) shows a tailing band, which overlaps with the emission spectra of the light source, as shown exemplary for the blue and green LED (Figure 3.24). We assume the formation of an EDA complex between THIQ **1** and nitromethane **5a**. Andrabi *et al.* described the formation of weak 1:1 molecular CT complexes of nitromethane with different *N,N*-dialkylanilines (*N,N*-diethylaniline: λ_{CT} = 377 nm, K(25°C) = 0.31 l mol^{-1}) a structural motif, which is present in THIQ **1**. Based on the UV-Vis measurements we assume that the peak of the EDA band is below 400 nm. Attempts to spectroscopically isolate the EDA band failed, which we ascribe to the high UV cut-off nitromethane (L_0: >400 nm, L_1: 380 nm).

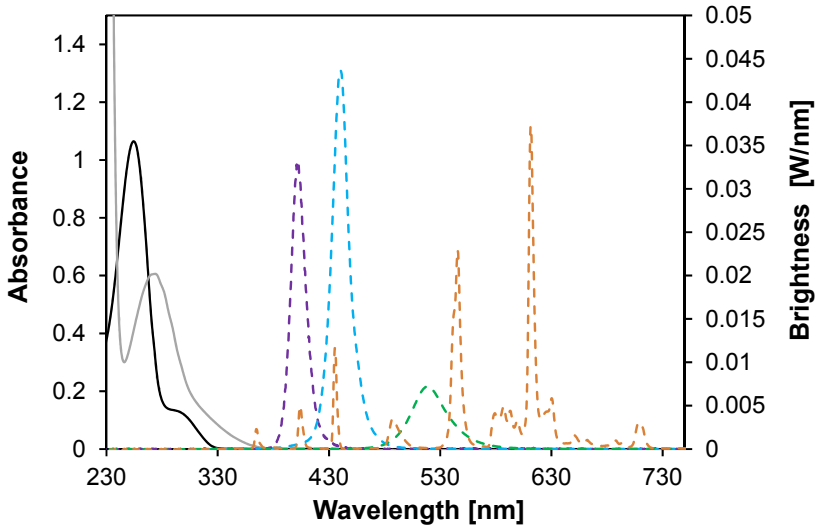

Figure 3.23 Absorption spectrum of THIQ **1** in MeCN (0.4 mM, d=2mm, solid black line) and nitromethane in MeCN (200 mM, d=2mm, solid grey line) at UV-Vis concentrations. Emission spectrum of high power LEDs with peak wavelength of 400 nm (dashed purple line), 440 nm (dashed blue line), 520 nm (dashed green line) and an energy-saving light bulb (dashed orange line).

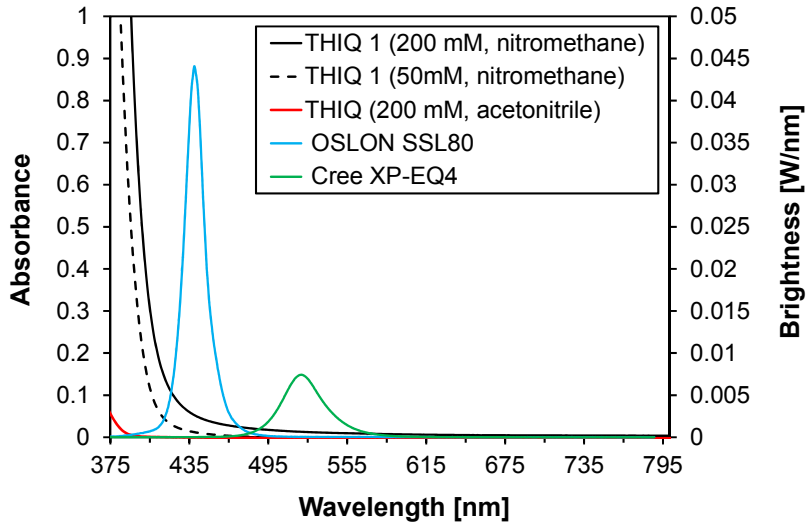

Figure 3.24 Absorption spectrum of THIQ **1** in nitromethane **5a** (200 mM, d=2mm, solid black line; 50 mM, d=2mm, dashed black line) and in acetonitrile (200 mM, d=2mm, solid red line) at the reaction concentrations and emission spectra of the applied light sources.

3.5.11 ESR investigations

In order to investigate the involved active oxygen species ESR measurements were performed. DMPO (5,5-dimethyl-1-pyrroline*N*-oxide) was used as probe for superoxide radical anion.[37,41,42,137]

3.5.11.1 General procedure

For ESR measurements concentrations (THIQ **1** (1.5 x 10^{-3} mol/L), DMPO (2 x 10^{-2} mol/L),) and $Ru(bpy)_3Cl_2$ (1.0 x 10^{-4} mol/L) in nitromethane) according to Wu *et al*.[37] were used. The samples were kept in the dark and saturated with oxygen before measuring. The samples were measured at room temperature in the dark and during *in situ* irradiation in the ESR device with blue LEDs.

3.5.11.2 Photocatalysed CDC reaction

In the dark no $O_2^{\bullet-}$ is formed (Figure 3.25 a and c). Upon irradiation with blue LEDs in the presence of THIQ (Figure 3.25 d) $O_2^{\bullet-}$ is generated as expected by the proposed mechanism. The superoxide radical anion is also formed in the absence of THIQ (Figure 3.25 b), as the adduct of $O_2^{\bullet-}$ and DMPO could be detected by ESR. It is reported that oxygen can quench the excited state of $Ru(bpy)_3^{2+}$ not only by energy transfer, but also by electron transfer generating $O_2^{\bullet-}$ and the corresponding $Ru(bpy)_3^{3+}$ species.

In the dark no $O_2^{\bullet-}$ is formed (Figure 3.25 a and c). Upon irradiation with blue LEDs in the presence of THIQ (Figure 3.25 d) $O_2^{\bullet-}$ is generated as expected by the proposed mechanism. The superoxide radical anion is also formed in the absence of THIQ (Figure 3.25 b), as the adduct of $O_2^{\bullet-}$ and DMPO could be detected by ESR. It is reported that oxygen can quench the excited state of $Ru(bpy)_3^{2+}$ not only by energy transfer, but also by electron transfer generating $O_2^{\bullet-}$ and the corresponding $Ru(bpy)_3^{3+}$ species.

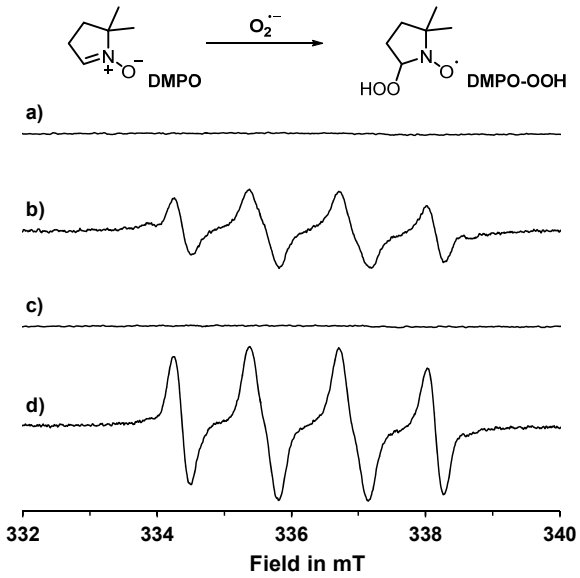

Figure 3.25 (a) and (b): ESR spectra of a solution of $Ru(bpy)_3Cl_2$ (1.0×10^{-4} molL^{-1}) and DMPO (2.0×10^{-2} molL^{-1}) in air-saturated nitromethane in the dark (a) and under the irradiation with blue LEDs (b); (c) and (d): ESR spectra of a solution of THIQ (1.5×10^{-3} molL^{-1}), $Ru(bpy)_3Cl_2$ (1.0×10^{-4} molL^{-1}) and DMPO (2.0×10^{-2} molL^{-1}) in air-saturated nitromethane in the dark (c) and under the irradiation with blue LEDs (d).

3.5.11.3 Light induced CDC reaction

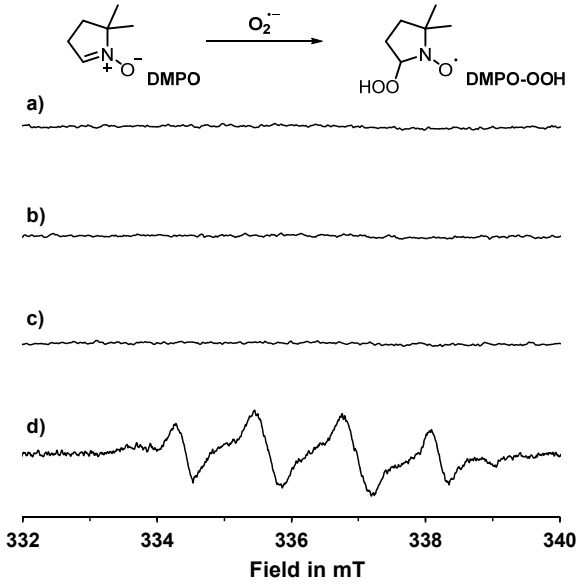

Figure 3.26 (a) and (b): ESR spectra of DMPO (2.0×10^{-2} molL^{-1}) in air-saturated nitromethane in the dark (a) and under the irradiation with blue LEDs (b); (c) and (d): ESR spectra of a solution of THIQ **1** (1.5×10^{-3} molL^{-1}) and DMPO (2.0×10^{-2} molL^{-1}) in air-saturated nitromethane in the dark (c) and under the irradiation with blue LEDs (d).

The formation of $O_2^{\bullet-}$ could be confirmed by ESR measurements using the radical trap DMPO. Control experiments showed that $O_2^{\bullet-}$ is only formed when both reaction partner are present in the solution upon irradiation with blue LEDs.

3.5.12 Investigations on the involvement of radical intermediates

3.5.12.1 Effect of radical inhibitors on reaction rate and profile

Scheme 3.12 Photocatalyzed CDC of nitromethane **5a** with THIQ **1** in the presence of the radical inhibitor TEMPO.

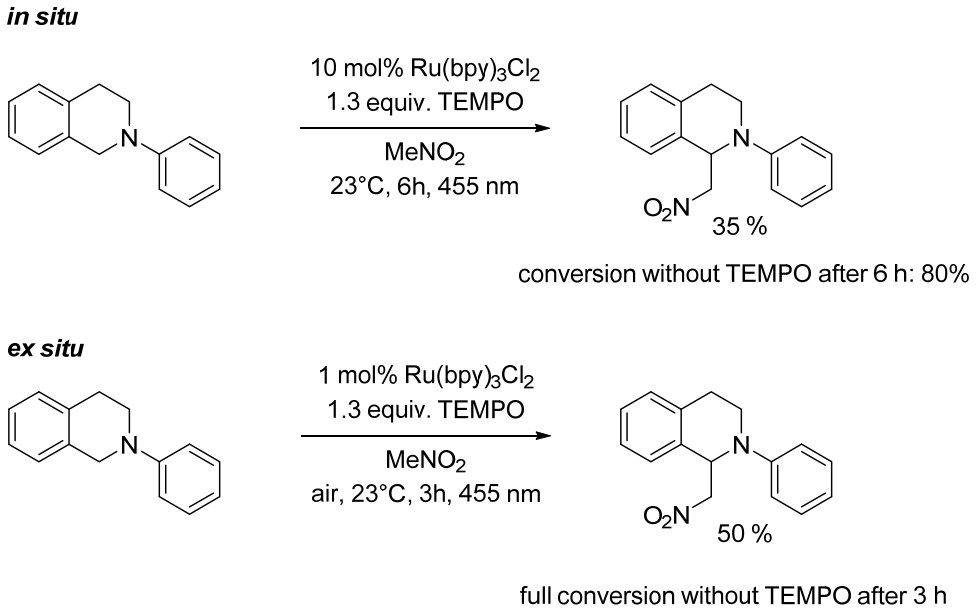

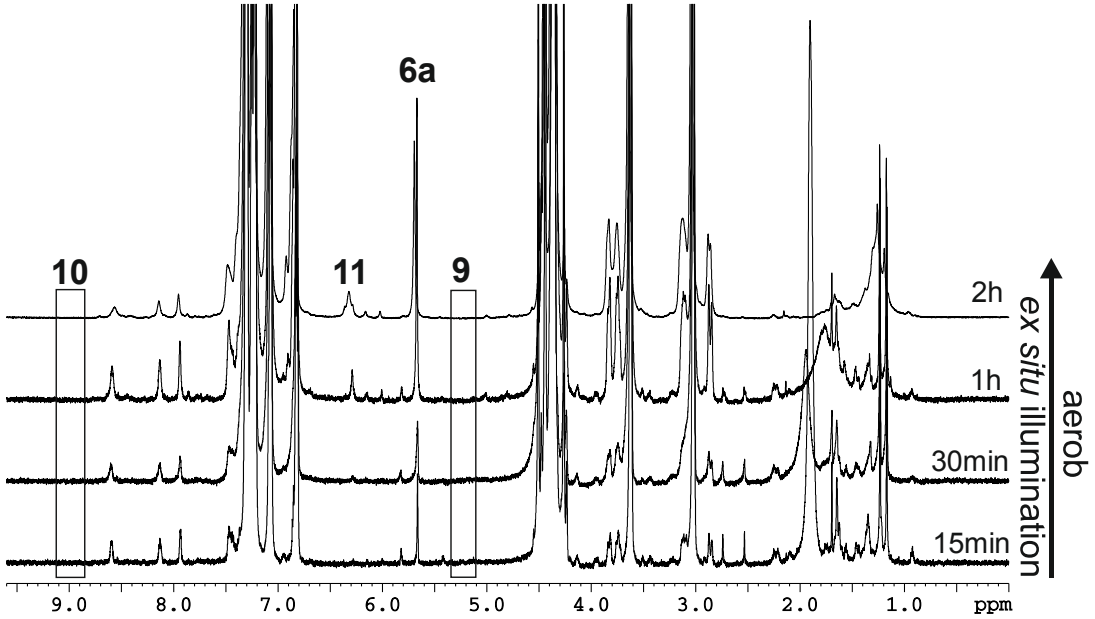

Figure 3.27 ^{1}H NMR spectra of the aerob photocatalyzed CDC of nitromethane **5a** with THIQ **1** in the presence of the radical inhibitor TEMPO under continuous illumination with blue LEDs.

The yield of the aza-Henry reaction in the absence and presence of TEMPO (1.3 equiv.) was compared after 6 h for the *in situ* irradiation (general procedure A) and after 3 h for the *ex situ* irradiation (general procedure B). The addition of 1.3 equiv. of TEMPO to the reaction

mixture slows down the reaction in both cases. Under *in situ* conditions only 35 % of the product **6a** is formed after 6 h compared to 80%. For *ex situ* conditions 50 % instead of full conversion was obtained after 3 h in the presence of TEMPO. The decrease in rate and yield upon TEMPO addition indicates the involvement of a radical mechanism. Further, a ^{1}H NMR reaction kinetic in the presence of TEMPO was monitored open to air, see Figure 3.27. Under continuous illumination with blue LEDs the THIQ hydroperoxide **11** as well as the product **6a** increase during the reaction. In contrast, the dimer **9** and the ring opened intermediate **10** were not detected at all.

Scheme 3.13 Light-induced CDC of nitromethane **5a** with THIQ **1** in the presence of the radical inhibitors TEMPO and BHT.

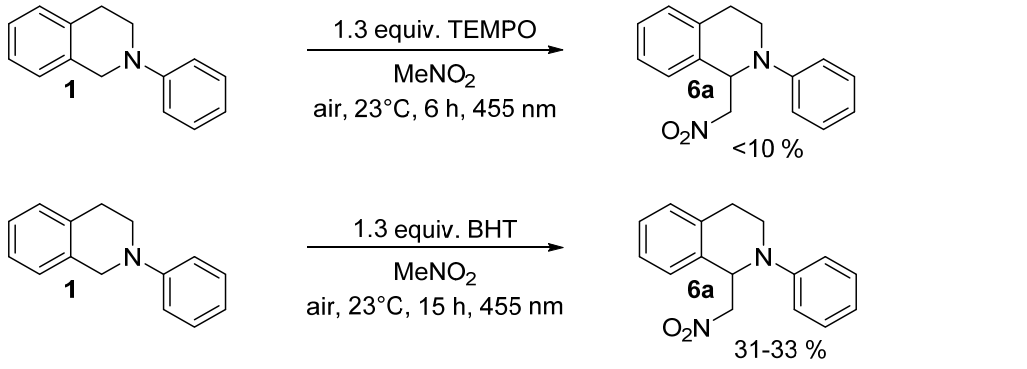

The influence of radical inhibitors TEMPO and BHT on rate and yield of the photoinduced CDC of THIQ **1** and nitromethane **5a** was investigated. The conversion of the aza-Henry reaction in the absence and presence of TEMPO (1.3 equiv.) was compared after 6 h. In the sample without TEMPO the ratio between THIQ/product is 46:54, in the sample with TEMPO THIQ/product 93:7. Almost no degradation products were detected in the sample containing TEMPO. TEMPO slowed down the reaction rate remarkably. Due to the intense red color of TEMPO, the decrease in rate could also be explained by light absorption. In order to exclude this effect we repeated the experiment with the colorless radical inhibitor BHT. Without BHT after 15 h of illumination 62-65% product were formed, with BHT (1.3 equiv.) only 31-33%. The decrease in rate and yield upon addition of radical inhibitors indicates the involvement of a radical mechanism.

3.5.12.2 Radical capturing experiments (TEMPO trapping of radical reaction intermediates)

Photocatalytic system

In a 5 mL crimp cap vial equipped with a magnetic stirring bar THIQ **1** (33.5 mg, 0.16 mmol, 1 equiv.), $Ru(bpy)_3Cl_2$ (6 mg, 0.008 mmol, 0.05 equiv.) and 2,2,6,6-tetramethylpiperidinyloxyl (TEMPO) (32.5 mg, 0.21 mmol, 1.3 equiv.) were dissolved in nitromethane (0.20 mmol/mL). The resulting mixture was irradiated through the vial's plane bottom side with blue LEDs for 5 h. The temperature was kept constant at 23 °C with a cooling device connected to a thermostat. After irradiation the reaction mixture was submitted to mass spectrometry (LC-MS) without any further work-up.

Light induced aza-Henry reaction

In a 5 mL crimp cap vial equipped with a magnetic stirring bar THIQ **1** (33.5 mg, 0.16 mmol, 1 equiv.) and TEMPO (32.5 mg, 0.21 mmol, 1.3 equiv.) were dissolved in nitromethane (0.20 mmol/mL). The resulting mixture was irradiated through the vial's plane bottom side with blue LEDs for 7 h. The temperature was kept constant at 23 °C with a cooling device connected to a thermostat. After irradiation the reaction mixture was submitted to mass spectrometry (LC-MS) without any further work-up.

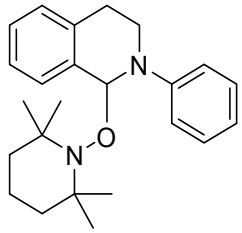

Chemical Formula: $C_{24}H_{32}N_2O$
Exact Mass: 364,2515
Molecular Weight: 364,5330
MS (ESI): m/z = 365.26 (MH^+)

Photocatalytic system

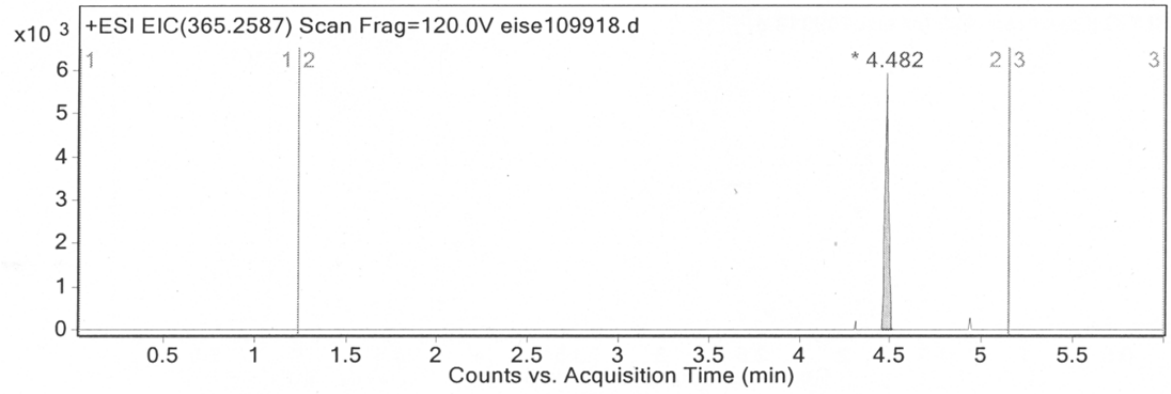

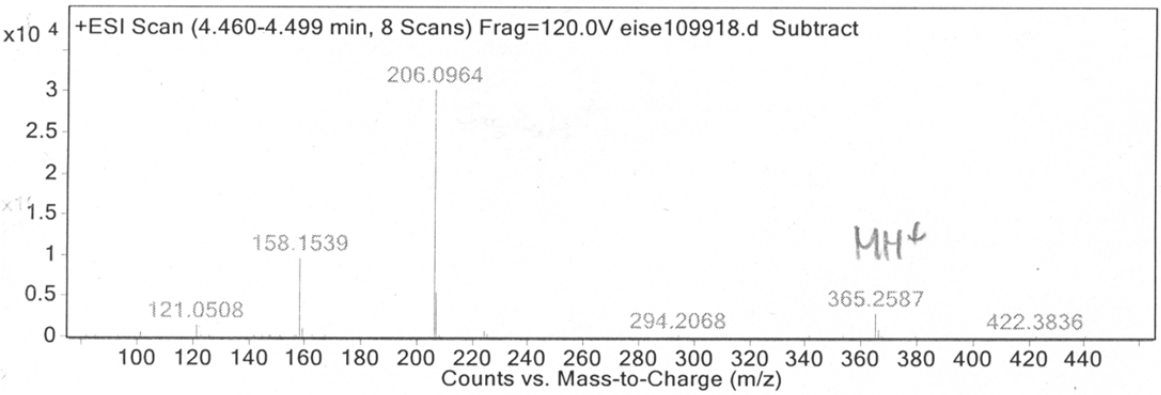

Light induced aza-Henry reaction

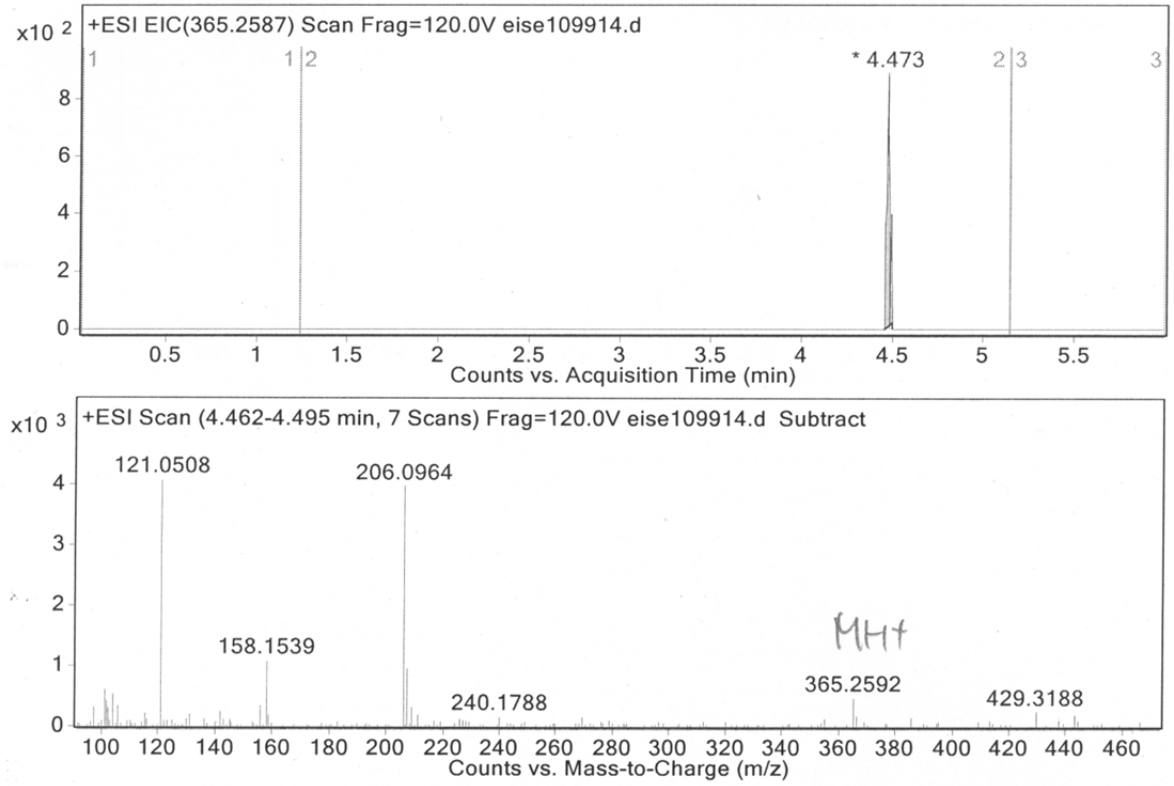

3.5.13 Photocatalyzed aza-Henry reaction – Literature overview

The visible light induced functionalization of tertiary amines, especially the formation of β-nitrosamine by the aza-Henry reaction is one of the most exploited photocatalytic transformations. A large variety of visible light absorbing photocatalysts (Figure 3.28) have been used for the cross-dehydrogenative coupling (CDC) aza-Henry reaction: Metal complexes, such as ruthenium, iridium, palladium, platinum, cobalt or copper complexes,[28,32–35] organic dyes,[37,38,40–42,138] heterogeneous photocatalyst like TiO_2, Cu_2O, CdS or mpg-C_3N_4,[44–47] metal organic frameworks (MOFs),[48,49] and polymeric photocatalysts.[50–53] Table 3.5 summarizes the applied conditions and yields of the different literature reported photocatalytic oxidative aza-Henry reactions. The literature overview does not cover the usage of $BrCCl_3$ as terminal oxidant[29,63] and approaches with microflow conditions.[30,31,43] Stephenson *et al.* noted that the photocatalytic reaction is accompanied by a slow photoinduced background reaction in the absence of the catalyst.[28] As the applied light source is often rather tailor-made to the absorption spectrum of the catalytic system or based on the already established equipment of the respective laboratory a multitude of different light sources was reported varying from high intensity mercury and xenon lamps with cut-off filter, light emitting diodes (LEDs) with narrow emission spectrum to low intensity household fluorescent bulbs with broad emission spectrum. Despite significant differences in the applied light source considering intensity and wavelength (see Table 3.5) the background reaction isn't described in some publications.

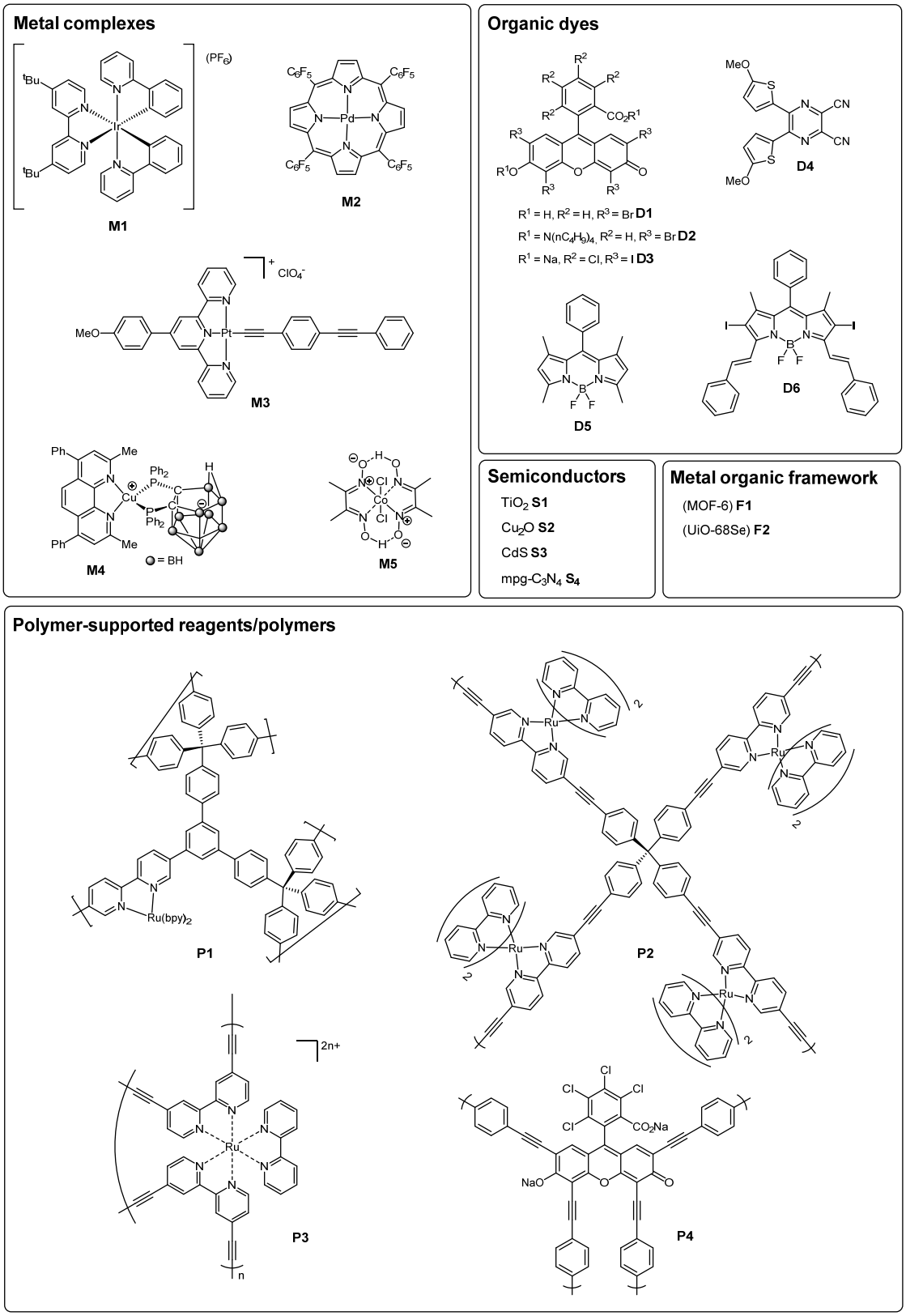

Figure 3.28 Selected literature reported photocatalysts for the aza-Henry reaction of THIQ **1** with nitromethane. ($Co(dmgH)_2Cl_2$ is formed *in situ* from $CoCl_2$ and dmgH; Cu_2O constitutes of mesoporous spheres with a large pore size; MOF-6: $[Ru(bpy)_2(dcbpy)]Cl_2$ (where bpy is 2,2′-bipyridine and dcbpy is 2,2′-bipyridine-5,5′-dicarboxylic acid) incorporated into a highly stable and porous $Zr_6O_4(OH)_4(bpdc)_6$ (UiO-67, bpdc = para-biphenyl-dicarboxylic acid) framework; UiO-68Se: A zirconium (IV)-based UiO-topological metal–organic framework containing benzoselenadiazole.[28,32–35,37,38,40–42,44–53,138]

Table 3.5 Literature overview Aza-Henry reaction.[a]

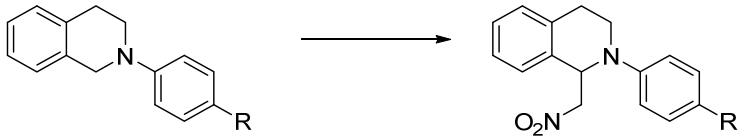

Entry	R	t [h]	yield [%][b]	light source	catalyst	conditions[c]
1[d]	H	10	92	**fluorescent lamp** (15 W, distance app. 10 cm)	**M1** (1 mol%)	0.25 M, rt, air
2[d]	OMe	18	96		**M1** (1 mol%)	0.25 M, rt, air
3[d]	H	180	83[q]		-	0.25 M, rt, air
4[d]	H	24	20 [q]		-	0.25 M, rt, air
5[d]	H	48	0[q]	No light	**M1** (1 mol%)	0.25 M, rt, air
6[e]	H	3	83[r]	**Xenon lamp** (300 W, λ > 400 nm)	**M2** (0.05 mol%)	0.08 M, O_2 bubbling
7[e]	OMe	3	80[r]		**M2** (0.05 mol%)	0.08 M, O_2 bubbling
8[f]	H		81	**blue LEDs** (1 W, λ = 450±10 nm, 145 lm @700 mA)	**M3** (0.25 mol%)	0.05 M, DMF, air, 3 equiv. $MeNO_2$, 2 equiv. $FeSO_4$
9[f]	Ome		83		**M3** (0.25 mol%)	0.05 M, DMF, air, 3 equiv. $MeNO_2$, 2 equiv.$FeSO_4$
10[e]	H	8	87	**Xenon lamp** (300 W, λ > 420 nm)	**M4** (1.5 mol%)	0.02 M, rt, O_2-sat. solution
11[e]	OMe	8	79		**M4** (1.5 mol%)	0.02 M, rt, O_2-sat. solution
12[e]	H	8	10[r]		-	0.02 M, rt, O_2-sat. solution
13[e]	H	8	0[r]	No light	**M4** (1.5 mol%)	0.02 M, rt, O_2-sat. solution
14[f]	H	24	83	**blue LEDs** (3 W, λ = 450±10 nm, 145 lm @700mA)	**M5**[s]	0.1 M, H_2O, air, 4 equiv. $MeNO_2$
15[g]	H	8	80	**green LEDs** (1 W, λ = 530±10 nm, 145 lm @700mA)	**D1** (2 mol%)	0.25 M, rt, air
16[g]	OMe	10	78		**D1** (2 mol%)	0.25 M, rt, air
17[g]	H	180	78		-	0.25 M, rt, air
18[g]	H	72	0	No light	**D1** (2 mol%)	0.25 M, rt, air
19[f]	H	4+12[t]	86	**high pressure mercury lamp** (500 W, λ > 450 nm)	**D2** (2 mol%)	0.02 M, rt, O_2
21[f]	OMe	4+12[t]	81		**D2** (2 mol%)	0.02 M, rt, O_2
22[f]	H	24	trace		-	0.02 M, rt, **Ar** atmosphere
23[h]	H	10	92	**green LEDs** (0.5-5 W)	**D3** (5 mol%)	0.1 M, rt
24[h]	H	20	0[q]	No light	**D3** (5 mol%)	0.25 M, rt
25[i]	H	5	95	**fluorescent lamp** (9W)	**D4** (0.1 mol%)	0.1 M, 28 °C, air
26[i]	OMe	5	95		**D4** (0.1 mol%)	0.1 M, 28 °C, air
27[f]	H	3	71 (80[r])	**white LEDs** (3W, 350 mA, radiometric power 80 mW)	**D5** (1 mol%)	0.05 M, rt, air
28[f]	OMe	3	73 (88[r])		**D5** (1 mol%)	0.05 M, rt, air
29[f]	H	3	9[r]		-	0.05 M, rt, air
30[f]	H	3	23[r]		**D5** (1 mol%)	0.05 M, rt, **no O_2**
31[f]	H	4	0[r]	No light	**D5** (1 mol%)	0.05 M, rt, air
32[j]	H	2	79	**Xenon lamp** (35 W, λ = 385 nm, 20 mW cm^{-2})	**D6** (1 mol%)	0.13 M, 20°C, air
33[j]	OMe	2-3	81		**D6** (1 mol%)	0.13 M, 20°C, air
34[j]	H	5	19		-	0.07 M, 20°C, air
35[k]	H	40	93	**fluorescent bulb**	**S1** (1 equiv.)	0.1 M, EtOH, 10 equiv.

36[k]	OMe	40	68	(11W, app. distance 3 cm, cold white, 6400 K)	**S1** (1 equiv.)	$MeNO_2$ 0.1 M, EtOH, 10 equiv. $MeNO_2$
37[l]	H	8	90	**blue LEDs** (4 W, 460 nm)	**S2**[u]	0.1 M, rt, O_2
38[l]	OMe	8	83		**S2**[u]	0.1 M, rt, O_2
39[l]	H	8	5		-	0.1 M, rt, O_2
40[g]	H	24	97[q]	**blue LEDs** (3 W, 440 nm)	**S3** (1 equiv.)	MeCN/$MeNO_2$ (1:2; v/v), N_2
41[m]	H	22-34	92	**energy saving bulb** (60 W)	**S4**[v]	0.25 M, MeCN, 5 equiv. $MeNO_2$, rt,O_2 (1 bar)
42[m]	OMe	22-34	89		**S4**[v]	0.25 M, MeCN, 5 equiv. $MeNO_2$, rt,O_2 (1 bar)
43[n]	H	12	86[q]	**fluorescent lamp** (26 W, distance 5-10 cm)	**F1** (1 mol %)	0.1 M, rt, air
44[n]	OMe	12	97[q]		**F1** (1 mol %)	0.1 M, rt, air
45[n]	H	12	19[q]		-	0.1 M, rt, air
46[n]	OMe	12	28[q]		-	0.1 M, rt, air
47[n]	H		< 5	No light	**F1**	0.1 M, rt, air
48[o]	H	4	90[r]	**blue LEDs** (3 W, λ_{max} = 450 nm)	**F2**[w]	0.1 M, rt, air
49[o]	OMe	4	88[r]		**F2**[w]	0.1 M, rt, air
50[o]	H	4	trace[r]		-	0.1 M, rt, air
51[o]	H	6	0[r]	No light	**F2**[w]	0.1 M, rt, air
52[n]	H	8	90[q]	**fluorescent lamp** (26W, distance app. 10 cm)	**P1** (0.2 mol%)	0.25 M, rt, air
53[n]	OMe	8	>99[q]		**P1** (0.2 mol%)	0.25 M, rt, air
54[n]	H	8	10[q]		-	0.25 M, rt, air
55[n]	H	8	<5[q]	No light	**P1** (0.2 mol%)	0.25 M, rt, air
56[n]	H	8	97[q]	**fluorescent lamp** (26W, distance app. 5 cm)	**P2** (0.2 mol%)	0.1 M, rt, air
57[n]	OMe	8	>99[q]		**P2** (0.2 mol%)	0.1 M, rt, air
58[n]	H	8	10[q]		-	0.1 M, rt, air
59[n]	OMe	8	19[q]		-	0.1 M, rt, air
60[n]	H	8	<5[q]	No light	**P2** (0.2 mol%)	0.1 M, rt, air
61[n]	H	8	85[x]	**fluorescent lamp** (26W, distance app. 5 cm)	**P3** (0.2 mol%)	0.1 M, rt, air
62[n]	OMe	8	90		**P3** (0.2 mol%)	0.1 M, rt, air
63[p]	H	15	95	**household bulb** (60 W)	**P4** (2 mol%)	0.5 M, rt, air
64[p]	OMe	15	97		**P4** (2 mol%)	0.5 M, rt, air
65[p]	H	15	0[q]	No light	**P4** (2 mol%)	0.5 M, rt, air

[a] Control experiments with irradiation in the absence of an absorbing catalyst and without light in the presence of the catalyst were included if mentioned in the original publication.

[b] Isolated yields, if not stated otherwise.

[c] $MeNO_2$ was used as solvent if not stated otherwise.

Data reported by: [d] Stephenson *et al.*[28]; [e] Che *et al.*[32,35]; [f] Wu *et al.*[33,34,37,41]; [g] König *et al.*[46,138]; [h] Tan *et al.*[38]; [i] Jiang *et al.*[40]; [j] Zhao *et al.*[42]; [k] Rueping *et al.*[44]; [l] Fan *et al.*[45]; [m] Antonietti *et al.*[47]; [n] Lin *et al.*[48,50–52]; [o] Wang *et al.*[49]; [p] Cooper *et al.*[53];

[q] Conversion calculated on basis of crude ^{1}H NMR analysis.

[r] The yields were determined by ^{1}H NMR spectroscopic analysis using an internal standard.

[s] $CoCl_2$ (8 mol%), dmgH (16 mol%)

[t] 4 h of irradiation + 12 h stirring in the dark.

[u] 2 mg catalyst / 0.15 mmol THIQ

[v] 15 mg catalyst / 0.25 mmol THIQ

[w] 4-5 mg catalyst / 0.1 mmol THIQ

[x] Low conversions to the product (<20%) were detected in the absence of either light or the catalyst.

3.6 Additional Findings

3.6.1 Aza-Henry Reaction

3.6.1.1 Influence of the $Ru(bpy)_3^{2+}$ Counter Ions

The chemical and photophysical properties of tris(2,2'-bipyridyl) ruthenium(II) complexes have been studied extensively since the last century.[139–142] In the last decades, the application of these catalysts became of high importance for chemical photocatalysis, due to the stability of the complexes at room temperature,[4] the good photoredox properties and its commercial availability. Several studies reported that $Ru(bpy)_3X_2$ (X= Cl^-, Br^-, NCS^-) complexes undergo photosubstitution under elevated temperatures, under acidic or alkaline conditions, in the presence of strong coordinating anions or in many organic solvents.[140,141,143–145] In contrast, the PF_6^- salt is proposed to be photoinert,[145,146] which is in accordance with our observations in DMF-d_7 and acetonitrile-d_3.[147] Despite the superiority of $Ru(bpy)_3(PF_6)_2$ regarding photostability, the chloride salt is preferentially used in photocatalysis,[6,11,12] e.g. in the aza-Henry reaction.[28,29,31] Surprised by this, we investigated the aza-Henry reaction in terms of the catalyst counter ion (Cl^- or PF_6^-).

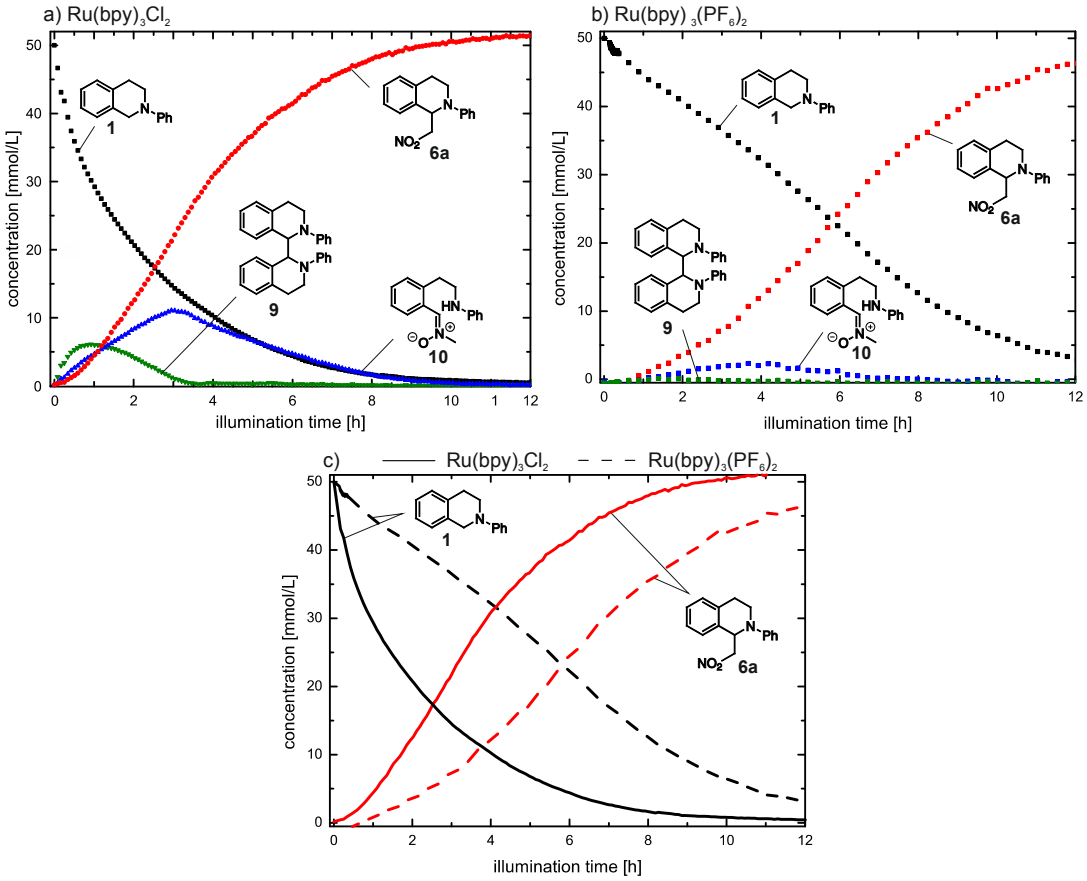

Figure 3.29 ^{1}H NMR kinetic, showing reduced reaction rates, together with reduced concentrations of the intermediates **9** and **10** for the $Ru(bpy)_3(PF_6)_2$ catalyzed reaction. Kinetic of the (a) $Ru(bpy)_3Cl_2$ (10 mol%) or (b) $Ru(bpy)_3(PF_6)_2$ (10 mol%) catalyzed aza-Henry reaction of THIQ **1** (50 mM) in nitromethane-d_3 at 300 K under illumination with blue light. (c) Product **6a** formation rates in the presence of $Ru(bpy)_3X_2$ at 300 K in nitromethane-d_3.

Anaerobic Reaction Profiles Samples containing THIQ **1** (50 mM) and $Ru(bpy)_3X_2$ (10mol%) in deuterated nitromethane-d_3 were monitored under anaerobic conditions and under continuous irradiation with blue light at 300 K. The ^1H NMR kinetic of the chloride salt, shown in Figure 3.29 a, has been discussed above in detail (refer to Figure 3.1 c). In contrast, the reaction profile of the $Ru(bpy)_3(PF_6)_2$ catalyzed reaction, monitored under otherwise stated conditions, showed significantly decreased intermediate concentrations and reaction rates, see Figure 3.29 b. The ring opened intermediate **10** only reached maximum concentrations of 5 mM for the hexafluorophosphate complex; in contrast to 11 mM for the chloride one. The dimer **9** concentration decreased close to the detection limit, in contrast to 6 mM for Cl^-. While the overall concentrations of the intermediates decreased for the hexafluorophosphate catalyst, the relative ratios of **9** and **10** remained constant.

For both photocatalytic systems a sigmoidal product **6a** formation curve was observed, see Figure 3.29 c. The rate of the $Ru(bpy)_3(PF_6)_2$ catalyzed reaction is approximately two-fold decelerated, in contrast to the chloride catalyst. After 6 h 50% of product **6a** were gained using $Ru(bpy)_3(PF_6)_2$, in contrast to 50% of product **6a** after 3 h for $Ru(bpy)_3Cl_2$. No reduced solubility was observed for the PF_6^- salt. The reaction conditions and parameters beside the counter ions were identical, reproducibility of the results was given and the same trends were observed performing the reaction with the substrate MeO-THIQ **15**, refer to section 3.6.2.

Counter Ion Effect Thus, the varying reaction profiles were ascribed to the influence of the counter ions itself. Possible explanations are steric or electronic effects, resulting from e.g. the diverse size of the counter ion, $Cl^- < PF_6^-$ [148] or the differences in the coordination properties (Cl^- strong coordinating anion, PF_6^- weak coordinating anion).[149,150] Furthermore, the redox potentials of the complexes and the stabilization of the cationic species were investigated.

Firstly, the redox potentials of the two complexes $Ru(bpy)_3Cl_2$ and $Ru(bpy)_3(PF_6)_2$ were determined in dependence of the counter ion and solvent by cyclic voltammetry. The measurements shown in Table 3.6 and Figure 3.30 were performed by Anna Eisenhofer. The redox potentials revealed to be identical, e.g. in acetonitrile $E_{1/2}(Ru^{2+}/Ru^+)$ = -1.35 V for both catalysts, see entry 1 and 2. Thus, the enhanced reaction rate of $Ru(bpy)_3Cl_2$ cannot be explained by the redox potentials.

Table 3.6 Redox potentials of $Ru(bpy)_3Cl_2$ and $Ru(bpy)_3(PF_6)_2$.

Entry	Analyte	Supporting Electrolyte	Solvent	$E_{1/2}(Ru^0/Ru^{-1})$[a]	$E_{1/2}(Ru^+/Ru^0)$[a]	$E_{1/2}(Ru^{2+}/Ru^+)$[a]	$E_{1/2}(Ru^{3+}/Ru^{2+})$[a]
1	$Ru(bpy)_3Cl_2$	Tetraethylammonium chloride	MeCN	-1.78	-1.54	-1.35	
2	$Ru(bpy)_3(PF_6)_2$	Tetrabutylammonium hexafluorophosphate	MeCN		-1.54	-1.35	+1.28
3	$Ru(bpy)_3(PF_6)_2$	Tetrabutylammonium hexafluorophosphate	$MeNO_2$[b]				+1.30
4	$Ru(bpy)_3^{2+}$ (literature)[143]	-	MeCN	-1.76	-1.52	-1.33	+1.29

[a] vs. SCE [V].
[b] For nitromethane as solvent the reductive part of the catalyst is outside of the electrochemical window, therefore only the oxidative potential was measured.

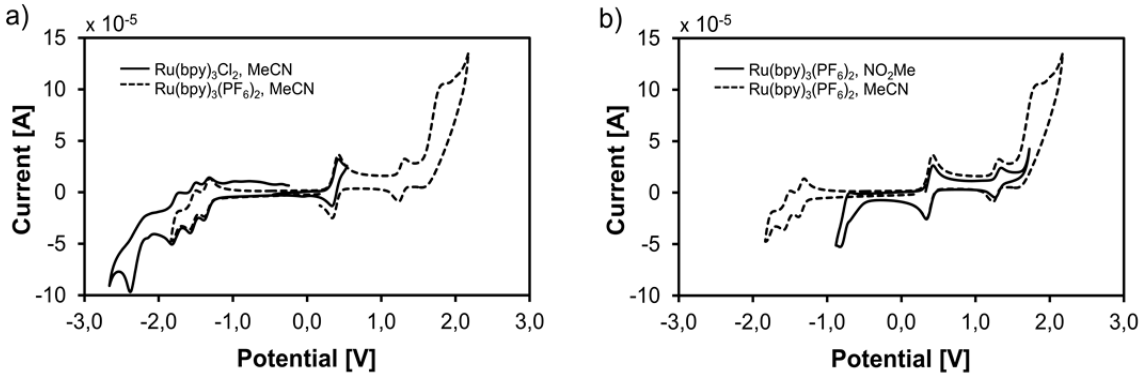

Figure 3.30 Cyclic voltammograms of $Ru(bpy)_3X_2$ in MeCN in dependence of the counter ion. (a) Dotted line: Tetrabutylammonium hexafluorophosphate was used as supporting electrolyte. Solid line: Tetraethylammonium chloride was used as supporting electrolyte. (b) Cyclic voltammograms of $Ru(bpy)_3(PF_6)_2$ – solvent effects. Tetrabutylammonium hexafluorophosphate was used as supporting electrolyte. Solid line: Nitromethane was used as solvent. Dotted line: MeCN was used solvent. The potentials are given in Volt vs. SCE. Ferrocene was used as internal standard.[4]

Another attempt to explain the different reaction profiles and reaction rates is based on the stability of the iminium ions **2**. As reported in literature, the reactivity and thus the stability of the iminium ions **2** can be triggered by the counter ion.[62] For THIQ iminium chloride **2f** respectively hexafluorophosphate **2g** different stabilities were observed in DMF-d_7, as the THIQ iminium chloride **2f** was detectable by ^{1}H NMR spectroscopy, while the THIQ iminium hexafluorophosphate **2g** concentration remained below the detection limit.[147] However, in nitromethane the concentration of the THIQ iminium ion **2** revealed to be identical for both photocatalysts. Based on this observation, we excluded the stabilization of the iminium ions **2** to be decisive for the subsequent reaction rate in nitromethane.

Therefore, we suggest that the key step decisive for the further reaction is the stabilization of the radical cation $\mathbf{1}^{\bullet+}$ and the therewith correlated efficiency to undergo back electron transfer or subsequent reaction steps (deprotonation, H$^\bullet$-abstraction), see Scheme 3.14. Whether the BET and/or the subsequent process are accelerated or decelerated by the stabilization of the radical cation remained unclear.

Scheme 3.14 Electron transfer (ET) between THIQ **1**/$Ru(bpy)_3X_2$ resulting in a contact ion pair and follow-up processes of the α-amino radical cation. (BET = back electron transfer).

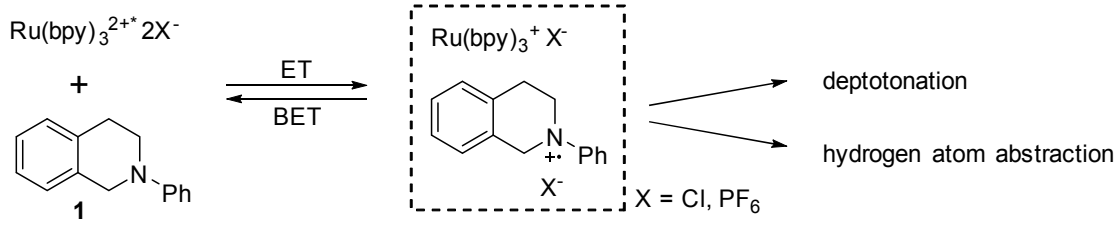

For the $Ru(bpy)_3(PF_6)_2$ catalyzed reaction the concentrations of the intermediates formed via the radical pathway (dimer **9** and THIQ-nitrone **10**) were significantly decreased. In addition, the reaction rate of the $Ru(bpy)_3(PF_6)_2$ catalyzed reaction is two-fold decelerated in contrast to the chloride counter ion complex.

According to the results obtained for the $Ru(bpy)_3Cl_2$ catalyzed aza-Henry reaction described in Scheme 3.8, under anaerobic conditions only the radical pathway is active. Thus, the reduced reaction rates and concentrations of the radical-derived intermediates were ascribed to an increased preference to undergo BET and/or a less favored deprotonation step leading to the α-amino radical anion **7**.

Conclusion and Outlook From experimental data we observed, that the product **6a** formation rate as well as the intermediate **9** and **10** concentrations decreased when exchanging the counter ion from chloride to hexafluorophosphate. The reaction rates are proposed to correlate with the stabilization of the radical cation $\mathbf{1}^{\bullet+}$. However, due to the lack of information, the complexity of the processes and the multitude of possibilities influencing back electron transfer and the other involved steps, an elaborated study together with a broader range of experimental data (variation of catalysts and substrates, aerobic conditions) is essential for a profound discussion.

3.6.1.2 2-(4-Methoxyphenyl)-1,2,3,4-tetrahydroisoquinoline (15) Studies

To gain deeper insight into the general validity of the reaction pathways described in 3.3 and 3.4 ($H^{\bullet}$- vs. H^{+}-abstraction), the substrate scope was extended to 2-(4-methoxyphenyl) -1,2,3,4-tetrahydroisoquinoline (MeO-THIQ) **15** (see Figure 3.31 a). The methoxy group in *para*-position is selected due to its strong electron-donating character, increasing the electron density surrounding the nitrogen. Because of this, the stabilization of the cationic species (the radical cation $\mathbf{15}^{\bullet+}$ and the MeO-THIQ iminium ion **17**, see Figure 3.31 b) and a reduced basicity of MeO-THIQ **15** were expected.

Aerobic and Anaerobic Reaction Profiles In consistency with the mechanistic study of THIQ **1** described in section 3.3, the photocatalytic aza-Henry reaction of MeO-THIQ **15** was investigated by ^{1}H NMR reaction profiles, regarding the influence of the terminal oxidant, the catalyst and the reaction intermediates. As described above, the *in situ*[75] and the *ex situ* setup were used to realize the systematic study. Samples containing MeO-THIQ **15** (50 mM) and 10 mol% $Ru(bpy)_3Cl_2$ in deuterated nitromethane-d_3 were irradiated with blue LEDs at room temperature (see Figure 3.31 c, d).

Under anaerobic conditions, the MeO-THIQ dimerization product **20** (Scheme 3.15) as well as the ring opened intermediate **18** were observed (likewise the THIQ **1** kinetic, Figure 3.1 c). However, in contrast to THIQ **1** the accumulation of the intermediates **18** and **20** was significantly reduced. The dimer of MeO-THIQ **20** is only observed within the first hour of the reaction and with maximal concentrations close to the detection limit (0.05 mM) (THIQ-dimer **9**: 6 mM; Figure 3.1 c). The ring opened species **18** constitutes the main intermediate, however with also reduced concentration of maximum 1.5 mM (THIQ ring opened intermediate **10**: 11 mM; Figure 3.1 c). Under aerobic conditions neither the MeO-THIQ dimer **20** nor the ring opened intermediate **18** nor the respective MeO-THIQ hydroperoxide **21** (refer to THIQ-OOH **11**; Figure 3.1 a) were observed.

The decreased intermediate concentration of the MeO-THIQ species **18** and **20** for both (anaerobic and aerobic) settings is ascribed to the electron-donating methoxy group. We suggest that the deprotonation of the radical cation $\mathbf{15}^{\bullet+}$, leading to the amino radical **16** is less favored, due to the reduced basicity of the radical cation $\mathbf{15}^{\bullet+}$. A reduced deprotonation rate is

in accordance with the reduced concentration of the radical-derived intermediate species **18** and **20**.

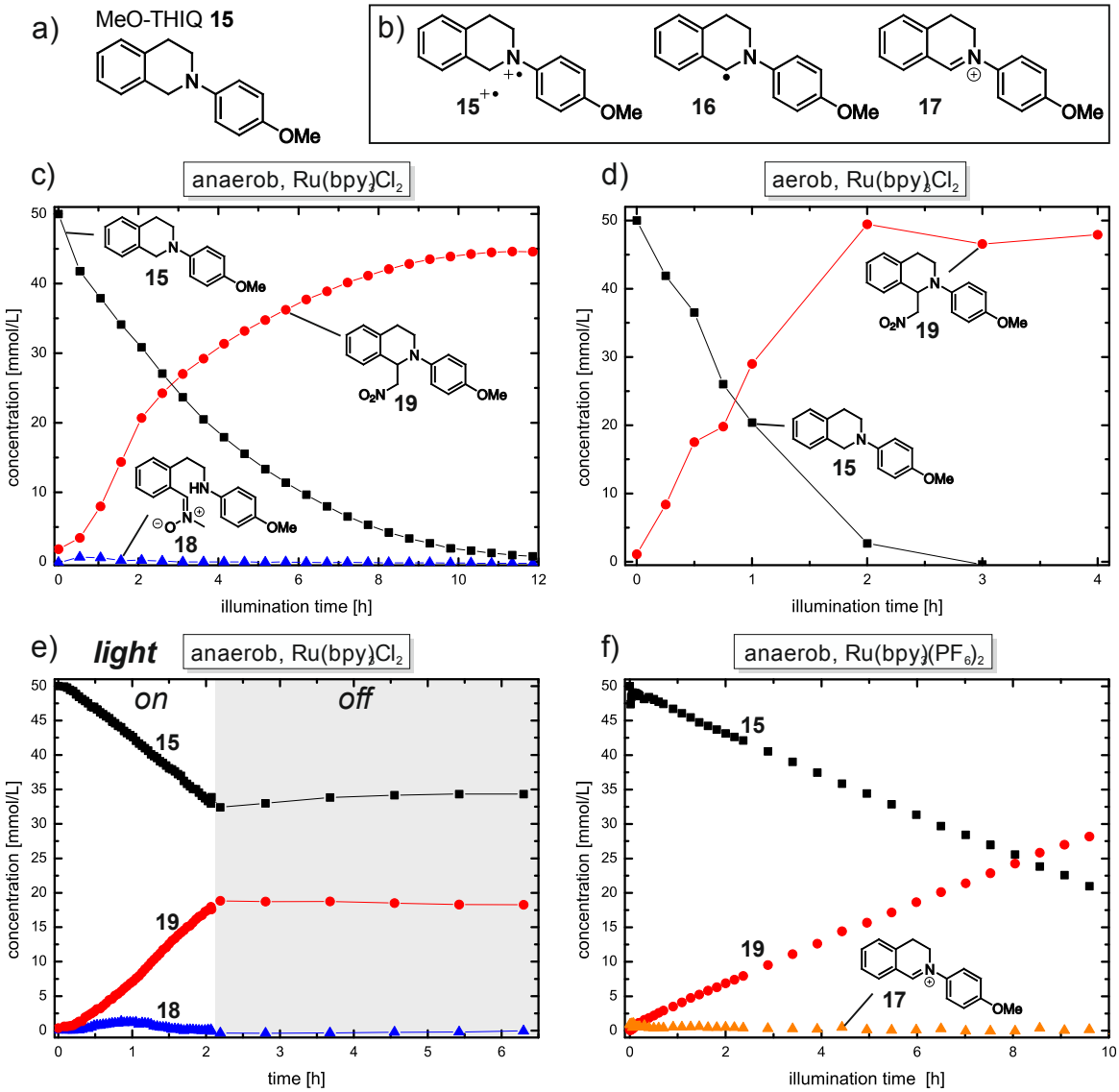

Figure 3.31 Structures of 2-(4-methoxyphenyl)-1,2,3,4-tetrahydroisoquinoline **15** (a) and the corresponding MeO-THIQ radical cation **15** $^{\bullet+}$, neutral radical **16** and iminium ion **17** (b).The photocatalytic aza-Henry reaction of MeO-THIQ **15** (50 mM) and 10mol% $Ru(bpy)_3Cl_2$ in NO_2Me-d_3 under continuous illumination with blue light at room temperature under anaerobic (c) or aerobic conditions (d). Light on-off study of MeO-THIQ **15**, revealing that no intermediate species contribute to the product formation in the dark (e) ^{1}H NMR reaction profile of the photocatalyzed aza-Henry reaction of MeO-THIQ (50 mM) at 300 K under continuous illumination with blue LEDs using $Ru(bpy)_3(PF_6)_2$ and *in situ* conditions (f).

Under aerobic conditions no MeO-THIQ hydroperoxide species **21** was detected, in contrast to THIQ **1** (refer to Figure 3.1 a). This is possibly due to the proposed stabilization of the iminium ion **17** by the methoxy group. By stabilization of the iminium ion **17**, a reduced preference to form MeO-THIQ hydroperoxide **21** in an off-cycle can be assumed. The proposal is supported by the slight acceleration of the product **19** formation rate, in contrast to **6a**, (both under aerobic conditions) and the comparability of the rates of **19** and **6a** under anaerobic conditions, where the iminium ion **17/2** is not that much taken into account. (see discussion below).

The MeO-THIQ iminium ion **17**, detected in the initial minutes of the anaerobic and the aerobic reaction is not depicted, due to maximum concentration <0.5 mM and fast decrease within the first hour.

Scheme 3.15 Structures of MeO-THIQ dimer **20** and MeO-THIQ hydroperoxide **21**.

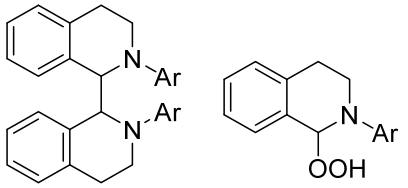

20 **21** Ar = -Ph-OMe

As observed for the substrate THIQ **1** (refer to section 3.3 and Figure 3.1), the aerobic reaction is significantly accelerated with respect to the anaerobic one. Full conversion to the product **19** is achieved after 2 h in the presence of oxygen, in contrast to 10 h under anaerobic conditions. Under anaerobic reaction conditions 50% of the coupling product was obtained after 3 h for both **19** and **6a**. The aerobic reaction rates slightly differ, as for THIQ **1** 90 % of product were obtained after 3 h compared to 2 h for MeO-THIQ **19**.

The exponential decrease of the starting material **15** and the sigmoidal shaped product **19** formation curve under anaerobic conditions respectively the linear product formation **19** under aerobic conditions are in good agreement with the reaction profile of THIQ **1** under otherwise stated conditions (Figure 3.31 c, d).

Light On-Off Studies To address the question, whether additional intermediates contribute to the product **19** formation in the dark, light on-off studies were performed *in situ*, see Figure 3.31 e. Under blue light illumination product **19** and the ring opened intermediate **18** were formed, while the starting material decreases **15**. After an irradiation period of 2 h, the ^{1}H NMR reaction profile of the dark reaction was monitored. In the absence of ligth, the conversion of MeO-THIQ **15** to product **19** stopped immediately, revealing that no additional intermediate species, not detectable by NMR spectroscopy contributes to the product **19** formation independent from light. These results are in good accordance to the THIQ **1** reaction profiles.

Background Reaction Control experiments were performed revealing the necessity of light as well as catalyst for an efficient product **19** formation under anaerobic (*in situ)* conditions. Under illumination with blue LEDs 8% of product **19** were obtained after 9 h in the absence of $Ru(bpy)_3Cl_2$. Up to 4% of product **19** were yielded after 12 h without illumination in the presence of 10 mol% $Ru(bpy)_3Cl_2$.

Influence of the Catalyst Counter Ion As discussed above (see 3.6.1) the counter ion of the $Ru(bpy)_3X_2$ catalyst significantly influences the reaction profiles. Likewise to the THIQ **1** studies the influence of the counter ion was investigated by comparing the ^{1}H NMR kinetics of the Cl^- and the PF_6^- salt. Samples containing MeO-THIQ **15** (50 mM) and 10 mol% $Ru(bpy)_3X_2$ were irradiated with blue LEDs at 300 K, see Figure 3.31 c (Cl^-) and Figure 3.31 f (PF_6^-).

Interestingly, the combination of $Ru(bpy)_3(PF_6)_2$ and MeO-THIQ **15** seemed to reinforced the suppression of the radical pathway, as now neither the open intermediate **18** nor the dimer **20** were observed during the reaction, see Figure 3.31 f. The concentration of the iminium

ion **17** reached maximum 1 mM, as observed before, however the iminium ion **2** was detected within the initial 5 h. Surprisingly, the decrease of the starting material MeO-THIQ **15** and the formation of the coupling product **19** are almost linear, indicating a pseudo-zero order product formation.

As described above, we suggest, that the methoxy group as well as the application of the $Ru(bpy)_3(PF_6)_2$ catalyst lead to a reduced preference to undergo deprotonation, and thus to a reduced intermediate (dimer **9/20** and ring opened intermediate **10/18**) concentration and product formation rate. If these assumptions are valid the radical pathway is expected to be suppressed significantly for the $Ru(bpy)_3(PF_6)_2$ catalyzed MeO-THIQ **15** reaction. In consequence, if no other pathway is operative, the reaction is expected to be inefficient.

The product **19** is formed in reasonable reaction times (50% yields after 8 h). Thus, we assume that another pathway is operative. The absence of the radical-based intermediates **18** and **20**, together with the linear curves of starting material **15** and product **19** hint towards a iminium pathway. The detection of the iminium ion **17** for exceptional long reaction times and the lacking of THIQ-OOH **21** can be assumed to result from the stabilization of the iminium ion **17** by the methoxy group, as discussed above. However, this is in contrast to the mechanism observed for the aza-Henry reaction of THIQ **1**, where nitromethane only functions as a base promoting the radical pathway. For the THIQ **1** reaction the iminium pathway is only observed in the presence of oxygen.

Summary and Conclusion For the $Ru(bpy)_3Cl_2$ catalyzed aza-Henry the reaction mechanisms obtained for THIQ **1** and MeO-THIQ **15** appeared to be consistent. The linear product **19** formation together with the accelerated reaction rate in the presence of air and the in contrast sigmoidal product **19** formations under anaerobic conditions are in good accordance with the THIQ **1** starting material. Furthermore, the intermediates MeO-THIQ dimer **20** and MeO-THIQ ring opened intermediate **18** were observed *in situ*, however in significantly reduced amounts. Light on-off studies revealed that no additional intermediates contribute to the product formation in the dark.

In addition, the $Ru(bpy)_3(PF_6)_2$ catalyzed aza-Henry reaction of MeO-THIQ **15** was monitored under anaerobic conditions. The intermediates **18**, **20** were not detected during the kinetic. Furthermore, the product **6a** exhibits a linear, instead of a sigmoidal curve. The reaction profile hints towards an operative iminium pathway, thus the $H^{\bullet}$-acceptor remained unclear, as the reaction was performed in the absence of oxygen. The underlying reaction mechanism could so far not be elucidated.

Outlook To gain further insight into the reaction mechanism, the application of a broader substrate scope including weak electron-donating and electron-withdrawing groups is suggested. With increasing basicity of the substrate, we expect a to MeO-THIQ contrary effect regarding the intermediate concentrations (higher amounts of the intermediate species formed via α-amino radical), possibly revealing an even more predominant radical pathway. Further, a wider range of $Ru(bpy)_3^{2+}$ counter ions (differing in size and coordination properties) and in general of photocatalysts are expected to contribute to an more profound valuation of the role of the catalyst besides the initial electron transfer step. The investigation of the counter ion effect should help to estimate, whether the reaction pathways are valid in general. The

influence of oxygen on the hexafluorophosphate catalyzed reaction has not been investigated, yet. We suggest that the stability of the contact ion pair, formed after initial electron transfer, is dependent on the counter ion, which influences the BET and thus the efficiency of the reaction. Therefore, the influence of oxygen is expected to vary for the Cl^- and the PF_6^- catalyst.

3.6.1.3 Influence of H_2O_2

During the progressing reaction hydrogen peroxide can be detected, dependent on the oxygen content of the solution. Under air the catalyst is regenerated by oxygen under formation of superoxide radical anion $O_2^{\bullet-}$. Superoxide radical anion is known to react as base or as hydrogen atom abstractor, forming $OOH^\bullet$ respectively OOH^-.[68,89–98] Hydrogen peroxide can thus be formed within the reaction by protonation or hydrogen atom abstraction of a oxygen species or via conversion of the THIQ-OOH **11** species to product **6a** (refer to 3.5.9.3). After investigation of the reaction profiles in the absence and presence of oxygen, the influence of H_2O_2 to the reaction mixture was studied.

Reaction Profiles A sample containing THIQ **1** and $Ru(bpy)_3Cl_2$ 10 mol% in deuterated nitromethane-d_3 was prepared and 2 equivalents of hydrogen peroxide were added to the mixture. The reaction kinetic was measured *in situ* at 300 K under illumination with blue LEDs. The ^1H NMR kinetic is shown in Figure 3.32 a. In contrast to the *in situ* reaction profiles in the absence of hydrogen peroxide (refer to Figure 3.1), the only intermediate formed is THIQ-OOH **11**, with up to 35% during reaction progress. This is not remarkably, as an excess of H_2O_2 was added.

The sigmoidal product **6a** formation is in accordance with the anaerobic reaction profiles detected without hydrogen peroxide. By comparing the reaction rates in the presence and absence of hydrogen peroxide, we observed identical reaction rates (each 80% product **6a** was obtained after 6 h) (Figure 3.32 a and Figure 3.31 a). Control experiment showed that the anaerobic reaction with H_2O_2 in the absence of catalyst is inefficient, as only 7% product were obtained after 15 h.

Based on the reaction profile we rather suggest that a radical pathway is active in the presence of additional H_2O_2 under anaerobic conditios. The product **6a** formation curve exhibits a sigmoidal shape and the reaction rate is in the range of the anaerobic not the aerobic H_2O_2-free reaction. The experiment showed that the role of oxygen differs from the one of hydrogen peroxide. However, it has to be considered, that the addition of H_2O_2 significantly changed the reaction system. Because no other intermediates, the dimer **9** or the ring opened intermediate **10**, were detected during the kinetic, we assume that the excess of hydrogen peroxide is responsible for the exclusive detection of THIQ-OOH **11**. (The relative stabilities of the intermediate species have to be considered for a reliable estimation.) To gain detailed information about the trends regarding stability and reactivity, we added H_2O_2 to a progressing reaction.

Delayed H_2O_2 Addition After around 4 h of continuous irradiation, hydrogen peroxide was added to the reaction mixture, see Figure 3.32 b. Immediately after addition of H_2O_2 the concentration of the ring opened intermediate **10** and the dimer **9** (Figure 3.32 c) dropped below the detection limit and THIQ-OOH **11** was formed in comparable concentrations. The conver-

sion of the intermediate **9** and **10** elapsed during the time of mixing and remeasuring, and thus is assumed to occur in the dark.

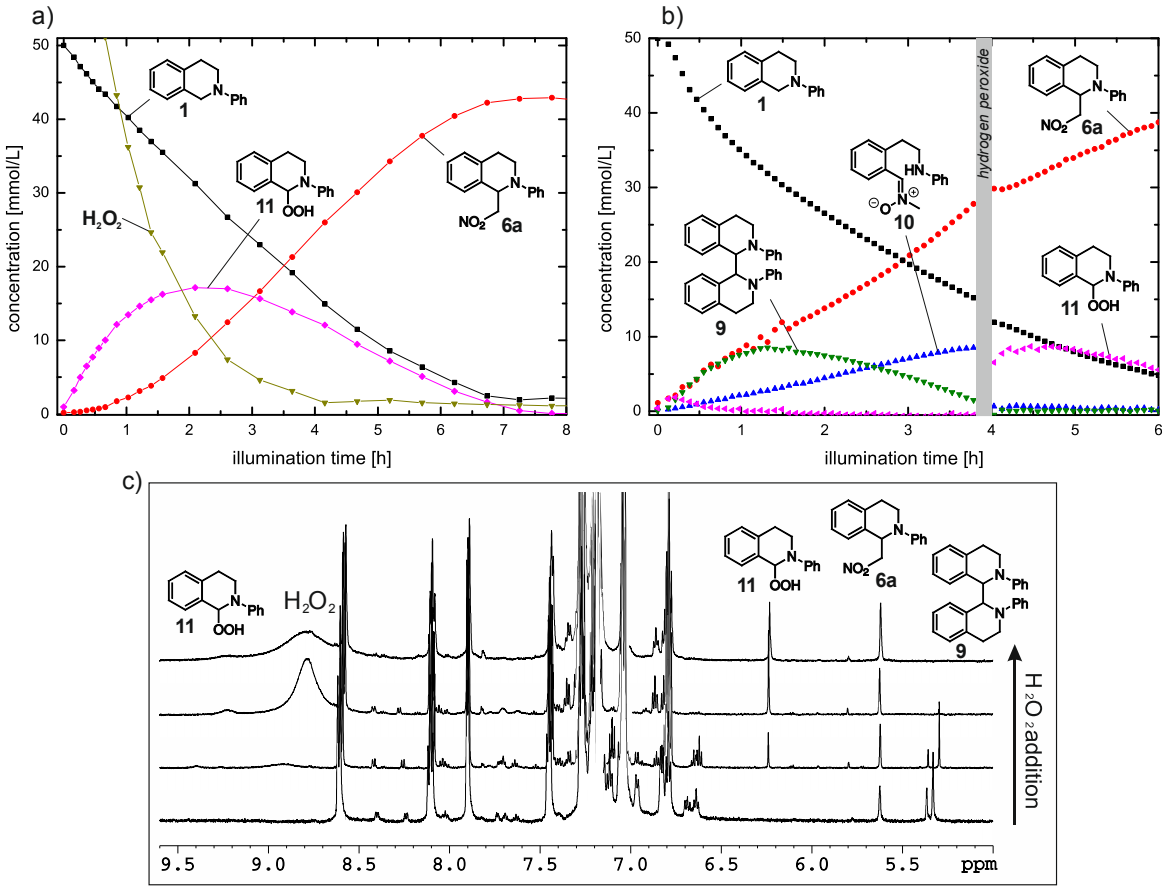

Figure 3.32 ^{1}H NMR kinetic, showing the influence of additional hydrogen peroxide on the aza-Henry reaction. (a) ^{1}H NMR kinetic of THIQ **1** (50 mM), H_2O_2 (2 equiv.) and $Ru(bpy)_3Cl_2$ 10 mol% in deuterated nitromethane-d_3 irradiated with blue LEDs at 300 K. (b) ^{1}H NMR kinetic of THIQ **1** (50 mM) and $Ru(bpy)_3Cl_2$ 10 mol% in deuterated nitromethane-d_3 at 300 K irradiated with blue LEDs for 4 h, followed by addition of H_2O_2 (~1 equiv.) and illumination for 2 h. (c) Row of ^{1}H spectra before and during the addition of hydrogen peroxide to the reaction mixture.

This observation corroborates both, the above mentioned relative stability of THIQ-OOH **11** to be higher than for the dimer **9** or the opened intermediate **10** or an equilibrium between THIQ-OOH **11** and the intermediates, shifted by the excess of hydrogen peroxide. For a reliable estimation the system needs to be thoroughly investigated.

Due to the formation of THIQ-OOH **11** from the opened intermediate **10** and the dimer **9** in the dark, a conversion occurring via the THIQ iminium ion **2** is likely. An equilibrium between the open intermediate **10** and iminium ion **2** has been proposed before (refer to Scheme 3.5). Thus, the conversion of the ring opened intermediate **10** to THIQ-OOH **11** via iminium ion **2** is reasonable (see Scheme 3.16). In contrast, the dimer **9** revealed to be stable in the dark in the absence of hydrogen peroxide, and the oxidative cleavage of the dimer **9** under formation of the iminium ion **2** and the amino radical **7** is observed in the precence of light and photocatalyst. Thus, the question remains, which mechanism is active converting the THIQ dimer **9** to the THIQ-OOH **11** in the dark.

Scheme 3.16 Proposed equilibrium between the ring opened intermediate **10** and THIQ hydroperoxide **11** via THIQ iminium ion **2**.

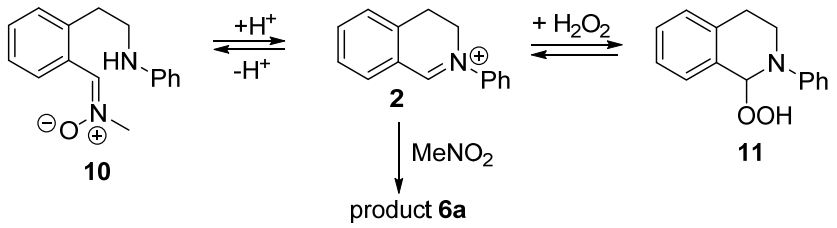

Conclusion The kinetic of the hydrogen peroxide containing reaction shows a reaction profile comparable to the anaerobe reaction profiles without H_2O_2. The only intermediate detectable constitutes the THIQ-OOH **11** species, in contrast to the reaction in the absence of H_2O_2. The addition of H_2O_2 to a progressing reaction revealed that the radical-derived intermediates **9** and **10** are immediately converted into the THIQ-OOH **11** in the dark. Based on the reaction profile and the immediate and complete conversion of the intermediates **9** and **10** to THIQ-OOH **11**, it seems likely that the radical pathway is still active under anaerobic conditions in the presence of H_2O_2 and that the hydrogen peroxide does not contribute to the catalytic cycle, but intercepts the formed intermediate species **9** and **10**. However, the contribution of the iminium pathway cannot be excluded, due to the formation of THIQ-OOH **11**. The iminium ion **2** may be provided by hydrogen atom abstraction from the radical cation $\mathbf{1}^{\bullet+}$ by hydrogen peroxide species e.g. $HOO^{\bullet}$.

Further investigation regarding the correlation of the intermediate species and the reaction pathway responsible for the formation of the THIQ-OOH **11** and product **6a** are recommended. The aerobic reaction profile containing hydrogen peroxide has not been monitored, yet. We expect the investigation of the reaction profile to provide a deeper insight into the reaction mechanism by revealing the roles as well as possible interaction of oxygen and hydrogen peroxide within the catalytic cycle.

3.6.2 Phosphonlyation Reaction

The aza-Henry reaction stands out from the photocatalytic transformations converting C-H into C-C or C-X bonds, as oxygen as well as nitromethane are capable of acting as terminal oxidants, enabling the investigation of the reaction mechanism under anaerobic and aerobic conditions. In chapter 3.3 and 3.4 we were able to show that depending on the terminal oxidant either H^+- or $H^\bullet$ -abstraction represent the predominate pathway of the aza-Henry reaction. Encouraged by these results, we extended our study to a boarder scope of reactions. Another typical example for photocatalytic transformations of THIQ **1** are phosphonylation reactions, where new C-P bonds are formed.[28,44,138,151]

In analogy to the aza-Henry reaction the substrate THIQ **1** and the catalysts $Ru(bpy)_3^{2+}$ were chosen. The nucleophile diethyl phosphite was selected, because of short reaction times of 3 h and reasonable yields of 86% for the α-amino phosphonate, reported for the starting material THIQ **1**.[138] The reactions were performed in DMF-d_7 at room temperature. In line with the aza-Henry reaction, the phosphonylation reaction was performed in the absence and presence of the terminal oxidant oxygen (*in situ* and *ex situ*) and in addition, the light-induced background reaction was studied.

3.6.2.1 Photocatalyzed Reaction

Aerobic Reaction Profiles Samples containing THIQ **1** (50 mM respectively 400 mM), $Ru(bpy)_3Cl_2$ (~ 10 mol%) and an excess of 3.5 equivalents of diethyl phosphite (dep) **5b** were prepared in DMF-d_7. The mixtures were irradiated with blue LEDs open to air, using the *ex situ setup* and the general procedure B described in 3.5.2.4. The ^{1}H NMR reaction profiles are shown in Figure 3.33.

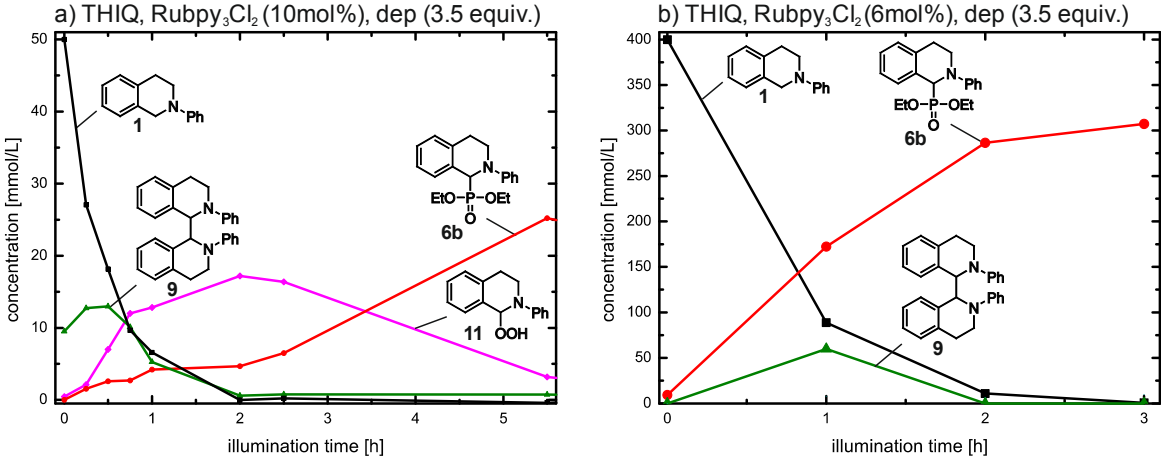

Figure 3.33 ^{1}H NMR kinetics of the phosphonylation reaction of THIQ **1** and $Ru(bpy)_3Cl_2$ in DMF-d_7 under aerobic conditions at 300 K under continuous illumination at room temperature.

Both aerobic ^{1}H NMR kinetics revealed that after initiation of the reaction the THIQ dimer **9** intermediate is formed, reaching a maximum amount of 30% after 30 min in Figure 3.33 a. In Figure 3.33 b the first data point taken after one hour of irradiation excluded a reliable estimation of the maximum dimer **9** concentrations. The detection of the dimer **9** under aerobic conditions in the presence of the photocatalyst is in line with the results obtained from the aza-Henry reaction.

However, in contrast to the aza-Henry reaction here no nitromethane — serving as a base — is present. Oxygen in form of $O_2^{\bullet-}$ is reported as $H^{\bullet}$- and H^+-acceptor in literature.[68,89–98] But, as the dimer **9** is also formed under anaerobic conditions (see below) and under anaerobic conditions in the absence of dep **5b** (see below), oxygen is unlike to be involved in the formation of the α-amino radical anion **7**. The dimer **9** formation is observed for samples containing only THIQ **1**, $Ru(bpy)_3Cl_2$, DMF-d_7 and residual water. Thus, the solvent is suggested to contain the species responsible for the deprotonation of the radical cation $\mathbf{1}^{\bullet+}$. As reported in literature, the weak base dimethylamine constitutes a predominate impurity of DMF[152] and thus, is suggested to act as a base deprotonating the radical cation $\mathbf{1}^{\bullet+}$ under formation of the α-amino radical anion **7**.

The intermediate THIQ-OOH **11** was only observed for the reaction kinetic shown in Figure 3.33 a. Here, THIQ-OOH **11** exhibits the main intermediate (40%). The product formation **6b** curve showed a sigmoidal shape, starting to increase after the maximal THIQ-OOH **11** concentration is reached. In contrast, no THIQ-OOH **11** intermediate is monitored during the kinetic depicted in Figure 3.33 b. The linear product **6b** formation curve is in line with the fast conversion. After 1 h 75% product **6b** was obtained in (b), in contrast to 10% for the kinetic shown in (a). The deceleration of the reaction rate in the presence of THIQ-OOH **11** (Figure 3.33 a) can be ascribed to the off-cycle equilibrium between the iminium ion **2** and THIQ-OOH **11**. The two reaction kinetics significantly differ in the concentration of THIQ **1**, thus the influence of the sample concentration as well as the oxygen content (variation in the THIQ-OOH **11** concentration) have to be further investigated. A systematic study is expected to help reproducing the reaction profiles and thus provide a deeper insight into reaction mechanism.

Conclusion and Outlook The reaction profiles considered individually are consistent and can be explained by the iminium and the radical pathways described above (section 3.4). Under aerobic conditions the radical pathway is active, leading to the formation of the THIQ dimer **9**, which is in agreement with the photocatalyzed aza-Henry reaction. The base, deprotonating the α-amino radical anion **7** has to be confirmed. The detection of THIQ-OOH **11** respectively the linear product **6b** formation suggested the additional contribution of the iminium pathway, where oxygen in form of the $O_2^{\bullet-}$ is proposed to undergo hydrogen atom abstraction. However, the detection of the THIQ-OOH species **11** and the reaction profiles were indistinct. Thus, for a reliable conclusion the reaction has to be further investigated.

Fluctuations in the saturation with oxygen (refer to Figure 3.36), sample volume, temperature or light intensity/distribution, latter e.g. due to the different sample concentration, may be possible explanations for the deviations in the reaction profiles. A repetition of the experiments together with further mechanistic studies is essential for a thoroughly insight. In addition, the performance of reaction kinetics in other solvents and with a broader scope of nucleophiles is recommended.

Anaerobic Reaction Profiles Further, the reaction profile was investigated in the absence of the terminal oxidant oxygen using the *in situ* setup. A ^1H kinetic was monitored in the absence of nucleophile to investigate the intermediates and the side reactions occurring. Then, the kinetic was recorded in the presence of the nucleophile diethyl phosphite.

Absence of Nucleophile For the ^{1}H NMR kinetic a sample containing THIQ **1** (50 mM) and $Ru(bpy)_3Cl_2$ (10 mol%) was prepared in oxygen saturated deuterated DMF-d_7. The kinetic was monitored under continuous illumination with blue LEDs at 230 K, see Figure 3.34.

By performing the reaction *in situ* in the absence of nucleophile the dimer **9** constitutes the main species with yields up to 8%. In the initial hours of the reaction THIQ iminium ion **2** and THIQ-OOH **11** were detected, reaching maximum amounts of 1% respectively 4%. The starting material is mainly converted to the dimer **9** via the radical pathway. In addition, the residual oxygen inside the solution is proposed to undergo hydrogen atom abstraction, leading to small amounts of THIQ-OOH **11** and THIQ iminium ion **2**, as described for the aza-Henry reaction in detail. An optimization of the reaction conditions temperature, solvent and catalyst as well as catalyst loading for the detection and characterization of the intermediate species and products was performed during the master thesis.[147]

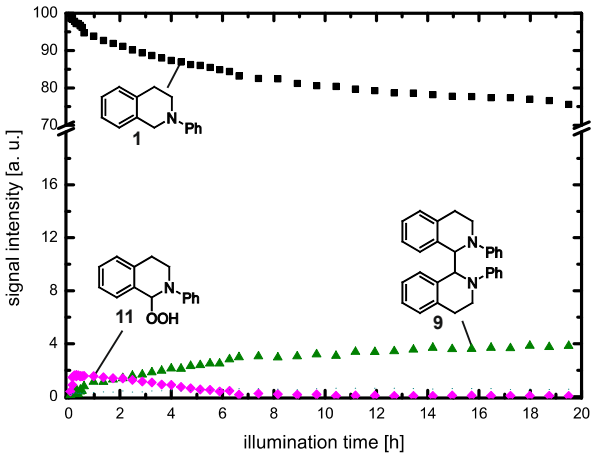

Figure 3.34 ^{1}H NMR kinetics of THIQ **1** and $Ru(bpy)_3Cl_2$ (10 mol%) in DMF-d_7 at 300 K under continuous illumination at room temperature in the absence of nucleophile.

Presence of Nucleophile In addition to the kinetics described above, the reaction was investigated in the presence of the nucleophile diethyl phosphite under anaerobic conditions. The absence of oxygen or another terminal oxidant (capable of regenerating the catalyst) led to a reduced product yield **6b** of the photocatalytic transformation, under the conditions described above (max 10mol% catalyst). Therefore, for a detailed investigation of the reaction mechanism variations of the experimental conditions were applied, see Figure 3.35.

Firstly, the reaction kinetic of a sample containing THIQ **1** (50 mM), $Ru(bpy)_3Cl_2$ (10mol%) and 10 equivalents of dep **5b** in DMF-d_7 was recorded, confirming that under anaerobic conditions the dimer **9** is formed as the main intermediate species (see Figure 3.35 a). Delayed, the coupling product **6b** is obtained in low amounts. After full consumption of the photocatalyst the formation of dimer **9** stopped. The dimer **9** concentration further increased after addition of new catalyst. Surprisingly, the products concentration remained constant during the time intervals. The ongoing addition of $Ru(bpy)_3Cl_2$ to the reaction mixture enabled the further formation of dimer **9** and product **6b**. However, the product **6b** concentration only increased immediately after addition of the catalyst. As the conversion of dimer **9** to the coupling product **6b** is expected to occur photocatalyzed, according to the results obtained for the isolated dimer **9** kinetic, see Figure 3.2, the results of the measurement have to be investigated in

more detail. As expected, the yield of the reaction is restricted by the regeneration of the catalyst.

To perform the reaction efficiently in the absence of oxygen (*in situ*) an alternative terminal oxidant was introduced. The regeneration of the catalyst was achieved by the addition of hydrogen peroxide (2 equiv.) to the solution.[37,153] Figure 3.35 b depicts the ^{1}H reaction profile of a sample containing THIQ **1**, photocatalyst, nucleophile dep **5b** and H_2O_2 in DMF. While the reaction proceeded, THIQ-OOH **11** was formed as the main intermediate yielding up to 35%, whereas the dimer **9** was observed in concentration close to the detection limit. This observation is in accordance with the results obtained for the aza-Henry reaction in section 3.6.1.3, where the influence of additional hydrogen peroxide is discussed. Correlated to the formation of the intermediate **11** the phosphonylation product **6b** is obtained, exhibiting a sigmoidal initial product formation rate. The kinetic confirmed that H_2O_2 acts as terminal oxidant, efficiently regenerating the catalyst and thus revealing a possibility to monitor the reaction under anaerobic conditions. However, the addition of a new reaction partner is capable of changing the reaction mechanism significantly.

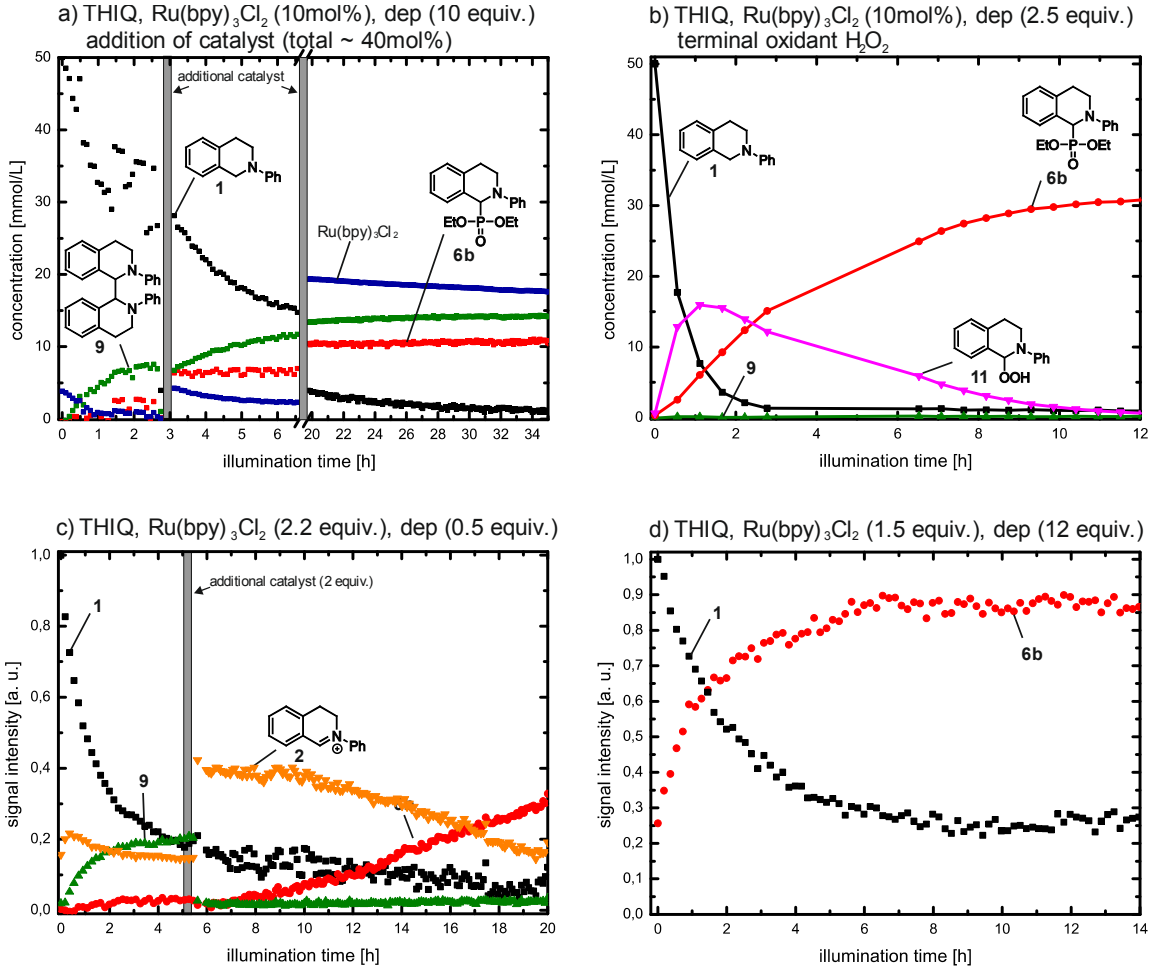

Figure 3.35 ^{1}H NMR reaction profiles of THIQ, $Ru(bpy)_3Cl_2$ and dep **5b** in DMF-d_7 at 300 K and continuous illumination with blue LEDs. (a) Addition of $Ru(bpy)_3Cl_2$ during the reaction progress. (b) Addition of hydrogen peroxide as terminal oxidant. Insufficient concentration (c) or excess (d) of the nucleophile.

In the absence of H_2O_2 (Figure 3.35 a and c) the detection of dimer **9** and a sigmoidal product **6b** formation curve indicate, that the radical pathway is operative. In the presence of hy-

drogen peroxide mainly THIQ-OOH **11** is obtained, however the product formation exhibits a sigmoidal curve, suggesting that the radical pathway is still present, for detailed discussion refer to 3.6.1.3. The formation of THIQ-OOH **11** as the main intermediate is in accordance with the results obtained in 3.6.1.3.

Further the influence of the nucleophile concentration was investigated (see Figure 3.35 c and d). In Figure 3.35 c the amount of the nucleophile dep **5b** (0.5 equiv.) is restricted. The ^{1}H NMR kinetic revealed that THIQ **1** is converted into the iminium ion **2** and the dimer **9**. Within the first 5 h 20% of each intermediate were obtained, while the reaction yielded less than 1% product **6b**. After addition of two more equivalents of photocatalyst to the reaction mixture, the dimer **9** is immediately converted into the iminium ion **2**, now yielding 40%. The photocatalytic transformation of the dimer **9**, resulting in a THIQ iminium ion **2** and an α-amino radical is discussed in 3.3. The surprisingly high amount of iminium ion **2** is ascribed to the deficit of nucleophile, resulting in a steady transformation of the iminium ion **2** into the phosphonylation product **6b** within the next 15 h. The insufficient concentration of the nucleophile is also reflected in the product **6b** yield of less than 40%.

By significantly increasing the amount of the nucleophile (12 equivalents) the reaction kinetic obtained, drastically changed (Figure 3.35 d). The THIQ **1** is converted directly into product **6b** on the NMR time scale, obtaining 80% product yield after 4 h. This is in contrast to reaction times of more than 20 h for limited amounts of the nucleophile (Figure 3.35 c). Furthermore, a linear product formation curve was obtained and no intermediate species were detected.

Conclusion and Outlook The efficiency of the phosphonylation reaction is not limited to aerobic reaction conditions. By performing the reaction with the help of an additional terminal oxidant or with high catalyst loadings full conversion can be achieved, thus enabling the investigation of the anaerobic pathway. The comparison of the different reaction profiles and experimental conditions suggested that for the *in situ* reaction still a radical pathway is operative. The iminium pathway under anaerobic conditions cannot be excluded due to the high amounts of iminium ion **2** obtained (Figure 3.35 c) and the linear product formation (Figure 3.35 d). Thoroughly investigations of the phosphonylation reaction are expected to elucidate the reaction mechanism and the species acting as a hydrogen atom acceptor, if the iminium pathway confimed to be operative under anaerobic conditions.

3.6.2.2 Light-Induced Reaction

In analogy to the light-induced aza-Henry reaction the phosphonylation reaction was performed in the absence of catalyst (refer to section 3.3) together with Anna Eisenhofer. To the best of our knowledge an effective light-induced background reaction of phosphonylation reactions has not been reported so far.

A sample containing THIQ **1** (200 mM) and diethyl phosphite (4 equiv.) in DMF-d_7 was irradiated extern with blue LEDs at room temperature (general procedure B). The reaction was performed under aerobic as well as anaerobic conditions, revealing that oxygen again is mandatory for an efficient conversion to the coupling product **6b**.

The reaction profile of the aerobic ^{1}H NMR kinetic is shown in Figure 3.36 a. Under air and continuous illumination the THIQ **1** starting material is converted into product **6b**. Both, the

decrease of THIQ **1** as well as the product formation appeared to be linear and after 6 h of illumination 30% of **6b** are obtained. The intermediate THIQ-OOH **11** concentration reached a maximum 2 mM. In contrast to the photocatalyzed reaction no dimer **9**, the intermediate of the radical pathway, was detected.

The product formation curve, the absence of dimer **9** and the requirement of oxygen for an efficient conversion are in good accordance with the reaction profiles of the light-induced aza-Henry reaction, suggesting that the light-induced phosphonylation occurs again via the iminium pathway, not via the radical pathway. However, as discussed above for the aza-Henry reaction an autoxidation mechanism (Scheme 3.9) cannot be excluded.

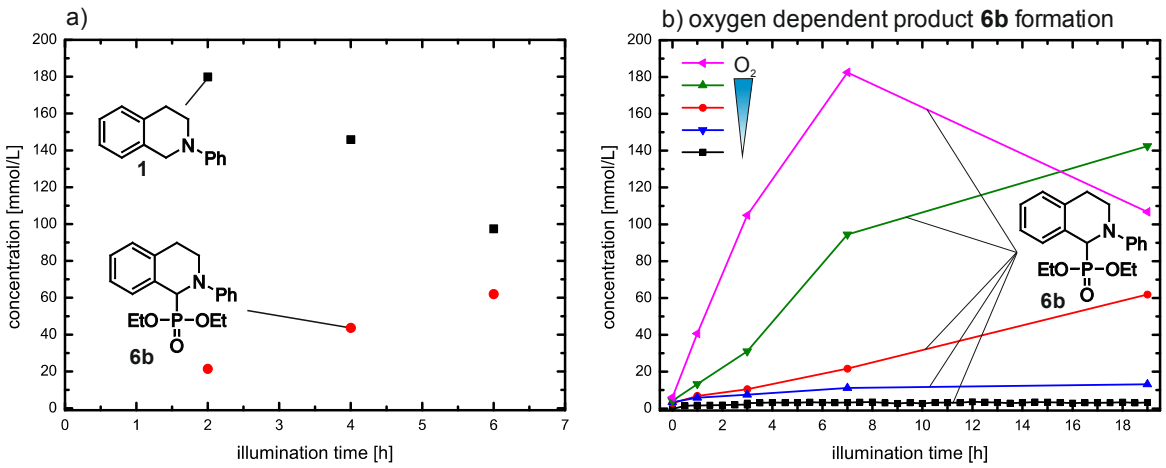

Figure 3.36 ^{1}H NMR reaction profile of the light induced phosphonlyation reaction of THIQ **1** in DMF-d_7 at room temperature (a) and influence of oxygen on the reaction rate and product **6b** yield (b).

In addition, the influence of oxygen was investigated, see Figure 3.36 b. Therefore, the reactions were performed *in situ* and *ex situ* with increased amounts of oxygen. The increased concentration of oxygen lead to an accelerated product **6b** formation rate and a product yield of 91% was obtained after 7 h (black), compared to 2% for *in situ* measurements. We could demonstrate that oxygen is mandatory for an efficient product **6b** formation and that the reaction rate is significantly accelerated by increasing oxygen content. Further control experiments confirmed, that light is also mandatory for an efficient product **6b** formation. In the absence of light 7% product **6b** were obtained after 16.5 h in the dark.

Illumination of the sample exceeding the full conversion to the phosphonylation product **6b** led to a significantly decreased product **6b** yield, together with the formation of the THIQ amides **22** and **23** shown in Figure 3.37 and Scheme 3.17. Based on the kinetic measurements performed we assume, that the amide formation is caused by over-oxidation of the product **6b** (Figure 3.37), in contrast to literature reports, where the THIQ amide **22** is described as a by-product under aerobic conditions, originating from interception of the iminium ion **2** or the α-amino radical by oxygen species (e.g superoxide).[11,12,31,82,99,151,154,155]

Scheme 3.17 Structures of the THIQ amides **22** and **23** obtained from over-oxidation.

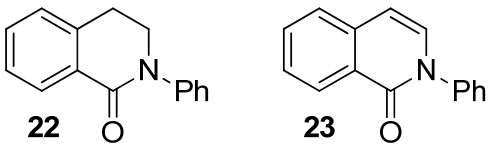

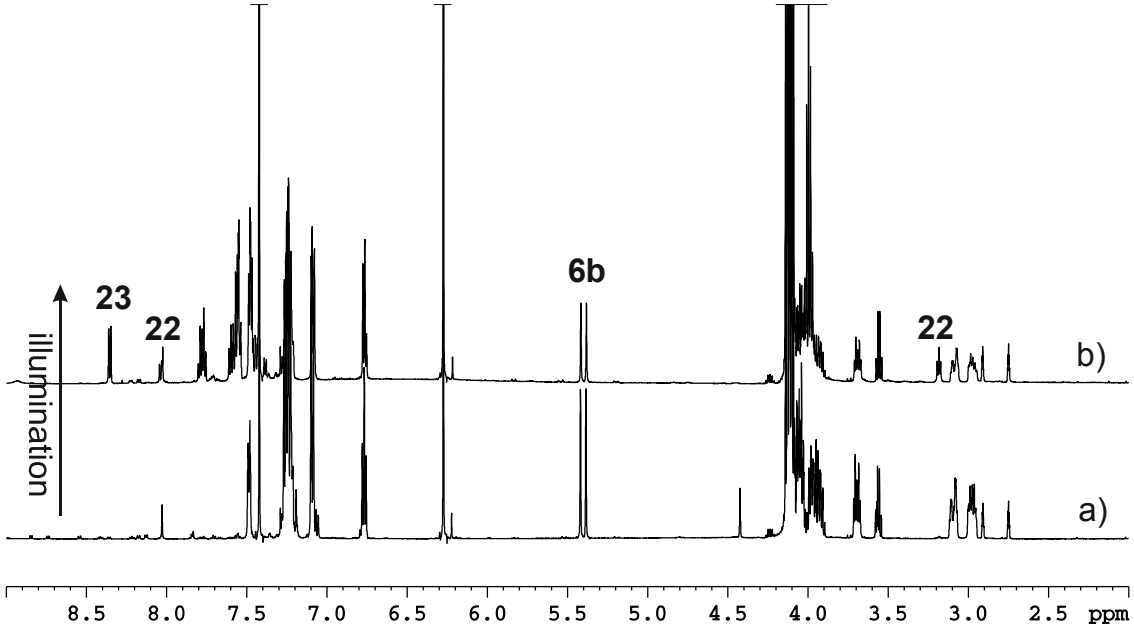

Figure 3.37 Stacked ^{1}H NMR spectra of product **6b** (a) and a mixture of **6b**, **22** and **23** after illumination with blue light (b) at 300 K in nitromethane-d_3.

Based on the experimental data described above, we suggest that the reaction mechanism is in accordance to the one described in Scheme 3.8. The detection of THIQ-OOH **11** and the absence of dimer **9**, as well as the linear product formation curve and the necessity of oxygen and light are in analogy to the aza-Henry reaction. The initiation of the initial electron transfer leading the THIQ radical cation $\mathbf{1}^{\bullet+}$ remained so far unclear, and needs further investigation.

3.6.3 Chemical Shift Assignment

2-(4-Methoxyphenyl)-1,2,3,4-tetrahydroisoquinoline (15)

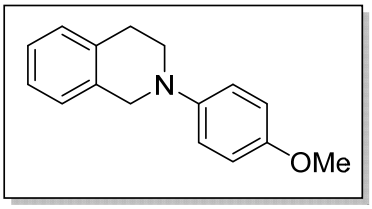

Synthesized according to the general procedure. NMR data are in accordance with literature reported values.[125]

^{1}H NMR (400 MHz, $CDCl_3$, 298 K): δ [ppm] = 7.17-7.1 (m, 4H), 7.01-6.99 (m, 2H), 6.87-6.83 (m, 2H), 4.30 (s, 2H), 3.76 (s, 3H), 3.45 (t, *J* = 5.8 Hz, 2H), 2.98 (t, *J* = 5.7 Hz, 2H).

^{13}C NMR (100 MHz, $CDCl_3$, 298 K): δ [ppm] = 153.7, 145.3, 134.6, 134.5, 128.9, 126.4, 126.2, 118.3, 114.7, 55.9, 53.0, 48.7, 29.4.

2-(4-Methoxyphenyl)-1-(nitromethyl)-1,2,3,4-tetrahydroisoquinoline (19)

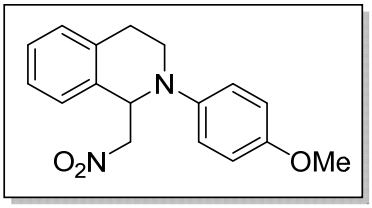

Synthesized according to the general procedure B. NMR data are in accordance with literature reported values.[36] Coupling pattern differs due to deuterated nitromethane-d_3.

^{1}H NMR (600 MHz, NO_2Me-d_3, 300 K): δ [ppm] =7.30-7.28 (m, 1H), 7.27-7.25 (m, 1H), 7.26-7.24 (m, 1H), 7.20-7.19 (m, 1H), 6.99 (d, *J* = 9.1 Hz, 2H), 6.84 (d, *J* = 9.1 Hz, 2H), 5.46 (s, 1H), 4.95, 4.78, 3.73 (s, 3H), 3.69-3.63 (m, 2H), 3.02-2.97 (m, 1H), 2.73 (dt, *J* = 16.8 Hz, *J* = 3.3 Hz, 1H).

^{13}C NMR (150 MHz, NO_2Me-d_3, 300 K): δ [ppm] = 155.3, 144.7, 137.5, 134.2, 130.8, 129.1, 128.6, 127.7, 119.9, 115.8, 79.5, 59.7, 56.1, 43.7, 26.1.

1-Phenyl-2-diethylphosphonate-1,2,3,4-tetrahydroisoquinoline (6b)

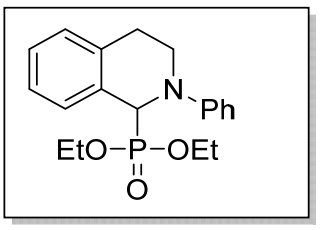

Synthesized according to the general procedure B. NMR data are in accordance with literature reported values.[36]

^{1}H NMR (600 MHz, DMF-d_7, 291 K): δ [ppm] = 7.50-7.47 (m, 1H), 7.28-7.21 (m, 5H), 7.09 (*J* = 8.5 Hz, 2H), 6.77 (t, *J* = 7.13 Hz, 1H), 5.40 (d, *J* = 20.7 Hz, 1H), 4.09-3.90 (m, 5H), 3.72-

3.67 (m, 1H), 3.12-3.07 (m, 1H), 3.00-2.94 (m, 1H), 1.22 (t, *J* = 7.0 Hz, 3H), 1.12 (t, *J* = 7.0 Hz, 3H).

2-Phenyl-3,4-diahydroisoquinolin-1(*2H*)-one (22)

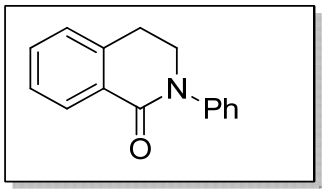

Synthesized according to Kohls *et al*.[82] by Anna Eisenhofer. NMR data are in accordance with literature reported values.

^{1}H NMR (600 MHz, NO_2Me-d_3, 300 K): δ [ppm] = 8.01 (dd, *J* = 7.7 Hz, *J* = 0.9 Hz, 1H), 7.52 (td, *J* = 7.5 Hz, *J* = 1.4 Hz, 1H), 7.5-7.28 (m, 6H), 4.02 (t, *J* = 6.6 Hz, 2H), 3.20 (t, *J* = 6.5 Hz, 2H).

2-Phenyl-isoquinolin-1(*2H*)-one (23)

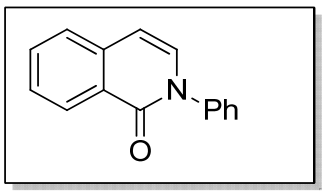

Synthesized according to Sugahara *et al.*[156] by Anna Eisenhofer. NMR data are in accordance with literature reported values.

^{1}H NMR (600 MHz, NO_2Me-d_3, 300 K): δ [ppm] = 8.33 (d, *J* = 8.0 Hz, 1H), 7.75 (td, *J* = 7.2 Hz, *J* = 1.3 Hz, 1H), 7.68 (d, *J* = 7.8 Hz, 1H), 7.58-7.54 (m, 3H), 7.50-7.47 (m, 3H), 7.32 (d, *J* = 7.4 Hz, 1H),6.68 (d, *J* = 7.4 Hz, 1H).

3.7 NMR spectra

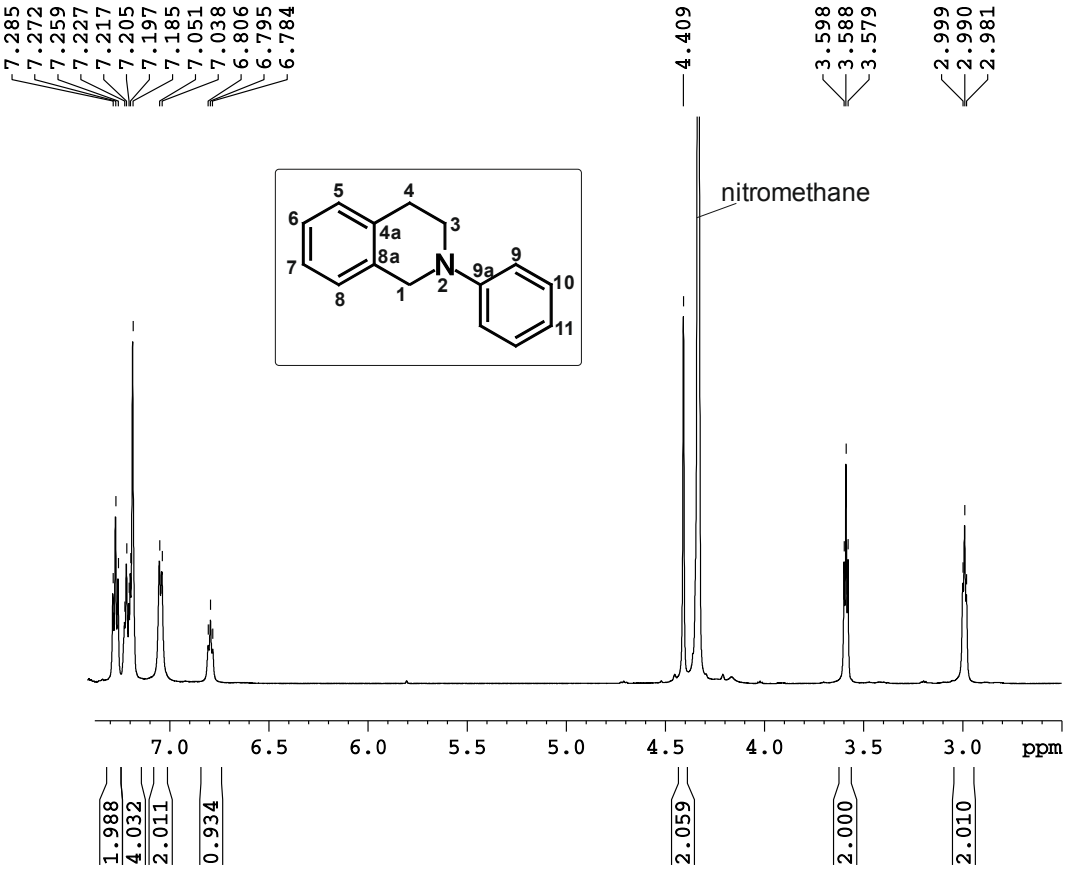

Figure 3.38 ^{1}H NMR spectrum of THIQ **1** in nitromethane-d_3 at 300 K.

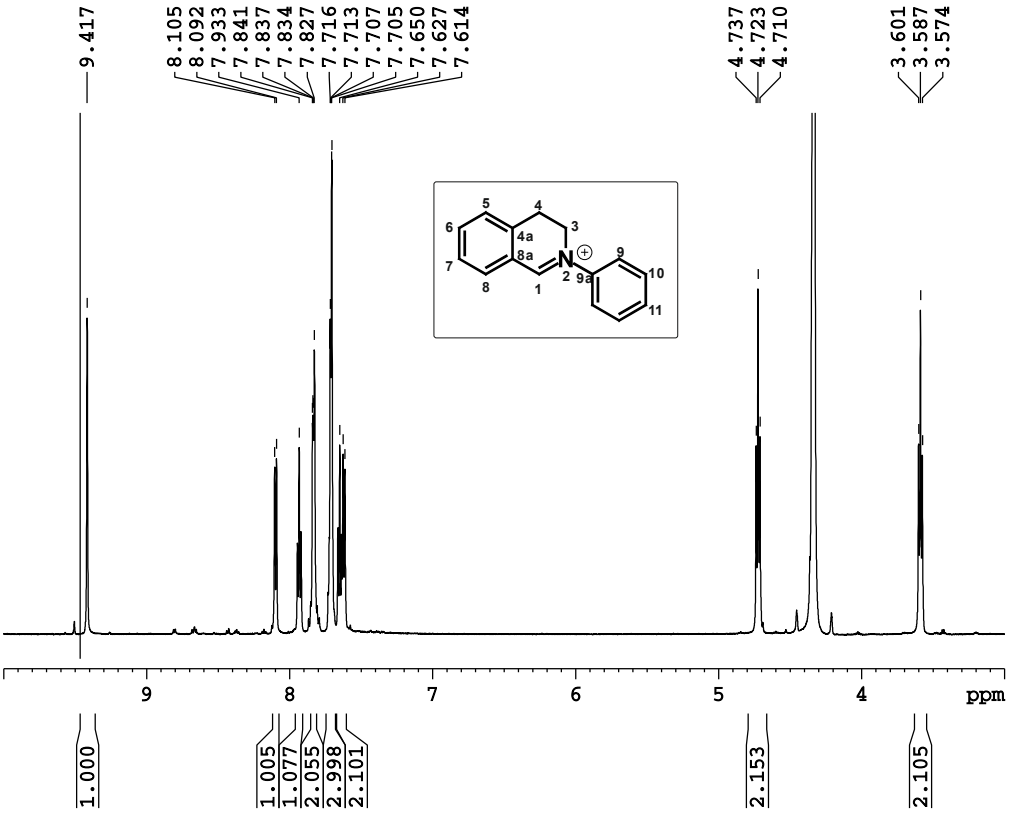

Figure 3.39 ^{1}H NMR spectrum of THIQ iminium bromide **2d** in nitromethane-d_3 at 300 K.

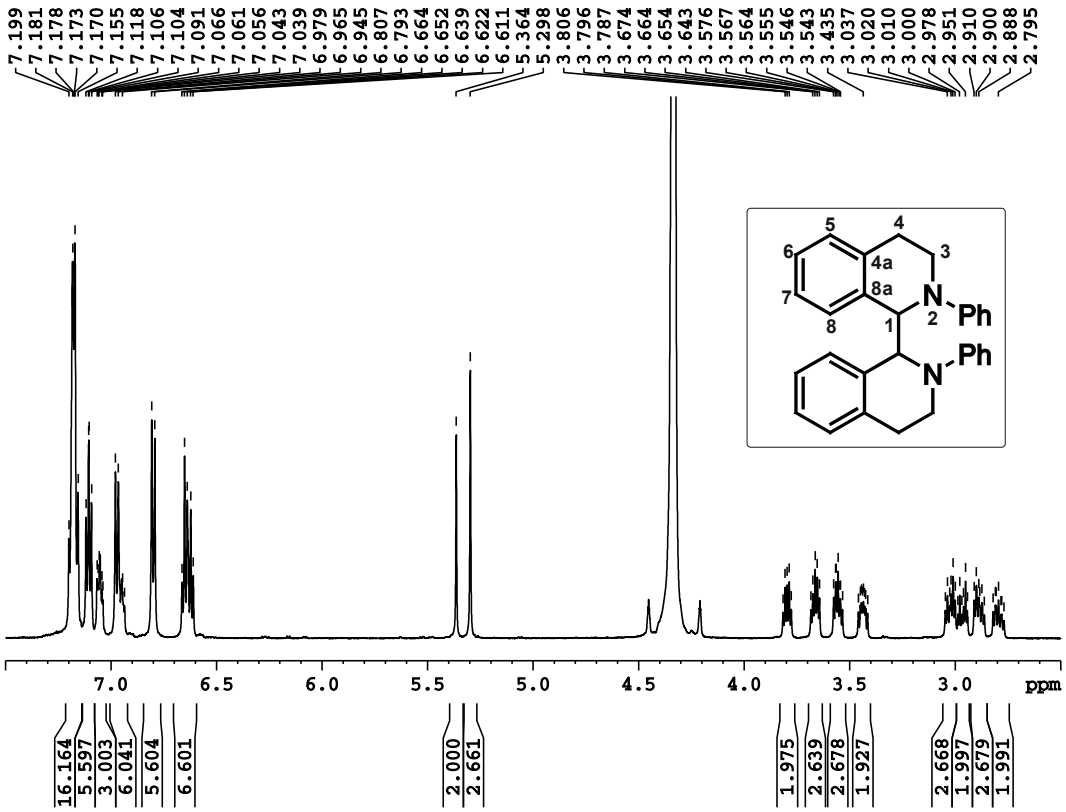

Figure 3.40 ^{1}H NMR spectrum of THIQ dimer **9** in nitromethane-d_3 at 298 K.

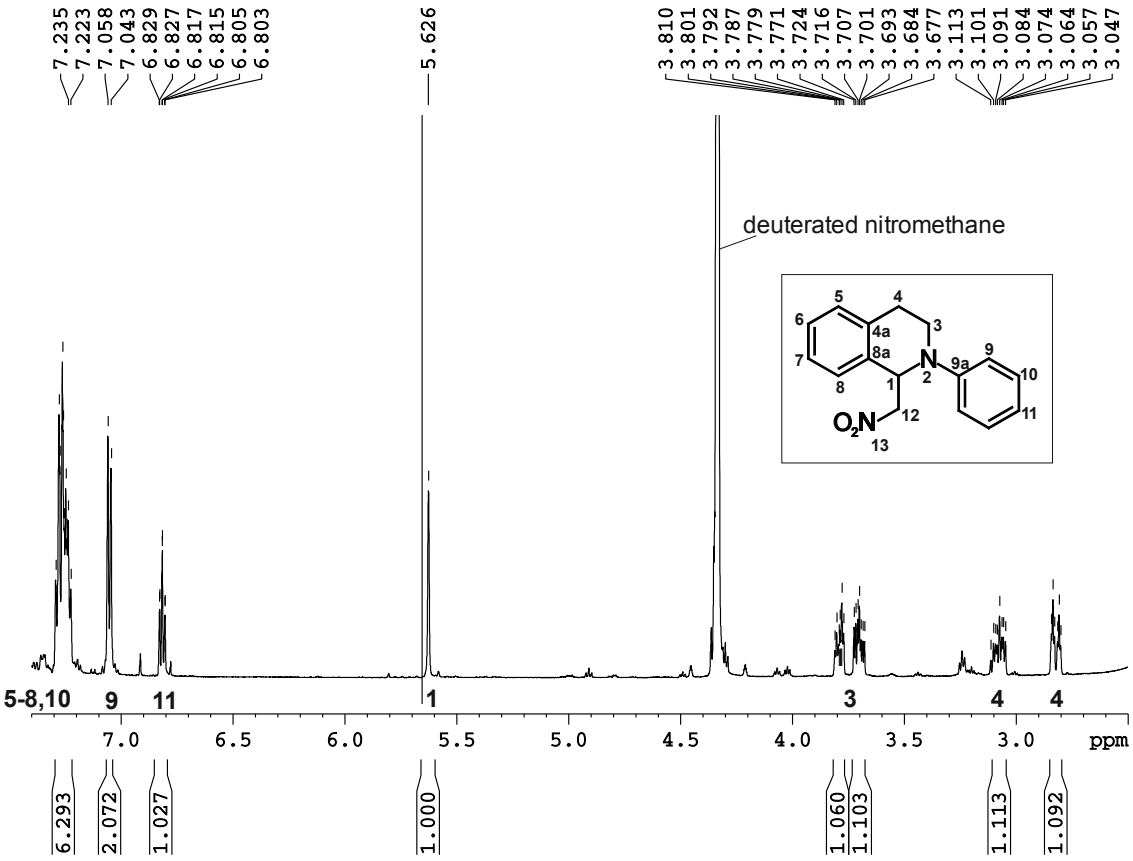

Figure 3.41 ^{1}H NMR spectrum of β-nitroamine coupling product **6a** in nitromethane-d_3 at 300 K.

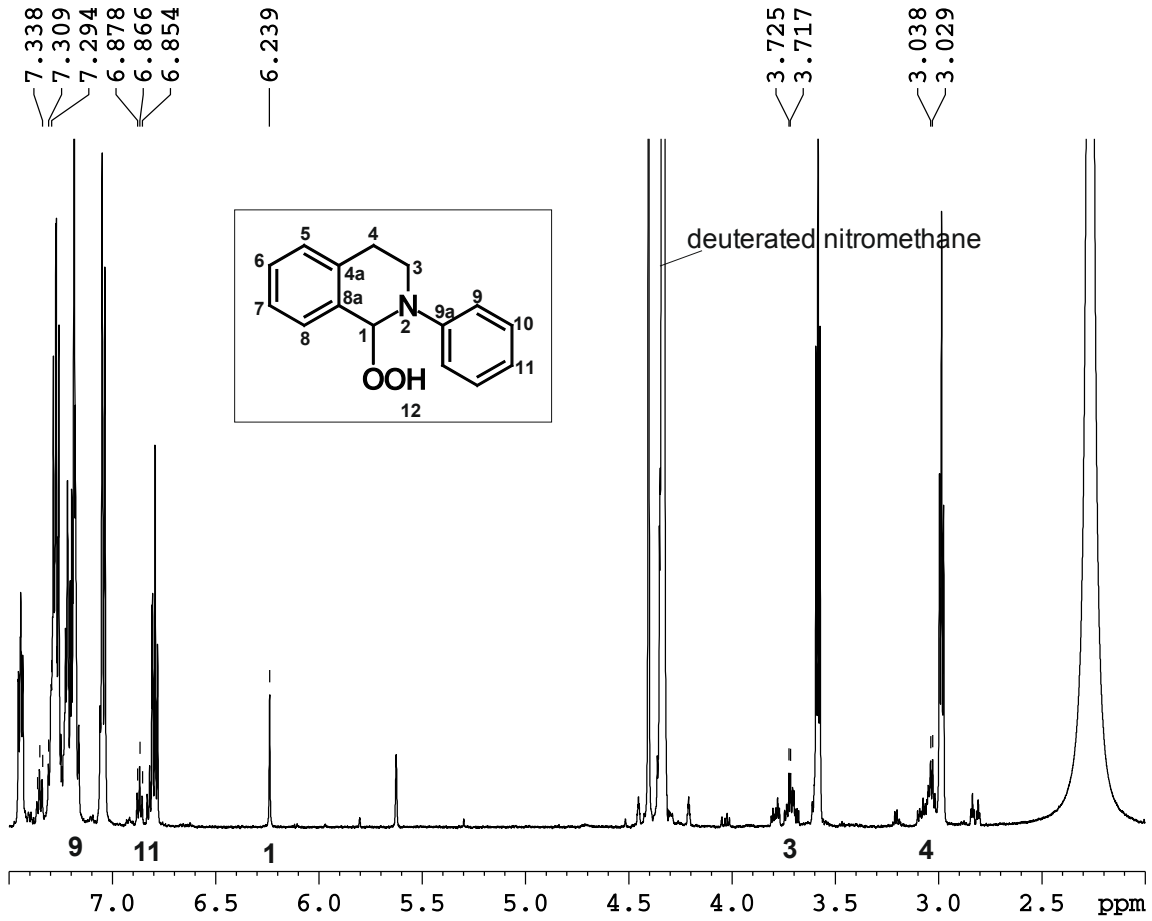

Figure 3.42 ^{1}H NMR spectrum of THIQ-OOH **11** in nitromethane-d_3 at 300 K.

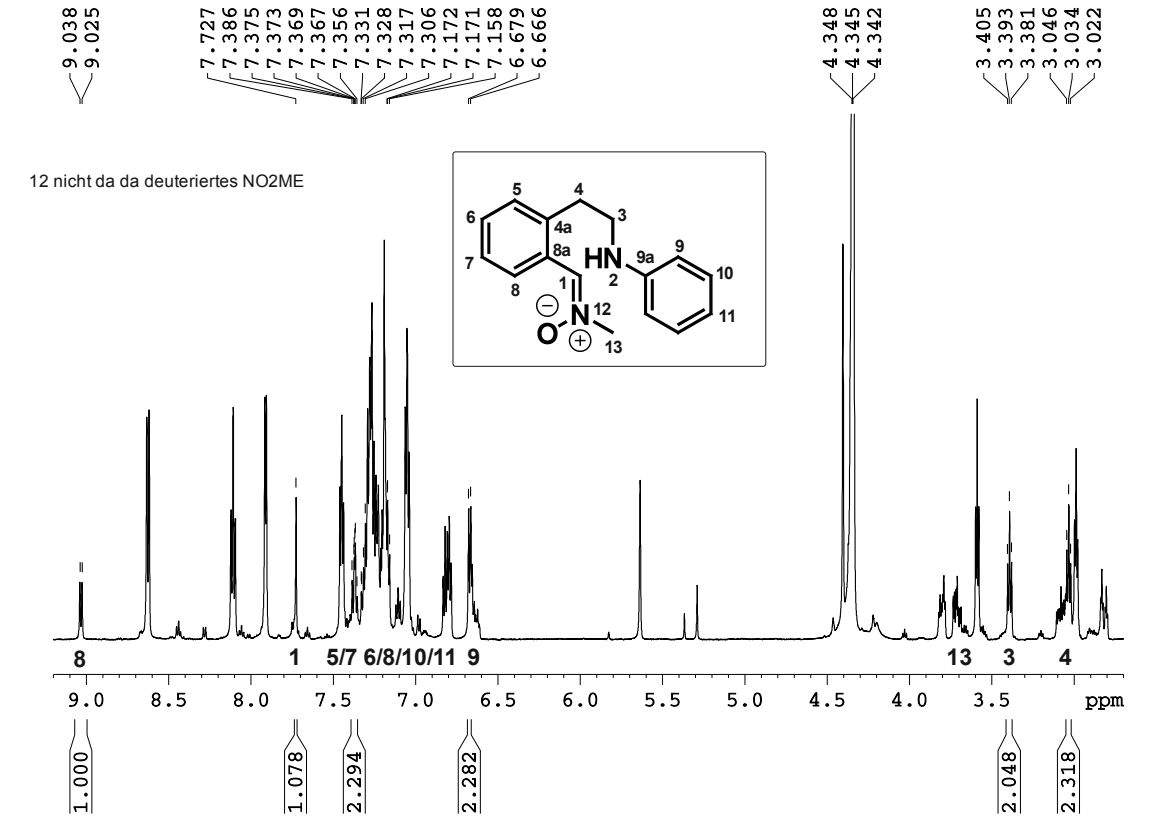

Figure 3.43 ^{1}H NMR spectrum of the ring-opened THIQ intermediate **10** in nitromethane-d_3 at 280 K.

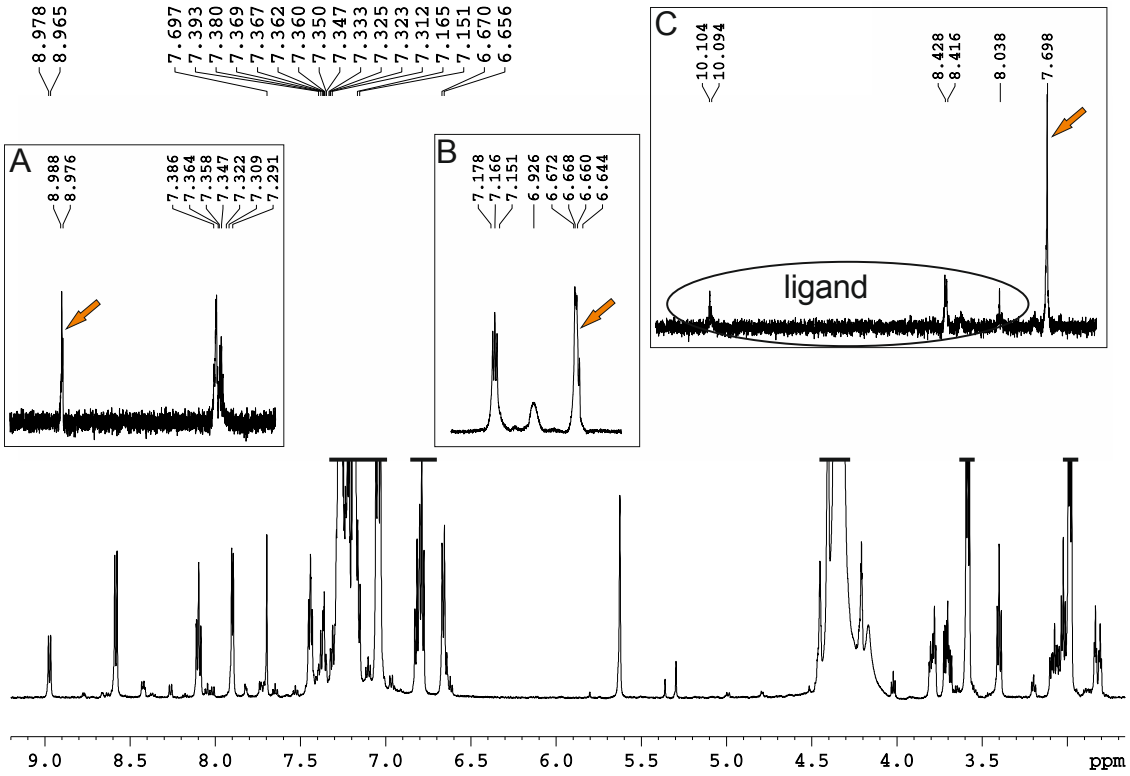

Figure 3.44 1D selective tocsy spectra showing the spin systems of the intermediate **10** at 300 K.

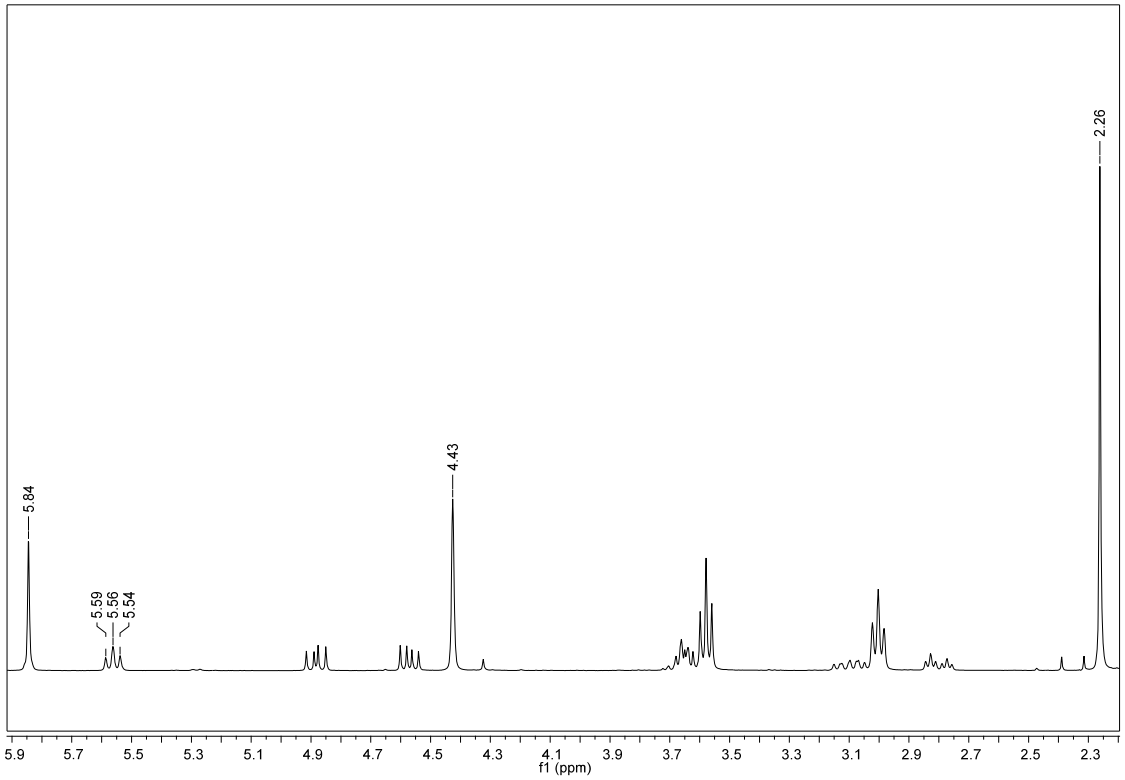

Figure 3.45 Crude ^{1}H NMR spectrum (300 MHz, $CDCl_3$) of the aza-Henry reaction between amine **1** and nitromethane **5a**. 2,5-Dimethylfuran was added as internal standard (5.84 ppm (s, 2H), 2.26 ppm (s, 6H)).[126] For entry 1-4 (Table 3.1), the product peak at 5.56 ppm and the substrate peak at 4.43 ppm were used to calculate the product yield and the amount of unreacted starting material.

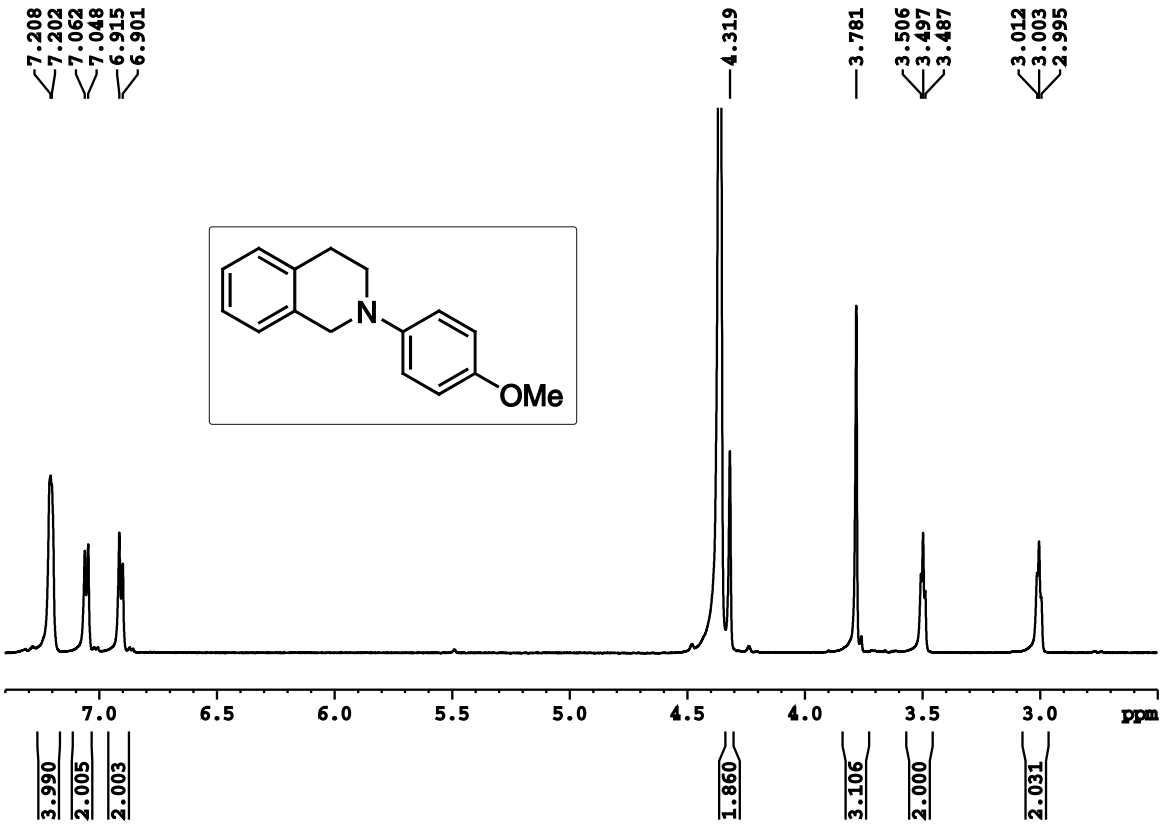

Figure 3.46 ^{1}H NMR spectrum of 2-(4-Methoxyphenyl)-1,2,3,4-tetrahydroisoquinoline **15** in nitromethane-d_3 at 300 K.

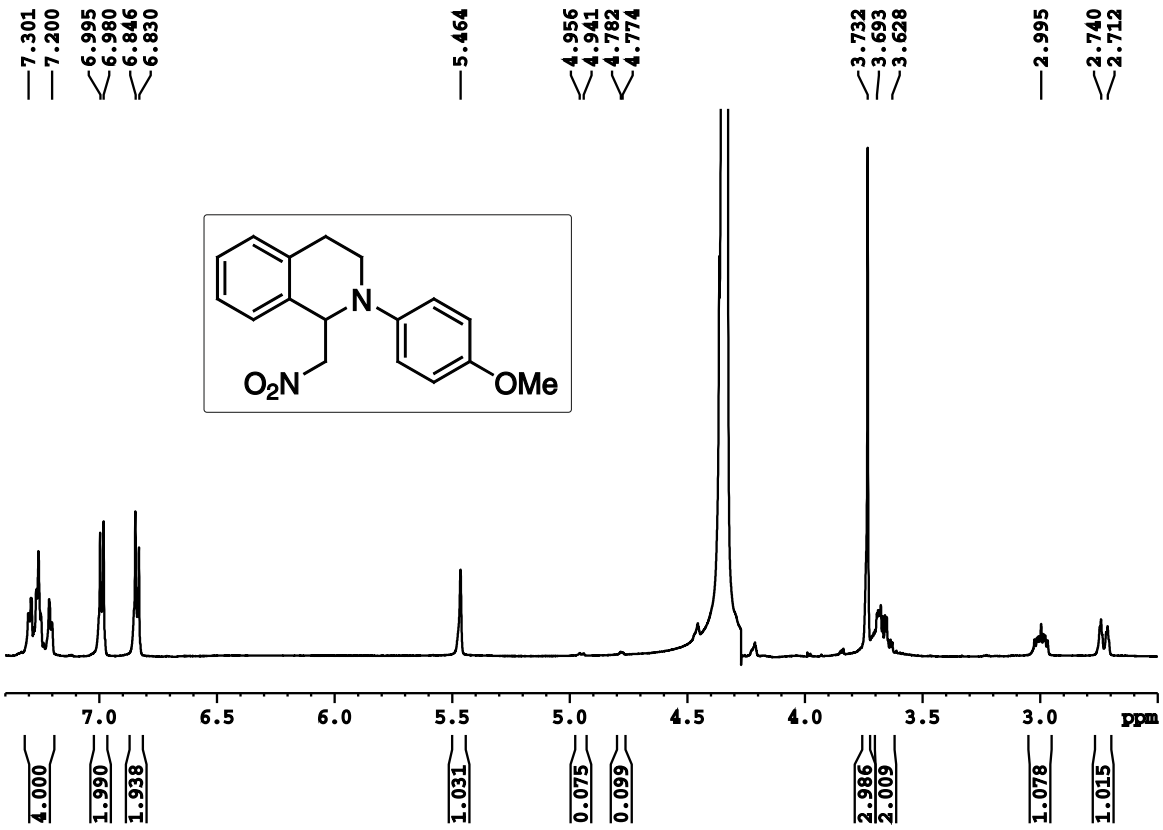

Figure 3.47 ^{1}H NMR spectrum of 2-(4-Methoxyphenyl)-1-(nitromethyl)-1,2,3,4-tetrahydroisoquinoline **19** in nitromethane-d_3 at 300 K.

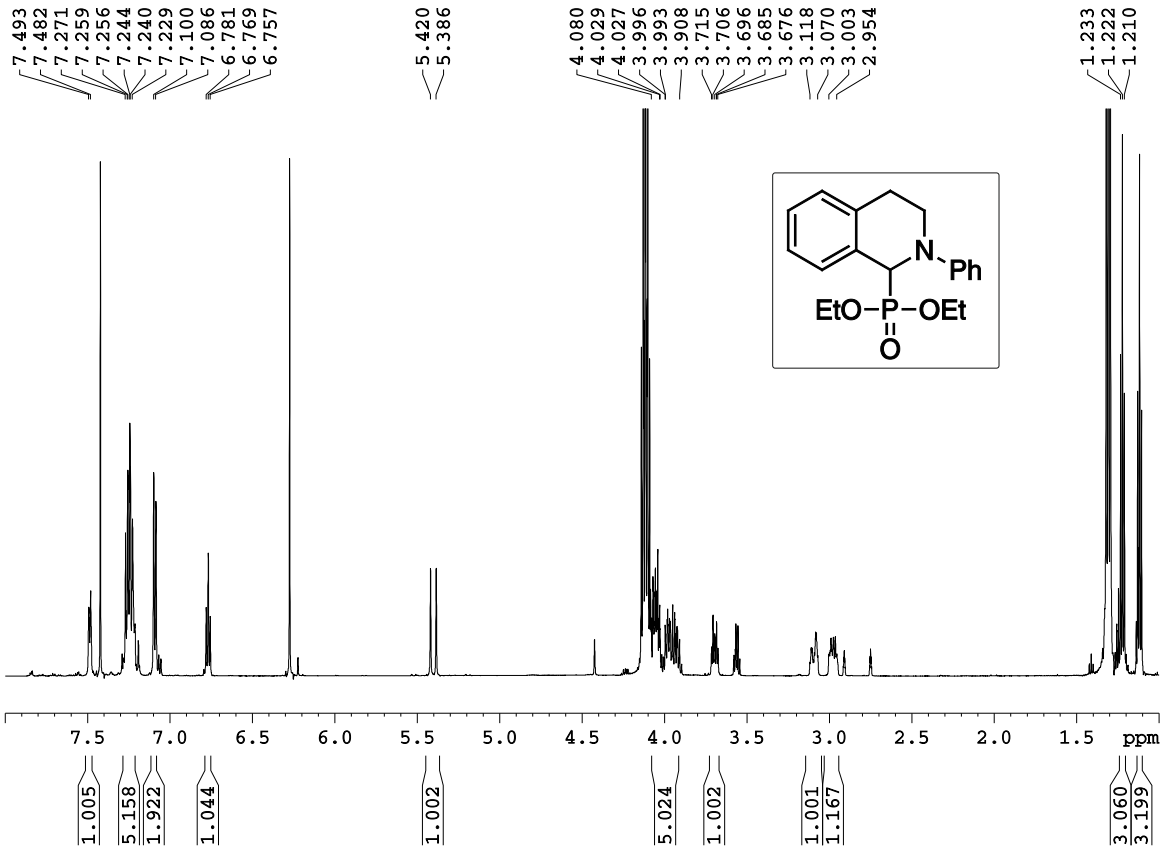

Figure 3.48 ^{1}H NMR spectrum of 1-Phenyl-2-diethylphosphonate-1,2,3,4-tetrahydroisoquinoline **6b** in DMF-d_7 at 291 K.

3.8 References

[1] C.-J. Li, *Acc. Chem. Res.* **2009**, *42*, 335–344.

[2] W.-J. Yoo, C.-J. Li, in *Top. Curr. Chem.* (Eds.: J.-Q. Yu, Z. Shi), Springer-Verlag, Berlin Heidelberg, **2009**, pp. 281–302.

[3] C. S. Yeung, V. M. Dong, *Chem. Rev.* **2011**, *111*, 1215–1292.

[4] J. M. R. Narayanam, C. R. J. Stephenson, *Chem. Soc. Rev.* **2011**, *40*, 102–113.

[5] T. P. Yoon, M. A. Ischay, J. Du, *Nat. Chem.* **2010**, *2*, 527–532.

[6] F. Teplý, *Collect. Czechoslov. Chem. Commun.* **2011**, *76*, 859–917.

[7] L. Shi, W. Xia, *Chem. Soc. Rev.* **2012**, *41*, 7687–7697.

[8] J. Xuan, W.-J. Xiao, *Angew. Chem. Int. Ed.* **2012**, *51*, 6828–6838.

[9] T. P. Yoon, *ACS Catal.* **2013**, *3*, 895–902.

[10] C. K. Prier, D. A. Rankic, D. W. C. MacMillan, *Chem. Rev.* **2013**, *113*, 5322–5363.

[11] J. Hu, J. Wang, T. H. Nguyen, N. Zheng, *Beilstein J. Org. Chem.* **2013**, *9*, 1977–2001.

[12] M. Reckenthäler, A. G. Griesbeck, *Adv. Synth. Catal.* **2013**, *355*, 2727–2744.

[13] Y. Xi, H. Yi, A. Lei, *Org. Biomol. Chem.* **2013**, *11*, 2387–2403.

[14] D. P. Hari, B. König, *Angew. Chemie - Int. Ed.* **2013**, *52*, 4734–4743.

[15] J. W. Beatty, C. R. J. Stephenson, *Acc. Chem. Res.* **2015**, *48*, 1474–1484.

[16] J. Xie, H. Jin, P. Xu, C. Zhu, *Tetrahedron Lett.* **2014**, *55*, 36–48.

[17] For pioneering work from Murashi and Li refer to: (a) Murahashi, S.-I.; Nakae, T.; Terai, H.; Komiya, N. *JACS*, **2008**, *130*, 11005. (b) Li, Z.; Bohle, D. S.; Li, C.-J. *PNAS* **2006**, *103*, 8928. (c) Li, C.-J. *Acc. Chem. Res*. **2009**, *42*, 335; For mechanistic studies of Doyle and Klussmann refer to: [70], [72].

[18] T. Chiba, Y. Takata, *J. Org. Chem.* **1977**, *42*, 2973–2977.

[19] T. Shono, Y. Matsumura, K. Tsubata, *J. Am. Chem. Soc.* **1981**, *103*, 1172–1176.

[20] O. Baslé, N. Borduas, P. Dubois, J. M. Chapuzet, T.-H. Chan, J. Lessard, C.-J. Li, *Chem. - A Eur. J.* **2010**, *16*, 8162–8166.

[21] A. S.-K. Tsang, M. H. Todd, *Tetrahedron Lett.* **2009**, *50*, 1199–1202.

[22] A. S.-K. Tsang, P. Jensen, J. M. Hook, A. S. K. Hashmi, M. H. Todd, *Pure Appl. Chem.* **2011**, *83*, 655–665.

[23] H. Wang, X. Li, F. Wu, B. Wan, *Tetrahedron Lett.* **2012**, *53*, 681–683.

[24] G. Zhang, Y. Ma, S. Wang, W. Kong, R. Wang, *Chem. Sci.* **2013**, *4*, 2645–2651.

[25] G. Pandey, *Tetrahedron Lett.* **1988**, *29*, 4153–4156.

[26] G. Pandey, G. Kumaraswamy, P. Y. Reddy, *Tetrahedron* **1992**, *48*, 8295–8308.

[27] G. Pandey, S. R. Gadre, *ARKIVOC* **2003**, 45–54.

[28] A. G. Condie, J. C. González-Gómez, C. R. J. Stephenson, *J. Am. Chem. Soc.* **2010**, *132*, 1464–1465.

[29] D. B. Freeman, L. Furst, A. G. Condie, C. R. J. Stephenson, *Org. Lett.* **2012**, *14*, 94–97.

[30] J. W. Tucker, Y. Zhang, T. F. Jamison, C. R. J. Stephenson, *Angew. Chemie - Int. Ed.* **2012**, *51*, 4144–4147.

[31] M. Neumann, K. Zeitler, *Org. Lett.* **2012**, *14*, 2658–2661.

[32] W.-P. To, Y. Liu, T.-C. Lau, C.-M. Che, *Chem. - A Eur. J.* **2013**, *19*, 5654–5664.

[33] J.-J. Zhong, Q.-Y. Meng, G.-X. Wang, Q. Liu, B. Chen, K. Feng, C.-H. Tung, L.-Z. Wu, *Chem. - A Eur. J.* **2013**, *19*, 6443–6450.

[34] C.-J. Wu, J.-J. Zhong, Q.-Y. Meng, T. Lei, X.-W. Gao, C.-H. Tung, L.-Z. Wu, *Org. Lett.* **2015**, *17*, 884–887.

[35] B. Wang, D. P. Shelar, X.-Z. Han, T.-T. Li, X. Guan, W. Lu, K. Liu, Y. Chen, W.-F. Fu, C.-

M. Che, *Chem. - A Eur. J.* **2015**, *21*, 1184–1190.

[36] D. P. Hari, B. König, *Org. Lett.* **2011**, *13*, 3852–3855.

[37] Q. Liu, Y.-N. Li, H.-H. Zhang, B. Chen, C.-H. Tung, L.-Z. Wu, *Chem. - A Eur. J.* **2012**, *18*, 620–627.

[38] Y. Pan, C. W. Kee, L. Chen, C.-H. Tan, *Green Chem.* **2011**, *13*, 2682–2685.

[39] M. N. Gandy, C. L. Raston, K. A. Stubbs, *Chem. Commun.* **2015**, *51*, 11041–11044.

[40] Y. Zhao, C. Zhang, K. F. Chin, O. Pytela, G. Wei, H. Liu, F. Bures, Z. Jiang, *RSC Adv.* **2014**, *4*, 30062–30067.

[41] X.-Z. Wang, Q.-Y. Meng, J.-J. Zhong, X.-W. Gao, T. Lei, L.-M. Zhao, Z.-J. Li, B. Chen, C.-H. Tung, L.-Z. Wu, *Chem. Commun.* **2015**, *51*, 11256–11259.

[42] L. Huang, J. Zhao, *RSC Adv.* **2013**, *3*, 23377–23388.

[43] M. Rueping, C. Vila, T. Bootwicha, *ACS Catal.* **2013**, *3*, 1676–1680.

[44] M. Rueping, J. Zoller, D. C. Fabry, K. Poscharny, R. M. Koenigs, T. E. Weirich, J. Mayer, *Chem. - A Eur. J.* **2012**, *18*, 3478–3481.

[45] J. Wang, J. Ma, X. Li, Y. Li, G. Zhang, F. Zhang, X. Fan, *Chem. Commun.* **2014**, *50*, 14237–14240.

[46] T. Mitkina, C. Stanglmair, W. Setzer, M. Gruber, H. Kisch, B. König, *Org. Biomol. Chem.* **2012**, *10*, 3556–3561.

[47] L. Möhlmann, M. Baar, J. Rieß, M. Antonietti, X. Wang, S. Blechert, *Adv. Synth. Catal.* **2012**, *354*, 1909–1913.

[48] C. Wang, Z. Xie, K. E. DeKrafft, W. Lin, *J. Am. Chem. Soc.* **2011**, *133*, 13445–13454.

[49] W.-Q. Zhang, Q.-Y. Li, Q. Zhang, Y. Lu, H. Lu, W. Wang, X. Zhao, X.-J. Wang, *Inorg. Chem.* **2016**, *55*, 1005–1007.

[50] Z. Xie, C. Wang, K. E. DeKrafft, W. Lin, *J. Am. Chem. Soc.* **2011**, *133*, 2056–2059.

[51] C. Wang, Z. Xie, K. E. DeKrafft, W. Lin, *ACS Appl. Mater. Interfaces* **2012**, *4*, 2288–2294.

[52] J.-L. Wang, C. Wang, K. E. DeKrafft, W. Lin, *ACS Catal.* **2012**, *2*, 417–424.

[53] J.-X. Jiang, Y. Li, X. Wu, J. Xiao, D. J. Adams, A. I. Cooper, *Macromolecules* **2013**, *46*, 8779–8783.

[54] A summary of the different literature reported photo-catalytic aerobic aza-Henry reactions including the applied conditions and yields is given in Table 3.5.

[55] In some cases singlet oxygen generated photochemically from the excited state of the respective catalyst was proposed as active oxidant: [32]; (a) Xue, Q.; Xie, J.; Jin, H.; Cheng, Y.; Zhu, C. *Org. Biomol. Chem*. **2013**, *11*, 1606. (b) Pan, Y.; Wang, S.; Kee, C. W.; Dubuisson, E.; Yang, Y.; Loh, K. P.; Tan, C.-H. *Green Chem*. **2011**, *13*, 3341.

[56] P. J. DeLaive, J. T. T. Lee, H. W. Sprintschnik, H. Abruna, T. J. Meyer, D. G. Whitten, *J. Am. Chem. Soc.* **1977**, *99*, 7094–7097.

[57] P. J. DeLaive, T. K. Foreman, C. Giannotti, D. G. Whitten, *J. Am. Chem. Soc.* **1980**, *102*, 5627–5631.

[58] J.-J. Zhong, Q.-Y. Meng, B. Liu, X.-B. Li, X.-W. Gao, T. Lei, C.-J. Wu, Z.-J. Li, C.-H. Tung, L.-Z. Wu, *Org. Lett.* **2014**, *16*, 1988–1991.

[59] J.-J. Zhong, C.-J. Wu, Q.-Y. Meng, X.-W. Gao, T. Lei, C.-H. Tung, L.-Z. Wu, *Adv. Synth. Catal.* **2014**, *356*, 2846–2852.

[60] Further proof for the radical cation is provided by Menche et al. for the Cu-catalyzed CDC reaction: Wang, T.; Schrempp, M.; Berndhäusler, A.; Schiemann, O.; Menche, D. *Org. Lett*. **2015**, *17*, 3982.

[61] The extent of the acidifing effect upon oxidation of tertiary amines is a topic under debate. (a) Nelson, S. F.; Ippoliti, J. T. *J. Am. Chem. Soc*. **1986**, *108*, 4879. (b) Lewis, F. D. *Acc. Chem. Res*. **1986**, *19*, 401. (c) Parker, V. D.; Tilset, M. *J. Am. Chem. Soc*. **1991**,

113, 8778.; (d) Dombrowski, G. W.; Dinnocenzo, J. P.; Zielinski, P. A.; Farid, S.; Wosinska, Z. M.; Gould, I. R. *J. Org. Chem*. **2005**, *70*, 3791.

[62] E. Boess, D. Sureshkumar, A. Sud, C. Wirtz, C. Farès, M. Klussmann, *J. Am. Chem. Soc.* **2011**, *133*, 8106–8109.

[63] J. F. Franz, W. B. Kraus, K. Zeitler, *Chem. Commun.* **2015**, *51*, 8280–8283.

[64] J. Xuan, T.-T. Zeng, Z.-J. Feng, Q.-H. Deng, J.-R. Chen, L.-Q. Lu, W.-J. Xiao, H. Alper, *Angew. Chemie - Int. Ed.* **2015**, *54*, 1625–1628.

[65] C. R. Bock, J. A. Connor, A. R. Gutierrez, T. J. Meyer, D. G. Whitten, B. P. Sullivan, J. K. Nagle, *J. Am. Chem. Soc.* **1979**, *101*, 4815–4824.

[66] D. D. M. Wayner, J. J. Dannenberg, D. Griller, *Chem. Phys. Lett.* **1986**, *131*, 189–191.

[67] C. P. Anderson, D. J. Salmon, T. J. Meyer, R. C. Young, *J. Am. Chem. Soc.* **1977**, *99*, 1980–1982.

[68] D. T. Sawyer, M. J. Gibian, M. M. Morrison, E. T. Seo, *J. Am. Chem. Soc.* **1978**, *100*, 627–628.

[69] J. Xie, Q. Xue, H. Jin, H. Li, Y. Cheng, C. Zhu, *Chem. Sci.* **2013**, *4*, 1281–1286.

[70] M. O. Ratnikov, M. P. Doyle, *J. Am. Chem. Soc.* **2013**, *135*, 1549–1557.

[71] E. Boess, D. Sureshkumar, A. Sud, C. Wirtz, C. Farès, M. Klussmann, *J. Am. Chem. Soc.* **2011**, *133*, 8106–8109.

[72] E. Boess, C. Schmitz, M. Klussmann, *J. Am. Chem. Soc.* **2012**, *134*, 5317–5325.

[73] E. Boess, L. M. Wolf, S. Malakar, M. Salamone, M. Bietti, W. Thiel, M. Klussmann, *ACS Catal.* **2016**, *6*, 3253–3261.

[74] Xia et al. adopted the principle of an off-cycle equilibrium for the photoredox catalyzed Mannich reaction to suppress the formation of amide by-product: Zhao, G.; Yang, C.; Guo, L.; Sun, H.; Chen, C.; Xia, W. *Chem. Commun*. **2012**, *48*, 2337.

[75] C. Feldmeier, H. Bartling, E. Riedle, R. M. Gschwind, *J. Magn. Reson.* **2013**, *232*, 39–44.

[76] Low to not detectable yields of iminium ion **2** are in accordance with the results obtained by Klussmann et al. [72]. They suggested, that the detection of the iminium ion **2** is pKa dependent and that more acidic conditions shift the equilibrium from THIQ peroxide species **8** towards iminium ion **2**. Further increasing pH values are reported in the progressing reaction.

[77] K. Lammertsma, B. V Prasad, *J. Am. Chem. Soc.* **1993**, *115*, 2348–2351.

[78] K. Lammertsma, P. V. Bharatam, *J. Org. Chem.* **2000**, *65*, 4662–4670.

[79] R. Balamurugan, S. Manojveer, *Chem. Commun.* **2011**, *47*, 11143–11145.

[80] R. Engelke, W. L. Earl, C. McMichael Rohlfing, *J. Phys. Chem.* **1986**, *90*, 545–547.

[81] As previously reported by Todd et al. [22] and Stepenson et al. [29] we found isolated THIQ iminium bromide **2d** in nitromethane to be unreactive until triethylamine (TEA) is added to the reaction mixture. After the addition of 2 equiv. of TEA the iminium ion **2d** is fully converted into the product **6a** within 90 s (elapsed time before measuring), showing the necessity of the activation of the pronucleophile nitromethane to its reactive aci anion form.

[82] P. Kohls, D. Jadhav, G. Pandey, O. Reiser, *Org. Lett.* **2012**, *14*, 672–675.

[83] L. Ruiz Espelt, E. M. Wiensch, T. P. Yoon, *J. Org. Chem.* **2013**, *78*, 4107–4114.

[84] Y. Miyake, K. Nakajima, Y. Nishibayashi, *J. Am. Chem. Soc.* **2012**, *134*, 3338–3341.

[85] X. Liu, X. Ye, F. Bures, H. Liu, Z. Jiang, *Angew. Chemie - Int. Ed.* **2015**, *54*, 11443–11447.

[86] Wu and coworkers detected traces of dimer **9** under aerobic conditions for the photocatalyzed aza-Henry reaction [41].

[87] S. Murata, K. Teramoto, M. Miura, M. Nomura, *Heterocycles* **1993**, *36*, 2147–2153.

[88] M. Nishino, K. Hirano, T. Satoh, M. Miura, *J. Org. Chem.* **2011**, *76*, 6447–6451.
[89] P. Bernhard, A. M. Sargeson, F. C. Anson, *Inorg. Chem.* **1988**, *27*, 2754–2760.
[90] P. Bernhard, F. C. Anson, *Inorg. Chem.* **1988**, *27*, 4574–4577.
[91] D. T. Sawyer, M. J. Gibian, *Tetrahedron* **1979**, *35*, 1471–1481.
[92] J. Wilshire, D. T. Sawyer, *Acc. Chem. Res.* **1979**, *12*, 105–110.
[93] E. J. Nanni, D. T. Sawyer, *J. Am. Chem. Soc.* **1980**, *102*, 7591–7593.
[94] D. T. Sawyer, J. S. Valentine, *Acc. Chem. Res.* **1981**, *14*, 393–400.
[95] D. T. Sawyer, T. S. Calderwood, C. L. Johlman, C. L. Wilkins, *J. Org. Chem.* **1985**, *50*, 1409–1412.
[96] Z.-R. Zheng, N. T. Kjaer, H. Lund, *Acta Chem. Scand.* **1998**, *52*, 362–365.
[97] D. T. Sawyer, E. J. Nanni, J. L. Roberts, *Adv. Chem.* **1982**, *201*, 585–600.
[98] M. Hayyan, M. A. Hashim, I. M. Alnashef, *Chem. Rev.* **2016**, *116*, 3029–3085.
[99] L. Möhlmann, S. Blechert, *Adv. Synth. Catal.* **2014**, *356*, 2825–2829.
[100] M. Rueping, S. Zhu, R. M. Koenigs, *Chem. Commun.* **2011**, *47*, 12709–12711.
[101] Hydroperoxylradical, *No Title*, **n.d.**
[102] B. Maillard, K. U. Ingold, J. C. Scaiano, *J. Am. Chem. Soc.* **1983**, *105*, 5095–5099.
[103] A. Tanoue, W.-J. Yoo, S. Kobayashi, *Org. Lett.* **2014**, *16*, 2346–2349.
[104] H. Ueda, K. Yoshida, H. Tokuyama, *Org. Lett.* **2014**, *16*, 4194–4197.
[105] A. Rieche, E. Höft, H. Schultze, *Chem. Ber.* **1964**, *97*, 195–201.
[106] B. Raju, R. Ragul, B. N. Sivasankar, *Indian J. Chem.* **2009**, *48B*, 1315–1318.
[107] F. Prieto, I. Navarro, M. Rueda, *J. Phys. Chem.* **1996**, *100*, 16346–16355.
[108] M. I. Christie, C. Gillbert, M. A. Voisey, *J. Chem. Soc.* **1964**, 3147–3155.
[109] We have to point out that the open intermediate **10** can also be formed via an nucleophilic attack of the methyl-hydroxylamine **14** on the iminium species **2** which is however not in line with the observations in the presence of radical inhibitors.
[110] L. W. Reichel, G. W. Griffin, A. J. Muller, P. K. Das, S. Ege, *Can. J. Chem.* **1984**, *62*, 424–436.
[111] L. Y. C. Lee, X. Ci, C. Giannotti, D. G. Whitten, *J. Am. Chem. Soc.* **1986**, *108*, 175–177.
[112] E. R. Gaillard, D. G. Whitten, *Acc. Chem. Res.* **1996**, *29*, 292–297.
[113] Residual oxygen due to structural conditions as described above.
[114] The pKa value for nitromethane has been determined as 10.2 (a) Nagakura, S. *Molecular Physics* **1960**, *3*, 152.; (b) Gruzdkov, Y. A.; Gupta, Y. M. *J. Phys. Chem. A* **1998**, *102*, 2322.; for THIQ **1** no pKa value is reported, for comparison the value for protonated *N,N*-diethyl-*N*-phenylamine is 6.57-6.92 (c) Rived, F.; Rosés, M.; Bosch, E. *Anal. Chim. Acta* **1998**, *374*, 309.
[115] By cyclic voltammetry the redox potentials were measured as $E_{p/2}$ = -1.65 V for nitromethane **5a** and $E_{p/2}$ = +0.83 V for THIQ **1**.
[116] S. Muzaffar, A. Andrabi, *Indian J. Chem.* **2002**, *41A*, 2306–2309.
[117] C. P. Constantinou, C. Pereira, M. M. Chaudhri, *Propellants, Explos. Pyrotech.* **1995**, *20*, 200–205.
[118] D. A. DiRocco, T. Rovis, *J. Am. Chem. Soc.* **2012**, *134*, 8094–8097.
[119] Wu *et al*. performed similar ESR trapping studies for the TBA-eosin Y catalyzed aza-Henry reaction. Trapping with DMPO showed that $O_2^{\bullet-}$ was the active oxygen species.
[120] BHT is a hindered phenol antioxidant, which act as inhibitor for radical-chain processes. A major pathway of BHT to interrupt radical species is by hydrogen atom transfer, the formed phenoxy radical is relatively unreactive due to steric hindrance by the ortho tert-butyl groups. Yehye, W. A.; Rahman, N. A.; Ariffin, A.; Abd Hamid, S. B.; Alhadi, A. A.; Kadir, F. A.; Yaeghoobi, M. *Eur. J. Med. Chem*. **2015**, *101*, 295.

[121] Whitten *et al*. [56] and Rüping *et al*. [100] suggest a hydrogen atom transfer to the nitrogen atom of amine radical cations forming the respective unreactive protonated amine, which can in agreement with our mechanistic proposal be an explanation for the reduced rate.

[122] C. Huo, H. Xie, M. Wu, X. Jia, X. Wang, F. Chen, J. Tang, *Chem. - A Eur. J.* **2015**, *21*, 5723–5726.

[123] Á. Pintér, A. Sud, D. Sureshkumar, M. Klussmann, *Angew. Chemie - Int. Ed.* **2010**, *49*, 5004–5007.

[124] F. Y. Kwong, A. Klapars, S. L. Buchwald, *Org. Lett.* **2002**, *4*, 581–584.

[125] Z. Li, C.-J. Li, *J. Am. Chem. Soc.* **2005**, *127*, 6968–6969.

[126] S. W. Gerritz, A. M. Sefler, *J. Comb. Chem.* **2000**, *2*, 39–41.

[127] H.-O. Kalinowski, S. Berger, S. Braun, *13C-NMR Spectroskopie*, Georg Thieme, Stuttgart, **1984**.

[128] R. N. Ram, V. K. Soni, *J. Org. Chem.* **2013**, *78*, 11935–11947.

[129] I. Sorribes, K. Junge, M. Beller, *J. Am. Chem. Soc.* **2014**, *136*, 14314–14319.

[130] R. Goumont, M. Sebban, F. Terrier, *Chem. Commun.* **2002**, 2110–2111.

[131] K. Alagiri, K. R. Prabhu, *Org. Biomol. Chem.* **2012**, *10*, 835–842.

[132] S. Berger, S. Braun, H.-O. Kalinowski, *NMR Spektroskopie von Nichtmetallen - 15N-NMR Spektroskopie*, Georg Thieme Verlag, Stuttgart, **1992**.

[133] V. V. Pavlishchuk, A. W. Addison, *Inorganica Chim. Acta* **2000**, *298*, 97–102.

[134] R. Francke, R. D. Little, *Chem. Soc. Rev.* **2014**, *43*, 2492–2521.

[135] Y. A. Gruzdkov, Y. M. Gupta, *J. Phys. Chem. A* **1998**, *102*, 2322–2331.

[136] F. Rived, M. Rosés, E. Bosch, *Anal. Chim. Acta* **1998**, *374*, 309–324.

[137] H. Zhao, J. Joseph, H. Zhang, H. Karoui, B. Kalyanaraman, *Free Radic. Biol. Med.* **2001**, *31*, 599–606.

[138] D. P. Hari, B. König, *Org. Lett.* **2011**, *13*, 3852–3855.

[139] J. N. Demas, G. A. Crosby, *J. Am. Chem. Soc.* **1971**, *93*, 2841–2847.

[140] J. Van Houten, R. J. Watts, *J. Am. Chem. Soc.* **1976**, *98*, 4853–4858.

[141] M. Gleria, F. Minto, G. Beggiato, P. Bortolus, *J. Chem. Soc. Chem. Commun.* **1978**, 285.

[142] F. H. Burstall, *J. Chem. Soc.* **1936**, *127*, 173–175.

[143] K. Kalyanasundaram, *Coord. Chem. Rev.* **1982**, *46*, 159–244.

[144] P. E. Hoggard, G. B. Porter, *J. Am. Chem. Soc.* **1978**, *100*, 1457–1463.

[145] A. Juris, V. Balzani, F. Barigelletti, S. Campagna, P. Belser, A. von Zelewsky, *Coord. Chem. Rev.* **1988**, *84*, 85–277.

[146] K. Kalyanasundaram, in *Photochem. Polypyridine Porphyr. Complexes*, Accademic Press, London, **1992**, pp. 136–199.

[147] H. Bartling, Masterarbeit, University of Regensburg, **2012**.

[148] E. R. Nightingale, *J. Phys. Chem.* **1959**, *63*, 1381–1387.

[149] S. H. Strauss, *Chem. Rev.* **1993**, *93*, 927–942.

[150] M. Dartiguenave, Y. Dartiguenave, A. Mari, A. Guitard, M. J. Olivier, A. L. Beauchamp, *Can. J. Chem.* **1988**, *66*, 2386–2394.

[151] M. Rueping, S. Zhu, R. M. Koenigs, *Chem. Commun.* **2011**, *47*, 8679–8681.

[152] J. Juillard, *Pure Appl. Chem* **1977**, *49*, 885–892.

[153] K. Alagiri, P. Devadig, K. R. Prabhu, *Chem. - A Eur. J.* **2012**, *18*, 5160–5164.

[154] M. Rueping, R. M. Koenigs, K. Poscharny, D. C. Fabry, D. Leonori, C. Vila, *Chem. - A Eur. J.* **2012**, *18*, 5170–5174.

[155] B. Schweitzer-Chaput, M. Klussmann, *European J. Org. Chem.* **2013**, 666–671.

[156] M. Sugahara, T. Ukita, *Chem. Pharm. Bull.* **1997**, *45*, 719–721.

4 LED-illuminated NMR Studies of Flavin-Catalyzed Photooxidations Reveal Solvent Control of the Electron-Transfer Mechanism

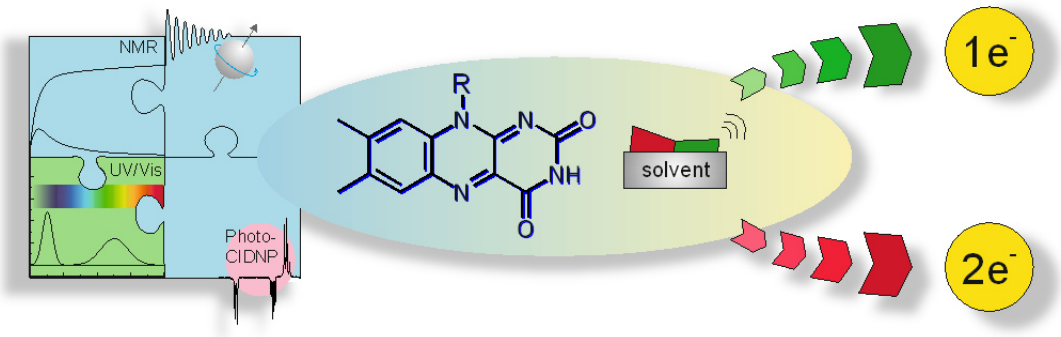

The sample preparation and the NMR measurements of the CD_3CN sample, the oxygenated CD_3CN/D_2O sample, Photo-CIDNP and UV/Vis measurements were performed by Dr. Christian Feldmeier. The sample preparation and NMR measurements of the fully deoxygenated sample in CD_3CN/D_2O were performed by Hanna Bartling. Parts of the Supporting Information have been published before in the Ph.D. thesis of Dr. C. Feldmeier.[1]

Christian Feldmeier, Hanna Bartling, Kathrin Magerl, Ruth M. Gschwind

Angew. Chem. Int Ed. **2015**, *54*, 1347-1351.

Angew. Chem. **2015**, *127*, 1363-1367.

DOI: 10.1002/anie.201409146

4.1.1 Abstract

Mechanistic insights into chemical photocatalysis are mainly the domain of UV/Vis spectroscopy, because NMR spectroscopy has been limited by the type of illumination so far. An improved LED-based illumination device can be used to obtain NMR reaction profiles of photocatalytic reactions under synthetic conditions and perform both photo-CIDNP and intermediate studies. Flavin-catalyzed photooxidations of alcohols show the potential of this setup. After identical initial photoreaction steps the stabilization of a downstream intermediate is the key to the further reaction mechanism and the reactivity. As a chemical photocatalyst flavin can act either as a one- or a two-electron mediator when the stability of the zwitterionic radical pair is modulated in different solvents. This demonstrates the importance of downstream intermediates and NMR-accessible complementary information in photocatalytic reactions and suggests the control of photoorganic reactions by solvent effects.

4.2 Introduction

Chemical photocatalysis has developed into a booming field with various synthetic applications.[2–5] Mechanistic insights into photocatalytic reactions are so far mainly the domain of UV/Vis spectroscopy due to its ability to characterize even excited states of the photocatalysts with ultrafast time resolution and high sensitivity (demonstrated for the mechanism of a flavin-catalyzed photooxidation in Figure 4.1[6]).However, even the most elaborate UV/Vis study is limited by the principle drawbacks of this method. Thus, UV/Vis focuses on the initial reaction steps of the photocatalyst but can gain only little information about the structures, aggregation trends, solvent effects, and substrates. Also the investigation of entire reaction pathways and especially the effects of downstream intermediates is difficult. These structural aspects and timescales are the classical domain of NMR spectroscopy, which in turn is a very slow and insensitive method and in many aspects complementary to UV/Vis spectroscopy. NMR spectroscopy can directly detect diamagnetic intermediates but neither excited states nor most of the radical species (Figure 4.1 blue highlights), which is reflected in many elaborate NMR studies of photoreactions, for example, in solid-state NMR spectroscopy,[7,8] protein folding,[9–11] organometallic photochemistry,[12] and photocatalysis.[13] Through the use of modern NMR photo-CIDNP techniques (CIDNP = chemically induced dynamic nuclear polarization)[14–18] with laser illumination, also transient radical pairs in photochemical reactions can be studied indirectly (purple frames in Figure 4.1).[9,10] However, the detection and interpretation of CIDNP effects in closed catalytic cycles, typical for photocatalysis, are difficult.[19] Moreover, the high light intensity of a laser often leads to fast degradation of the photocatalyst. As a result the detection of whole reaction profiles including both catalyst and substrate/product is difficult with laser setups and the results often are not comparable to synthetic applications using lower light intensities.

4.3 Materials and Methods

Recently, we developed an LED illumination device for NMR spectroscopic investigations and were able to increase the light intensity inside the sample by a factor of ca. 800.[20] This LED device can be used in a pulsed and in a continuous-wave mode and facilitates time-resolved photo-CIDNP as well as the detection of entire reaction pathways. Therefore, with this LED setup now the full potential of NMR spectroscopy can be applied to study the mechanisms of photocatalytic reactions. This device now can be used to investigate the relevance of downstream intermediates and solvent effects in photocatalysis as well as the informative value of NMR reaction profiles for mechanistic studies, which is well known for organocatalytic reactions.[21–25]

For the present study the flavin-catalyzed photooxidation of benzyl alcohols[6,26–28] was chosen (Figure 4.1). Flavins are able to catalyze a huge variety of different biochemical reactions in various proteins; their photoreactions in proteins are well investigated[9,29] and flavins are known to produce CIDNP effects.[15] Flavins can act as both one-electron and two-electron mediators in redox reactions[30–34] by modulating the stability of the semiquinone radical in the protein.[31,32,35] Furthermore, flavin derivatives are successfully used as photocatalysts[2,26,34] for the oxidation of various substrates,[2,36–40] but to our knowledge the modification of the electron-transfer properties of flavin in synthetic applications has never been reported so far.

The flavin-catalyzed photooxidation of benzylic alcohol was the subject of an in-depth mechanistic UV/Vis study (Figure 4.1).[6] After excitation of the photocatalyst by blue light, two electrons and two protons are transferred from methoxybenzyl alcohol (MBA) to riboflavin tetraacetate (RFTA) yielding methoxybenzyl aldehyde (MBAld) and reduced RFTA (RFTA-H_2). The reduced form of flavin is referred to as RFTA-H_2 hereafter, although the spectra indicate a mixture of RFTA-H_2 and RFTA-H$^{\bullet}$ as expected for a CD_3CN/D_2O mixture. Subsequently RFTA is recovered by reaction with oxygen leading to H_2O_2. The UV/Vis study revealed the flavin triplet state as the key intermediate for a productive electron transfer and a subsequent protonation of the flavin radical anion.[6] The strong solvent dependence of the yields and reaction rates[26] (high yields, fast reaction in CD_3CN/D_2O; low yields, slow reaction in CD_3CN) remained unclear. In previous mechanistic NMR studies, the interruption of catalytic cycles, for example, by omitting substrates, has proven to be a successful strategy for the stabilization and NMR detection of otherwise inaccessible intermediates.[21-23,40-42] Therefore, oxygen was excluded to interrupt the catalytic cycle of flavin, preventing the reoxidation of the reduced flavin species and allowing their characterization by combined NMR and UV/Vis studies (see 4.6.2). In addition, the stoichiometry of the product and the reduced flavin species can be monitored and CIDNP effects are not cancelled by closing the cycle. As solvent both pure CD_3CN and CD_3CN/D_2O (1:1) were chosen to elucidate the influence of solvent, particularly with regard to the flavin oxidation state and the associated role of flavin as a one- or two-electron acceptor in photooxidations.

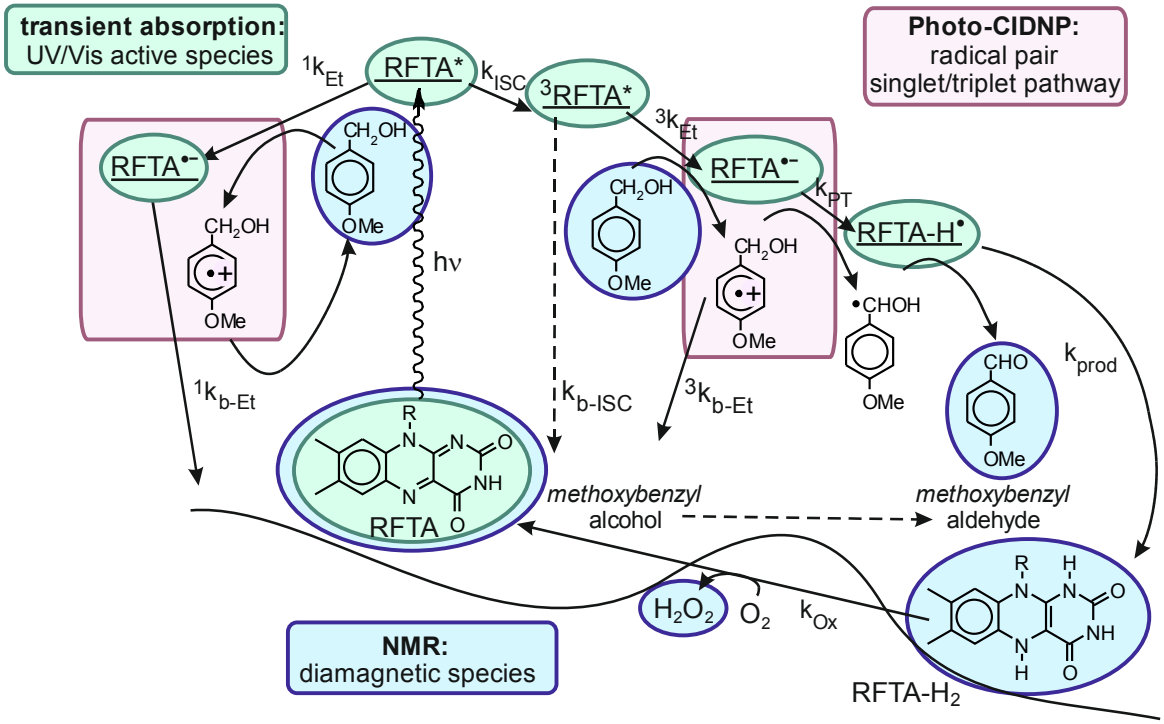

Figure 4.1 NMR complements UV/Vis spectroscopy with regards to structure information and time resolution in photocatalytic reactions. In RFTA-catalyzed photooxidations of alcohols, the initial excited states and radicals are accessible by UV/Vis spectroscopy (green).[3] LED illumination for *in situ* NMR spectroscopy provides reaction profiles of substrates, products, and diamagnetic states of the photocatalyst (blue) and information about transient radical pairs via CIDNP (purple).

4.4 Results and Discussion

First, the reduced flavin species (semiquinone or hydroquinone) was studied in pure CD_3CN. Figure 4.2 c shows ^1H NMR spectra of the reaction mixture in deoxygenated CD_3CN before illumination and after 2 h of illumination time. With continued illumination the amount of the product methoxybenzyl aldehyde (MBAld, black) increases, while the amount of the oxidized flavin (RFTA, blue) decreases and a complete new set of signals (green) appears, which was assigned to the two-electron reduced hydroquinone form of flavin (RFTA-H_2) (refer to 4.6.4). The linewidths of all the signals are extremely small even during the reaction, indicating a very short lifetime of the proposed transient flavin semiquinone radicals (Figure 4.2). Photo-CIDNP measurements[14,15,19,43] on this sample proved that this reaction nevertheless involves radical pairs. The opposite signs of the CIDNP phases of the oxidized and the reduced flavin signals (Figure 4.2 g and section 4.6.13) are in line with the initial reaction mechanism proposed by UV studies in CD_3CN/D_2O:[3] First an electron transfer occurs from MBA to RFTA. The subsequent spin-correlated zwitterionic radical pair in the singlet state recombines and results in photo-CIDNP effects in the set of RFTA signals. In the case of intersystem crossing the radical pair in the triplet state yields the product and causes the photo-CIDNP polarizations in the set of RFTA-H_2 signals. Thus, the combined information from ^1H NMR spectra and CIDNP effects show that also in pure CD_3CN the product is formed from the triplet states of the zwitterionic radical pairs. However, the absolute amount of these radicals is very low and their lifetime extremely short.

Next, entire reaction profiles were investigated revealing the relative stoichiometry of the involved species. Figure 4.2 e shows the reaction profile in deoxygenated pure CD_3CN. Upon illumination RFTA is directly reduced to RFTA-H_2 on the NMR timescale without the semiquinone radical altering the kinetics. The lack of oxygen prevents reoxidation and the concentration of RFTA-H_2 increases at a rate corresponding to the decrease of RFTA. In addition, the product MBAld is initially formed at the same rate as the reduced flavin. This reveals the requirement of one molecule of RFTA for the oxidation of one molecule of MBA and proves a formal two-electron process in pure CD_3CN. The reaction proceeds very slowly indeed, as observed by synthetic investigations[25] and shows yields of only about 50% after 4 h.

The combined information obtained from ^1H NMR spectra, CIDNP effects, and reaction kinetics shows that the triplet state of the flavin semiquinone radical is decisive for the product formation, but its lifetime extends beyond the NMR timescale affecting neither the NMR spectra nor the associated kinetics. That means that the formation of zwitterionic radical pairs in pure CD_3CN is energetically unfavorable to such an extent[20] that a formal two-electron process is observed on the NMR timescale. Furthermore, the significant CIDNP effects in combination with slow reaction rates and low yields indicate the presence of zwitterionic radical contact ion pairs allowing for an effective intersystem crossing and a fast back electron transfer in the singlet state. To sum up, the spectra and the reaction kinetics show a formal two-electron process in pure CD_3CN with the insufficient formation and stabilization of the zwitterionic radical pair as most probable rate-limiting step.

With deoxygenated CD_3CN/D_2O (1:1) as the solvent the character of the dominating reduced flavin species changes drastically. Upon illumination the signals of RFTA rapidly decrease and broaden, whereas those of the starting material, product, and solvent remain sharp (Figure

4.2 d). After a time delay RFTA-H_2 is formed showing also broad signals (Figure 4.2 d). The signals for RFTA and (less pronounced) RFTA-H_2 show the typical distance dependence of the linewidths expected for a chemical exchange with a semiquinone radical, which was also previously described for flavin mononucleotide (FMN) ring systems in deoxygenated solution.[20] The line broadening is most pronounced for the protons of the isoalloxazine ring system; the signals of the side chain show reduced line broadening with increasing distance from the radical (see 4.6.5). After the light was turned off, the product formation stops immediately and the broadened lines remain for hours. Upon addition of oxygen the flavin signals recover to sharp lines indicating the reoxidation of the semiquinone radicals to RFTA (see 4.6.6). In contrast to experiments in CD_3CN no photo-CIDNP polarizations are detected in deoxygenated CD_3CN/D_2O (1:1) (refer to 4.6.7 and 4.6.13).

The change of the reaction profiles in CD_3CN/D_2O reveals the role of the semiquinone radicals in the reaction mechanism (Figure 4.2 f). First, the product formation is strongly accelerated (50% yield after 10 min compared to 4 h in CD_3CN); second, the relative stoichiometries of RFTA, RFTA-H_2, and the product MBAld change drastically. While MBAld is rapidly formed, the concentration of RFTA drops close to zero and RFTA-H_2 increases with a significant time delay and at a reduced rate. This reaction profile is typical for the presence of a stabilized reaction intermediate in the mechanism. The line broadening of the NMR signals reveal flavin semiquinone radicals as intermediate species (see above and Figure 4.2 f) The high amount of flavin radical intermediates and the concurrent immediate oxidation of the alcohol to the aldehyde impressively show that RFTA acts in CD_3CN/D_2O as a one-electron oxidation agent for the oxidation of MBA. Under synthetic conditions, that is, with varying amounts of oxygen, similar line broadening of the flavin resonances is observed in CD_3CN/D_2O as well as identical reaction profiles after the full consumption of oxygen (see 4.6.2; 4.6.8 and 4.6.9). This confirms that the one-electron mechanism is generally valid in CD_3CN/D_2O.

The semiquinone radical intermediate was identified as the anionic semiquinone radical $RFTA^{\bullet-}$ by UV/Vis spectroscopy, which has proven effective for the detection and characterization of flavin semiquinone radicals[3,48] (section 4.6.2). The dominant occurrence of $RFTA^{\bullet-}$ and the immediate oxidation of the alcohol without a radical intermediate detectable on the NMR timescale (see 4.6.9 and 4.6.11) clearly indicate that flavin acts as a one-electron oxidizing agent and that two flavin molecules are necessary for the complete oxidation of the alcohol. The resulting $RFTA^{\bullet-}$ radicals have significantly longer lifetimes in the presence of oxygen, which is a strong hint that in the presence of oxygen mainly $RFTA^{\bullet-}$ is reoxidized to RFTA. Previous diffusion-ordered spectroscopy (DOSY) experiments with RFTA and derivatives in CD_3CN, D_2O, and CD_3CN/D_2O (1:1) combined with reactivity studies indicated not only a significant amount of RFTA dimers in CD_3CN/D_2O (1:1) (aggregation number 1.7) but also an increasing reactivity and decreasing stability of the flavin photocatalysts with reduction of the aggregation.[25] Therefore, monomeric RFTA molecules are assumed to be the reactive catalytic species. The dimer is proposed to be important only for the disproportionation process under the exclusion of oxygen (refer to 4.6.2).

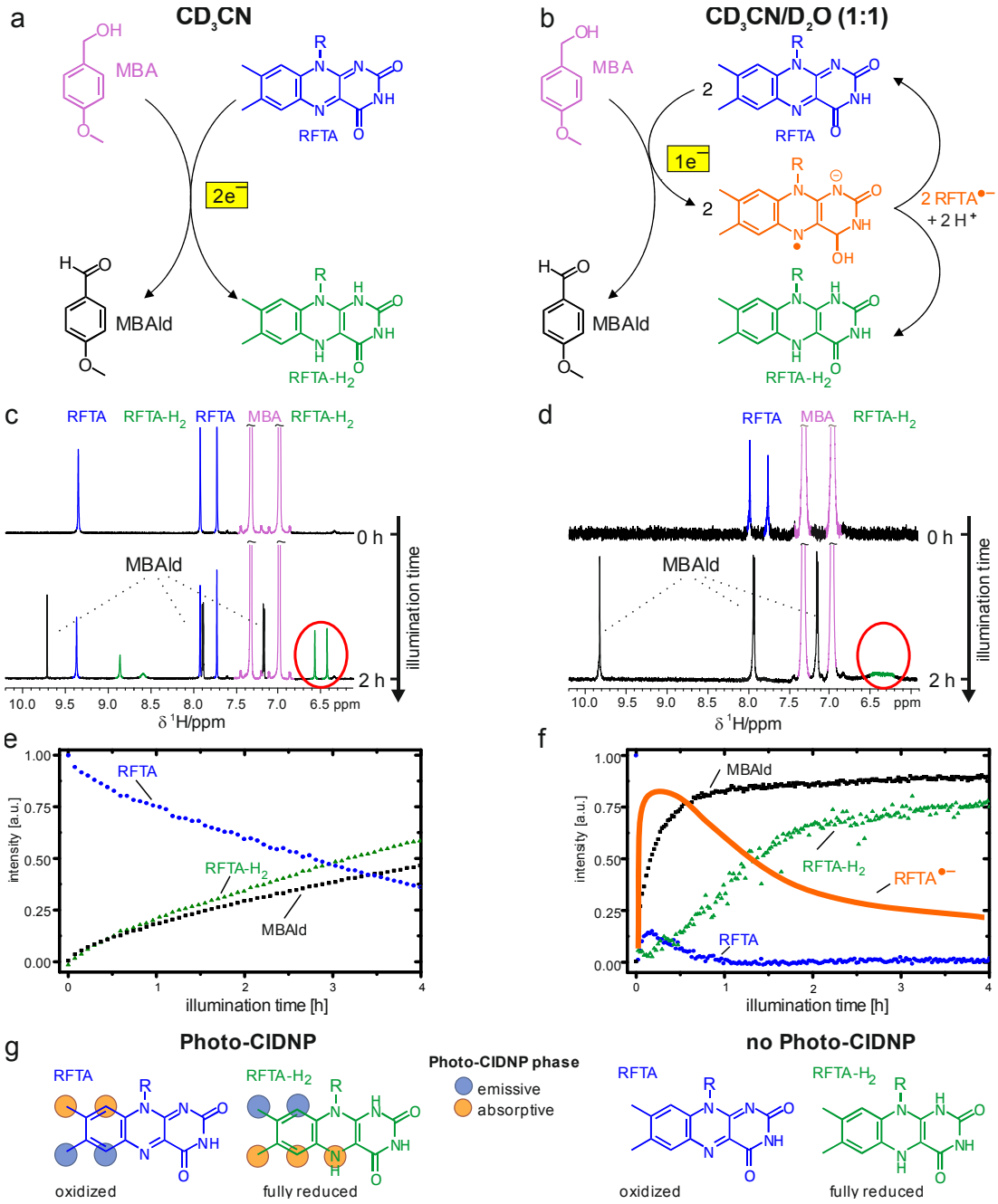

Figure 4.2 NMR reaction profiles reveal that chemical photooxidations by flavin can be switched between one- and two-electron-transfer mechanisms by solvent properties. Oxygen exclusion interrupts the catalytic cycle of flavin and allows for the identification of the reductive pathway: a formal two-electron transfer in CD_3CN (a) and a one-electron transfer in CD_3CN/D_2O (1:1) (b). Selected ^1H NMR spectra recorded before and during the reaction show no line broadening of any signal in CD_3CN (c), whereas in CD_3CN/D_2O (1:1) (d) both detectable flavin species show broad linewidths indicating chemical exchange with a flavin radical. The corresponding reaction profile in CD_3CN (e) shows a slow formal two-electron-transfer mechanism on the NMR timescale. In CD_3CN/D_2O (1:1) (f) fast product formation, high amounts of the anionic semiquinone radical $RFTA^{\bullet-}$ as intermediate (smoothened curve for details see 4.6.8), and delayed formation of the twofold reduced flavin RFTA-H_2 is observed indicating a one-electron-transfer process. Photo-CIDNP polarizations detected in the oxidized and fully reduced flavin species (g) in CD_3CN in combination with the results from recent UV/Vis studies[3] in CD_3CN/D_2O (1:1) show that the product formation via triplet zwitterionic radical pairs is identical in the two solvents. However, the NMR reaction profiles reveal that the stabilization of these downstream intermediates controls the further reaction mechanism.

Based on this NMR study including reaction profiles and CIDNP effects in combination with the results of a time-resolved UV/Vis study[3] we propose an extended mechanism for the flavin-catalyzed photooxidation of methoxybenzyl alcohol. The time-resolved UV/Vis study in CD_3CN/D_2O (1:1) and the CIDNP studies in pure CD_3CN show that the initial photoexcitation steps and the formation of the excited triplet state as the key intermediate for the product formation are identical in these solvent systems. However, starting from the electron-transfer step creating a zwitterionic radical pair, the solvent interactions determine the further mechanistic pathway. In CD_3CN/D_2O (1:1) the radical counter ions are stabilized and separated, leading to a fast one-electron oxidation process. In pure CD_3CN the formation energy of the charge separation is much higher. The resulting zwitterions form contact ion pairs and facilitate an effective back electron transfer after intersystem crossing. Both effects lead to a slow reaction with a formal two-electron-transfer mechanism on the NMR timescale.

4.5 Conclusions

In conclusion, the new LED setup, which made both NMR reaction profiles and CIDNP studies possible, led to new insights into the reaction mechanism of photocatalytic reactions. The new findings are not only complementary to the results of UV/Vis studies but crucial for the understanding of the mechanism. Downstream intermediates, especially ion pairs, and processes accessible on the NMR timescale can be decisive for the mechanistic pathway of photoreactions. Thus, this study shows that the control of the one- versus two-electron processes of flavin and potentially also other photocatalysts is possible without any protein but by just making use of solvent and solvation properties.

4.6 Supporting Information[1]

4.6.1 Shortcut of the Experimental Section (Most Important Methods)

The reaction was conducted directly inside the NMR spectrometer by illuminating the NMR sample inside the NMR tube by the improved LED based illumination device.[20] In this way photochemical reactions can be run directly inside the spectrometer under synthetic conditions, i.e. 2 mM riboflavin tetraacetate (RFTA) and 20 mM methoxybenzyl alcohol (MBA). The samples were deoxygenated by freeze-pump-thaw or purged with argon for 1 h (partially deoxygenated). NMR spectra were all recorded of dark samples to avoid intensity changes by CIDNP effects.[15,19] The whole reaction profiles were investigated based on a quantitative analysis of the ^{1}H signal intensities during the reaction.

In deoxygenated samples the light was switched off after a short illumination time. The signal of RFTA-H_2 remains unchanged, indicating an oxygen free sample. In contrast, the addition of oxygen to the reaction mixture leads to immediate reoxidation of the flavin.

The time dependent formation of the radical species was calculated by subtracting the detectable flavin species RFTA and RFTA-H_2 from the known total amount of flavin before illumination (see orange smoothed curve in Figure 4.2 f main text Figure 4.3 a, for raw data see 4.6.8).

In the reaction profiles (Figure 4.2 f and Figure 4.3 a) after the decay of RFTA a small amount of a mixed dimer (RFTA/RFTA-H_2), indicated by chemical shift changes, reappears, which then decreases gradually (see 4.6.12). Small amounts of RFTA-H_2 appear right from the start of illumination but its main formation occurs with a significant delay relative to the product formation. Both RFTA-H_2 and MBAld approach a saturation concentration with prolonged illumination time corresponding to one catalytic cycle of a two-electron reduction of the flavin and a two-electron oxidation of the alcohol.

The nature of the semiquinone radical intermediate was investigated by UV/Vis spectroscopy, because UV/Vis has proven effective for the detection and characterization of flavin semiquinone radicals[6,48] Compared to the absorption spectrum of RFTA with its characteristic well-resolved absorption bands located at about 450 nm (S0→S1 transition) and at about 360 nm (S0→S2 transition) (see 4.6.10) the absorption spectra of the semiquinone radicals are characterized by an additional spectral feature at about 580 nm.[6,48] The neutral protonated semiquinone radical RFTA-H$^{\bullet}$ has a small but pronounced absorption band at 580 nm (ε(580) = 4.0 [10^3 LM^{-1} cm^{-1}]),[6] whereas the anionic semiquinone radical RFTA$^{\bullet-}$ has an extinction coefficient, which is about 40 times lower at 580 nm (ε(580) = 0.1 [10^3 LM^{-1} cm^{-1}]). The full reduction of flavin is usually associated with bleaching of the sample and disappearing of the well-resolved absorption bands. The corresponding UV/Vis spectra have rather structureless and atypical absorption in the near UV and visible range strongly changing with conditions most probably caused by the butterfly-bending conformational changes.[49,50] For the identification of the radical intermediate in CD_3CN/D_2O now the difference in the ε values at 580 nm between the protonated and the anionic semiquinone radical were used. From the UV/Vis spectra the respective concentration of the two radicals were calculated and compared to the amount derived from the NMR reaction kinetics.

4.6.2 Summary of Reaction Profiles under Synthetic Conditions and the Identification of RFTA$^{\bullet-}$

Under synthetic conditions, i.e. saturation with oxygen, or only partial deoxgenation a similar line broadening of the flavin resonances is observed directly after the start of the illumination as well as identical reaction profiles after the full consumption of oxygen (see 4.6.8 and 4.6.9). This is shown on the reaction profiles in CD_3CN/D_2O with only partial deoxygenation (see Figure 4.3 a). Again high amounts of flavin radicals are formed immediately after the start of the illumination (see smoothed orange curve in Figure 4.3 a, raw data see 4.6.8.2). With proceeding consumption of oxygen the reoxidation of flavin slows down and the amount of oxidized flavin becomes smaller. At the moment oxygen is fully consumed (see Figure 4.3 c, red line) the identical reaction profile as in Figure 4.2 f main text starts to develop. This shows clearly that the one-electron mechanism is generally valid in CD_3CN/D_2O (1:1) mixtures.

Next the nature of the semiquinone radical intermediate was investigated by UV/Vis spectroscopy, because UV/Vis has proven effective for the detection and characterization of flavin semiquinone radicals.[6,48] The neutral protonated semiquinone radical RFTA-H$^{\bullet}$ has a small but pronounced absorption band at 580 nm (ε(580) = 4.0 [10^3 $LM^{-1}cm^{-1}$],[6] whereas the anionic semiquinone radical RFTA$^{\bullet-}$ has an extinction coefficient, which is about 40 times lower at 580 nm (ε(580) = 0.1 [10^3 $LM^{-1}cm^{-1}$]). Thus, from the UV/Vis spectra the respective concentration of the two radicals can be calculated and compared to the amount derived from the NMR reaction profiles. After 5 min and 30 min of illumination the amount of radical was estimated from the UV/Vis absorption band at 580 nm of the respective spectra (see Figure 4.3 a). For the exclusive stabilization of anion radicals RFTA$^{\bullet-}$ a radical concentration between 0.78 - 2.00 mM was calculated, corresponding to 39-100% of the overall flavin concentration. The significantly higher ε (580) of the neutral radicals RFTA-H$^{\bullet}$ leads to very low radical concentrations between 0.02 - 0.05 mM, which corresponds only to 1.0 - 2.5% of the overall flavin concentration (for details about the estimation see 4.6.10). From the amount of intermediate flavin radicals calculated from the NMR reaction kinetics it can be concluded that the stabilized semiquinone radical appears mainly in the anionic form (see Figure 4.3 a).

Additional UV/Vis experiments in deoxygenated CD_3CN and with different RFTA and MBA ratios in deoxygenated CD_3CN/D_2O (1:1) mixtures showed that the presence of water as well as sufficient amounts of both RFTA and MBA are necessary to stabilize the semiquinone radical. These experiments furthermore revealed that the formation of the semiquinone radical results from the intermolecular electron transfer from MBA to RFTA, also observed by Megerle et al.[6] (for details see 4.6.11).

The dominant occurrence of RFTA$^{\bullet-}$ and the immediate oxidation of the alcohol without a radical intermediate detectable on the NMR time scale (see 4.6.9 and 4.6.11.) clearly indicate that flavin acts as an one electron oxidizing agent and that two flavin molecules are necessary for the full oxidation of the alcohol. The resulting RFTA$^{\bullet-}$ radicals have different life time's depending on the presence or absence of oxygen. Under the exclusion of oxygen no protonation of RFTA$^{\bullet-}$ to RFTA-H$^{\bullet}$ was observed within a measurement time of 100 µs.[51] In contrast with oxygen a much shorter life time of 5.5 µs was measured for RFTA$^{\bullet-}$ and a unexpected long life time of 129 µs for RFTA-H$^{\bullet}$.[6] This change of the lifetimes of RFTA$^{\bullet-}$ with and without oxygen is a strong hint that in the presence of oxygen mainly RFTA$^{\bullet-}$ is reoxidized to RFTA.

Without oxygen a disproportionation pathway is highly probable. Under oxygen exclusion (see Figure 4.2 f) or after consumption of oxygen (see Figure 4.3 a) the signals of RFTA reappear after the decay to zero. This reappearance indicates another rate of $RFTA^{\bullet-}$ formation from this species compared to pure RFTA, which can be explained by a mixed dimer consisting of RFTA and RFTA-H_2 as indicated by the chemical shift changes (4.6.12). The formation of this mixed dimer at the beginning of the reaction in combination with the missing CIDNP effect supports a disproportionation mechanism under the exclusion of oxygen. The extremely long lifetimes of $RFTA^{\bullet-}$ under the exclusion of oxygen (> 100 µs)[51] and of RFTA-$H^{\bullet}$ in the presence of oxygen (~129 µs)[6] reveal that the disproportionation process is slow compared to the direct reoxidation of $RFTA^{\bullet-}$ by oxygen but may also occur as a minor side reaction under oxygen. Previous diffusion ordered spectroscopy (DOSY) experiments of RFTA and derivatives in CD_3CN, D_2O and CD_3CN/D_2O (1:1) combined with reactivity studies revealed not only a significant amount of RFTA dimers in CD_3CN/D_2O (1:1) (aggregation number 1.7) but also an increasing reactivity and decreasing stability of the flavin photocatalysts with reduction of the aggregation.[25] Therefore, monomeric RFTA molecules are assumed as the reactive catalytic species. The dimer is proposed to be only important for the disproportionation process.

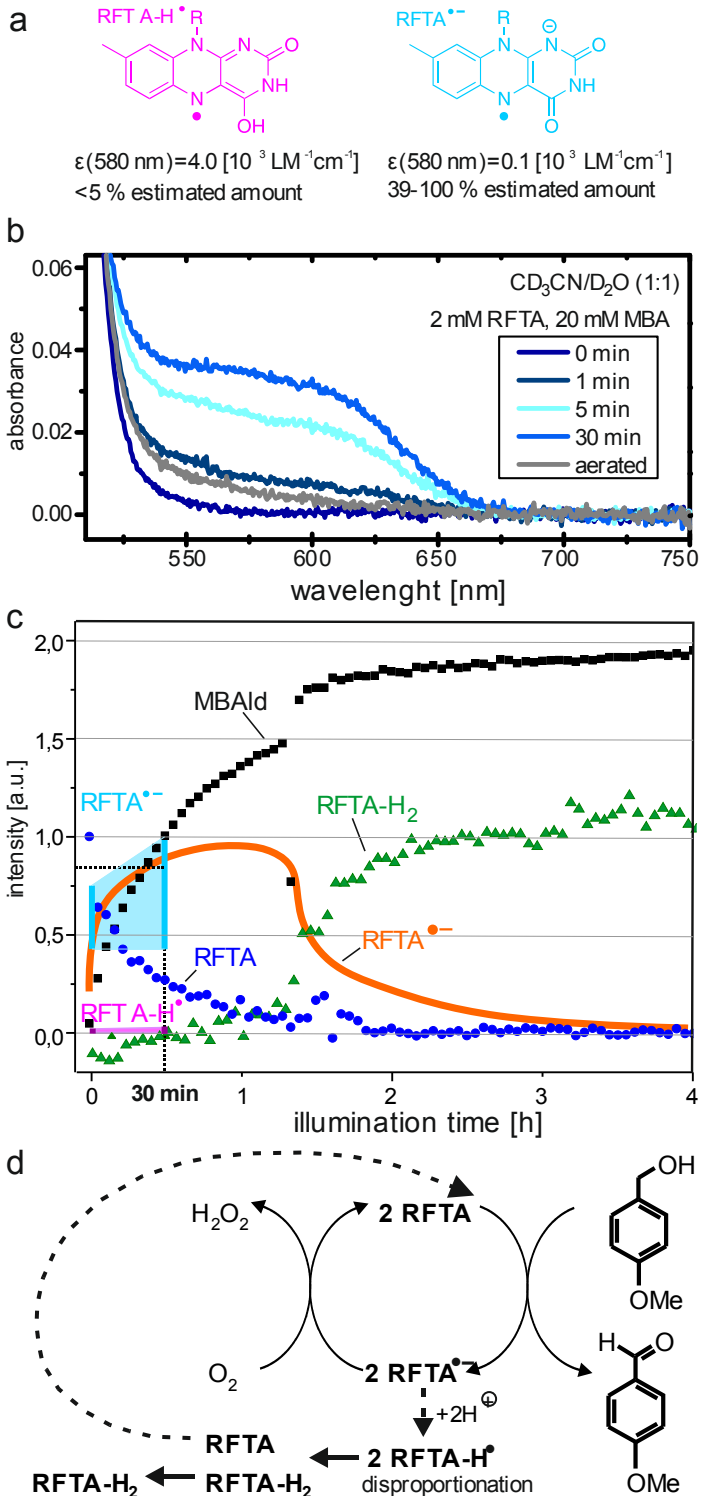

Figure 4.3 One-electron transfer mechanism of flavin catalyzed photooxidation of paramethoxybenzyl alcohol also in the presence of O_2 and identification of the intermediate as anionic semiquinone radical RFTA$^{\bullet-}$. (a) The semiquinone radicals RFTA$^{\bullet-}$ and RFTA-H$^{\bullet}$ differ significantly in their ε values at 580 nm. Therefore, the UV/Vis spectra during the reaction (b) can be used to calculate the amount of the respective radical. The time range of the UV/Vis spectra is indicated by the blue lines and the purple dots (5 – 30 min). The range of concentration of RFTA$^{\bullet-}$ calculated from the UV/Vis spectra is given in light blue, that of RFTA-H$^{\bullet}$ in light purple. A comparison with the corresponding NMR reaction profile (c) reveals the anionic semiquinone radical RFTA$^{\bullet-}$ as main intermediate. Results from NMR and UV/Vis[6] (for details see text) indicate that mainly RFTA$^{\bullet-}$ is oxidized by O_2 and disproportionation is only a minor pathway (c).

4.6.3 General Information

4.6.3.1 Materials

The solvents D_2O and acetonitril-d_3 were purchased from Deutero and Aldrich. 4-methoxybenzyl alcohol (MBA) was purchased from Aldrich and used without further purification. Riboflavin tetraacetat (RFTA) was prepared according to the reported procedures.[52]

4.6.3.2 General Methods

4.6.3.2.1 Sample Preparation

For the measurements 0.5 ml solutions of 2 mM riboflavin tetraacetate (RFTA) and 20 mM methoxybenzyl alcohol (MBA) in CD_3CN and in CD_3CN/D_2O (1:1) were prepared in amberized Rototec-Spintec 5 mm NMR-Tube 7 inch 535-PP-7, to protect the samples from unwanted exposition to light. The solvents were deoxygenated in a Schlenk flask by means of Freeze-Pump-Thaw cycling and transferred under argon atmosphere to the NMR tube which was sealed airtight after insertion of a transparent inlet. The samples with residual oxygen were purged with argon for 1 h and sealed after insertion of a transparent inlet to prevent oxygen from entering.

4.6.3.2.2 Deoxygenation

The solvents were deoxygenated by Freeze-Pump-Thaw cycling or for partially oxygenated samples purged with argon for 1 hour. The deoxygenation of the samples was verified by the instantaneous appearance of the ^1H NMR signal set of the fully reduced flavin RFTA-H_2 right from the beginning of the photooxidation. This is employed as an indicator for the complete deoxygenation of the reaction solution as the reduced species can only be stabilized when oxygen is excluded. H_2O_2 as the second product from the reoxidation of the reduced flavin appears in the ^1H spectra at a chemical shift of 8.60 ppm. The absence of the H_2O_2 resonance provides a second evidence for the complete deoxygenation. The amount of residual oxygen can be estimated from the maximal amount of formed H_2O_2. If D_2O is present in the solution, however, H_2O_2 cannot be employed as an indicator for the grade of deoxygenation as it is deuterated by chemical exchange. The stoichiometry of the reduced flavin and the aldehyde at the end of the reaction provides a third indicator for the deoxygenation of the reaction mixture. In the case of complete deoxygenation both the signal intensity of RFTA-H_2 and MBAld approximate the same value at the end of the reaction. With residual oxygen more MBAld than RFTA-H_2 is formed due to the delayed interruption of the catalytic cycle. The amount of residual oxygen can be estimated from the stoichiometry of RFTA-H_2 and the product MBAld. The line broadening of the ^1H NMR signals of the flavin in CD_3CN/D_2O (1:1) mixture cannot be employed as an indicator for deoxygenation or full consumption of oxygen as the lines begin to broaden before complete consumption of oxygen.

4.6.3.2.3 In situ NMR by an LED based illumination device

NMR spectra were recorded on a Bruker Avance 600 spectrometer with a 5 mm broadband triple resonance z-gradient probe. Constant temperatures were controlled by a Bruker BVTE 3000 unit. The 2D spectra for the assignments were partially recorded at a BRUKER Avance III 600 (600.25 MHz) spectrometer with a TCI z-gradient cryoprobe. The spectra were processed, evaluated and plotted with Bruker Topspin 3.2. For the illumination of the samples a Cree XP-

E high power LED with a center wavelength of 455 nm and 500 mW optical output power was used. The LED was used together with a setup consisting of an optical fiber to guide the light directly into the sample and a transistor circuit operated by the spectrometer to switch the LED automatically. In order to ensure that the NMR signal intensities are not distorted by unwanted additional Photo-CIDNP polarizations ^{1}H spectra were recorded alternating with and without illumination. Starting with a ^{1}H spectrum of the not illuminated spectrum a row of ^{1}H spectra was taken and the light was switched on and off between two consecutive ^{1}H spectra. For the reaction profiles only the dark spectra were used. The kinetics were derived from the integrals of the ^{1}H signals C(6)-H and C(9)-H (fully reduced flavin RFTA-H_2 and oxidized flavin RFTA) and from the C(1)-H proton of the aldehyde (MBAld) (see Figure 4.4) and referenced each to these signals in the first spectrum. Assignments were made by a complete standard set of 1D and 2D NMR spectra consisting of ^{1}H, ^{13}C, $^{1}H,^{1}H$ cosy, $^{1}H,^{1}H$-noesy, $^{1}H,^{13}C$-hsqc and $^{1}H,^{13}C$-hmbc. An exception is the assignment of the fully reduced riboflavin tetraacetate in CD_3CN/D_2O (1:1). The line broadening inhibits the assignment by 2D NMR and the proton resonances were assigned in analogy to the fully reduced riboflavin tetraacetate in CD_3CN, see Figure 4.4. The chemical shifts were referenced to the ^{1}H chemical shift of tetramethylsilane (TMS) of 0.00 ppm.

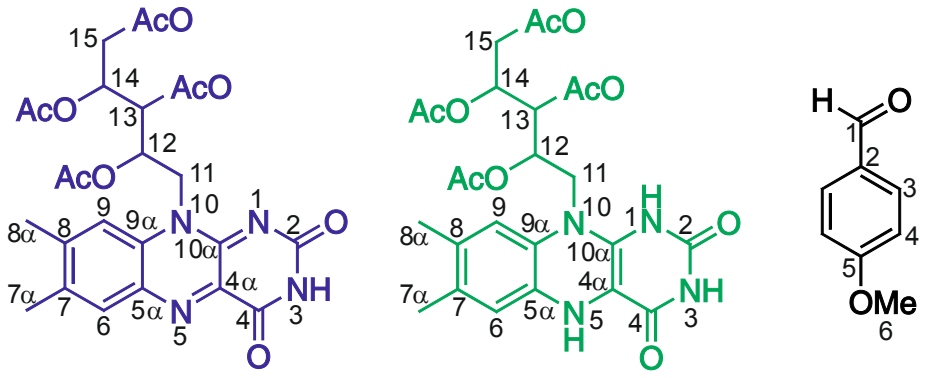

Figure 4.4 Numeration of RFTA (blue), RFTA-H_2 (green) and MBAld (black) as used for the assignment and further characterization.

4.6.3.2.4 UV/Vis

UV/Vis spectra were measured at a Perkin-Elmer Lambda 9a spectrometer with a modified cuvette holder. Temperature was thermostated at 20°C. The samples were prepared in HELLMA 110-QS 2.00 mm cuvettes. For the measurements different samples of the concentrations used in NMR and synthesis (c(RFTA) = 2 mM; c(MBA) = 20 mM) and the concentrations used for UV/Vis spectroscopy (c(RFTA) = 40 µM; c(MBA) = 400 µM) were prepared each in pure CD_3CN and in CD_3CN/D_2O (1:1) mixture and purged with Argon for 30 min to exclude oxygen, then closed airtight and sealed with parafilm. The small thickness of 2.00 mm of the cuvette keeps the light path in the UV/Vis measurement small so that even the relative high concentrations used for NMR can be measured by UV/Vis spectroscopy. The samples were illuminated outside the spectrometer all arranged in a distance of about 1 cm from a Cree XP-E high power LED with a center wavelength of 455 nm and 500 mW optical output power operated at a current of 700 mA.

4.6.4 Assignment of the Starting Material, Catalyst and Product

Assignments were made by a complete standard set of 1D and 2D NMR spectra consisting of ^{1}H, ^{13}C, $^{1}H,^{1}H$-cosy, $^{1}H,^{1}H$-noesy, $^{1}H,^{13}C$-hscq and $^{1}H,^{13}C$-hmbc.

The fully reduced riboflavin tetraacetate (RFTA) in CD_3CN/D_2O (1:1) was not assignable by 2D NMR because of line broadening and the proton resonances were assigned in analogy to the fully reduced riboflavin tetraacetate in CD_3CN. With the proton resonances at 1.93 ppm and 2.09 ppm corresponding to the methyl groups in positions 7 and 8 (2.03 ppm and 2.06 ppm for pure CD_3CN) and the signals at 6.30 ppm and 6.45 ppm corresponding to the aromatic protons C(6)-H and C(9)-H (6.28 ppm and 6.43 ppm for pure CD_3CN). Strong changes of the chemical shifts of the reduced form compared to the oxidized form are detected. The reduction of flavins causes a notable upfield shift of the isoalloxazine NMR resonances as it was reported for all ^{13}C resonances except C(5a), C(9) and C(10a).[53-55] The resonances of the side chain are not affected by this shift. N(3)-H is readily assigned to the broad proton resonance at 8.64 ppm. For N(5)-H a proton signal of integral 1 (relative to the reduced flavin molecule) is detected at 5.01 ppm and assigned by means of $^{1}H,^{13}C$-hmbc and ^{1}H-dosy experiments and the NOE contact to C(6)-H. A double protonation of N(5) can be ruled out by the signal integral. For N(1)-H no clear signal is detected in the ^{1}H spectra.

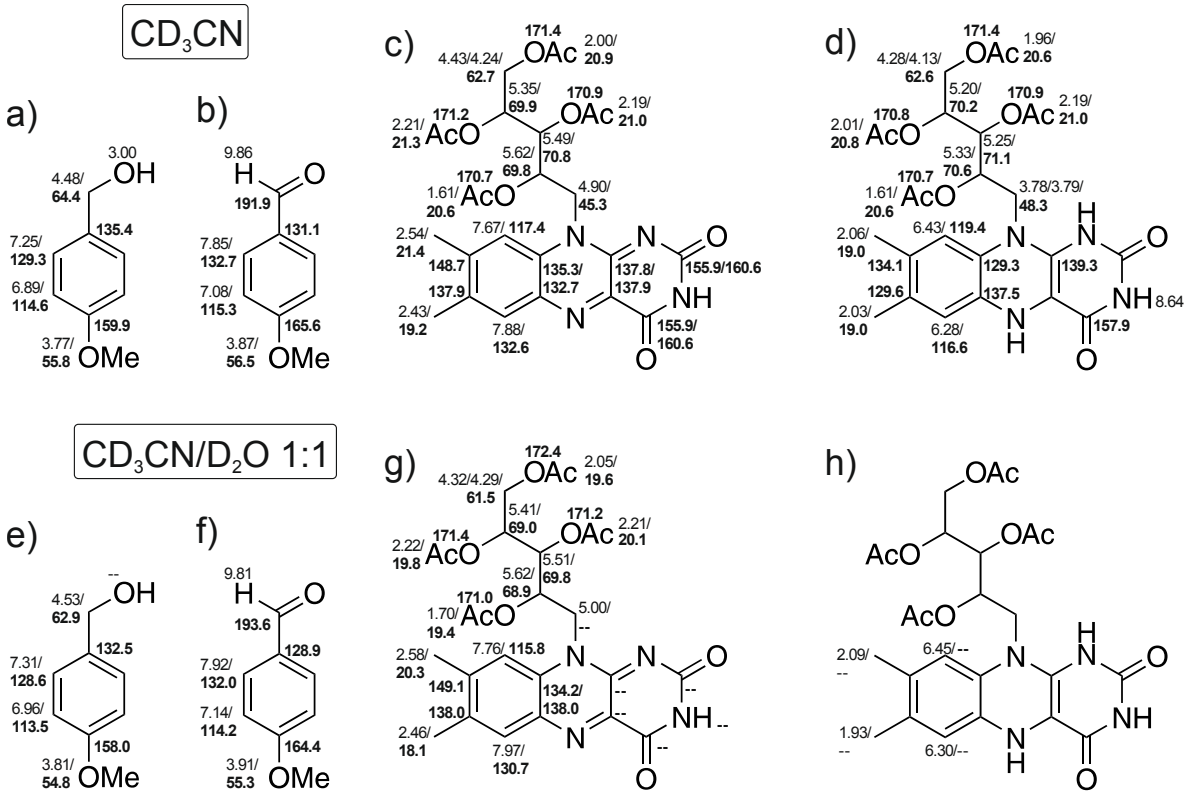

Figure 4.5 Proton and carbon chemical shift assignment of (a,e) para-methoxy benzyl alcohol (MBA); (b,f) para-methoxy benzyl aldehyde (MBAld); (c,g) riboflavin tetra acetate oxidized (RFTA) and (d,h) riboflavin tetra acetate reduced (RFTA-H_2/ RFTA-H^-) in CD_3CN (a,b,c,d) and CD_3CN/D_2O (1:1) (e,f,g,h) by 1D and 2D NMR.

However, all assigned N-H resonances of both the quinone and the hydroquinone, the MBA-OH group and the signal of H_2O show strong and broad exchange cross peaks to a chemical shift of 8.68 ppm in the $^{1}H,^{1}H$-noesy spectrum (mixing time 350 ms), see Figure 4.6. From the

broadness of the exchange peak and the characteristic chemical shift it is very probable that the N(1)-H proton resonance of the fully reduced RFT appears at a ^{1}H chemical shift of 8.68 ppm. The strong broadening of the resonance is most probably caused by strong exchange and partial deprotonation corresponding to an in N(1) only partially protonated fully reduced flavin species. The N(5)-H signal is the sharpest among the N-H resonances with a line width of 4 Hz, followed by N(3)-H with 24 Hz and N(1)-H with 337 Hz. The line widths correlate with the pKa values[56] for the fully reduced flavin of pK_a = 6.8 for N(1)-H, pK_a = 14 for N(3)-H and pK_a > 20 for N(5)-H and reflect the relative acidity of the different flavin N-H.

For the case of CD_3CN/D_2O (1:1) mixture no information about the nature of the reduced flavins can be gained from NMR spectroscopy due to the chemical exchange of the crucial N-H protons with D_2O.

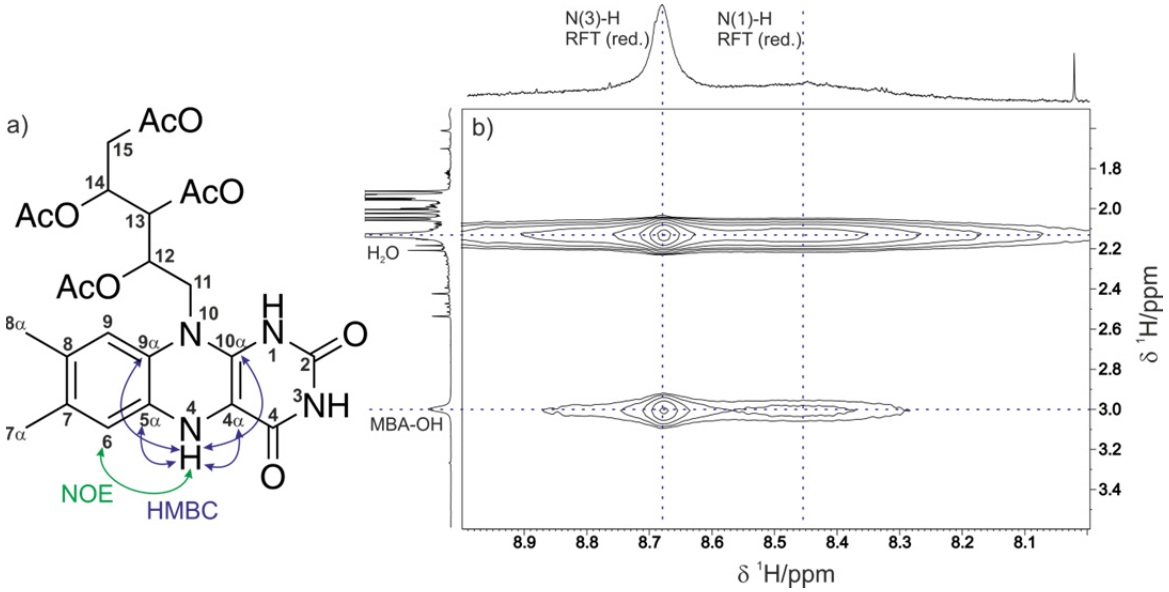

Figure 4.6 Ionization state of the fully reduced RFT (a) scheme of the fully reduced flavin N-H assignment by 1H,1H-noesy and $^{1}H,^{13}C$-hmbc (b) Section of the $^{1}H,^{1}H$-noesy spectrum showing exchange peaks of N(3)-H and the N(1)-H of the fully reduced flavin to H_2O and the MBA-OH group.

4.6.5 Spin Density Dependent Line Broadening

The line broadening of the RFTA signals dependents from the distance to the radical center. A sample of 2 mM RFTA and 20 mM MBA in not deoxygenated CD_3CN/D_2O (1:1) was sealed airtight and then a row of ^{1}H spectra was taken during the illumination with 455 nm. A selection of these spectra is shown in Figure 4.7. The first spectrum was taken before starting the illumination and shows only sharp signals for all proton resonances. By ongoing illumination the ^{1}H spectra show a gradual broadening of the RFTA resonances. The line broadening is exclusively detected for the RFTA resonances, neither substrate, product or solvent signals are affected. In flavin mononucleotide (FMN) ring systems in deoxygenated solution line broadening of the ^{1}H and ^{13}C NMR resonances was described before[46] and attributed to the formation of the semiquinone radical. Further the RFTA resonances reveal that the line broadening is not consistent in the whole molecule but distance dependent. The RFTA signals C(6)-H, C(9)-H, C(11)-H2, C(12)-H, C(13)-H and C(14)-H show that the broadening of the signal is more prominent with shorter distance of the corresponding proton from the isoalloxazine ring

system. Especially the signals C(12)-H, C(13)-H and C(14)-H show a very clear dependence of the broadening on the distance from the isoalloxazine ring system, as they are less affected by the line broadening.

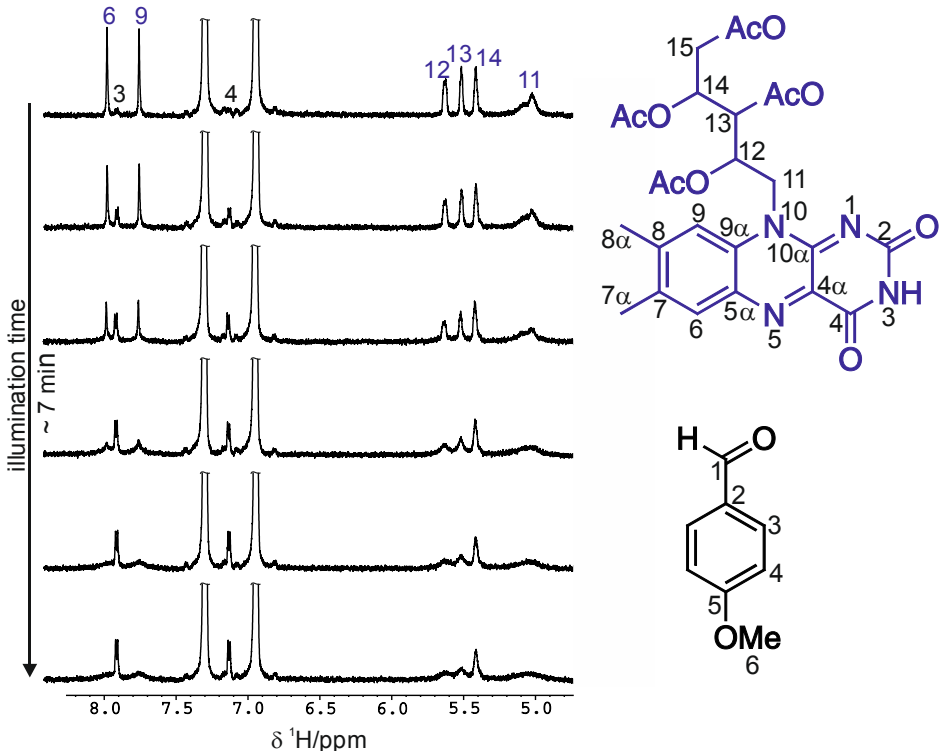

Figure 4.7 Selection of ^{1}H spectra taken during illumination with 455 nm of a sample of 2 mM RFTA and 20 mM MBA in CD_3CN/D_2O (1:1) sealed airtight. The first spectrum was recorded before illumination. MBA shows sharp signals during whole the illumination, whereas the RFTA signals broaden with increasing illumination time.

4.6.6 Stability of the Semiquinone Radical

The illumination of samples of 2 mM RFTA and 20 mM MBA in deoxygenated CD_3CN/D_2O (1:1) mixture causes broadened flavin signals in the ^{1}H NMR spectra, see Figure 4.8. So a sample of 2 mM RFTA and 20 mM MBA in deoxygenated CD_3CN/D_2O (1:1) mixture was illuminated with 455 nm. In the first ^{1}H spectrum the RFTA resonances broadened, while the signals of the aldehyde, the alcohol and the solvents (not shown) are not affected by the broadening. Than the light was switched off and ^{1}H spectra were recorded in the dark during 16 hours. Figure 4.8 shows the aromatic protons C(6)-H, C(9)-H of these ^{1}H spectra. The broadened RFTA signals reappear not before hours in the dark.

Further a sample of 2 mM RFTA and 20 mM MBA in deoxygenated CD_3CN/D_2O (1:1) mixture was illuminated with 455 nm until the RFTA resonances broadened and then aerated. Upon addition of oxygen the flavin signals recover again to sharp lines indicating the reoxidation of the semiquinone radicals to RFTA.

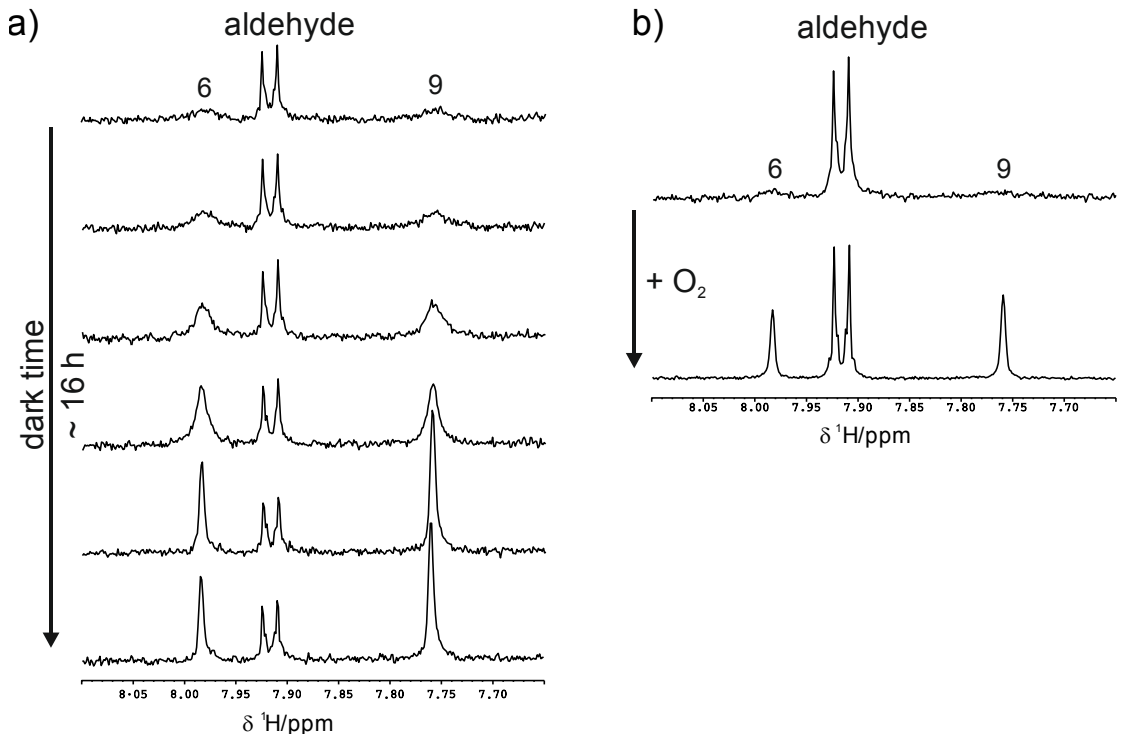

Figure 4.8 (a) Row of ^{1}H spectra showing the reappearance of the broadened RFTA signals in the dark over a time interval of ~16 h. (b) ^{1}H spectra of RFTA showing the reappearance of the broadened signals after aerating the sample.

4.6.7 Disproportionation

In contrast to pure CD_3CN no Photo-CIDNP polarizations are detected when the reaction is conducted in a deoxygenated CD_3CN/D_2O (1:1) mixture. This can be caused by disproportionation of the flavin radicals to their diamagnetic counterparts and degenerated exchange cancelation of Photo-CIDNP polarizations,[15,57,58] chemical exchange between the flavin species and or the faster separation of the initial ionic radical pair associated with the high polarity of water. Disproportionation of the semiquinone radicals makes 50% of the Photo-CIDNP sorted nuclear spins end up as recombination products (oxidized flavin) and thus reduces Photo-CIDNP polarizations. The broadened NMR resonances of the oxidized and fully reduced flavin that get sharper at lower temperatures (data not shown) suggest facilitated exchange between the different RFTA redox states. This exchange mixes the nuclear spins that were sorted by nuclear spin dependent intersystem crossing at the stage of the electron spin correlated RFTA/MBA radical pair. Thus the nuclear spin sorting is redone and deletes Photo-CIDNP polarizations in the diamagnetic products. A third factor likely to contribute to the Photo-CIDNP cancelation upon the addition of water to the reaction mixture is the faster separation of the initial ionic radical pair associated with the high polarity of water. The back electron transfer is hampered by the solvent separated radical pair and thus the sorting of nuclear spins by the Photo-CIDNP effect in the recombination product (oxidized RFTA) diminished.

4.6.8 NMR Reaction Profiles

4.6.8.1 Reaction profile in deoxygenated samples

The whole reaction profiles were investigated revealing the relative stoichiometry of the involved species. Therefore samples of 2 mM RFT and 20 mM MBA in deoxygenated CD_3CN/D_2O (1:1) were prepared and reaction profiles were recorded from a row of ^1H spectra. For the kinetic only spectra recorded in the dark were taken. After starting the illumination the signal of RFTA rapidly decreases. The formation of MBAld starts immediately, while RFTA-H_2 is formed after a time delay. The semiquinone radical anion $RFTA^{\bullet-}$ (Figure 4.9, orange points) is here shown in the raw data as well as in a smoothened curve (Figure 4.9, turquoise smoothed curve). $RFTA^{\bullet-}$ (orange points) is calculated by subtracting the detectable flavin species RFTA and RFTA-H_2 from the known total amount of flavin before illumination. But at the beginning of the reaction the high radical concentration leads to extremely broad linewidths. In addition the signals, which are integrated, are very small. For such combinations it is well known that the resulting integrals are too small and in the reverse the calculated radical concentration (100% minus integrals) is too large. Therefore, the strongly smoothed function is in our opinion the best solution to this problem.

The measuring points were smoothened in OriginPro 8G by using the smoothening function. Used method: moving average; weighted average; points of window 50, boundary conditions: none.

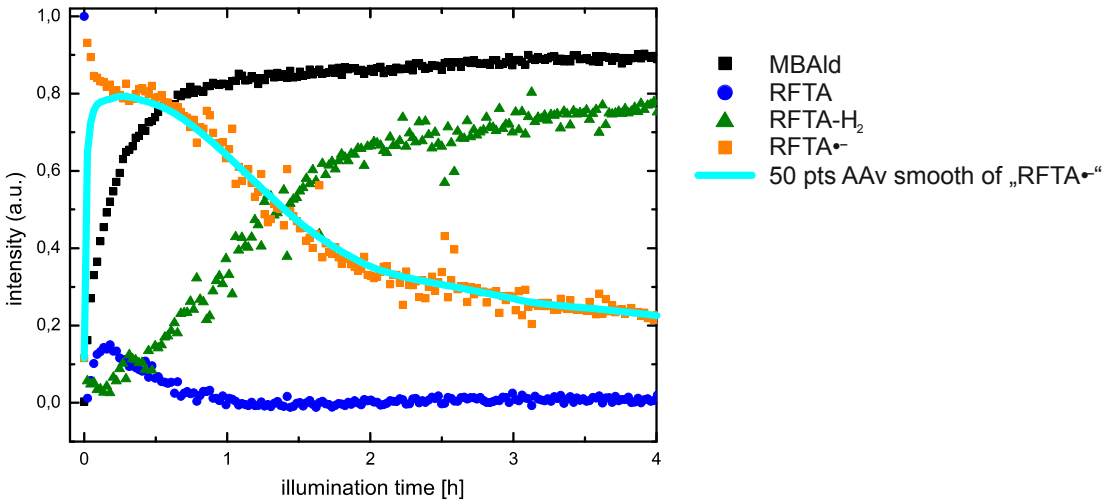

Figure 4.9 ^1H-NMR kinetic recorded in the course of the formation of methoxy benzyl aldehyde (MBAld, black) from 20 mM methoxybenzyl alcohol (not shown) catalyzed by 2 mM riboflavin tetraacetate (oxidized RFTA: blue, fully reduced RFTA-H_2: green) in deoxygenated CD_3CN/D_2O (1:1). The amount of the semiquinone radical anion $RFTA^{\bullet-}$ is first calculated by subtracting the detectable flavin species RFTA and RFTA-H_2 from the known total amount of flavin before illumination (orange data points) and then fitted by using a smoothening function (turquoise curve).

4.6.8.2 Reaction profile in partially oxygenated samples

Samples of 2 mM RFT and 20 mM MBA in partially oxygenated (solvents purged with argon for 1 hour) CD_3CN/D_2O (1:1) were prepared and reaction profiles were recorded from a row of ^1H spectra. For the kinetic only spectra recorded in the dark were taken. After starting the illumination the signal of RFTA slowly decrease. Again high amounts of flavin radicals are formed immediately after the start of the illumination (see Figure 4.10, orange curve). With

proceeding consumption of oxygen, the reoxidation of flavin slows down and the amount of oxidized flavin becomes smaller. At the moment oxygen is fully consumed the identical reaction profile as in Figure 4.9 starts to develop.

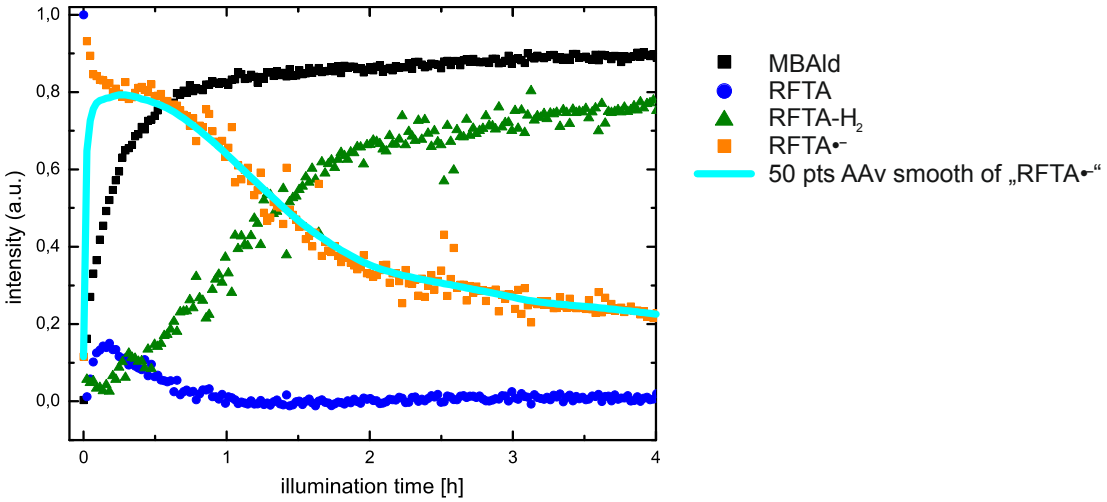

Figure 4.10 ^{1}H-NMR kinetic recorded in the course of the formation of methoxy benzyl aldehyde (black) from 20 mM methoxybenzyl alcohol (not shown) catalyzed by 2 mM riboflavin tetraacetate (oxidized RFT: blue, fully reduced RFT: green) in partially oxygenated CD_3CN/D_2O (1:1), the semiquinone radical anion $RFTA^{\bullet -}$ (orange) is calculated by subtracting the detectable flavin species RFTA and RFTA-H_2 from the known total amount of flavin before illumination.

4.6.9 Reaction profile and line broadening in the presence of oxygen.

Samples with residual amounts of oxygen were tested as well. Therefore 2 mM RFTA and 20 mM MBA in CD_3CN/D_2O (1:1) were purged with argon for 1 hour. The oxygen left in the solution was estimated from the stoichiometry of the reduced flavin and the product (Figure 4.11 a) to be about 2 mM.

The reaction profiles of the NMR signals of the RFTA, RFTA-H_2 and the product MBAld are shown in Figure 4.11 a. The signals of the oxidized flavin decrease quickly due to line broadening. Compared to the measurements under anaerobic conditions, however, this happens at a slower rate due to the concurrent reoxidation of the reduced flavin species by oxygen. The oxidized flavin signals begin to broaden and decrease right from the beginning of the reaction, even though not all oxygen is consumed. However, the fully reduced flavin species starts to appear much later when all oxygen has been consumed.

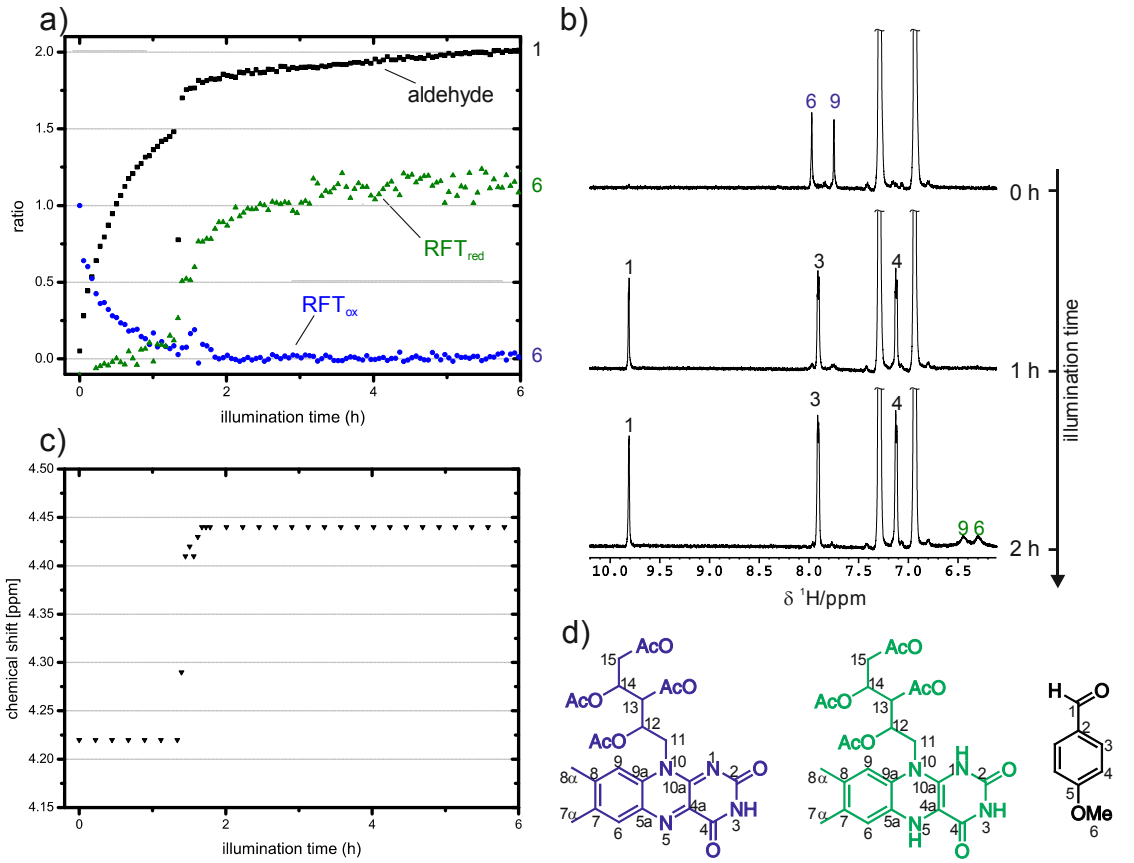

Figure 4.11 Formation of methoxy benzyl aldehyde (black) from 20 mM methoxybenzyl alcohol (not shown) catalyzed by 2 mM riboflavintetraacetate (oxidized RFTA: blue, fully reduced RFTA-H_2: green) in CD_3CN/D_2O (1:1) in the presence of ~2 mM oxygen. (a) reaction profile of RFTA, RFTA-H_2 and methoxybenzyl aldehyde referenced to the amount of the oxidized RFTA in the beginning (1.0) (b) exemplary fractions of ^{1}H spectra before, after 1 h and after 2 h of continuous illumination, (c) change of the H_2O ^{1}H chemical shift during illumination (d) structures of the oxidized and fully reduced flavin species and MBAld.

4.6.10 Calculation of the Amount of Semiquinone Radicals

To estimate the amount of the stabilized radical species the characteristic absorption band of the semiquinone radicals at 580 nm were used. Table 4.1 shows the extinction coefficients from the species associated spectra[6] of the oxidized riboflavin tetraacetate (RFTA), the corresponding anion radical (RFTA$^{\bullet-}$) and the neutral radical (RFTA-H$^{\bullet}$) for three selected wavelengths (360 nm, 450 nm and 580 nm). The characteristic absorption band of the flavin semiquinone radical is represented by the absorption at 580 nm. The absorptions at 360 nm and 450 nm represent the other absorption bands of RFTA. The UV/Vis spectra of RFTA-H_2 show absorptions for wavelengths shorter than 550 nm.[48] As only the semiquinone radicals (anion and neutral) show absorption in the spectral range above 550 nm,[6,48] the absorption band at 580 nm was used to calculate the amount of the semiquinone radical species.

The optical density (OD) of the absorption band at 580 nm (Figure 4.12) was used to estimate the amount of semiquinone radical for the cases that 100% of the detected semiquinone radical is protonated or that 100% of the detected semiquinone radical is deprotonated (anionic or neutral radical). The Beer–Lambert law[59] gives the concentration of the radical species

c from the optical density and the extinction coefficient ε of the corresponding radical at 580 nm and the path length d.

$$c = \frac{OD}{\varepsilon * d}$$

Table 4.1 Extinction coefficients ε of RFTA, the one-electron reduced flavin anion RFTA$^{\bullet-}$and the flavin neutral radical RFTA-H$^{\bullet}$ at 360 nm, 450 nm and 580 nm according to Megerle *et al*..[6]

	ε [10^3 L M^{-1} cm^{-1}]		
	360 nm	450 nm	580 nm
RFTA	8.5	12.5	0
RFTA$^{\bullet-}$	22	8.5	0.1
RFTA-H$^{\bullet}$	13.5	8.5	4.0

The OD of 0.016 at the wavelength of 580 nm (Figure 4.12), an optical path length of 2.00 mm and an extinction coefficient of $0.1 \cdot 10^3$ L mol^{-1} cm^{-1} for the anion flavin radical RFTA$^{\bullet-}$ and an extinction coefficient of $4.0 \cdot 10^3$ L mol^{-1} cm^{-1} for the neutral flavin radical RFTA-H$^{\bullet}$ are used to estimate the amount of radical stabilized in the reaction mixture after 5 minutes and after 30 minutes of illumination. At 5 minutes the anion radical RFTA$^{\bullet}$- gives an estimated amount of 0.775 mM of stabilized radical which would correspond to 39% of the overall flavin concentration. For the neutral radical RFTA-H$^{\bullet}$ the estimation gives an amount of 0.019 mM of stabilized radical which would correspond to 1% of the overall flavin concentration. The same estimations were made for 30 min, giving 100% for RFTA$^{\bullet-}$ and 2.5% for RFTA-H$^{\bullet}$ (data not shown). Further the UV/Vis measurements shown in Figure 4.12 b were used for the same calculations. In summary the estimated amount of the anion radical RFTA$^{\bullet-}$ is in the range of 39-100% and the amount of the neutral radical RFTA-H$^{\bullet}$ in the range of 1-2.5%.

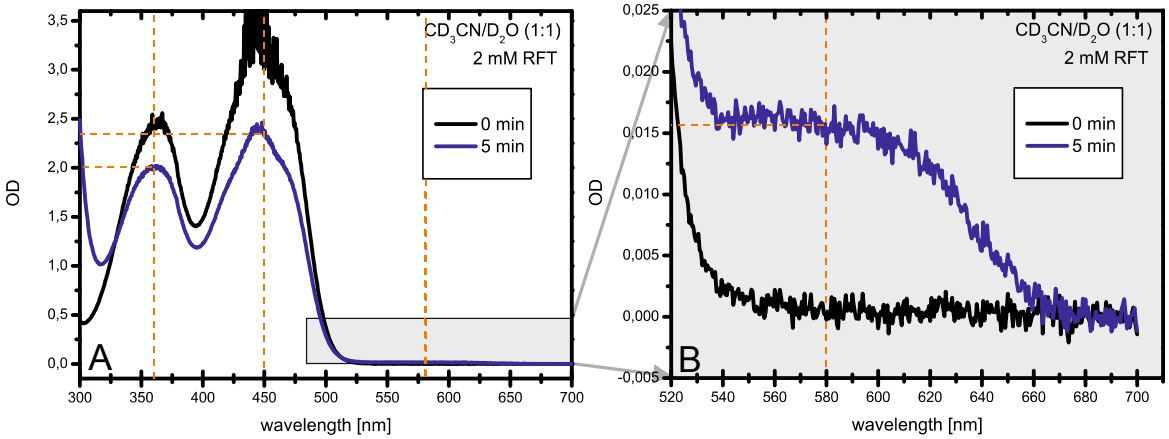

Figure 4.12 UV/Vis spectra of a deoxygenated reaction mixture of 20 mM MBA and 2 mM RFTA as a photocatalyst in CD_3CN/D_2O (1:1) mixture. UV/Vis spectra were taken before illumination and after 5 min of continuous illumination. (a) full spectrum and (b) close up in the rage of 500 nm – 700 nm. The OD of 0.016 at 580 nm was used for the estimation of the amount of the radical species.

4.6.11 Combined NMR and UV/Vis Measurements

4.6.11.1 In deoxygenated CD_3CN/D_2O

A sample of 2 mM RFTA and 20 mM MBA solved in deoxygenated CD_3CN/D_2O (1:1) was prepared to provide direct comparability of the UV/Vis measurements with the NMR measurements. The line broadening of the flavin signals in the NMR spectra (Figure 4.13 b) was found to be caused by the formation of a stable semiquinone radical by means of UV/Vis spectroscopy. Figure 4.13 c and d shows the UV/Vis spectra of the reaction mixture after different illumination times with 455 nm light. Figure 4.13 c shows the spectra with the characteristic absorption bands of RFTA in the oxidized ground state. With increasing illumination time the intensity of the two absorption bands decreases and their ratio to each other changes indicating the formation of additional flavin species. The close up view in Figure 4.13 d shows that upon irradiation of the sample a new optical feature appears at a wavelength of about 58 nm. The new absorption correlates with the species associated spectra for the semiquinone radicals reported by Megerle et al.[6]

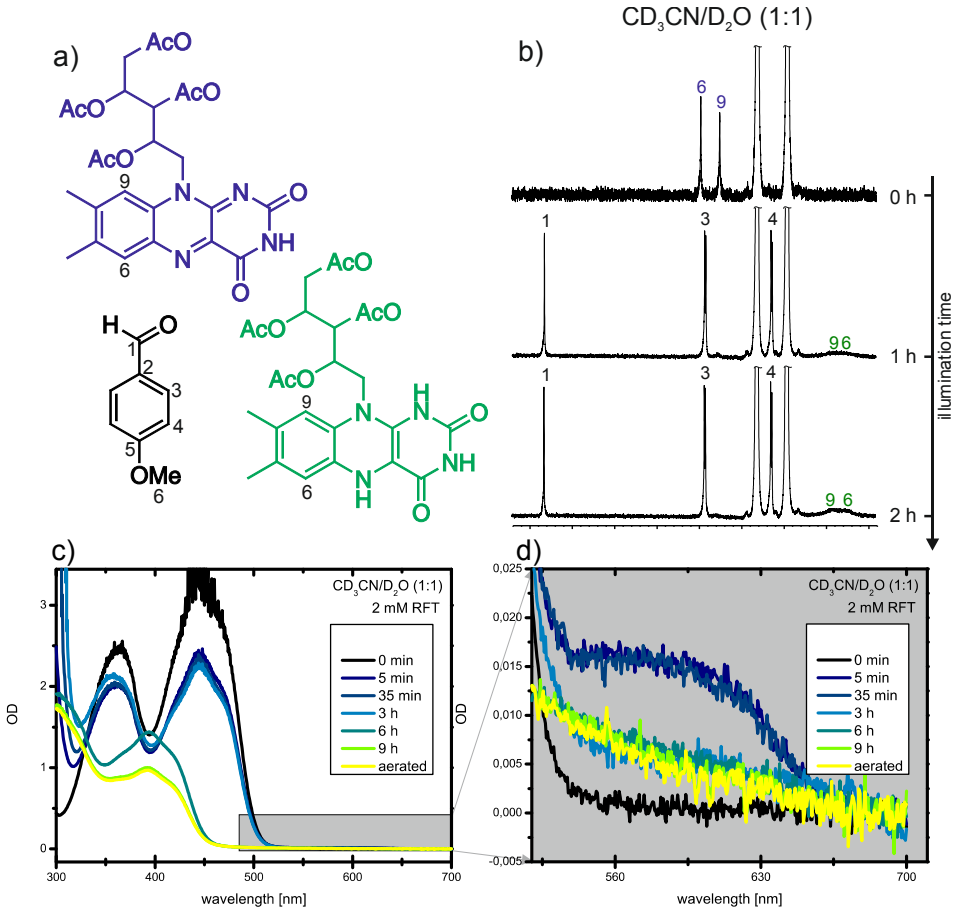

Figure 4.13: (a) Molecule structures and numbering of riboflavin tetraacetate oxidized (blue, RFTA) and reduced (green, RFTA-H_2) and methoxybenzyl aldehyd (black, MBAld) (b) ^1H NMR spectra recorded in the course of the formation of MBAld from 20 mM methoxybenzyl alcohol (MBA, not shown) catalyzed by 2 mM RFTA in deoxygenated CD_3CN/D_2O (1:1) (c) UV/Vis spectra of a degassed solution of 2 mM RFTA and 20 mM of MBA in CD_3CN/D_2O (1:1) before illumination and after 5 min, 35 min, 3 h, 6 h and 9 h of continuous illumination, after nine hours of illumination the samples were aerated (yellow spectrum, degradation of RFTA). (d) shows a close up of the absorption of the flavin in the range

of 500 nm up to 700 nm the range of the characteristic absorption band of the flavin semiquinone radical.

4.6.11.2 In deoxygenated CD_3CN

The NMR data show the broadening of the signals only for the case of the solvent mixture CD_3CN/D_2O (1:1) (Figure 4.13 b) and not for pure CD_3CN (Figure 4.14 b) which suggests that the addition of D_2O to the reaction mixture is at least partially responsible for the stabilization of the radical. So the influence of the solvent on the stabilization of the semiquinone radical was studied by means of UV/Vis spectroscopy. A solution of 2 mM RFTA and 20 mM MBA in CD_3CN illuminated with 455 nm light over different time periods and UV/Vis spectra were taken after each illumination period. The spectra are shown in Figure 4.14 c and d. The observation that no semiquinone radical is stabilized if the reaction is performed in pure CD_3CN correlates with the NMR studies of the reaction in the two different solvents. In the case of pure CD_3CN the ^1H resonances of the oxidized and the fully reduced flavin species appear as sharp signals indicating no stabilization of the radical.

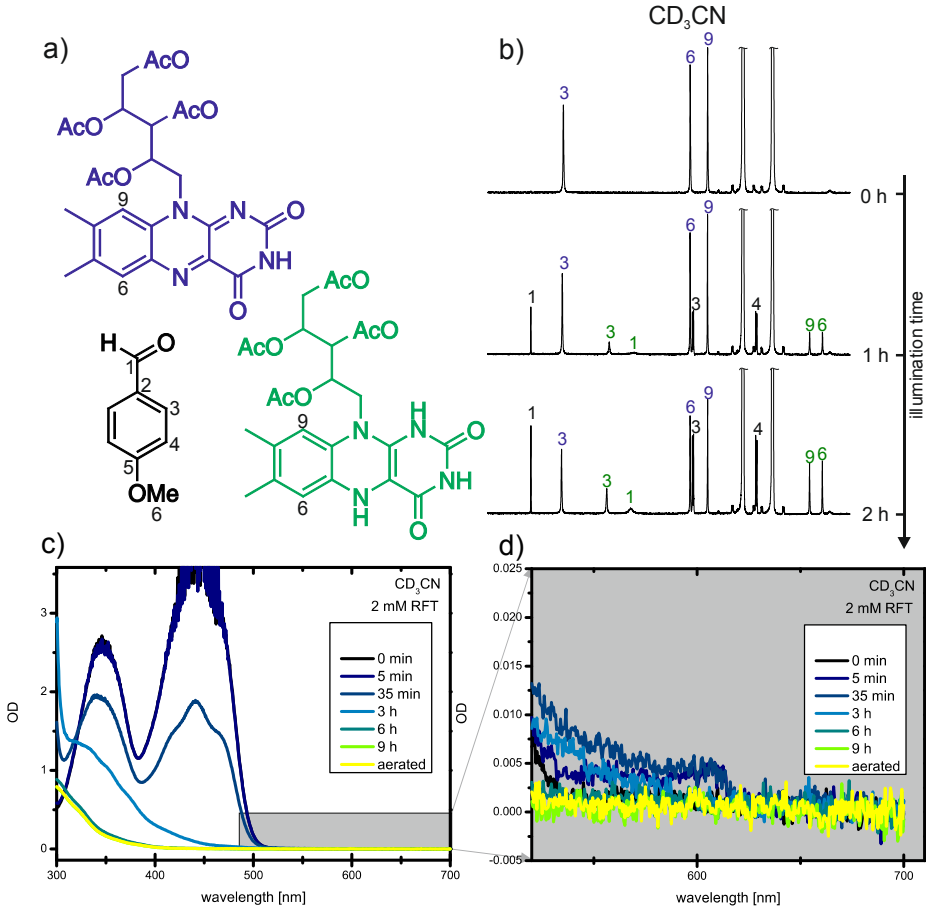

Figure 4.14 (a) Molecule structures and numbering of riboflavin tetraacetate oxidized (blue, RFTA) and reduced (green, RFTA-H_2) and methoxybenzyl aldehyd (black, MBAld) (b) ^1H NMR spectra recorded in the course of the formation of MBAld from 20 mM methoxybenzyl alcohol (MBA, not shown) catalyzed by 2 mM RFTA in deoxygenated CD3CN (c) UV/Vis spectra of a degassed solution of 2 mM RFTA and 20 mM of MBA in CD_3CN before illumination and after 5 min, 35 min, 3 h, 6 h and 9 h of continuous illumination, after nine hours of illumination the samples were aerated (yellow spectrum). (d) shows a close up of the absorption of the flavin in the range of 500 nm up to 700 nm the range of the characteristic absorption band of the flavin semiquinone radical.

4.6.11.3 Influence of the ratio of RFTA/MBA

The ratio between the concentrations of MBA and RFTA is influencing the semiquinone stabilization. Therefore samples with different concentrations (2 mM RFTA; 2 mM RFTA and 400 µM MBA; 2 mM RFTA and 20 mM MBA) in deoxygenated CD_3CN/D_2O (1:1) were investigated. The different samples were illuminated for 1 min, 5 min and 30 min and the UV/Vis spectra were recorded after the illumination periods. Figure 4.15 c shows the UV/Vis spectra of only RFTA.

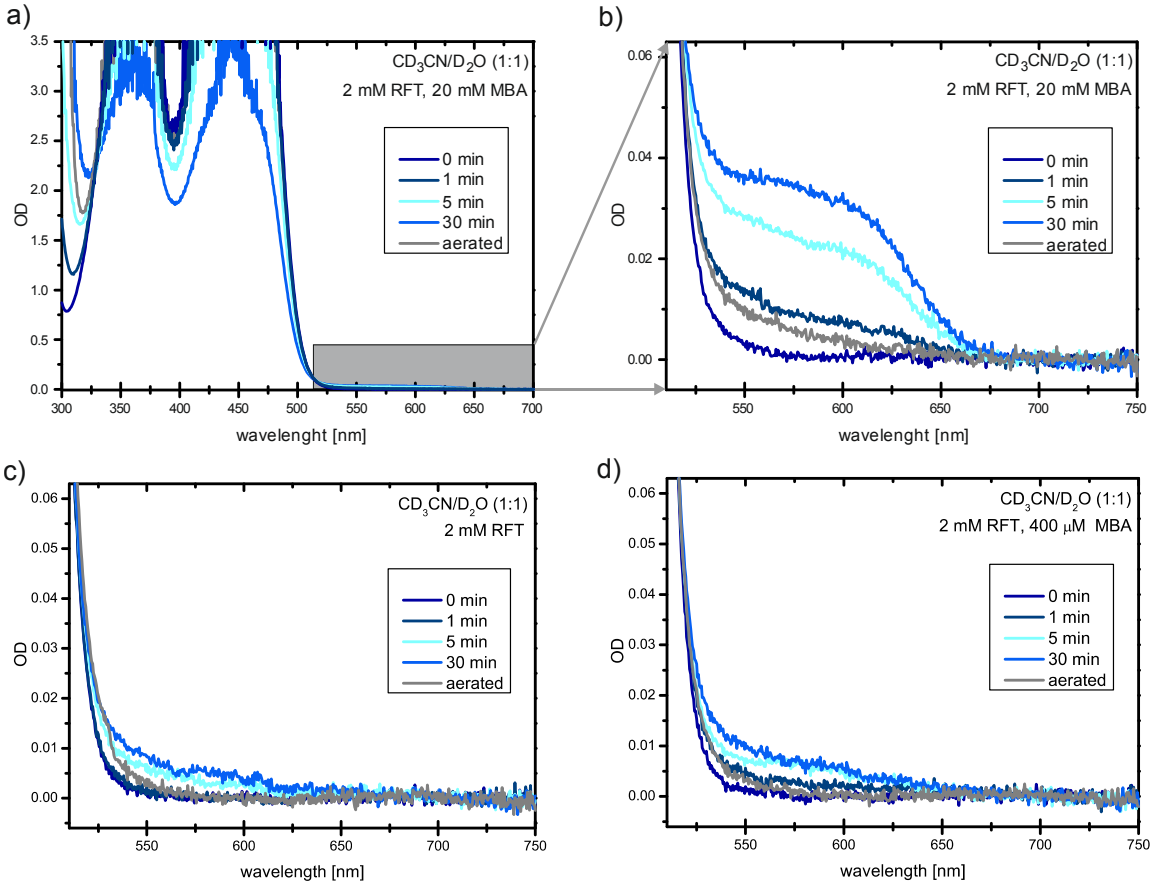

Figure 4.15 UV/Vis spectra of deoxygenated reaction mixtures of riboflavin tetraacetate (RFTA) and methoxybenzyl alcohol (MBA) of different concentrations in CD_3CN/D_2O (1:1) before and after 1 min, 5 min and 30 min of continuous illumination with 455 nm and after subsequent aeration of the solution (grey spectra). (a) Full spectrum of the standard concentration used for NMR studies (2 mM RFTA and 20 mM MBA) and (b) close up in the range of 500 nm – 700 nm with the characteristic absorption band of the flavin semiquinone radical at 580 nm, (c) only 2 mM RFTA without MBA, (d) low MBA concentration (2 mM RFTA and 400 µM MBA).

The first spectrum shows the formation of the semiquinone radical by the characteristic absorption band at 580 nm after 5 min of irradiation and becomes more pronounced after 30 min illumination. To study the influence of MBA on the radical formation the measurement was conducted with 2 mM RFTA and 400 µm MBA concentrations. The UV/Vis spectra (Figure 4.15 d) show no significant increase in amount of formed semiquinone compared to the case that only RFT is present in the solution (Figure 4.15 c). A sample containing 20 mM MBA and 2 mM RFTA was measured. Figure 4.14 a shows the full UV/Vis spectrum and Figure 4.15 b shows a close up of the spectra. The semiquinone radical is already formed after 1 min of irradiation and becomes more pronounced after 5 min and 30 min illumination. Compared to

the cases of only 2 mM RFTA or of 2 mM RFTA and 400 µM MBA the increased amount of MBA causes the formation and stabilization of more semiquinone radical. This reveals that a significant amount of semiquinone radical is only formed and stabilized when both RFTA and MBA are present in sufficient concentrations. Overall, the experiments with different RFTA and MBA ratios showed that both RFTA and MBA are necessary in significant amounts to stabilize the semiquinone radical and that the stabilized semiquinone radical predominantly results from the oxidation of MBA by RFTA.

4.6.12 Mixed dimers RFTA/RFTA-H_2

In the reaction profiles of the deoxygenated and the partially oxygenated CD_3CN/D_2O (1:1) mixture a small amount of a mixed dimer (RFTA/RFTA-H_2) reappears after the decay of RFTA, indicated by chemical shift changes, which than decreases gradually. The initial fast decrease of the oxidized flavin is caused by the fast semiquinone radical formation at the beginning of the reaction leading to broadened lines. The oxidized flavin species reappears with the typical behavior of an intermediate. However, it is not the rate determining intermediate because the maximum of its intensity does not correlate with the maximal slope in product formation. This shows that it is a downstream intermediate to aldehyde formation. The reappearing of the signal set of the oxidized RFT is accompanied with a downfield shift of the C(9)-H resonance of about 0.2 ppm. The chemical shift change is due to the formation of mixed dimers consisting of one oxidized and one fully reduced RFT molecule as products of disproportionation of the two semiquinone radicals, because the same chemical shift changes are observed if the reaction is conducted in pure CD_3CN with the C(9)-H resonance shifting downfield in the course of the reaction. The formation of the mixed dimer species also explains the different rate constants in consumption of pure oxidized flavin dimers and mixed dimers.

4.6.13 ^{1}H CIDNP-Spectra

4.6.13.1 ^{1}H CIDNP Spectra in CD_3CN/D_2O

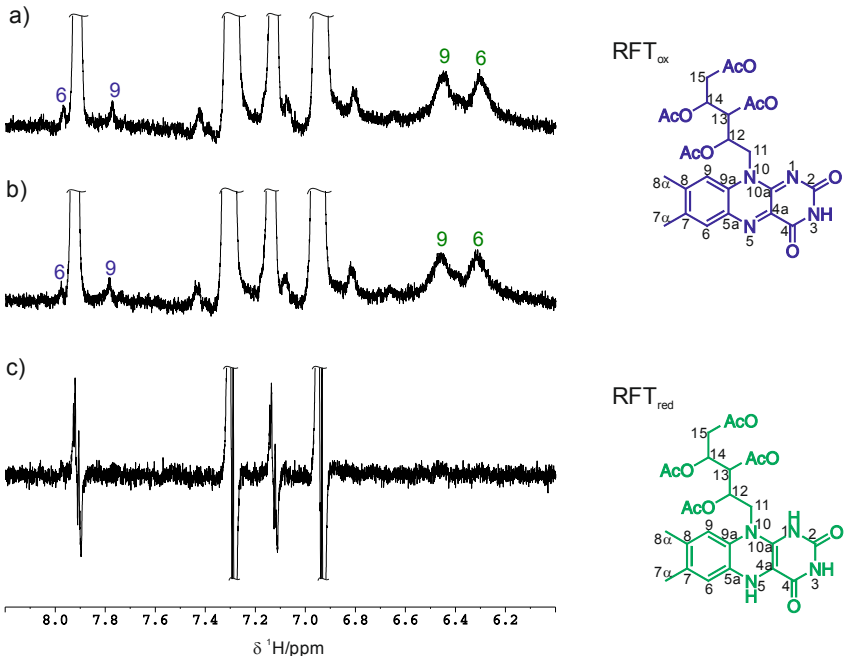

Figure 4.16 ^{1}H spectra of the reaction mixture of 2 mM RFT and 20 mM MBA in deoxygenated CD_3CN at 300 K after one hour of *in situ* illumination with 455 nm light. (a) shows the spectrum of the not illuminated sample (b) the spectrum of the illuminated sample (c) the Photo-CIDNP spectrum as the difference spectrum of (b) and (a).

4.6.13.2 ^{1}H CIDNP Spectra in CD3CN

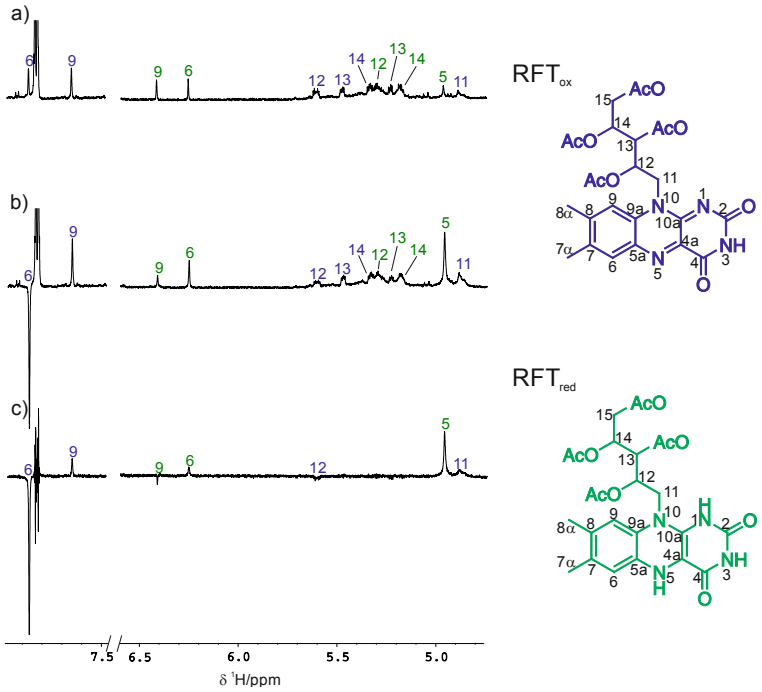

Figure 4.17 ^{1}H spectra of the reaction mixture of 2 mM RFT and 20 mM MBA in deoxygenated CD_3CN/D_2O (1:1) at 280 K after *in situ* illumination with 455 nm light. (a) shows the spectrum of the not illuminated sample, (b) the spectrum of the illuminated sample (c) the Photo-CIDNP spectrum as the difference spectrum of (b) and (a).

4.7 References

[1] C. Feldmeier, Ph.D. thesis, University of Regensburg, Regensburg **2014**.

[2] B. König, S. Kümmel, R. Cibulka, in *Chem. Photocatal*. (Ed.: B. König), De Gruyter, Berlin, **2013**, pp.45-66.

[3] J. W. Tucker, C. R. J. Stephenson, *J. Org. Chem*. **2012**, *77*, 1617-1622.

[4] C. K. Prier, D. A. Rankic, D. W. C. MacMillan, *Chem. Rev*. **2013**, *113*, 5322-5363.

[5] T. P. Yoon, M. A. Ischay, J. Du, *Nat. Chem*. **2010**, *2*, 527-532.

[6] U. Megerle, M. Wenninger, R.-J. Kutta, R. Lechner, B. König, B. Dick, E. Riedle, *Phys. Chem. Chem. Phys*. **2011**, *13*, 8869-8880.

[7] S. J. Hwang, C. Petucci, D. Raftery, *J. Am. Chem. Soc*. **1998**, *120*, 4388-4397.

[8] S. Pilkenton, S.J. Hwang, D. Raftery, *J. Phys. Chem*. B **1999**, *103*, 11152-11160.

[9] J. Wirmer, T. Kühn, H. Schwalbe, *Angew. Chemie - Int. Ed*. **2001**, *40*, 4248-4251.

[10] T. Kühn, H. Schwalbe, *J. Am. Chem. Soc*. **2000**, *122*, 6169-6174.

[11] K. H. Mok, T. Nagashima, I. J. Day, J. A. Jones, C. J. V Jones, C. M. Dobson, P. J. Hore, *J. Am. Chem. Soc*. **2003**, *125*, 12484-12492.

[12] G. E. Ball, in *Spectrosc. Prop. Inorg. Organomet. Compd. Tech. Mater. Appl.*, Bd. 41, The Royal Society Of Chemistry, London, **2010**, pp. 262-287.

[13] A. Mills, C. O'Rourke, *Catal. Today* **2014**, *230*, 256-264.

[14] M. Goez, in *Adv. Photochem*., (Eds. D.C. Neckers, D.H. Volman, G. von Bünau), Wiley, New York, **1997**.

[15] P. J. Hore, R.W. Broadhurst, *Prog. Nucl. Magn. Reson. Spectrosc*. **1993**, *25*, 345-402.

[16] H. Hayashi, *Introduction to Dynamic Spin Chemistry: Magnetic Field Effects upon Chemical and Biochemical Reactions*, World Scientific, **2004**.

[17] L. Kuhn, *Top. Curr. Chem*., Springer, Berlin/Heidelberg, **2013**, pp.1-72.

[18] N. J. Turro, V. Ramamurthy, J. C. Scaiano, *Modern Molecular Photochemistry of Organic Molecules*, University Science Books, Sausalito, **2010**.

[19] M. Goez, in *Adv. Photochem*. (Eds.: D.C. Neckers, D.H. Volman, G. von Bünau), WILEY, New York, **2007**, pp. 63-163.

[20] C. Feldmeier, H. Bartling, E. Riedle, R. M. Gschwind, *J. Magn. Reson*. **2013**, *232*, 39-44.

[21] M. B. Schmid, K. Zeitler, R. M. Gschwind, *Angew. Chemie – Int. Ed.* **2010**, *49*, 4997-5003.

[22] M. B. Schmid, K. Zeitler, R. M. Gschwind, *J. Am. Chem. Soc*. **2011**, *133*, 7065-7074.

[23] M. B. Schmid, K. Zeitler, R. M. Gschwind, *J. Org. Chem*. **2011**, *76*, 3005-3015.

[24] D. G. Blackmond, *Angew. Chemie - Int. Ed*. **2005**, *44*, 4302-4320.

[25] J. Dadová, S. Kümmel, C. Feldmeier, J. Cibulková, R. Pažout, J. Maixner, R. M. Gschwind, B. König, R. Cibulka, *Chem. - A Eur. J*. **2013**, *19*, 1066-1075.

[26] R. Lechner, S. Kümmel, B. König, *Photochem. Photobiol. Sci*. **2010**, *9*, 1367-1377.

[27] J. Svoboda, H. Schmaderer, B. König, *Chem. - A Eur. J*. **2008**, *14*, 1854-1865.

[28] G. Richter, S. Weber, W. Römisch, A. Bacher, M. Fischer, W. Eisenreich, *J. Am. Chem. Soc*. **2005**, *127*, 17245–17252.

[29] R. Miura, *Chem. Rec*. **2001**, *1*, 183–194.

[30] A. M. Edwards, in *Flavins Photochem. Photobiol*. (Eds.: E. Silva, A.M. Edwards), RCS Publishing, Cambridge, **2006**, pp. 1-11.

[31] V. Massey, *Biochem. Soc. Trans*. **2000**, *28*, 283-296.

[32] M. W. Fraaije, A. Mattevi, *Trends Biochem. Sci*. **2000**, *25*, 126-132.

[33] G. DeGonzalo, M. W. Fraaije, *ChemCatChem* **2013**, *5*, 403-415.

[34] S. Ghisla, V. Massey, *Biochem. J*. **1986**, *239*, 1-12.

[35] K. Tatsumi, H. Ichikawa, S. Wada, *J. Contam. Hydrol*. **1992**, *9*, 207-219.

[36] C. B. Martin, M.-L. Tsao, C. M. Hadad, M. S. Platz, *J. Am. Chem. Soc*. **2002**, *124*, 7226-7234.

[37] E. Silva, A. M. Edwards, D. Pacheco, *J. Nutr. Biochem*. **1999**, *10*, 181-185.

[38] W. A. Massad, Y. Barbieri, M. Romero, N. A. García, *Photochem. Photobiol.* **2008**, *84*, 1201-1208.

[39] J. Kim, M. A. Bogdan, P.S. Mariano, *J. Am. Chem. Soc*. **1993**, *115*, 10591-10595.

[40] T. Gärtner, N. Yoshikai, M. Neumeier, E. Nakamura, R. M. Gschwind, *Chem. Commun*. **2010**, *46*, 4625-4626.

[41] K. Schober, H. Zang, R. M. Gschwind, *J. Am. Chem. Soc*. **2008**, *130*, 12310-12317.

[42] M. Neumeier, R. M. Gschwind, *J. Am. Chem. Soc*. **2014**, *136*, 5765-5772.

[43] M. Goez, *ChemInform* **2010**, *41.*

[44] M. Goez in *Annu. Reports NMR Spectrosc., Vol 66* (Ed.: A.W. Graham), Academic Press, **2009**, pp. 77-147.

[45] J. C. Scaiano, D. J. Lougnot, *J. Phys Chem*. **1984**, *88*, 3379-3382.

[46] D. D. Macmurchie, R. J.Cushley, *Can. J. Chem*. **1978**, *56*, 1045-1051.

[47] P. R. Andrews, M. D. Fenn, *Aust. J. Chem*. **1975**, *28*, 1609-1612.

[48] M. Sakai, H. Takahashi, *J. Mol. Struct*. **1996**, *379*, 9-18.

[49] S. Ghisla, V. Massey, J.-M. Lhoste, S.G. Mayhew, *Biochemistry* **1974**, *13*, 589-597.

[50] P. Hemmerich, S. Ghisla, U. Hartmann, F. Müller, in *First publ. Flavins Flavoproteins Proc. Third Int. Symp. Flavins Flavoproteins*, Durham, North Carolina **1971**.

[51] R.-J. Kutta, Ph.D. thesis, University of Regensburg, Regensburg **2012**.

[52] D. B. McCormick, *J. Heterocycl. Chem*. **1970**, *7*, 447-450.

[53] K. Kawano, N. Ohishi, A. T. Suzuki, Y. Kyogoku, K. Yagi, *Biochemistry* **1978**, *17*, 3854-3859.

[54] C. G. van Schagen, F. Müller, *Helv. Chim. Acta* **1978**, *61*, 3139-3142.

[55] C. G. van Schagen, F. Müller, *Helv. Chim. Acta* **1980**, *63*, 2187-2201.

[56] P. Macheroux, S. Ghisla, C. Sanner, H. Ruterjans, F. Muller, *BMC Biochemistry* **2005**, *6*, 26.

[57] R. Kaptein, K. Dijkstra, F. Müller, C. G. Van Schagen, A. J. W. G. Visser, *J. Magn. Reson*. **1978**, *31*, 171-176.

[58] P. J. Hore, E. R.]P. Zuiderweg, R. Kaptein, K. Dijkstra, *Chem. Phys. Lett*. **1981**, *83*, 376-383.

[59] P. Atkins, J. de Paula, *Physical* Chemistry, 9th Edition, W. H. Freeman & Co, **2009**.

5. Spiropyran/Merocyanine — Studies of a Photochromic Model System Using NMR with *Ex-Situ* and *In-Situ* Irradiation Devices

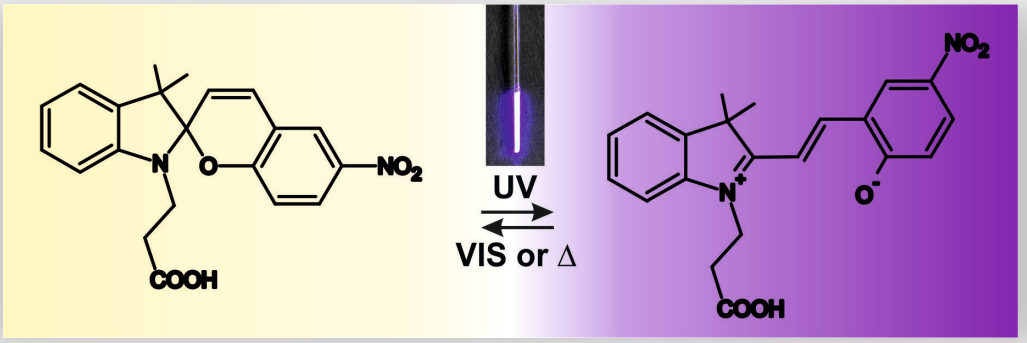

The synthesis of spiropyran and the UV measurements were performed by Dr. H. Schenderlein. *Ex-situ* NMR measurements were performed by Dr.-Ing. C. Wolff. *In-situ* NMR measurements were performed by H. Bartling.

Christiane Wolff, Jonas Kind, Helge Schenderlein, Hanna Bartling, Christian Feldmeier, Ruth M. Gschwind, Markus Biesalski, Christina M. Thiele

Magn. Res. Chem. **2016**, *54*, 485-491.

DOI: 10.1002/mrc.4403

5.1 Abstract

The switching behavior of a photochromic model system was investigated in detail via NMR spectroscopy in order to improve understanding of the compound itself and to provide ways to obtain insights into composition trends of a photo switchable (polymeric) material containing spiropyran/ merocyanine units. In addition to the classical irradiation performed outside the magnet (*ex-situ*), a device for irradiation inside the NMR spectrometer (*in-situ*) was tested. Both setups are introduced, their advantages and disadvantages as well as their limits are described and the setup for future investigations of photochromic materials is suggested.

The influence of different sample concentrations, irradiation procedures, and light intensities on the model system was examined as well as the dependence on solvent, temperature and irradiation wavelengths. Using the recently published LED illumination device, it was even possible to record two-dimensional spectra on this model system with rather short half-life (7 min in DMSO). This way ^{13}C chemical shifts of the merocyanine form were obtained, which were unknown before.

5.2 Introduction

The function and reactivity of a compound or a new material is largely determined by its structure-property relationship.[1,2] For a detailed description of the properties of a new material or its goal-oriented synthesis, a fundamental understanding of the before mentioned relationship is of utmost importance. If studying a new material itself would incorporate too many challenges simultaneously – as is the case for many multifunctional macromolecules, including the photochromic polymer further outlined below – investigating precursor compounds can facilitate a deeper insight into the properties of materials derived thereof.

In the last years, new compounds and materials with reversible light-induced change in properties have been synthesized and used in manifold applications[3] This includes the use in optical information storage or sunglasses[3,4] or the embedding of photochromic compounds in biomacromolecules.[5-7] The most prominent photochromic systems are the *cis/trans*-azobenzene and the spiropyran /merocyanine systems (Scheme 5.1).[3,5] For the latter, a closed colorless form (spiropyran) is in equilibrium with the open and colored merocyanine form. The ring-opening reaction to the (usually) metastable merocyanine can be promoted by irradiation with Ultraviolet (UV) light, while the back reaction occurs thermally or promoted by visible light.[3,8] The discovery of the spiropyran/merocyanine system in the 1950s by Hirshberg and Fischer was followed by an extensive investigation of spiropyrans[9,10] and derived compounds[11,12] as well as their usage in different fields.[8,13,14] One major benefit of photochromic systems is the high spatial and temporal precision of activation through light.[5]

We are interested in the photochromic properties (kinetics, half-life and maximum fraction of merocyanine) of a new photochromic copolymer containing the spiropyran/merocyanine photochromic moiety.[15] The light-induced conformational change between the spiropyran and the merocyanine leads to a change in the physical properties of the photochromic unit (color, polarity, and dipole moment), which also has an influence on the physical properties of the polymer itself. This light induced change of the polymer properties can be used for different kinds of applications, e. g. polymers with switchable interactions to analytes (ions, proteins, and living cells), variable wettability and solubility, tunable coloration.[16-20] Despite these applications, our fundamental understanding of the structure-property relation of stimulus-responsive spiropyran-polymers is still poor. The knowledge of the photochromic properties, in particular, allows the understanding of the macroscopic switching behavior of the material and enables the design and synthesis of material with desired bulk properties.[5,21] It thus needs to be characterized (structure, absorption spectra, solubility, and half-life of the metastable form[22]). For the investigation of the photochromic material or precursor system, a light source is needed, which is linked with an analytical method, which ideally does not affect the photochromic equilibrium between the stable and the metastable form of the system. While Ultraviolet-visible (UV/Vis) spectroscopy can easily be performed on photochromic systems for qualitative studies, a quantitative investigation can only be carried out if the extinction coefficient of the metastable form is known,[23] which was not the case in the present project. When using NMR spectroscopy, which also provides structural details for the study of photochromic equilibria,[9,11,12] one faces the challenge of illuminating the sample ideally within the NMR spectrometer. Several NMR illumination devices have been presented, which are suitable for the investigation of photochromic compounds via NMR.[24] Such

systems usually employ extensive probe alterations or use optical fibers guiding the light into the NMR sample.[24,25] A further advancement of the latter was recently published by the Gschwind group,[26] which uses standard inexpensive light emitting diodes (LEDs) for illuminating the sample inside the NMR spectrometer at a specific wavelength.

Scheme 5.1 Light-induced interconversion between the closed spiropyran form **1** and the open merocyanine form **2** (To determine the ratio between both forms the ^{1}H-NMR signals of the corresponding methyl groups (red) were integrated).

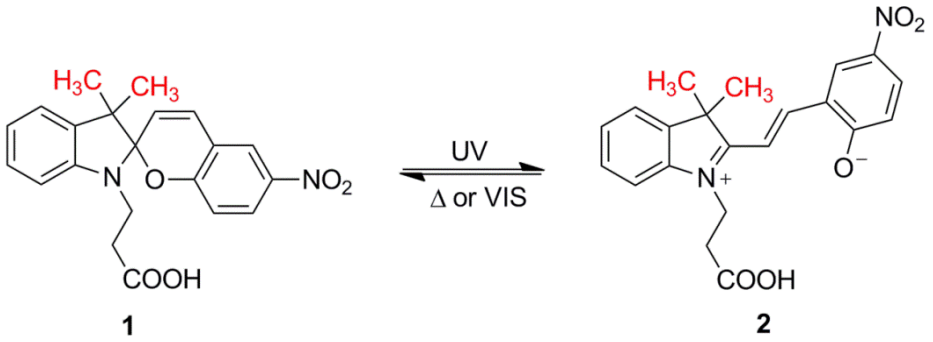

As the extinction coefficient was not known for the metastable form of the copolymer and cannot be determined easily, UV/Vis measurements could only be interpreted qualitatively. To circumvent these problems and to gain first insights, a simplified precursor model was investigated (Scheme 5.1) to establish methods which should then be transferable to the polymer.[27] The fractions of spiropyran **1** and merocyanine **2** were monitored online via different NMR illumination techniques (irradiation inside and outside of the magnet) and compared to standard UV/Vis measurements. By using NMR spectroscopy, not only the calculation of the extinction coefficient ε of the metastable form **2** of the precursor model was possible but also the determination of the fraction of merocyanine **2** in the photo stationary state. Through these measurements, new insights in the mentioned spiropyran/merocyanine equilibrium were obtained and handling trends for the copolymer hinted at.

5.3 Materials and Methods

The spiropyran compound **1** was prepared according to the synthesis described in Schenderlein *et al*.[15] and Fissi *et al*.[27]

5.3.1 Irradiation outside of the NMR spectrometer (*ex-situ*)

For the irradiation outside of the NMR spectrometer, a Lumatec DC-E mercury vapor lamp with a UV filter (transmission wavelengths range from 320 – 400 nm) was used. The spiropyran solutions (0.20, 0.36 and 0.59 wt.% in DMSO-d_6) were filled into a 3 mm NMR tube and irradiated at a distance of 8 cm between the liquid and the light guide tip for 10 min (energy density at this distance ~ 30 mW/cm^2).[1] Afterwards, the 3 mm tube was placed inside an amber 5 mm NMR tube and transferred into the NMR spectrometer. The respective dead-time, which includes the transport of the sample and locking, is between 60 and 90 s. For the

[1] The energy density was measured as a function of distance. At a wavelength of 365 nm and 100% light intensity the energy density at a distance of 8 cm is estimated to be 30 mW/cm^2.

measurements of the samples irradiated outside of the spectrometer a Bruker Avance III 600.4 MHz spectrometer with a triple broad-band inverse (TBI)-probe with a selective ^{31}P-coil and z-gradient was used. The measurements were recorded as single-scan ^{1}H-NMR spectra with variable time delays (time delay list: 1x0 s, 4x15 s, 14x60 s, 3x300 s, and 2x600 s). The time delays for the first data points were chosen as close to each other as possible but nevertheless ensuring complete relaxation of the system (~ 5*T_1, T_1 < 3.2 s for spiropyran **1** obtained via inversion-recovery experiment).[28]

5.3.2 Irradiation inside the spectrometer (*in-situ*)

The sample solution was placed in a 5 mm NMR tube with an insert for the glass fiber. The measurements were recorded with a Bruker Avance III 600.13 MHz spectrometer with 5 mm TBI-probe with selective ^{31}P-coil and z-gradient or a 5 mm Prodigy broad-band observe (BBO)-probe with z-gradient as single-scan ^{1}H-NMR spectra under continuous irradiation with light of the corresponding wavelengths using constant time delays. The *in-situ* irradiation device is the LED irradiation device described in Feldmeier *et al*.[26] LEDs of the following emission wavelengths were coupled to the device (365 nm: Nichia SMD LED UV NCSU033B (Tokushima, Japan) with 325 mW and 455 nm: Cree XP-E (Durham, North Carolina, USA), royal blue 500 mW; the power at the sample for the 365 nm LED is ~ 7 mW). The output power of the LED coupled to the optical fiber was measured with an energy meter (Coherent Power Max). Additionally, the same UV lamp as used for the *ex-situ* NMR irradiation was coupled to the same device.

5.3.3 Ultraviolet-visible measurements

Ultraviolet-visible spectra were recorded using a Varian Cary 50 SCAN UV/Vis spectrometer (Agilent, Santa Clara, California, USA). For irradiation of the sample the same mercury vapor lamp as used for the *ex-situ* NMR irradiation (see above) was employed. For UV illumination, the filter mentioned earlier was used, for illumination with visible light (Vis) a filter with transmission between 400 and 700 nm was used. The light guide was introduced at an angle of 45° to the sample surface into the sample chamber. Complete spectra were recorded from 200 to 800 nm (Figure 5.1). For kinetic investigations and to obtain half-lives the change in extinction at a fixed wavelength (λ_{max} of the merocyanine form) was monitored over time (Table 5.1).

5.4 Results and Discussion

As a first step the optimum conditions for the irradiation had to be found. By using UV/Vis spectroscopy the half-life $\tau_{½}$ of the thermal back reaction[14] of the spiropyran/merocyanine system in DMSO was determined to be larger as compared with other solvents [DMF, THF, and dioxane (Table 5.1)].[15]

The solvent induced change in absorption wavelength λ_{max} as well as half-life $\tau_{½}$ corresponds to the different relative permittivity of the solvents and has been widely discussed elsewhere.[10,29,30] UV/Vis spectra in DMSO showed that irradiation with UV light stimulates the interconversion of spiropyran **1** to merocyanine **2**, while visible light shifts the spiropyran/merocyanine equilibrium back to the more stable side of spiropyran **1** (Figure 5.1).

Table 5.1 Half-lives of the thermal back reaction of merocyanine **2** to spiropyran **1** in different solvents determined via ultraviolet-visible measurements (at 295K).[15]

Entry	Solvent	Half-life $\tau_{½}$ (s)	λ_{max} of the merocyanine form **2** (nm)
1	DMSO	408	565
2	DMF	126	570
3	THF	19	585
4	Dioxane	13	585

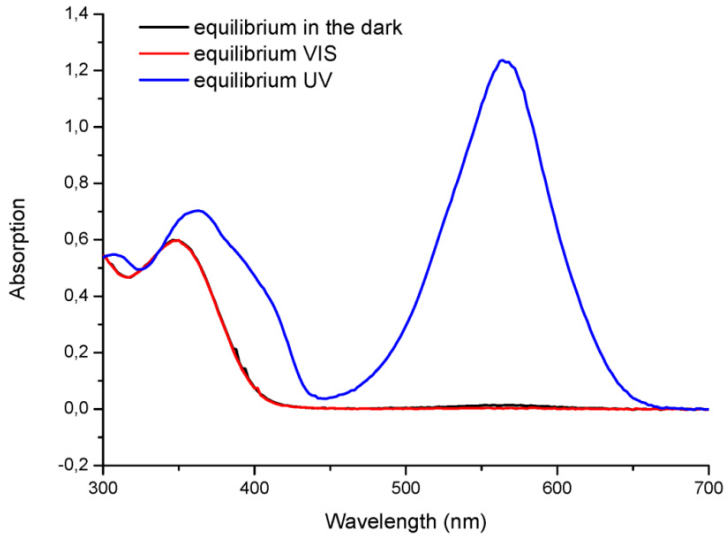

Figure 5.1 UV/Vis spectrum of merocyanine/spiropyran equilibrium in the dark (black), under irradiation with visible light (red, emission wavelengths 400 - 700 nm) and UV light (blue, emission wavelengths 320 - 400 nm).

Because of the much larger half-life of **2** in DMSO, the following NMR measurements were performed in DMSO-d_6, starting with *ex-situ* UV irradiation (outside the NMR spectrometer). To obtain as much signal of **2** as possible, one would want to use a high concentration of **1/2**. The relative fraction of merocyanine **2** that can be reached after 10 min of irradiation (UV lamp) and transferring the sample into the magnet is less for the higher concentrated sample [0.59 wt.% (Figure 5.2)]. While the irradiation of the 0.20 wt.% sample lead to reasonable amounts of **2** the experimental error of the NMR measurements becomes far too large.[2] Thus, we chose 0.30 wt.% (for the *in-situ* measurements, refer to later discussion) as the best compromise between spectrometer sensitivity and optical density.

As can be seen in Figure 5.2 by illuminating the sample outside of the spectrometer, only the thermal relaxation of merocyanine **2** can be monitored. The ring-opening reaction cannot be investigated. Neither the realization of a photo stationary state can be assured nor can the maximum obtainable fraction of merocyanine **2** be safely determined. It is estimated to be

[2] Due to the very low S/N ratio even formal negative values were obtained for the lowest concentration. For details how the error analysis was performed, see supporting information.

around 10% (Figure 5.2). The dead-time between sample illumination and collection of the first proton NMR spectrum makes the situation even worse. This dead-time (approximately 60-90 s) and monitoring problem can be avoided by using devices, which are capable of illuminating the sample inside the NMR spectrometer as described, for example in Kuprov *et al*., Kühn *et al*. and Feldmeier *et al*. [24-26]

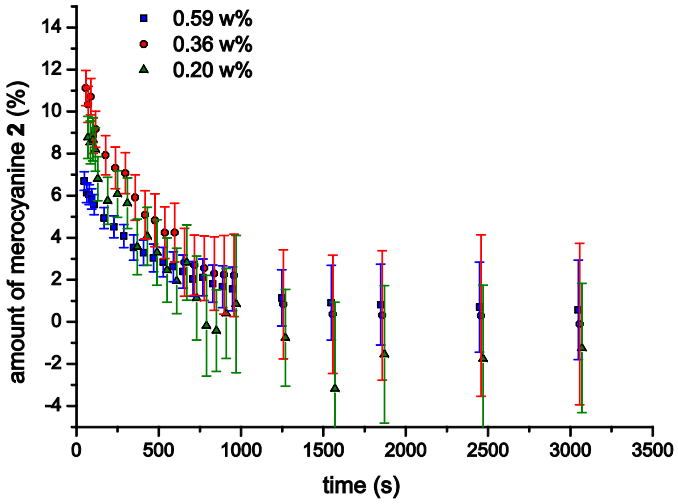

Figure 5.2 Thermal back reaction of the open merocyanine form **2** after irradiation of the sample outside the NMR spectrometer with a UV lamp (emission wave lengths 320-400 nm) for 10 minutes at different sample concentrations (blue squares: 0.59 wt.%, red dots: 0.36 wt.%, and green triangles: 0.20 wt.% in DMSO-d_6 at 300 K). The amount of merocyanine **2** was determined via integration of the methyl groups of spiropyran **1** and merocyanine **2** in single-scan ^{1}H-NMR-spectra. The first data point can be obtained after 60-90 seconds. For a discussion on how experimental errors were obtained see 5.6.4.

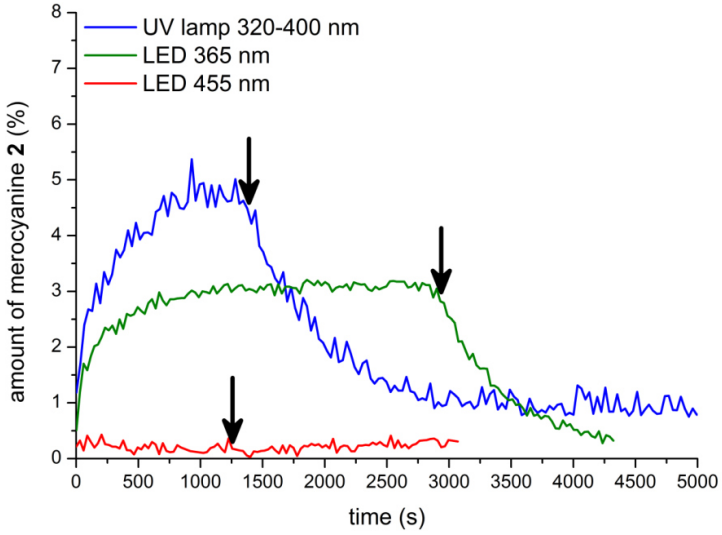

Figure 5.3 Behavior of the merocyanine **2** during and after (arrow) irradiation with different wavelengths (blue: UV lamp 320-400 nm, green: LED λ = 365 nm, and red: LED λ = 455 nm) in DMSO-d_6 at 300 K.

Thus, we changed our setup to the LED device described in Feldmeier *et al*.[26], which enabled us to monitor the ring-opening reaction (Figure 5.3 blue and green; 0 s to arrow) as well as

the back-reaction (Figure 5.3 blue and green; arrow to end) under continuous irradiation. A mono exponential equation was used to fit the decreasing amount of merocyanine **2** and to obtain the apparent rate constants accordingly (refer to 5.6).

With the irradiation device chosen here (Figure 5.3), the light source can be exchanged easily, enabling the irradiation with the same UV lamp as used for the irradiation outside of the spectrometer (Figure 5.3 blue), or enabling the irradiation with a LED most suited for the accumulation of merocyanine **2** (λ = 365 nm, Figure 5.3 green). The maximum amount of merocyanine **2** for the *in-situ* irradiation is lower than for the *ex-situ* irradiation regardless of the light source. We attribute this discrepancy to the applied light fluxes, which originate from different emission intensities of the light source, the high attenuation of light by the silica fiber in the UV spectral range, and the loss of light because of the coupling (refer to previous discussion). As the emission intensity is restricted for the LEDs and for the UV lamp, more powerful UV LEDs have yet to be checked.

Table 5.2 Rate constants in DMSO-d_6 at 300 K obtained via exponential fit of the data from different NMR irradiation procedures and from UV/Vis spectroscopy. Errors shown in this table are errors that are obtained for the fits; the total errors on *k*s are larger because of to the uncertainties that should be assumed for the molar ratios of merocyanine **2** (see 5.6.4).

Entry	Irradiation procedure	Concentration	Light source	10^{-3} k_1/s[a]	$\tau_{½}$ /min	R^2
1	*ex-situ* NMR	0.59 wt.%	UV lamp	2.36±0.14	4.90	0.99
2	*ex-situ* NMR	0.36 wt.%	UV lamp	2.16±0.16	5.35	0.99
3	*ex-situ* NMR	0.20 wt.%	UV lamp	1.91±0.19	6.05	0.97
4	*in-situ* NMR	0.30 wt.%	UV lamp	1.76±0.06	6.56	0.97
5	*in-situ* NMR	0.30 wt.%	LED 365 nm	1.99±0.08	5.81	0.99
6	UV/Vis[15]	0.05 mg/mL	UV lamp	1.7[b]	6.80	0.99

[a] The errors correspond to the standard errors of the mono exponential fit.

[b] UV/Vis data were normalized prior to fitting. Measurement was performed in non-deuterated DMSO at 295.15 K.

Independent of the lower amounts of **2** for the irradiation procedure inside the NMR spectrometer, an irradiation with a wavelength around 365 nm inside or outside the magnet leads to rate constants and half-lives of the same order of magnitude for the thermal back reaction. These two values are independent of the light flux applied before, and thus provide full comparability (Table 5.2). Data obtained by NMR measurements were fitted with a mono exponential function where the parameter A describes the initial concentration of merocyanine **2** and γ0 the thermal equilibrium concentration of **2**. For the *in-situ* measurement A can also be determined from the experiment. The A obtained from the fit is within the error margin obtained from the experiment A. A negative γ0 is obtained for the 0.20 wt.% measurement because of the uncertainty within the molar ratio (refer to previous discussion). Fitting with a fixed A and γ0 does not improve the quality of this fit.

As the LED device is easily compatible with different LEDs, in addition to the LED most suited for the accumulation of merocyanine **2** (λ = 365 nm, Figure 5.3 green) a LED favoring the back reaction was tested (λ = 455 nm, Figure 5.3 red and Figure 5.4) resulting in a decrease of the amount of merocyanine **2**. The decrease of merocyanine **2** concentration under irradiation with a wavelength of 455 nm is so small that it is in the range of the error of the measurement. However, in a detailed view of the methyl signals of merocyanine **2,** the decrease of the signal can be seen (Figure 5.4). To highlight the decrease even more, the spectra are shown in a shifted fashion (left) and on top of each other (right). Additionally to the spectrum without irradiation (dark red), the two spectra under irradiation with 455 nm (navy and green), and the spectrum after irradiation and thermal back reaction (blue), a spectrum while irradiating with 365 nm (purple) is shown to compare the signal heights and effects of irradiation with different wavelengths. Even if the change in signal height is only small, its disappearance can be seen, as well as its reoccurrence after switching-off of the light source and thermal back reaction.

The low amount of merocyanine **2** in general makes the assignment of the proton signals (except the methyl signals shown in Scheme 5.1) difficult. The proposed assignment of merocyanine **2** in DMSO-d_6 is presented in Table 5.3. The two protons (5 and 6) at the bridging part of the molecule cannot or can only be hardly seen in the spectra (Figure 5.9); therefore, a definite determination of the double bond configuration (*cis* or *trans)* cannot be made. Other sources describe the dis-appearance of the double bond protons in the presence of acids[9] as well as the existence of the *trans* merocyanine form as the energetic more favorable form for a similar system.[21] Considering these sources, we suggest that the most stable form of the merocyanine **2** is the *trans* form shown in all figures in this article. More indications are given in the supporting information in section 5.6.

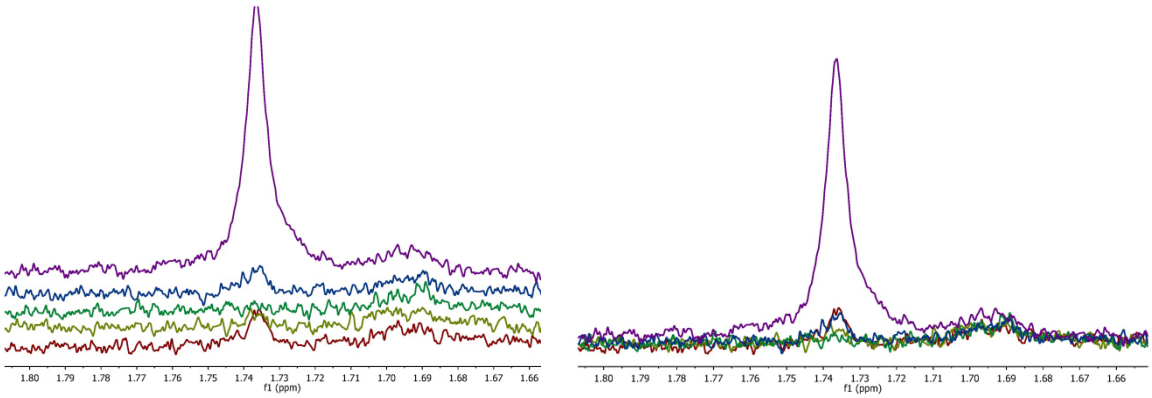

Figure 5.4 Detailed views of proton spectra of the methyl signals of merocyanine **2** under irradiation with different wavelength. Left: All spectra are shifted in the y-dimension. Right: All spectra lie on top of each other. The spectrum in equilibrium without irradiation is marked in dark red; the two spectra with irradiation with 455 nm are navy and green. Blue marks the spectra after irradiation with 455 nm and a certain time to ensure the thermal back-reaction. As a comparison of the aforementioned spectra to the irradiation with UV light, the purple spectrum shows the methyl signal of merocyanine **2** after irradiation with 365 nm.

By using the illumination device inside the magnet the half-life issue is nullified as continuous irradiation procedures are now feasible and photo stationary states with a constant molar ratio of **1** and **2** are accessible. We combined this advantage with a solvent change (to DMF-d_7), and a temperature decrease, which we believe to lead to a stabilization of **2**. This way,

we hoped to increase the amount of merocyanine **2**, which in turn should enable at least a partial chemical shift assignment. As envisioned the amount of merocyanine **2** was at least enhanced up to 20% by these procedure, even allowing the acquisition of 2D spectra (hsqc, hmbc and noesy also refer to 5.6.3). Although the assignment of the configuration at the double bond could not be made, these measurements gave access to carbon chemical shifts of the metastable form **2** which have not been reported until now (Figure 5.5, Table 5.3 and section 5.6). The addition of water (DMF/D_2O 4:1) did not further increase the amount of merocyanine **2** (only up to 5% of merocyanine **2** at 260 K after around 2.5 h of illumination) but allowed for the detection of the protons 5 and 6 of the double bond as well as for the detection of NOE cross peaks corroborating the chemical shift assignment (Figure 5.11). These new spectroscopic data were not accessible via irradiation outside of the NMR spectrometer as thermal relaxation is too fast as compared with the measurement time that is necessary for typical multidimensional NMR experiments.

To compare the aforementioned results with the data obtained via UV/Vis measurements, the extinction coefficient ε (not known at the beginning of this project) had to be calculated by using equilibrium compositions from NMR data and extinction values from UV/Vis measurements at different concentrations (a detailed calculation is shown in the 5.6.4).[15,21] Using the extinction coefficient calculated, the extinction behavior obtained by UV/Vis after irradiation with UV light can be transferred into fractions of merocyanine **2**. The maximum amount of merocyanine **2** for the UV/Vis measurements after irradiation can be determined to be around 40%.[15] The significant difference between this value and the percentage obtained with NMR measurements after irradiation outside of the spectrometer (around 10%, Figure 5.2 red) originates most probably from the concentration disparity (UV/Vis 0.05 mg/mL, NMR 0.36 wt.% ≙ 4.0 mg/mL). We reckon that the optical density of the two orders of magnitude more concentrated NMR sample results in stronger quenching of the UV light and in a decreased percentage of merocyanine **2** in comparison to the UV/Vis sample. Because of the low sensitivity of NMR spectrometers, a reduction of the sample concentration to 0.05 mg/mL is not feasible. Likewise, the UV measurement of more concentrated samples is not feasible, because of saturation effects. Nevertheless, the same reaction steps can be monitored with UV/Vis and NMR using different irradiation methods. Rate constants are obtained from exponential fits for the back-reaction of merocyanine **2** and are comparable (Table 5.2).

Table 5.3 Assignment of the proton chemical shifts in DMSO-d_6 (300 K), DMF-d_7 (248 K), and DMF-d_7/D_2O-d_2 of merocyanine **2**.[a]

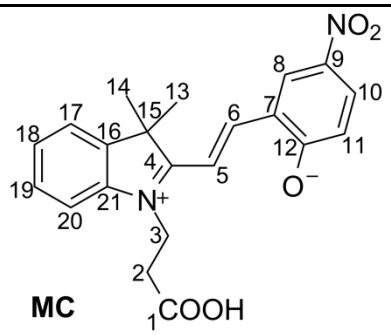

^{1}H chemical shift (ppm)			Multiplicity	Assignment	^{13}C chemical shift (ppm)	
DMSO-d_6	DMF-d_7	DMF-d_7/D_2O-d_2			DMF-d_7	DMF-d_7/D_2O-d_2
8.68	8.83	8.79	s (br)	8	118.4	-
8.41	8.67-8.60	8.39/8.63	m (br)	5/6?	-	-
7.73	7.93	7.86	d (br)	20	113.6	113.8
7.81	7.91	7.95	d (br)	10	128.1	128.7
7.73	7.86	7.81	d	17	123.1	122.5
7.51	7.59	7.62	pt	19	127.3	128.7
7.44	7.51	7.55	pt	18	128.9	127.7
6.26	6.35	6.54	d (br)	11	125.1	123.9
4.55	4.70	4.78	s (br)	3	41.8	-
2.87	3.06	2.95	t (br)	2	31.4	-
1.75	1.86	1.83	s	13/14	26.4	26.2
-	-	-	-	1	171.7	-
-	-	-	-	4	182.1	181.9
-	-	-	-	15	51.0	51.2
-	-	-	-	16	143.1	142.8
-	-	-	-	21	141.6	140.6

[a] The multiplicity is indicated by s (singlet), d (doublet), t (triplet), m (multiplet), and pt (pseudo triplet). Broad signals are marked with br. The carbon chemical shifts in DMF-d_7 (248 K) are extracted from the respective hsqc and hmbc spectra at 255 K, the carbon chemical shifts in DMF-d_7/D_2O-d_2 4:1 from hsqc and hmbc spectra at 260 K.

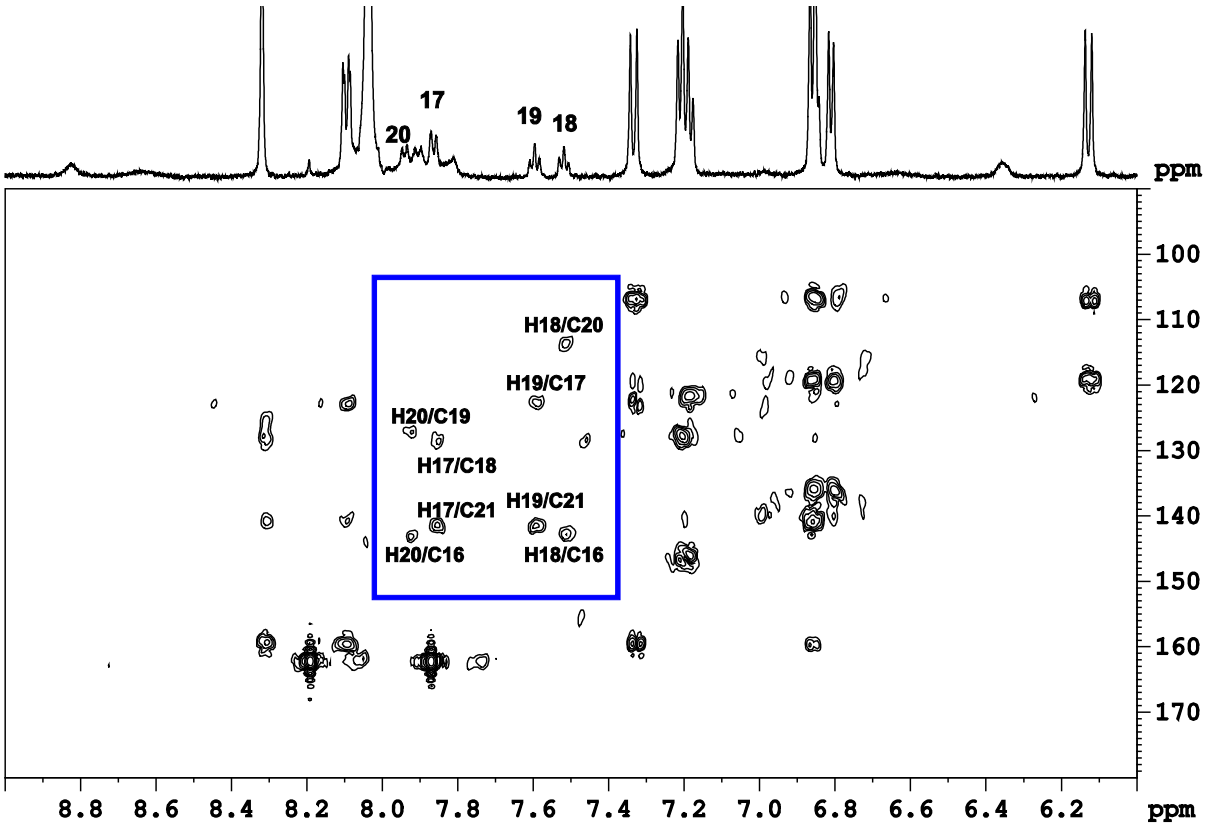

Figure 5.5 Expansion of a hmbc-NMR spectrum of spiropyran **1** (larger signals) and merocyanine **2** (smaller signals and highlighted signals in the box) in DMF-d_7 at 255 K under continuous irradiation (LED λ = 365 nm).

For future measurements of the spiropyran-containing copolymer concentration, the molar content of the light-responsive moiety within the copolymer - again - seems to be the strongest limitation. The light-switchable copolymer typically contains only a certain fraction of spiropyran/merocyanine units (between 2 and 5 mol-%[15]). As a result a decreased relative signal intensity of the desired NMR signals compared with the model system is expected. Although the use of the *in situ* illumination device in the NMR spectrometer gives a reduced light flux and thereby smaller absolute signal intensities, it seems to be most promising for the measurements of the copolymer, because even small changes of the spectra can be monitored during continuous illumination, the photo stationary state can be detected and no data loss arises through the absence of the dead-time.

5.5 Conclusions

Photochromic compounds are widely used for the synthesis of *stimuli responsive* materials. Therefore structures of the metastable compound and characteristic properties of the photo reaction like half-lives, thermal relaxation rates, and maximum fractions are subject to recent research. In this investigation, we compared *ex-situ* and *in-situ* illumination approaches for NMR studies of a spiropyran **1**/merocyanine **2** system. It revealed that *in-situ* illumination offers several advantages.

Firstly, excitation and relaxation of the photochromic system can be monitored *in-situ*. In contrast, *ex-situ* illumination approaches are restricted to the observation of relaxation

reactions. *Ex-situ* illumination, furthermore, is restricted to systems with thermal relaxation rates exceeding the dead-time necessary to transfer the sample into the spectrometer. In this context, thermal relaxation rates and half-lives of spiropyran **1**/merocyanine **2** were obtained from *ex-situ* and *in-situ* illumination NMR, and UV/Vis and compared for different sample concentrations, light sources, and temperatures. It was observed that the maximum fraction of merocyanine **2** in DMSO at room temperature was between 3 and 10% for NMR measurements, respectively, depending on the irradiation procedure as compared with 40% for UV/Vis. The variations in the values emanate from the different sample concentrations and light fluxes.

Secondly, *in-situ* illumination offers the possibility to observe saturation and stationary states of photochromic systems. In NMR spectroscopy, such stationary states are favorable as experiments with long acquisition times become accessible. As a result, more complex structural information like hetero nuclear correlations can be obtained. In this work, the *in-situ* illumination approach provided access to two dimensional spectra (hsqc and hmbc) as well as to carbon chemical shifts of the metastable merocyanine **2**, which were not accessible before. Furthermore, a continuous illumination offers the possibility to observe photo decomposition reactions and might provide insights into photo bleaching processes.

A disadvantage of *in-situ* illumination arises from the experimental setup. The light flux is damped by the wave guide materials in the UV leading to smaller illumination intensities compared with direct irradiation of the sample in *ex-situ* experiments, and thereby lower concentrations of photo intermediates are obtained. In our opinion, the mentioned advantages outbalance this drawback.

Taking together, the previously described NMR investigation provided access to a variety of composition data for the precursor model system, which will be very useful for the investigation of the spiropyran/merocyanine containing copolymer. The most favorable setup for NMR measurements of the copolymer seems to be the LED device equipped with more powerful UV LEDs under adjusted solvent/temperature conditions.

5.6 Supporting Information

5.6.1 Assignment of spiropyran 1

The assignment of spiropyran **1** in DMSO-d_6 at 300 K is shown in Figure 5.6.

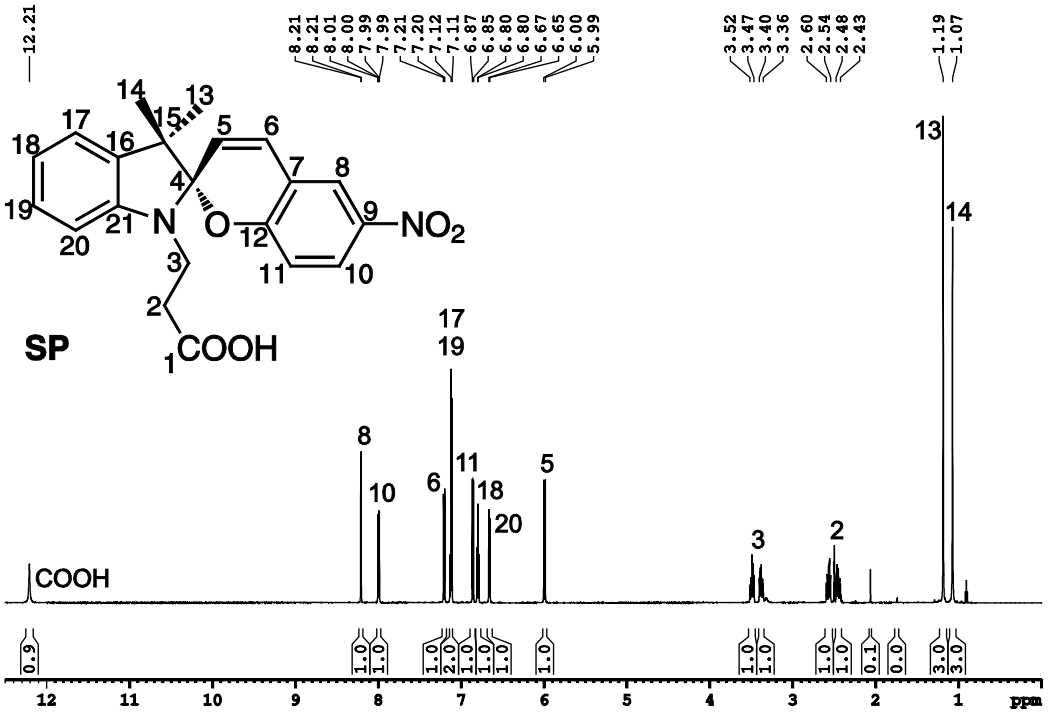

Figure 5.6 The signals and the corresponding assignment of spiropyran **1** in DMSO-d_6 (2.4 w% at 300 K and 600 MHz).

5.6.2 Assignment and discussion of merocyanine 2

As shortly discussed in the main text the assignment of merocyanine **2** is more difficult than the assignment of spiropyran **1**. Merocyanines can exist in a set of stereoisomers *cis* and *trans* and are described by various mesomeric formulas (zwitter ionic vs uncharged).[22,29]

A definite determination of the configuration of the double bond and the assignment of the proton chemical shifts cannot be made for the present system, because the signals for the protons 5 and 6 in DMSO are very broad and/or missing. Raymo et al. and others - who investigated very similar systems - proposed the *trans* form to be the most stable form of the merocyanine.[21,22] Other authors describe the broadening of the vinyl protons as well as the complete disappearance of these proton signals in the presence of acids.[9] Raymos as well as Hobleys assignments and chemical shift observations for the double bond protons are similar to ours (above 8 ppm), emphasizing the correctness of our assignment.

The prediction of proton spectra for the *cis* and *trans* merocyanine via ACD Labs (Figure 5.7, Figure 5.8) forecasts the signals of the protons 5 and 6 to have a chemical shift of 7.51 ppm and 7.79 ppm for the *cis* form as well as 7.65 ppm and 8.18 ppm for *trans*. In our proton spectra we find a broad signal at 8.4 ppm in DMSO (Figure 5.9) suggesting that the most stable isomer is the *trans* form shown in this article.

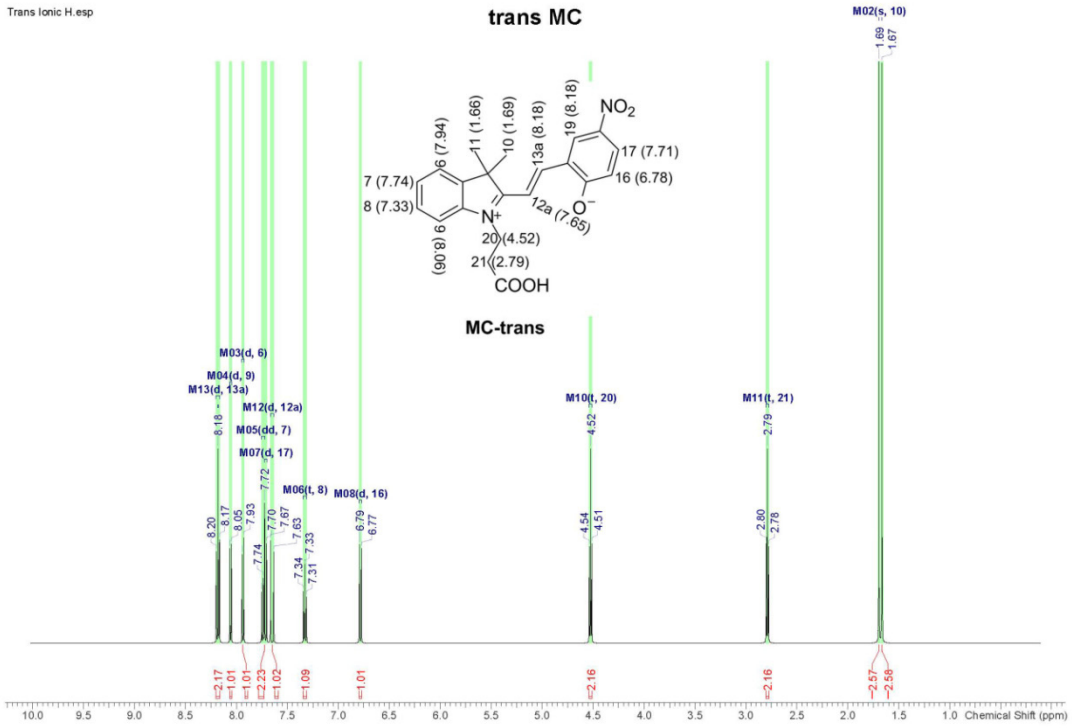

Figure 5.7 Calculated proton spectrum of the *trans* form of merocyanine **2**. The numeration in this figure corresponds to the automatic numeration of ACD Labs.

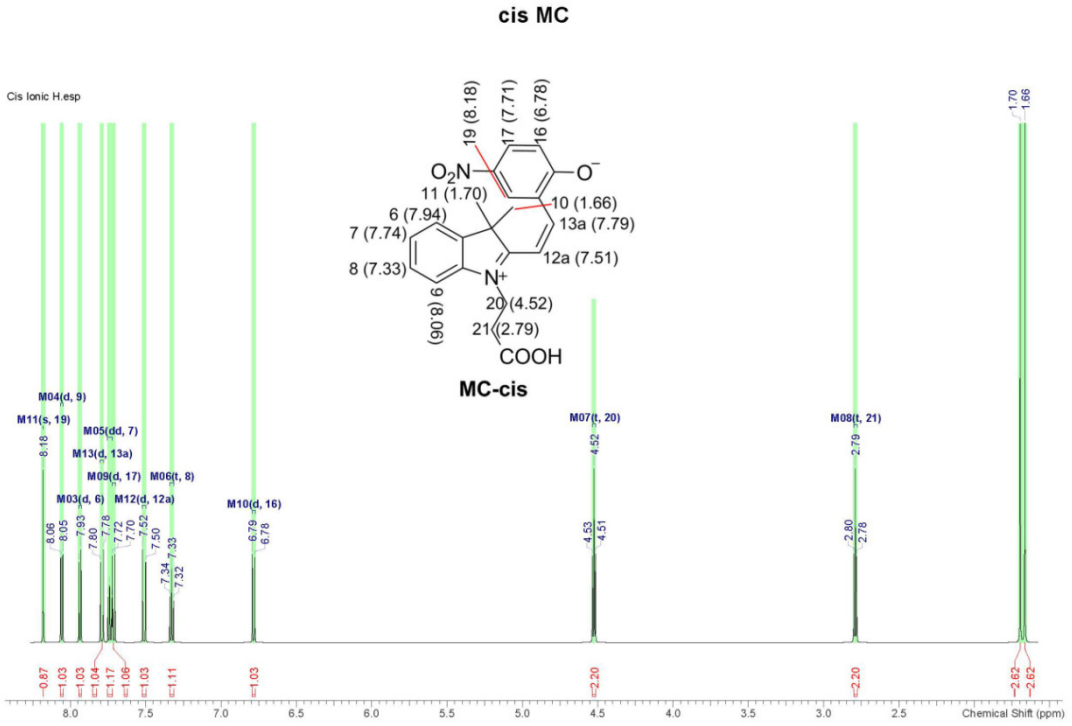

Figure 5.8 Calculated proton spectrum of the *cis* form of merocyanine **2**. The numeration in this figure corresponds to the automatic numeration of ACD Labs.

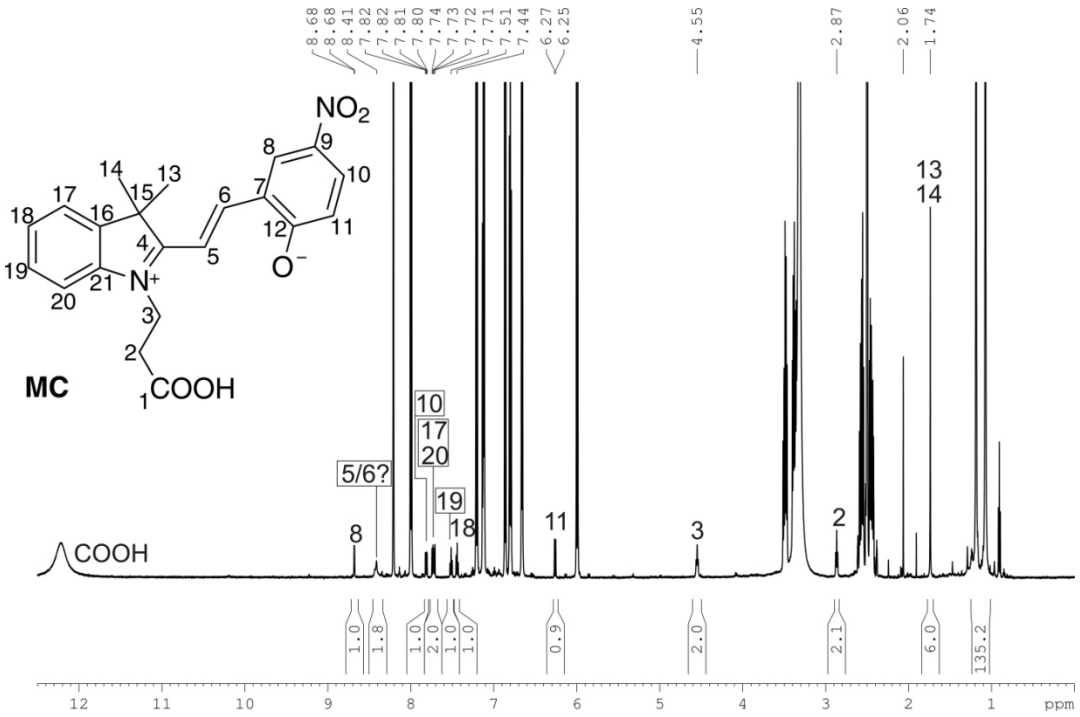

Figure 5.9 Proton spectrum of a mixture of merocyanine **2** and spiropyran **1** in DMSO-d_6 and the corresponding assignment of merocyanine **2** (2.4 w% at 300 K and 600 MHz).

5.6.3 NMR measurements in DMF-d_7

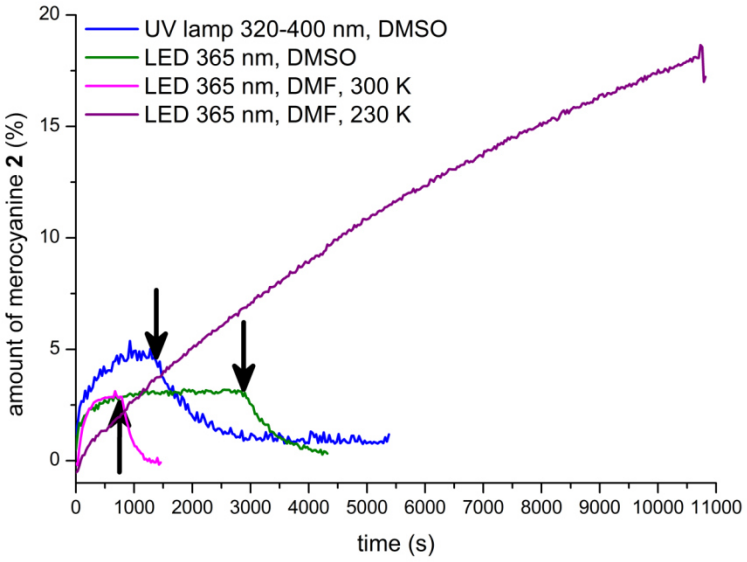

Figure 5.10 Amount of merocyanine **2** in DMSO-d_6 and irradiation with different wavelengths (blue: UV lamp, green: LED λ = 365 nm) as well as samples in DMF-d_7 at 300 K (pink) and 230 K (purple). The arrows mark the switching-off of the illumination device. The measurement in DMF-d_7 at 230 K was stopped after 2.9 h of illumination, without recording the back reaction.

One mayor benefit of the irradiation inside the magnet is the absence of dead-time and the opportunity to monitor the ring-opening reaction in addition to the thermal back-reaction. This enables us to monitor the amount of merocyanine **2** online. After a solvent change to

DMF-d_7 (Figure 5.10, pink) and after additional temperature decrease (Figure 5.10, purple) the amount of merocyanine **2** is enhanced at least up to 20% enabling 2D NMR measurements (refer to Figure 5.5 in the main text).

Trying to enable the assignment of merocyanine **2,** we additionally measured a sample in deuterated DMF/D_2O 4:1 at 260 K. The proton chemical shift pattern is comparable to that in pure deuterated DMF; the amount of **2** formed, however, is only approximately 5%. Nevertheless, a new proton signal at 8.39 ppm can be detected and several noesy cross peaks corroborate the assignment of the protons 5-11 (see Figure 5.11).

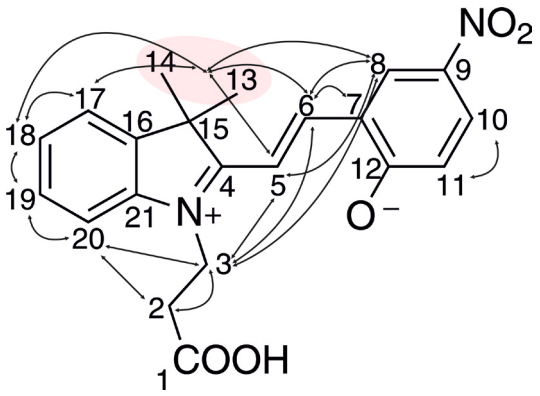

Figure 5.11 Illustration of the noesy cross peaks (depicted by arrows) of merocyanine **2** in DMF-d_7/D_2O-d_2 4:1 at 260 K measured at 600 MHz.

5.6.4 Calculation of the extinction coefficient

For low concentrations the Lambert-Beer law describes the correlation between the extinction E_λ and the concentration of the sample c at a specific wavelength λ.

$$E_\lambda = -lg\frac{I}{I_0} = \varepsilon_\lambda \cdot c \cdot d$$

I is the light intensity after passing through the sample and I_0 the light intensity before the sample. d is the sample length and ε_λ the extinction coefficient at the specific wavelength λ. Initially the concentration of merocyanine **2** and the extinction coefficient at the maximum wavelength of this form ε_{565nm} are not known (λ_{max} = 565 nm for merocyanine **2** in DMSO).[15] Therefore a translation of the extinction values into sample compositions is not possible.

To overcome this problem a method combining NMR and UV/Vis data is used.[21] The equilibrium composition of the photochromic compound in darkness consists of spiropyran **1** and a very low amount of merocyanine **2**. This composition results in a coloring of the sample solution even without UV irradiation and a corresponding UV/Vis spectrum. The merocyanine **2** fraction in equilibrium (0.62 ± 0.1 %) was determined to be constant over a concentration range (2 to 36 mg/mL) via ^{1}H-NMR spectroscopy (index MC stands for merocyanine **2**).[15] Sample concentration c_{all} (sum of c_{SP} and c_{MC}) was varied and extinctions were measured via UV/Vis spectroscopy and fitted using a linear regression (Figure 5.12).

$$E_{565\mathrm{nm}} = \varepsilon_{565\mathrm{nm}} \cdot c_{\mathrm{MC}} \cdot d = \varepsilon_{565\mathrm{nm}} \cdot c_{\mathrm{all}} \cdot 0.0062 \cdot d$$

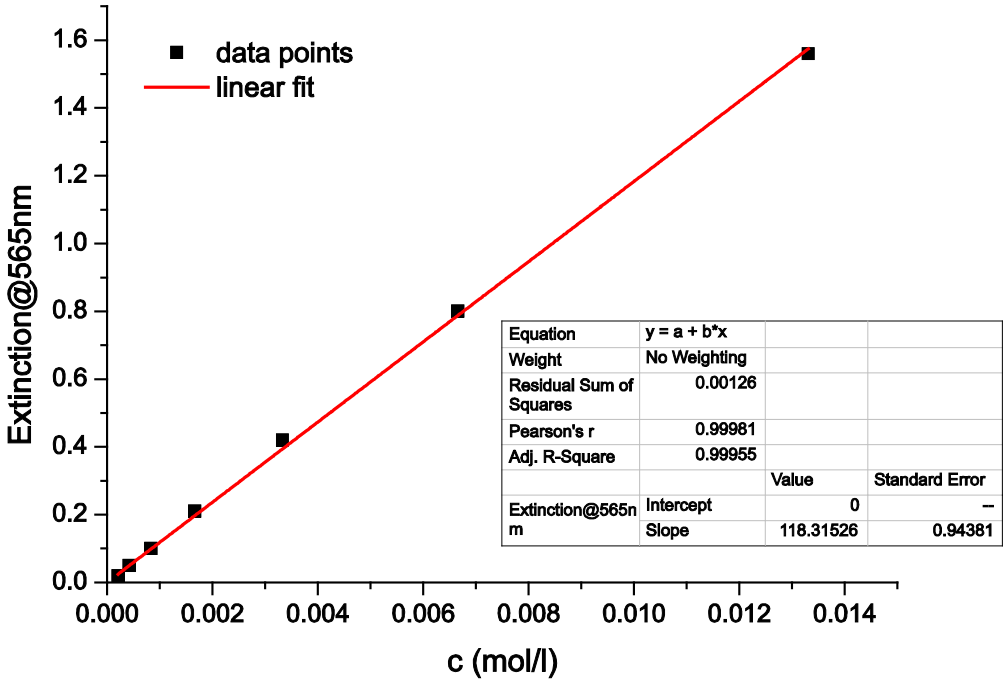

Figure 5.12 Linear regression of the extinction values at 565 nm depending on the concentration of the sample.[15]

Finally the extinction coefficient can be calculated by using the slope S of the linear regression and the merocyanine **2** fraction from the NMR data:

$$\varepsilon_{565\mathrm{nm}} = \frac{S}{0.0062 \cdot d} = \frac{118.32\ {}^{\mathrm{l}}/_{\mathrm{mol}}}{0.0062 \cdot 0.5\ \mathrm{cm}} \approx 3.8 \cdot 10^{4}\ {}^{\mathrm{l}}/_{\mathrm{mol \cdot cm}}$$

This value can be used to convert the extinction values E_{565nm} into an amount of merocyanine **2**.

Kinetic model, exponential fit and rate constants

Assuming that the thermal back reaction follows a first order rate law,[8,14] the reaction rate for the decrease of merocyanine **2** is given by:

$$v = -\frac{\mathrm{d}c_{\mathrm{MC}}}{\mathrm{d}t} = k_1 \cdot c_{\mathrm{MC}}$$

After the replacement of $c_{\mathrm{MC}} = \chi_{\mathrm{MC}} \cdot c_{\mathrm{all}}$, integration and transformation, the usual mono exponential behavior is received (c_{all} is constant and can be reduced).

$$\chi_{\mathrm{MC},t} = \chi_{\mathrm{MC},0} \cdot \exp(-k_1 \cdot t) + \chi_{\mathrm{MC,t}\to\infty}$$

The parameter $\chi_{\mathrm{MC,t}\to\infty}$ corresponds to the amount of merocyanine in equilibrium (which is not zero, see section above). Using an exponential fit ($y = y_0 + \mathrm{A} \cdot \exp(\mathrm{R}^0 \cdot \mathrm{x})$) the rate constant can be obtained by $\mathrm{R}^0 = -k_1$ (See example fit in Figure 5.12).

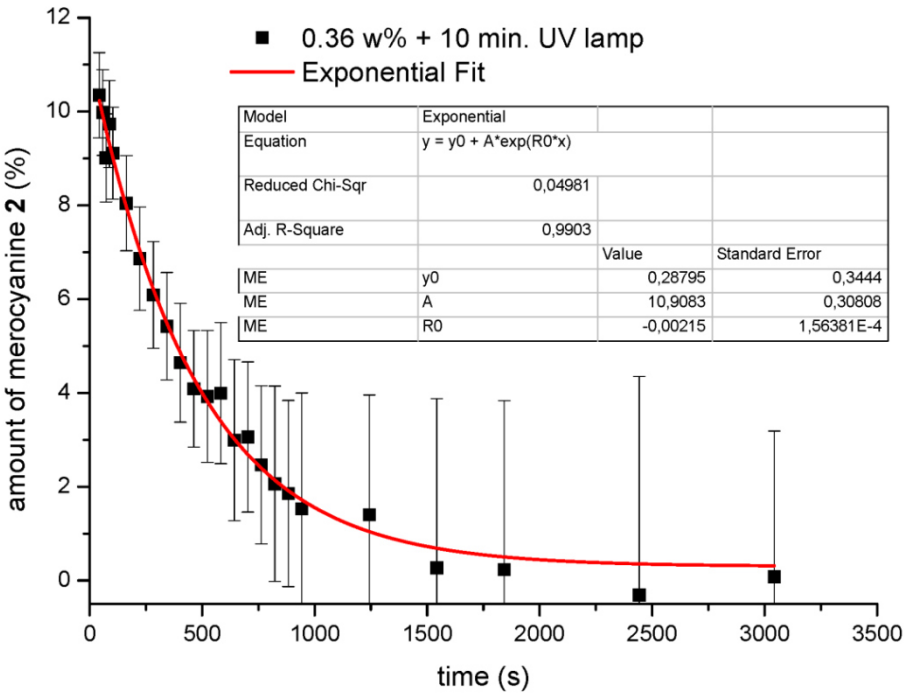

Figure 5.13 Example of an exponential fit (red) of the experimentally obtained merocyanine amount (black cubes, *ex-situ* irradiation, 0.36 w%, 10 min. UV lamp, see Figure 5.2 (red dots) in the main apart). The error bars originate from Gaussian error propagation (see below).

The rate constants (and half-lives $\tau_{½} = \frac{\ln 2}{k_1}$) obtained by this method for the different NMR illumination procedures and for the UV/Vis spectroscopy are all in the same value range.

Error analysis

The error bars shown in Figure 5.13 were estimated by Gaussian error propagation. Starting from a formula expressing the amount of merocyanine **2** through the integrals of merocyanine *I*(MC) and spiropyran *I*(SP)

$$G = \frac{I(\mathrm{MC})}{I(\mathrm{MC}) + I(\mathrm{SP})} = \frac{x}{x + y}$$

and the general equation for the Gaussian error propagation

$$\Delta G = \sqrt{\left(\frac{\delta G}{\delta x}\Delta x\right)^2 + \left(\frac{\delta G}{\delta x}\Delta y\right)^2}$$

a new formula representing the error on the amount of merocyanine **2** can be obtained

$$\Delta G = \sqrt{\left(\frac{y\Delta x}{(x+y)^2}\right)^2 + \left(-\frac{x\Delta y}{(x+y)^2}\right)^2}$$

Assuming that the error of the integral is depending mainly on the low S/N ratio (SN), the errors can be described as

$$\Delta I(\mathrm{MC})_i = \frac{1 + \frac{SN_{\mathrm{max,\,MC}}}{SN_{\mathrm{i,\,MC}}}}{2}$$

$$\Delta I(\mathrm{SP})_i = \frac{1 + \frac{SN_{\mathrm{max,\,SP}}}{SN_{\mathrm{i,\,SP}}}}{2}$$

The indices stand for the S/N ratio at a specific data point i, the maximal S/N ratio (for all data points) and the compounds merocyanine MC **2** and spiropyran SP **1,** respectively.

In the end the following expression can be obtained for the uncertainty of the merocyanine **2** amount:

$$\Delta G_i = \frac{\sqrt{(I(\mathrm{SP})_i \Delta I(\mathrm{MC})_i)^2 + (-I(\mathrm{MC})_i \Delta I(\mathrm{SP})_i)^2}}{(I(\mathrm{MC})_i + I(\mathrm{SP})_i)^2}$$

The error bars are thought to describe the uncertainty of the merocyanine **2** amount very well as the error is larger for smaller amounts of merocyanine **2** as the S/N ratio gets worse.

5.7 Additional Information

5.7.1 SP/MC Assignment in DMF-d_7

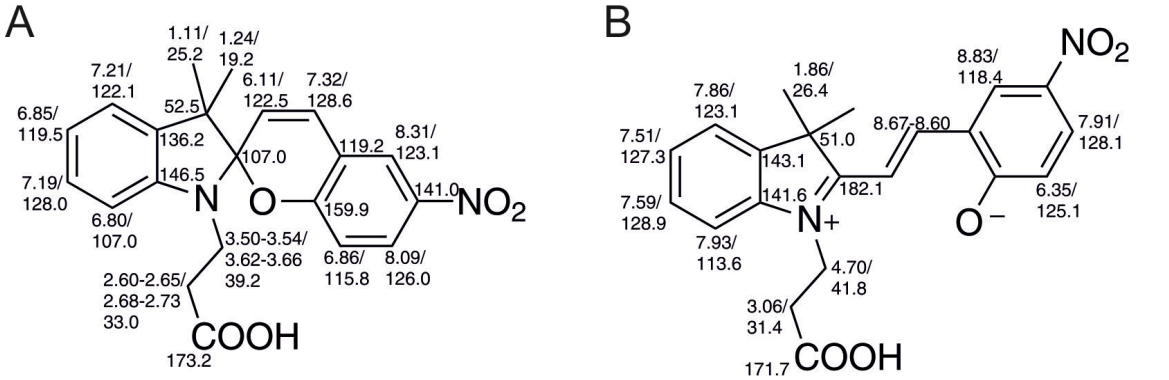

Figure 5.14 Proton and carbon chemical shift assignment of (a) spiropyrane **1** and (b) merocyanine **2** in DMF-d_7 at 248-255 K at 600 MHz. The sample was illuminated for 1 h with 365 nm, than the 2D spectra for the MC **2** assignment were recorded in the dark.

spiropyran **1**:

^{1}H NMR (600 MHz, DMF): δ [ppm] = 8.31 (d, *J* = 2.6 Hz, 1H), 8.09 (dd, *J* = 8.9 Hz and 2.6 Hz, 1H), 7.32 (d, *J* = 10.4 Hz, 1H), 7.21 (m, 1H), 7.19 (m, 1H), 6.86 (m, 1H), 6.85 (m, 1H), 6.80 (d, *J* = 7.8 Hz, 1H), 6.11 (d, *J* = 10.4 Hz, 1H), 3.66-3.62 (m, 1H), 3.54-3.50 (m, 1H), 2.73-2.68 (m, 1H), 2.65-2.60 (m, 1H), 1.24 (s, 3H), 1.11 (s, 3H).

^{13}C NMR (150 MHz, DMF): δ [ppm] = 173.2, 159.9, 146.5, 141.0, 136.2, 128.6, 128.0, 126.0, 123.1, 122.5, 122.1, 119.5, 119.2, 115.8, 107.0, 107.0, 52.5, 39.2, 33.0, 25.2, 19.2.

merocyanine **2**:

^{1}H NMR (600 MHz, DMF): δ [ppm] = 8.83 (br s), 8.67-8.60 (br m), 7.93 (br d, *J* = 8.3 Hz, 1H), 7.91 (br d, *J* = 9.5 Hz, 1H), 7.86 (d, *J* = 7.6 Hz, 1H), 7.59 (pt, *J* = 7.6 Hz 1H), 7.51 (pt, *J* = 7.6 Hz 1H), 6.35 (br d, *J* = 9.5 Hz 1H), 4.70 (br s, 2H), 3.06 (br t, *J* = 7.5 Hz, 2H), 1.86 (s, 6H).

^{13}C NMR (150 MHz, DMF): δ [ppm] = 182.1, 171.7, 143.1, 141.6, 128.9, 128.1, 127.3, 125.1, 123.1, 118.4, 113.6, 51.0, 41.8, 31.4, 26.4.

5.7.2 SP/MC Assignment in DMF-d_7/D_2O

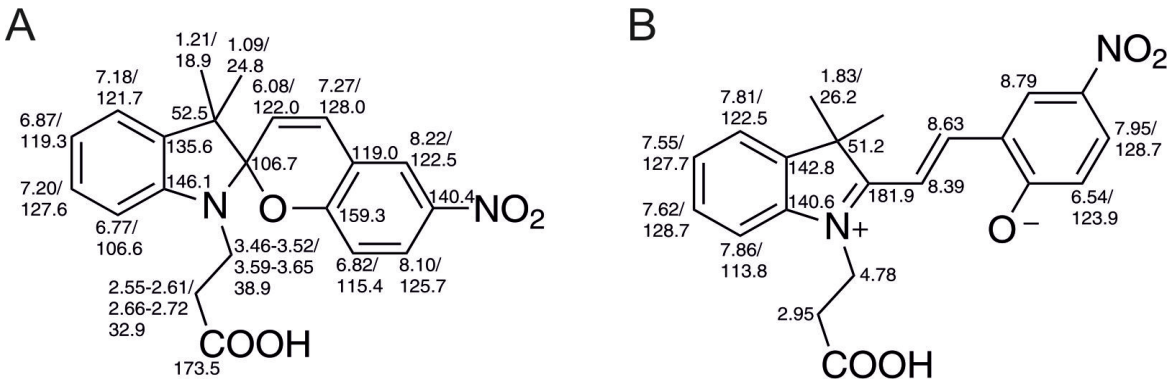

Figure 5.15 Proton and carbon chemical shift assignment of (a) spiropyrane **1** and (b) merocyanine **2** in DMF/D_2O 4:1 at 260 K at 600 MHz. The sample was illuminated for 1 h with 365 nm, than the 2D spectra for the MC **2** assignment were recorded in the dark.

spiropyrane **1**:
^{1}H NMR (600 MHz, DMF/D_2O): δ [ppm] = 8.22 (s, 1H), 8.10 (d, *J* = 8.9 Hz, 1H), 7.27 (d, *J* = 10.3 Hz, 1H), 7.20 (m, 1H), 7.18 (m, 1H), 6.87 (t, *J* = 7.2 Hz, 1H), 6.82 (d, *J* = 8.9 Hz, 1H), 6.77 (d, *J* = 7.6 Hz, 1H), 6.08 (d, *J* = 10.3 Hz, 1H), 3.65-3.46 (m, 2H), 2.72-2.55 (m, 2H), 1.21 (s, 3H), 1.09 (s, 3H).

^{13}C NMR (150 MHz, DMF): δ [ppm] = 173.5, 159.3, 146.1, 140.4, 135.6, 128.0, 127.6, 125.7, 122.5, 122.0, 121.7, 119.3, 119.0, 115.4, 106.7, 106.6, 52.5, 38.9, 32.9, 24.8, 18.9.

merocyanine **2**:
^{1}H NMR (600 MHz, DMF/D_2O): δ [ppm] =8.79 (br s, 1H), 8.63 (br d, 1H), 8.39, 7.95, 7.86 (d, *J* = 8.2 Hz, 1H), 7.81 (m, 1H), 7.62 (t, *J* = 7.5 Hz, 1H), 7.55 (t, *J* = 7.5 Hz, 1H), 6.54 (d, *J* = 9.7 Hz, 1H), 4.78, 2.95, 1.83 (s, 6H).

^{13}C NMR (150 MHz, DMF): δ [ppm] = 181.9, 142.8, 140.6, 128.7, 128.7, 127.7, 123.9, 122.5, 113.8, 51.2, 26.2.

The full assignment of merocyanine **2**, and thus the distinction between the different MC species was not possible by NMR spectroscopic data. The ^{1}H,^{1}H-cosy in DMF/D_2O 4:1 at 260 K shows only few cross peaks (see Figure 5.16, cross peaks depicted by arrows). In the ^{1}H,^{13}C-hmbc or ^{1}H,^{13}C-hsqc spectra no cross peaks of the double bond, the alkyl and parts of the benzyl moiety were found. At least the ^{1}H,^{1}H-noesy spectrum enabled the detection of a cross peak network, connecting the protons 13/14 and 3 with the protons of the double bond (5 and 6) as well as proton 8 (see Figure 5.11).

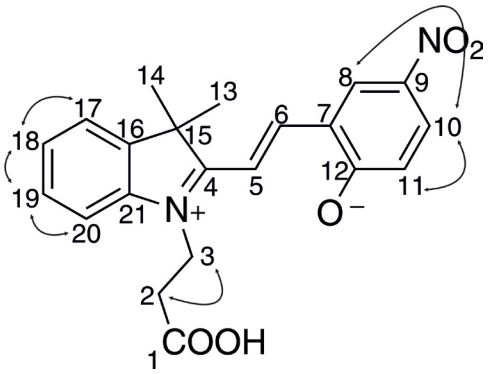

Figure 5.16 ^{1}H,^{1}H-cosy cross peaks of merocyanine 2 in DMF/D_2O 4:1 at 260 K. The cross peaks found between two protons are highlighted by arrows.

5.8 References

[1] A. D. Mcnaught, A. Wilkinson. *Compendium of Chemical Terminology*. Blackwell Scientific Publications, (XML online corrected version: http://goldbook.iupac.org (2006-) created by M. Nic, J. Jirat, B. Kosata; updates compiled by A. Jenkins): **1997**.

[2] G. Bifulco, P. Dambruoso, L. Gomez-Paloma, R. Riccio; *Chem. Rev.* **2007,** *107* (9), 3744-3779.

[3] H. Bouas-Laurent, H. Dürr; *Pure Appl. Chem.* **2001,** *73* (4), 639-665.

[4] B. Champagne, A. Plaquet, J. L. Pozzo, V. Rodriguez, F. Castet; *J. Am. Chem. Soc.* **2012,** *134* (19), 8101-8103.

[5] R. Klajn; *Chem. Soc. Rev.* **2014,** *43* (1), 148-184.

[6] B. Horstmann, M. Korbus, T. Friedmann, C. Wolff, C. M. Thiele, F. J. Meyer-Almes; *Bioorg. Chem.* **2014,** *57*, 155-161.

[7] A. A. Beharry, G. A. Woolley; *Chem. Soc. Rev.* **2011,** *40*, 4422-4437.

[8] E. Fischer,Y. Hirshberg; *J. Chem. Soc.* **1952**, 4522-4524.

[9] J. Hobley, V. Malatesta, R. Millini, L. Montanari, W. O Neil Parker, Jr.; *Phys. Chem. Chem. Phys.* **1999,** *1*, 3259-3267.

[10] G. Balasubramanian, J. Schulte, F. Müller-Plathe, M. C. Böhm; *Chem. Phys. Lett*. **2012**, *554*, 60-66.

[11] S. Delbaere, C. Bochu, N. Azaroual, G. Buntinx, G. Vermeersch; *J. Chem. Soc., Perkin Trans.* **1997**, 2 (8), 1499-1502.

[12] S. Delbaere, B. Luccioni-Houze, C. Bochu, Y. Teral, M. Campredon, G. Vermeersch; *J. Chem. Soc., Perkin Trans.* **1998**, 2 (5), 1153-1158.

[13] Y. Hirshberg; *J. Am. Chem. Soc.* **1956**, *78*, 2304-2312.

[14] G. Berkovic, V. Krongauz, V. Weiss; *Chem. Rev*. **2000**, *100* (5), 1741-1754.

[15] H. Schenderlein, A. Voss, R. W. Stark, M. Biesalski; *Langmuir* **2013,** *29* (14), 4525-34.

[16] J.-I. Edahiro, K. Sumaru, Y. Tada, K. Ohi, T. Takagi, M. Kameda, T. Shinbo, T. Kanamori,Y. Yoshimi; *Biomacromolecules* **2005,** *6* (2), 970-974.

[17] K. Kikuchi, K. Sumaru, J.-I. Edahiro, Y. Ooshima, S. Sugiura, T. Takagi,T. Kanamori; *Biotechnol. Bioeng.* **2009**, *103* (3), 552-561.

[18] K. H. Fries, S. Samanta, S. Orski, J. Locklin; *Chem. Commun.* **2008,** (47), 6288-6290.

[19] K. H. Fries, J. D. Driskell, S. Samanta, J. Locklin; *Anal. Chem.* **2010,** *82* (8), 3306-3314.

[20] H. Schenderlein; *Herstellung und Charakterisierung oberflächengebundener, lichtschaltbarer Polymernetzwerke*. Ph.D. thesis, Technische Universität Darmstadt, Darmstadt, **2013**.

[21] F. M. Raymo, S. Giordani; *J. Org. Chem.* **2003,** *68*, 4158-4169.

[22] J. T. C. Wojtyk, A. Wasey, P. M. Kazmaier, S. Hoz, E. Buncel; *J. Phys. Chem. A* **2000,** *104* (39), 9046-9055.

[23] E. Fischer; *J. Phys. Chem.* **1967,** *71* (11), 3704-3706.

[24] I. Kuprov, P. J. Hore; *J. Magn. Reson.* **2004,** *171* (1), 171-5.

[25] T. Kühn, H. Schwalbe; *J. Am. Chem. Soc.* **2000,** *122*, 6169-6174.

[26] C. Feldmeier, H. Bartling, E. Riedle, R. M. Gschwind; *J. Magn. Reson.* **2013,** *232*, 39-44.

[27] A. Fissi, O. Pieroni, G. Ruggeri, F. Ciardelli; *Macromolecules* **1995,** *28* (1), 302.309-302.309.

[28] J. S. Frey; *Concepts Magn Res*. **1989**, *1* (1), 27-33.

[29] N. A. Murugan, S. Chakrabarti, H. Agren; *J Phys Chem B* **2011,** *115* (14), 4025-4032.

[30] D. G. Patel, M. M. Paquette, R. A. Kopelman, W. Kaminsky, M. J. Ferguson, N. L. Frank; *J. Am. Chem. Soc.* **2010,** *132*, 12568-12586.

6 Summary

The efficient use of sunlight is one of the major challenges of our times, as the sun is the most powerful sustainable energy source our planet can provide. Thus, since the last century many concepts using visible light for chemical synthesis have been developed. While the number of synthetic applications rapidly increases, mechanistic insights into photochemical and photocatalytic reactions are still scarce. UV/Vis spectroscopy is frequently used to study light induced processes, whereas hardly any attention has been paid implementing NMR spectroscopy.

This thesis focuses on the application of NMR spectroscopy for the investigation of all kinds of light-induced transformations. The investigation of central photocatalytic and light-induced reactions as well as photochromic materials provided information of utmost importance for a better understanding and reaction design.

Firstly, an LED based illumination device was developed, enabling the illumination of a sample inside the magnet. Instead of lasers, commonly used for e.g. Photo-CIDNP spectroscopy, high power LEDs were implemented, because they are comparable to the light sources conventionally used in synthesis, easy to handle, reasonable priced and commercially available in a wide range of emission spectra. To increase the efficiency of this setup the application of commonly used shutters was avoided by switching the LEDs directly via the hardware of the NMR-spectrometer. Roughening the fiber tip ensured a uniform and efficient distribution of the light over the whole sector of the receiver coil. Triggering the LEDs by the spectrometer allows for continuous illumination as well as pulsed operations. The latter even enabled millisecond time resolved Photo-CIDNP spectroscopy, as under short duty cycles exceptional high powers can be applied to the LEDs. By those innovations the light intensity inside the sample could be increased significantly. This now provides access to all classical NMR techniques as well as Photo-CIDNP spectroscopy for the *in situ* investigation of light driven reactions. The LED based setup, applied to a variety of central issues in photochemistry to demonstrate its diversity, benefits and limitations, is further expected to shed light onto a huge variety of other light-induced processes. Furthermore, due to the small size of the setup it is highly presumably that modifications of the illumination device are also applicable in other fields.

Secondly, the prominent photocatalytic cross-dehydrogenative coupling reactions of *N*-aryltetrahydroisoquinolines were investigated by means of NMR in combination with ESR spectroscopy and synthetic strategies. Within the last two decades, those amine coupling reactions were and still are widely exploited photocatalytic transformations, yet their reaction mechanisms remained unclear. To provide a comprehensive picture, the aza-Henry reaction of 2-phenyl-1,2,3,4-tetrahydroiso-quinoline (THIQ) was studied thoroughly. The outstanding property of the nucleophile nitromethane, also serving as the solvent, to reoxidize the photocatalyst $Ru(bpy)_3Cl_2$ allows to investigate the reaction in the absence (*in situ* illumination) or in the presence (*ex situ* illumination) of oxygen. The reaction profiles and the distribution of the intermediates revealed two competitive pathways. Next to a THIQ-dimer and a THIQ-hydroperoxide an additional THIQ-nitrone intermediate was detected and characterized for

the first time. Furthermore, in contrast to previous assumptions the contribution of all intermediate species to the product formation was confirmed. Based on these results we propose that under anaerobic conditions a radical pathway is operative. Here, $NO_2Me^{\bullet-}$ functions as a base, deprotonating the THIQ radical cation, which is formed after initial electron transfer from THIQ. The resulting α-amino radical serves as precursor for the intermediates THIQ dimer and THIQ nitrone. Both species are subsequently converted to the aza-Henry product dependent (dimer) or independent (nitrone) of light. Under aerobic conditions, oxygen in form of superoxide radical anions was found to abstract hydrogen atoms of the THIQ radical cation, directly leading to the iminium ion. From an off-cylce equilibrium with THIQ-OOH the iminium ion is converted into the product. Surprisingly, an efficient background reaction was detected even in the absence of photocatalyst. This light-induced background reaction was also studied in detail, revealing the importance of oxygen and the correlation of wavelength and light intensity for an efficient conversion. In conclusion, an in-depth insight into the aza-Henry reaction is presented, revealing the different pathways operative and providing access to trigger the reaction by the experimental conditions. Thus, this study not only provides an exceptional overview of an entire reaction mechanism, but can also be seen as a guideline for further photochemical studies.

Thirdly, the flavin-catalyzed photooxidation of benzyl alcohols was studied in-depth by a combination of classical NMR, Photo-CIDNP and UV/Vis spectroscopy. By comparing ^{1}H NMR spectra and reaction profiles obtained in pure acetonitrile and in acetonitrile/D_2O mixtures, the presence of flavin semiqiunone radicals, detectable on the NMR time scale, is revealed for acetonitrile/D_2O mixtures. The observation of the radical species is ascribed to a solvent dependent stabilization of the zwitterionic radical pair. This radical pair is proposed to represent the central intermediate and the key of reactivity. After an identical initial electron transfer step the subsequent reaction pathways are controlled by the solvent properties. In acetonitrile, the NMR kinetic is not affected by the formation of (transient) flavin semiquinone radicals. Thus, this indicates an insufficient stabilization and a formal two-electron transfer process on the NMR time scale, directly leading to the formation of the fully reduced flavin. In contrast, in acetonitrile/D_2O mixtures the spectra revealed the involvement of a stabilized flavin semiquinone radical, which is formed via a one-electron transfer step. The regeneration to fully oxidized flavin is suggested to occur at this stage, in contrast to the reoxidation of fully reduced flavin in pure acetonitrile. The stabilized radical species was identified as the anionic semiquinone radical by UV/Vis spectroscopy. In summary, an explanation for the discrepancy in the reaction rates is given, resulting in an extended reaction mechanism, controllable by the experimental conditions. Furthermore, the detailed investigations revealed, that even in solution flavin is capable of acting as one- or two-electron mediator, a conduct which so far has only been observed for proteins, revealing the solvent dependent stabilization of a flavin semiquinone radical

Next to the mechanistic studies the LED based illumination device was applied for a detailed investigation of photochromic materials. These metastable compounds feature reversible light-induced property changes and thus are important for a various number of industrial applications, when embedded into polymers or macromolecules. As the investigation of polymers involves additional challenges, a spiropyran/merocyanine system was selected as a model unit. The thermodynamically stable spiropyran is converted into the metastable merocya-

nine form via irradiation with ultraviolet light. The system was investigated regarding the structure of the merocyanine form and its characteristic properties (half-lives, thermal relaxation rates, maximum fraction of merocyanine). The influence of sample concentration, solvent, temperature, emission wavelengths and intensity of the light source was investigated by a combination of the *ex situ* and *in situ* approaches. The application of the *in situ* device provided unprecedented access to the excitation of the photochromic system, stationary states and structural information of the metastable merocyanine form (carbon chemical shifts, two dimensional NMR). Thus, the *in situ* illumination is expected to become an important tool for the detailed investigation of photochromic materials and other types of light-induced transformations involving diamagnetic species.

In summary, within this thesis an LED based illumination setup was developed and applied to a variety of different photo-systems. By a combination of the *in situ* illumination technique with other classical approaches a new and easy access to important questions in the field of photochemistry was facilitated. The elucidation of single reaction pathways and whole reaction mechanisms was achieved, under consideration of the experimental conditions. Further, the detection and characterization of elusive intermediates and metastable compounds was realized by *in situ* illumination.

7 Zusammenfassung

Die effiziente Nutzung des Sonnenlichts ist eine der größten Herausforderungen unserer Zeit, da die Sonne als solche eine der ergiebigsten erneuerbaren Energiequellen unseres Planeten darstellt. Aus diesem Grund wurden seit dem letzten Jahrhundert viele Konzepte entwickelt, um sichtbares Licht für die chemische Synthese nutzen zu können. In Gegensatz zu der schnell wachsenden Anzahl an synthetischen Anwendungen, gibt es vergleichsweise immer noch wenige mechanistische Einblicke in photochemische und photokatalytische Reaktionen. Während die Untersuchung von Licht-induzierten Prozessen mittels UV/Vis Spektroskopie gängige Praxis ist, wurde das Potential der NMR Spektroskopie bisher unterschätzt.

Diese Arbeit befasst sich mit der Verwendung der NMR Spektroskopie für die Untersuchung diverser Licht-induzierter Umwandlungen. Die Analyse von zentralen photokatalytischen und Licht-induzierten Reaktionen, sowie photochromer Materialien liefert signifikante Informationen zu den Reaktionsabläufen, wodurch die Reaktionsprozesse weiter optimiert werden können.

Zunächst wurde ein spezielles auf LEDs basierendes Modul entwickelt. Dieses ermöglichte die direkte Beleuchtung von Proben im Inneren des Spektrometers bei laufender Reaktion. An Stelle der üblicherweise verwendeten Laser (z.B. in der Photo-CIDNP Spektroskopie) kommen hier Hochleistungs-LEDs zum Einsatz. Diese haben den Vorteil, dass sie mit den herkömmlichen Lichtquellen die in der Synthese benutzt werden vergleichbar sind. Zudem sind sie leicht zu handhaben, kostengünstig und in einer Vielzahl verschiedener Emissionsspektren erhältlich. Um die Effizienz des Aufbaus zu optimieren, wurde eine direkte Ansteuerung der Dioden über die Spektrometer-Hardware forciert, wodurch die vorher notwendige Verwendung von Shuttern hinfällig wurde. Das Anrauen der Glasfaserspitze bewirkte eine gleichmäßige und effiziente Verteilung des Lichts über den gesamten Bereich der Empfängerspule. Die Ansteuerung der LEDs mittels Spektrometer ermöglichte nun einen Dauer- und Pulsbetrieb. Durch den Pulsbetrieb können die LEDs mit geringem Auslastungsgrad und außergewöhnlich hoher Leistung betrieben und somit selbst für im Millisekunden Bereich aufgelöste Photo-CIDNP Spektroskopie verwendet werden. Mittels dieser Neuerungen konnte die Lichtintensität im Inneren der Probe maßgeblich gesteigert werden und ermöglicht somit die Untersuchung von lichtabhängigen Reaktionen im laufenden Prozess mittels klassischer NMR-, sowie Photo-CIDNP Spektroskopie. Der auf LEDs basierende Beleuchtungsaufbau wurde zur Untersuchung von diversen Fragestellungen in der Photochemie eingesetzt, um dessen Vielfältigkeit, Nutzen und Limitierung aufzuzeigen. Darüber hinaus kann angenommen werden, dass dieser Aufbau in der Zukunft über einige weitere lichtinduzierte Reaktionen Aufschluss geben wird. Durch seine Kompaktheit ist der Einsatz eines gegebenenfalls angepassten Aufbaus auch in anderen Bereichen denkbar.

Im Weiteren wurden die photokatalytisch relevanten dehydrierenden Kreuzkupplungen von *N*-aryltetrahydroisochinolinen mittels einer Kombination aus NMR-Spektroskopie, EPR-Spektroskopie und synthetischen Strategien untersucht. Innerhalb der letzten zwei Jahrzehnte wurden und werden die Kupplungsreaktionen dieser Amine für eine Vielzahl photokatalyti-

scher Umwandlungen ausgeschöpft. Trotz der immer noch andauernden Nutzung der Reaktion, konnte der zugrunde liegende Reaktionsmechanismus bisher nicht vollständig aufgeklärt werden. Um ein umfassendes Gesamtbild der Reaktion zu liefern wurde die aza-Henry Reaktion von 2-Phenyl-1,2,3,4-tetrahydroisochinolin (THIQ) sorgfältig untersucht. Die spezielle Eigenschaft des Nukleophils und zeitgleichen Lösungsmittels Nitromethan, den Katalysator $Ru(bpy)_3Cl_2$ zu reoxidieren, ermöglichte eine Untersuchung der Reaktion sowohl in Abwesenheit (*in situ* Beleuchtung) als auch in Anwesenheit (*ex situ* Beleuchtung) von Sauerstoff. Die Reaktionsprofile und die Intermediatverteilung zeigten zwei miteinander konkurrierende Reaktionswege auf. Neben dem THIQ-Dimer und dem THIQ-Hydroperoxid Intermediat konnte zusätzlich erstmals ein THIQ-Nitron nachgewiesen und charakterisiert werden. Weiterhin konnte entgegen bisheriger Annahmen eine Beteiligung aller Intermediate an der Produktbildung bestätigt werden. Basierend auf diesen Ergebnissen kann angenommen werden, dass unter anaeroben Bedingungen ein Radikalweg aktiv ist. In diesem fungiert $NO_2Me^{\bullet -}$ als eine Base, die in der Lage ist das THIQ Radikalkation zu deprotonieren, welches durch den anfänglichen Elektronentransfer aus dem THIQ gebildet wird. Das entstehende α-amino Radikal dient als Vorstufe für die Bildung der THIQ Dimere und THIQ Nitrone. Beide Spezies werden anschließend in das aza-Henry Produkt überführt. Dies kann lichtabhängig (Dimer) oder lichtunabhängig (Nitron) geschehen. Weiterhin konnte unter aeroben Bedingungen gezeigt werden, dass Sauerstoff, in Form von Superoxidradikalanionen, in der Lage ist Wasserstoffatome des THIQ Radikalkations zu abstrahieren, was zu einer direkten Bildung des Iminiumions führt. Das Iminiumion steht mit THIQ-OOH in einem außerhalb des Katalysezyklus liegenden Gleichgewicht, und führt zur Produktbildung. Überaschenderweise konnte auch in der Abwesenheit des Katalysators eine effiziente Hintergrundreaktion beobachtet werden. Bei einer detaillierten Untersuchung der lichtinduzierten Hintergrundreaktion konnten die ablaufenden Reaktionswege offengelegt und ein Zugang zur Steuerung der Reaktion mithilfe der experimentellen Bedingungen ermöglicht werden. Aus diesem Grund gibt diese Studie nicht nur einen außergewöhnlich detaillierten Überblick über den gesamten Reaktionsmechanismus, sondern kann auch als Wegweiser für zukünftige photochemische Studien angesehen werden.

Als Nächstes wurde die durch Flavin katalysierte Photooxidation von Benzylalkoholen mittels einer Kombination aus NMR-, EPR- und UV/Vis-Spektroskopie eingehend untersucht. Ein Vergleich der in reinem Acetonitril und in Acetonitril/D_2O Mischungen erhaltenen ^1H NMR Spektren und Reaktionsprofile zeigte die Anwesenheit eines Flavin-Semichinonradikals in Acetonitril/D_2O Mischungen auf der NMR Zeitskala. Das diese Radikalspezies indirekt mittels NMR-Spektroskopie erfasst werden konnte, wird einer lösungsmittelabhängigen Stabilisierung des zwitterionischen Radikalpaares zugeschrieben. Es wird angenommen, dass dieses Radikalpaar das zentrale Intermediat und damit den Schlüssel zur Reaktivität darstellt. Nach einem anfänglich identischen Elektronentransferschritt werden die nachfolgenden Reaktionswege durch die Eigenschaften des Lösungsmittels gesteuert. In Acetonitril wird die NMR Kinetik nicht von der Bildung eines (transienten) Flavin-Semichinonradikals beeinflusst. Aus diesem Grund wird eine unzureichende Stabilisierung der Radikalspezies angenommen, welche über einen formalen Zwei-Elektronen-Transferprozess auf der NMR Zeitskala direkt zur Bildung des vollständig reduzierten Flavins führt. In Gegensatz dazu weisen die Spektren in Acetonitril/D_2O Mischungen auf eine Beteiligung des stabilisierten Flavin Semichinonradikals hin, dass durch einen Ein-Elektron–Transferprozess gebildet wird. Es wird angenommen, dass die Regenerierung zum

vollständig oxidierten Flavin an dieser Stelle erfolgt, im Gegensatz zur Oxidation des vollständig reduzierten Flavins in reinem Acetonitril. Die stabilisierte Radikalspezies konnte mittels UV/Vis-Spektroskopie als das Flavin-Semichinonanion identifiziert werden. Zusammenfassend kann gesagt werden, dass in dieser Studie eine Erklärung für die unterschiedlichen Reaktionsraten gefunden wurde, die zu einem ausführlicheren Reaktionsmechanismus führte, welcher durch die Wahl der experimentellen Bedingungen beeinflusst werden kann. Des Weiteren konnte die detaillierte Studie zeigen, dass Flavin die Fähigkeit besitzt, auch in Lösung als Ein- bzw. Zwei-Elektronen-Vermittler zu fungieren. Dies ist ein Verhalten, welches bisher nur in Proteinumgebungen beobachtet werden konnte und die lösungsmittelabhängige Stabilisierung des Flavin-Semichinonradikals demonstriert.

Neben den mechanistischen Studien wurde der auf LEDs basierende Aufbau auch für die eingehende Untersuchung von photochromen Materialien eingesetzt. Diese metastabilen Komponenten besitzen die Fähigkeit ihre Eigenschaften bei Bestrahlung mit Licht reversibel zu ändern und sind daher - eigenbettet in Polymere oder Makromoleküle - für eine Vielzahl von industriellen Anwendungen relevant. Da die Untersuchung von Polymeren viele zusätzliche Herausforderungen mit sich bringt, wurde als Modelsystem die Spiropyran/Merocyanin Einheit gewählt. Das thermodynamisch stabile Spiropyran kann durch Bestrahlung mit ultraviolettem Licht in die metastabile Merocyaninform umgewandelt werden. Das Modelsystem wurde hinsichtlich seiner Merocyaninstruktur und seiner charakteristischen Eigenschaften (Halbwertszeiten, thermische Relaxationsgeschwindigkeiten, Maximalanteil von Merocyanin) untersucht. Der Einfluss der Probenkonzentration, des Lösungsmittels, der Temperatur, der Emissionswellenlänge und Intensität der Lichtquelle auf das System wurde mittels einer Kombination aus *ex situ* und *in situ* Strategien untersucht. Der Einsatz des *in situ* Beleuchtungsaufbaus ermöglichte einen bisher nicht dagewesenen Zugang zu Informationen bezüglich der Anregung des photochromen Systems, der stationären Zustände und der Struktur der metastabilen Merocyaninform (Kohlenstoffchemische Verschiebungen, Zweidimensionale NMR-Spektren). Aus diesem Grund kann erwartet werden, dass sich der *in situ* Beleuchtungsaufbau zu einem wichtigen Hilfsmittel für die eingehende Untersuchung photochromer Materialien und anderer lichtinduzierter Umwandlungen diamagnetischer Spezies entwickelt.

Zusammenfassend wurde in dieser Arbeit ein auf LEDs basierender Beleuchtungsaufbau entwickelt und auf verschiedene Photo-Systeme angewendet. Mittels Kombination aus *in situ* Beleuchtung und anderen klassischen Vorgehensweisen wurde ein neuer und leicht umsetzbarer Lösungsansatz für Kernproblematiken in der Photochemie gefunden. Die Aufklärung von einzelnen Reaktionswegen und von gesamten Mechanismen wurde unter Einbeziehung der experimentellen Bedingungen erreicht. Daneben wurde die Detektion und Charakterisierung von schwer fassbaren Intermediaten und metastabilen Komponenten durch die *in situ* Beleuchtung ermöglicht.